11:03:09 OCA PAD AMENDMENT - PROJECT HEADER INFORMATION 12/04/95

Active

Project #: E-16-M83 Cost share #: E-16-364 Rev #: 6
Center # : 10/24-6-R7760-0A0 Center shr #: 10/22-1-F7760-0A0 OCA file #:
Work type : RES
Contract#: F49620-93-1-0177 Mod #: BUDGET REVISION Document : GRANT
Prime #: Contract entity: GTRC

Subprojects ? : N CFDA: 12.800
Main project #: PE #: 61102F

Project unit: AERO ENGR Unit code: 02.010.110
Project director(s):
ZINN B T AERO ENGR (404)894-3033

Sponsor/division names: AIR FORCE / BOLLING AFB, DC
Sponsor/division codes: 104 / 001

Award period: 930301 to 960229 (performance) 960428 (reports)

Sponsor amount	New this change	Total to date
Contract value	0.00	461,934.00
Funded	0.00	461,934.00
Cost sharing amount		170,612.00

Does subcontracting plan apply ?: N

Title: INVESTIGATION OF ACTIVE CONTROL OF COMBUSTION INSTABILITIES IN CHEMICAL ...

PROJECT ADMINISTRATION DATA

OCA contact: Anita D. Rowland 894-4820

Sponsor technical contact

MITAT A BIRKAN
(202)767-4987

AFOSR/NA
110 DUNCAN AVENUE SUITE B115
BOLLING AFB DC 20332-0001

Sponsor issuing office

JENNIFER BELL
(202)767-4799

AFOSR/PKA
110 DUNCAN AVENUE, SUITE B115
BOLLING AFB, DC 20332-0001

Security class (U,C,S,TS) : U ONR resident rep. is ACO (Y/N): N
Defense priority rating : supplemental sheet
Equipment title vests with: Sponsor GIT X
>$5000-AFOSR MAY ELECT TITLE W/IN 120 D. AFTER COMPLETION.
Administrative comments -
PROCESSED 11.30 REQUEST

GEORGIA INSTITUTE OF TECHNOLOGY
OFFICE OF CONTRACT ADMINISTRATION

NOTICE OF PROJECT CLOSEOUT

4

Closeout Notice Date 06/12/96

Project No. E-16-M83 Center No. 10/24-6-R7760-0A0

Project Director ZINN B T School/Lab AERO ENGR

Sponsor AIR FORCE/BOLLING AFB, DC

Contract/Grant No. F49620-93-1-0177 Contract Entity GTRC

Prime Contract No.

Title INVESTIGATION OF ACTIVE CONTROL OF COMBUSTION INSTABILITIES IN CHEMICAL .

Effective Completion Date 960229 (Performance) 960428 (Reports)

Closeout Actions Required:	Y/N	Date Submitted
Final Invoice or Copy of Final Invoice	Y	
Final Report of Inventions and/or Subcontracts	Y	960507
Government Property Inventory & Related Certificate	Y	
Classified Material Certificate	N	
Release and Assignment	N	
Other	N	

Comments

Subproject Under Main Project No.

Continues Project No.

Distribution Required:

Project Director	Y
Administrative Network Representative	Y
GTRI Accounting/Grants and Contracts	Y
Procurement/Supply Services	Y
Research Property Managment	Y
Research Security Services	N
Reports Coordinator (OCA)	Y
GTRC	Y
Project File	Y
Other	N
	N

NOTE: Final Patent Questionnaire sent to PDPI.

GTA

AFOSR ANNUAL TECHNICAL REPORT

for the period
March 1993 - February 1994

on

INVESTIGATION OF ACTIVE CONTROL OF COMBUSTION INSTABILITIES IN CHEMICAL ROCKETS

Prepared for

Air Force Office of Scientific Research
Aerospace Sciences Directorate
Bolling Air Force Base

by

Ben T. Zinn
Brady R. Daniel
Yedidia Neumeier

School of Aerospace Engineering
Georgia Institute of Technology
Atlanta, GA 3032

March 1994

Approved for public release; distribution unlimited
Grant No. F49620-93-1-0177

Summary

This report summarizes the accomplishments under AFOSR Grant No. F49620-93-1-0177 during the period March 1, 1993 to February 28, 1994. The objective of this research is to investigate active control of detrimental combustion instabilities in chemical rockets by a periodic combustion process. These efforts resulted in the development of an active control approach consisting of a pressure transducer sensor, an observer that determines the characteristics of the instability in real time, a controller that incorporates appropriate phase shifts and amplitude gains into each of the identified (by the observer) combustor modes and sends the resulting signal to an actuator consisting of a secondary fuel injector with capabilities for injecting a periodic fuel flow rate into the combustor. This control system is designed to produce an oscillatory combustion process within the combustor that is out of phase with the combustor pressure oscillations, resulting in the attenuation of the unstable combustor modes. In a parallel effort, an experimental gas rocket setup that will be used to investigate the effectiveness of the developed active control system is being developed. To date, most of the software and hardware needed for the active control system have been developed. In addition, the development of the experimental setup is near completion. Also, the effectiveness of the developed active control system was demonstrated in independent theoretical and experimental studies. A theoretical model of an actively controlled rocket combustor was developed and used to demonstrate the effectiveness of the active control system. Furthermore, the effectiveness of the developed controller was demonstrated in cold flow experiments in which the active control system rapidly damped large amplitude resonant oscillations that were excited by a speaker. Finally, the possibility of using an open loop, high frequency, vibrational control approach to stabilize rocket motors was investigated and the conditions under which this approach can work were established.

Introduction

This report summarizes the accomplishments under AFOSR Grant No. F49620-93-1-0177 during the period March 1, 1993 to February 28, 1994. The objective of this research is to investigate active control of detrimental combustion instabilities in chemical rockets by a periodic combustion process. It is expected that this study will develop fundamental information that could be used to guide the development of active control systems for unstable rocket motors.

Combustion instabilities are generally driven by a periodic combustion process whose oscillations are in phase with the combustor pressure oscillations; a principle that is generally referred to as Rayleigh's criterion. The operation of the rocket motor becomes unstable if the driving provided by the periodic combustion process is larger than the damping inherently present within the system due to, for example, viscous dissipation and nozzle damping. The processes responsible for the establishment of a periodic combustion process generally involve complex interactions between the combustion process and acoustic oscillations in the combustor that depend upon the rocket motor design and operating conditions. For example, combustion instabilities may be driven by a periodic combustion heat release process that is occurring within periodically formed vortical structures[1], or by interaction between the compression wave and the reaction rate[2]. To date, such instabilities were generally suppressed by, for example, modification of the combustion process in an effort to reduce its driving and/or increasing the damping present within the system by, the addition of acoustic liners or metal rods[3]. Unfortunately, these efforts were generally costly and time consuming and often failed to attain their objectives. Alternate approaches that can be used to stabilize propulsion systems in general and chemical rockets in particular at a reasonable cost and within a reasonable time period are clearly needed.

Recent progress in electronics, computers, sensors and actuators has suggested that practical, active, control systems capable of damping detrimental combustion instabilities in rocket motors could be developed. Such a control system generally consists of a sensor that monitors the

rocket motor performance, a controller that analyzes the sensor's output and uses it to provide an input signal for an actuator that modifies the system's performance. The development of such a system and an understanding of the fundamental processes that govern its operation are the objectives of this investigation. The developed active control system will damp combustion instabilities by "driving" a periodic heat addition process within the combustor that will be out of phase with the combustor pressure oscillations. This study will investigate the attainment of this objective by use of periodic injection of a secondary fuel stream.

Control System Considerations

Rayleigh's criteria implies that acoustic oscillations are driven or suppressed when heat is added in phase or out of phase with the pressure oscillations, respectively. This suggests that combustion instability oscillations could be suppressed if effective means for driving heat addition oscillations that are out of phase with the combustor pressure oscillations could be developed.

Rocket motors instabilities are generally accompanied by the excitation of one or more natural acoustic modes of the combustor and sometimes, their harmonics. For example, the combustion process may drive longitudinal, transverse or radial combustor modes, or multi-dimensional modes whose oscillations consist of a combination of the motions produced by the above mentioned modes. Active control of combustion instabilities investigated to date[4] were based upon a time domain control approach and focused on the damping of combustion instabilities consisting of the fundamental longitudinal mode or, at most, a combination of low frequency longitudinal modes. Moreover, the application of these methods required apriori knowledge of the characteristics of the unstable modes. In reality, however, the characteristics of the excited instability are not known in advance. Furthermore, the characteristics of the instability (e.g., its modal content) often change with time in response to changes in cavity properties (e.g., change of propellant burning surface diameter in a solid rocket) and motor operating conditions.

Consequently, active control systems that are capable of real time identification of the characteristics of the instability must be developed. Such systems will have to utilize the acquired information about the characteristics of the instability to "drive" an oscillatory combustion process within the combustor that is out of phase with the time varying combustor pressure oscillations.

A new approach for active control of rocket motor combustion instabilities that overcomes the limitations of previous active control systems has been developed under this program. The developed system consists of a sensor (a pressure transducer) that monitors the performance of the combustor, an observer that analyzes the sensor output and determines the frequencies and amplitudes of the excited combustor oscillations in real time and a "controller" that introduces appropriate phase shifts and amplitude gains into the data provided by the observer prior to sending it to an actuator that controls the operation of a periodic fuel injection system. The novel components of this systems are its observer and "controller" whose tasks are to identify the characteristics of the instability in real time and provide the necessary phase shifts and gains to the oscillating combustor modes, respectively. The "controller's" output is then used to drive a novel actuator whose task is to produce an oscillatory fuel injection rate into the combustor that will produce combustion process heat release oscillations that are out of phase with the excited combustor oscillations.

Summary of Program Accomplishments

Overview

The efforts expended during the first year of this program consisted of a number of theoretical and experimental studies. The experimental efforts focused on the development of a small scale gas rocket that could be used to experimentally investigate the performance of the developed active control system. In addition, the experimental efforts focused on the development of needed sensors, electronic components, computer systems, and actuators. The theoretical studies were concerned with the development of an analytical approach for real time identification

of the characteristics of time varying rocket motor instabilities, the development of an effective control system methodology, simulating the performance of an actively controlled rocket motor, and investigating alternate control approaches for stabilizing unstable propulsion systems. Progress made under each of these studies is briefly summarized in the remainder of this section.

Gas Rocket Motor

In parallel with the theoretical efforts, the development of a small scale gas rocket setup for investigating the performance of the developed active control system was initiated at the onset of this program. A gas rocket was chosen for this study because past studies[5,6,7] have shown that such rocket motors experience instabilities similar to those observed in practical solid and liquid propellant rocket motors, and their design and operational characteristics have much in common with those of liquid rockets. The experimental gas rocket developed under this program is shown in Fig. 1. It consists of a reactants feed system, a combustor section with windows for observations and optical diagnostics, a nozzle and an exhaust system. To provide needed cooling, the combustor is submersed in a bath with running water. Also, the combustor section length can be changed by adding or subtracting sections having the same diameter, which will provide capabilities for exciting instabilities with different frequencies. Since the designed combustor has a large length to diameter ratio, it is expected that axial mode instabilities with high and low frequencies will be excited in the system when short and long combustor lengths will be tested, respectively. This will provide an opportunity to investigate the effectiveness of the developed active control system in the damping of low and high frequency instabilities. The need to damp high frequency instabilities will determine the frequency limit of the developed control system.

Reactants Injection System

It is expected that methane or propane fuel and air or air-oxygen mixture oxidizer will be used as propellants in the developed gas rocket. Consequently, the developed reactants feed system required capabilities for supplying pre specified flow rates of these propellants into the

combustor. Furthermore, since tests will be conducted at different mean combustor pressures, the developed reactants injection system needed capabilities for operating over comparable pressure ranges. Finally, the active control system requires capabilities for dividing the combustor fuel flow rate into two streams of accurately controlled flow rates, and oscillating the injection rate of one of these fuel streams in order to produce a (controlled) oscillatory combustion process within the combustor.

The developed propellants feed system is shown in Fig. 2. It consists of an oxidizer (i.e., air) injector and two fuel injectors. The primary and secondary fuel injectors supply the combustor with steady and oscillatory fuel flow rates, respectively. The secondary fuel flow rate is modulated by use of a recently developed "magnetostrictive" actuator [8]. It oscillates a tapered needle up and down, producing a periodic blockage of a cross sectional area of the secondary fuel orifice. The oxidizer and fuel streams are injected at approximately 45 degrees angle and axially, respectively, into a small volume upstream of the injector plate where they mix prior to entering the combustor through the injector plate orifices. The angles and dimensions of the orifices in the injector plate have been chosen to generate recirculation zones downstream of the injector plate where the combustion process will be stabilized.

In this feed system design, the main fuel flow rate is controlled by the size of the upstream orifice while the secondary fuel flow rate is regulated by the position of the actuator needle that is designed to oscillate up-and-down relative to some mean position. The oscillatory needle motion is controlled by an "Etrema" actuator consisting of a Terfenol-D rod that changes its length in response to changes in magnetic field intensity[9]. This recently developed actuator is capable of providing relatively large displacement (e.g., 100 μm) in a very short response time (e.g., .2 msec.)

The active control system

The active control system under development is shown in Fig. 3. It uses a piezoelectric pressure transducer to "sense" the combustor pressure oscillations. The measured pressure signal is fed to a Digital Signal Processor (DSP) TX320C40 DSP via an analog input board. The digital control signal that is generated by the DSP is converted into an analog signal and fed back to the actuator. The host computer will accommodate an as yet to be developed algorithm that will determine the optimal gain and phase shift for the controller on the DSP. The DSP and the I/O interface are integrated on a single DATA TRANSLATION 3801-G board that is installed in a host IBM PC personal computer.

The developed control scheme consists of two parts. A fast algorithm, which includes the observer and an observer signal modifier (to be denoted "controller"), that is run on the DSP and a slower adaptive-type algorithm that is run on the host computer. The function of the observer is to provide the controller with the frequency, amplitude and phase of the oscillations in the measured pressure signal. The observer continuously updates its output in response to changes in its input data. The frequency, amplitude and phase of each combustor oscillations, as identified by the observer, are used to generate a control signal with the same frequency but different amplitude and phase. The optimal amplitude and phase shift are determined by as yet to be developed adaptive control algorithm. This algorithm, which is naturally slow and requires a significant computational effort, will be performed on the host computer. This adaptive capability will enable the control system to maintain the stability of a rocket without any prior knowledge of the characteristics of its instability.

Since the developed active control approach significantly deviates from standard control approaches, its performance was investigated in the experimental setup (i.e., plant) shown in Fig. 4. It consists of a wooden rectangular box that serves as an acoustic resonator and speakers that simulate acoustic energy sources. Simulated acoustic instabilities were driven in the box by one of the speakers while the other was used to damp the oscillations using the developed control method.

In this setup, the controller consists of a "simple" Analog Devices I/O Interface and the 486/66 MHz. processor of the host computer performed the tasks of the DSP.

Initially, the observer's performances was investigated. For this purpose, an acoustic wave was excited in the box by one of the speakers that was driven with a computer generated sinusoidal signal. The amplitude of the sinusoidal signal sent by the computer to the speaker was fixed but its frequency varied slowly with time. The excited pressure signal in the box was measured by a transducer and sent to the observer, which determined its amplitude and frequency in real time. In this connection, it should be noted that the observer determined the characteristics of the pressure oscillation in the box without having any information about the signal supplied to the acoustic driver. The "observed" (real) time* dependence of the amplitude and frequency of the box oscillations are shown in Figs. 5-a and 5-b, respectively. The frequency response displayed in Fig. 5-a agrees very well with measurements of previous tests in which the dependence of the box amplitude upon the frequency of the driven signal was investigated. Figure 5-b indicates that the observer cannot accurately identify the frequency near anti resonance where the amplitudes of the pressure oscillations are virtually zero. This does not, however, present any problem to the controller because it can be shown[10] that when the observed frequency is wrong, the generated control signal still possesses the correct frequency but with a different phase. When anti-resonance oscillations occur in the combustor, this phase has no impact upon the pressure oscillations.

The steps-like structure of the curve in Fig. 5-b of the time dependence of the "observed" frequency is the result of the time required by the computer to calculate the frequency in the periods between data sampling. As the ratio of the computation time and the period of the oscillations increases, the width of the steps increases. Currently, the computation cycle requires about 180 μs, which limits the capability of the control system to frequencies below 1000 Hz. This limit will be extended in the future to 10 KHz. after the DSP board will be incorporated into the control system.

* Since the frequency of the driven signal changed with time, plotting the "observed" amplitude and frequency of the box oscillations as a function of frequency is equivalent to showing their time dependence.

In the next series of tests, the performance of the controller was investigated. For this purpose, the 250 Hz. resonant frequency of the box was driven by a speaker that was incorporated in a positive feedback loop, see Fig. 4. Once large amplitude oscillations were excited in the box, the controller (i.e., the second "loop" in Fig. 4) was turned on in an effort to damp the box oscillations. Subsequent "real time" rate of the damping of the box oscillations by the active control system, as determined by the observer, for different controller phases and gains are shown in Figs. 6-a and 6-b, respectively.

Figure 6-a describes the dependence of the controller's performance upon its phase shift. The results presented in Fig. 6-a indicate that the developed controller can rapidly damp large amplitude resonant oscillations, and that the rate of damping depends upon the controller's phase. At the optimum phase for which the rate of attenuation is maximum, the energy addition provided by the controller is exactly out of phase with the box pressure oscillations. As the controller's phase deviates from this phase, the controller's effectiveness decreases resulting in a lower attenuation rate of the oscillations. The phase margin for a given value of the controller's gain is determined by the total phase span in which the controller attenuates the oscillations. A large phase margin indicates that the controller is robust. Figure 6-a shows that the developed controller has a large phase margin of at least 120 degrees.

Figure 6-b describes the dependence of the controller's performance upon its gain. The results presented in Fig. 6-b show that the rate of damping the pressure oscillations increases as the controller's gain increases. In most high order linear systems the controller gain cannot be increased indefinitely, because the system becomes unstable when the gain exceeds a certain threshold value. An analysis of the developed controller predicts that it can perform effectively over a wide range of gain values. Figure. 6-b indicates that the developed controller performs effectively with a gain ratio of 8:1. It is expected that the developed controller has not yet reached its full potential and that additional (slight) modifications to its software will further increase its gain margin.

Theoretical Investigations

The objective of this study was to theoretically investigate the performance of the developed active control system. Initially, the characteristics of an instability were investigated by solving the one dimensional, nonlinear, Euler equations that describe the flow inside a rocket motor combustor, using a McCormack predictor corrector technique[11]. The driving of the instability by the combustion process was modeled by means of a simple linear feedback between the pressure and combustion heat addition oscillations. Next, the combustor model was "equipped" with the developed active control system and used to investigate the effectiveness of the active control systems. The results of numerical simulations confirmed the effectiveness of the developed control system. The results of this study are summarized in a paper that has been submitted for presentation at the Twenty Fifth International Symposium on Combustion that will be held in August 1994. A copy of this paper is included in the Appendix of this report.

At present, a more advanced numerical solution algorithm, based upon Roe's scheme, for solving the unsteady reacting flow equations in an unstable rocket motor is being developed. As part of this study, a new approach for proper numerical representation of the boundary conditions at the injector face and nozzle entrance plane has been developed and incorporated in the model. Furthermore, to improve the representation of the highly complex combustion heat release process in the simulation, a mixing model that can be incorporated into a one dimensional combustion model was developed. It accounts for the mixing of the fuel and air as well as the mixing of hot combustion products with reactants. The combustion heat release model utilizes an Arrhenius law to determine the reaction rate of the mixed reactants.

Numerical simulations of the rocket performance, which utilized the developed rocket model, indicate that the model predicts spontaneous onset of combustion instabilities that grow in amplitude and reach limit cycle oscillations similar to those observed in unstable rocket motors[12]. Since the developed model can predict unstable rocket motor performance using input data that

describes its operating conditions (e.g., air and fuel injection rates), it provides an excellent tool for evaluating the performance of the developed active control system.

Vibrational Control of Combustion Instabilities

In a parallel study, the potential use of vibrational control[13] to damp combustion instabilities was investigated. Vibrational control consists of the excitation of high frequency, open loop, oscillations within an unstable system. It has been shown in the past that such an approach could stabilize unstable mechanical system such as an inverted pendulum. Because of the relative simplicity of this approach, it has been decided to investigate whether it could be used to stabilize rocket motors.

This study has shown that pressure oscillations in acoustic cavity cannot be damped by classical linear vibrational control. Subsequently, this research was extended to explore the use of nonlinear vibrational control. It was found that nonlinear vibrational control can be effective in cases where linear vibrational control fails. However, while the application of linear vibrational control can be achieved with an open loop control system that does not require monitoring the system's behavior, the suggested nonlinear vibrational control must use measurement of the system's pressure oscillations. Future studies will investigate the advantages and disadvantages of the developed nonlinear vibrational control method relative to the active control method that are the main subject of interest of this program.

The results of this investigation were summarized in a paper that will be presented at an AIAA Student Conference in April 1994. This paper is listed in the related publication list and a copy is provided in the appendix.

Summary of Program Accomplishments and Expected Future Activities

(1) An active control method and the needed software were developed and tested in a simplified experimental setup.

(2) The design of an experimental, actively controlled, small scale gas rocket motor has been completed and the setup is being assembled

(3) The design of a periodic fuel injection system that will be used to produce an oscillatory heat release process within the rocket combustor has been completed. This injection system is currently being fabricated. In addition, the actuator that drives the periodic fuel injection system has been assemble and tested.

(4) The effectiveness of the developed active control system has been experimentally demonstrated in cold flow experiments in which speakers were used to simulate combustion instability oscillations and the out-of-phase driving that will be provided by the driven oscillatory combustion system.

(5) A theoretical model of an unstable rocket motor has been developed. Novel features of this model include a flow mixing sub model that is incorporated in the combustion process heat release model and a new approach for proper numerical representation of the injector face and nozzle entrance boundary conditions.

(6) A preliminary investigation of the feasibility of an open loop vibrational control of rocket instabilities has been performed.

Planned future activities will include:

(1) Assembly completion and checkout tests of the experimental rocket motor setup.

(2) Experimental studies to determine the conditions under which the rocket motor operation is unstable.

(3) Completion of the development of the active control system and its incorporation into the rocket motor setup.

(4) Check out tests of the active control system.

(5) Experimental investigation of the effectiveness of the active control system and determination of system parameters that optimize the controller performance.

(6) Development of an automatic optimization scheme that will be incorporated into the control system.

Related Publications

1. Matta, L. M. and Zinn, B. T., Theoretical Study of Flow Turning Losses in the Presence of Mean Temperature Gradients, AIAA 94-0099, Jan. 1994.

2. Sujith, R. I., and Waldherr, G. A. and Zinn, B. T., Exact Solution for One-Dimensional Acoustic Field in Ducts with Axial Temperature Gradient, AIAA 94-0359, Jan. 1994.

3. Shapiro B., "High frequency Nonlinear Vibrational Control", Accepted for presentation at the AIAA Southeastern Regional Student Conference, Huntsville, Alabama, April 6-10, 1994.

4. Neumeier Y. and Zinn B. T., "Active Control of Combustion Instabilities Using Real Time Identification of Unstable Combustor Modes. Submitted to the Twenty Fifth International Symposium of Combustion.

References

1. Sterling, J. D., Longitudinal Mode Combustion Instabilities in Air Breathing Engines. Ph.D. thesis, California Institute of Technology, 1987.

2. Sirignano, W. A. and Crocco, L., A shock Wave Model of Unstable Rocket Combustors. AIAA Journal Vol. 2, No. 7, July 1964, pp. 1285-1296.

3. Harjee, D. and Reardon, F. (eds.), Liquid Propellant Rocket Combustion Instability, NASA SP 194, 1972, Chap. 8.

4. Gutmark, E., Wilson, K. J., Parr, T. P. and Schadow, K. C., Feedback Control of Multi-Mode Combustion Instability, AIAA Paper 92-0778, 30th Aerospace Sciences Jan. 1992, Reno, Nevada.

5. Zucrow, M. J. and Osborn, J. R., An Experimental Study of High Combustion Pressure Oscillations, Jet Propulsion Vol. 28., No. 10, Oct. 1958 pp. 654-659.

6. Pelmas, R., Glassman, I. and Weleb M., An Experimental Investigation of Longitudinal Mode Combustion Instability in a Rocket Motor Using Premixed Gaseous Propellants, Aeronautical Engineering Laboratory, Report No. 589, Dec. 1961 Princeton.

7. Tsuji, H. and Takeno T., Studies of High Frequency Combustion Oscillations in a Gaseous Propellant Rocket Motor, Report No. 391, March 1964, University of Tokyo, Aeronautical Research Institute.

8. Savage, H. T., Clark, A. E. and Powers, J. M., Magnetomechanical Coupling and ΔE Effect in Highly Magnetostrictive Rare Earth-Fe_2 Compounds, IEEE Transactions on Magnetics, Vol. Mag-11, No. 5, Sep. 1975.

9. Savage, H. T., Abbundi, R. and Clark, A. E., Permeability, Magnetomechanical Coupling and Magnetostriction in Grain-oriented Rare earth-iron Alloys.

10. Neumeier Y. and Zinn B. T., Active Control of Combustion Instabilities Using Real Time Identification of Unstable Combustor Modes. Submitted to the Twenty Fifth International Symposium of Combustion.

11. MacCormack, R. W., The Effect of Viscosity in Hypervelocity Impact Cratering, AIAA Paper 69-354, 1969.

12. Bowman, C. T., Experimental Investigation of High Frequency Longitudinal Combustion Instability in Gaseous Propellant Rocket Motor, Technical Report No. 784, Jan. 1967, Princetone University, Department of Aerospace and Mechanical Sciences.

13. Meerkov, S. M., Principle of Vibrational Control; Theory and Application, IEEE Transaction on Automatic Control, Vol. AC-25, No. 4, Aug. 1980.

Personnel

Dr. Ben T. Zinn, David S. Lewis Chair of Aerospace Engineering and Regent's Professor.	Principal investigator
Mr. Brady R. Daniel, Senior Research Engineer	Principal investigator
Dr. Y. Neumeier	Post Doctoral Fellow
Mr. Rajendran Mohanraj	Ph.D. Student
Mr. Gershon Ordan	Research Engineer
Mr. Brian Stephens	Undergraduate Research Assistant
Mr. Benjamin Shapiro	Undergraduate Research Assistant

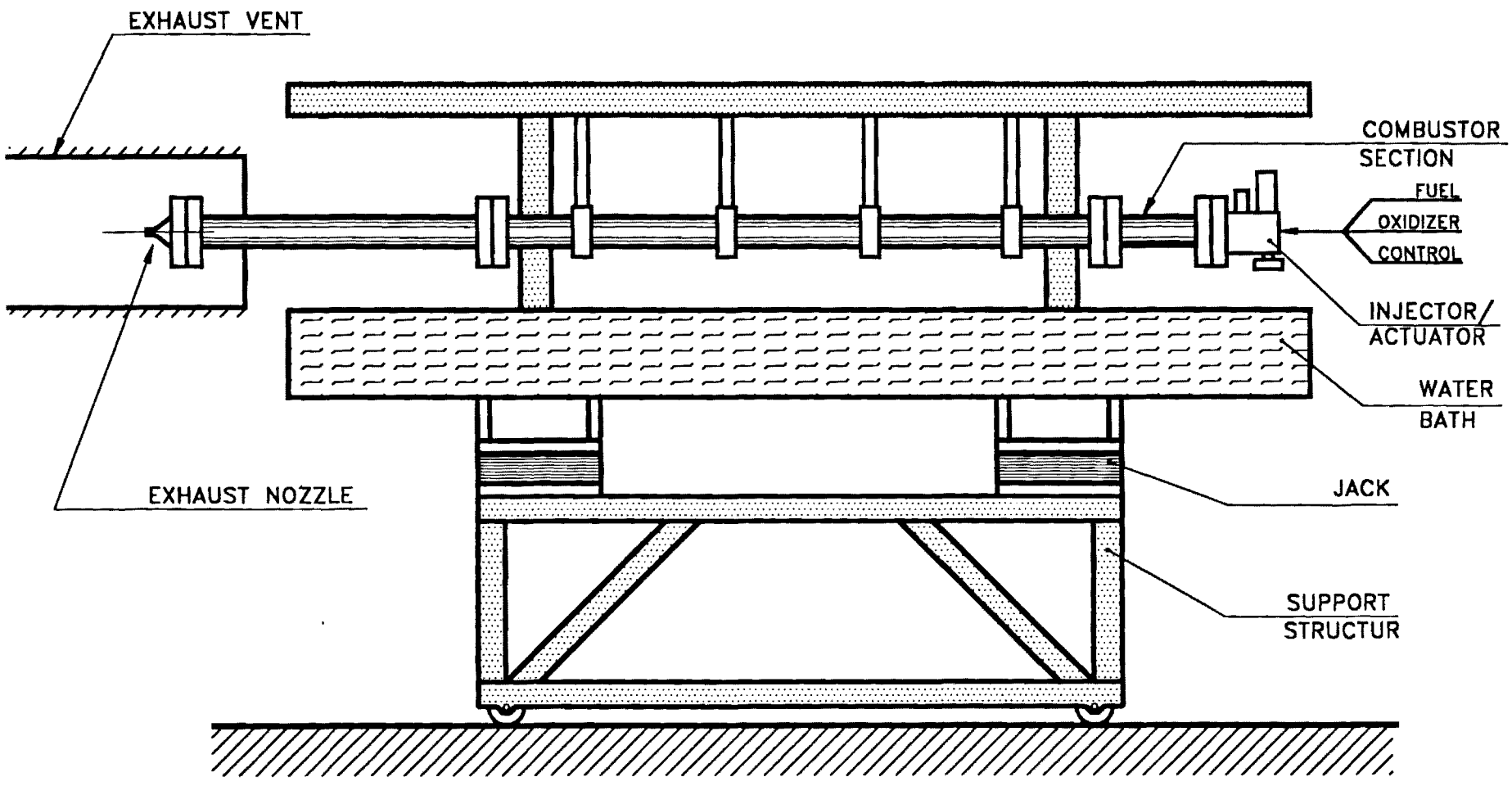

FIGURE 1. A SCHEMATIC OF THE DEVELOPED GAS ROCKET MOTOR SETUP

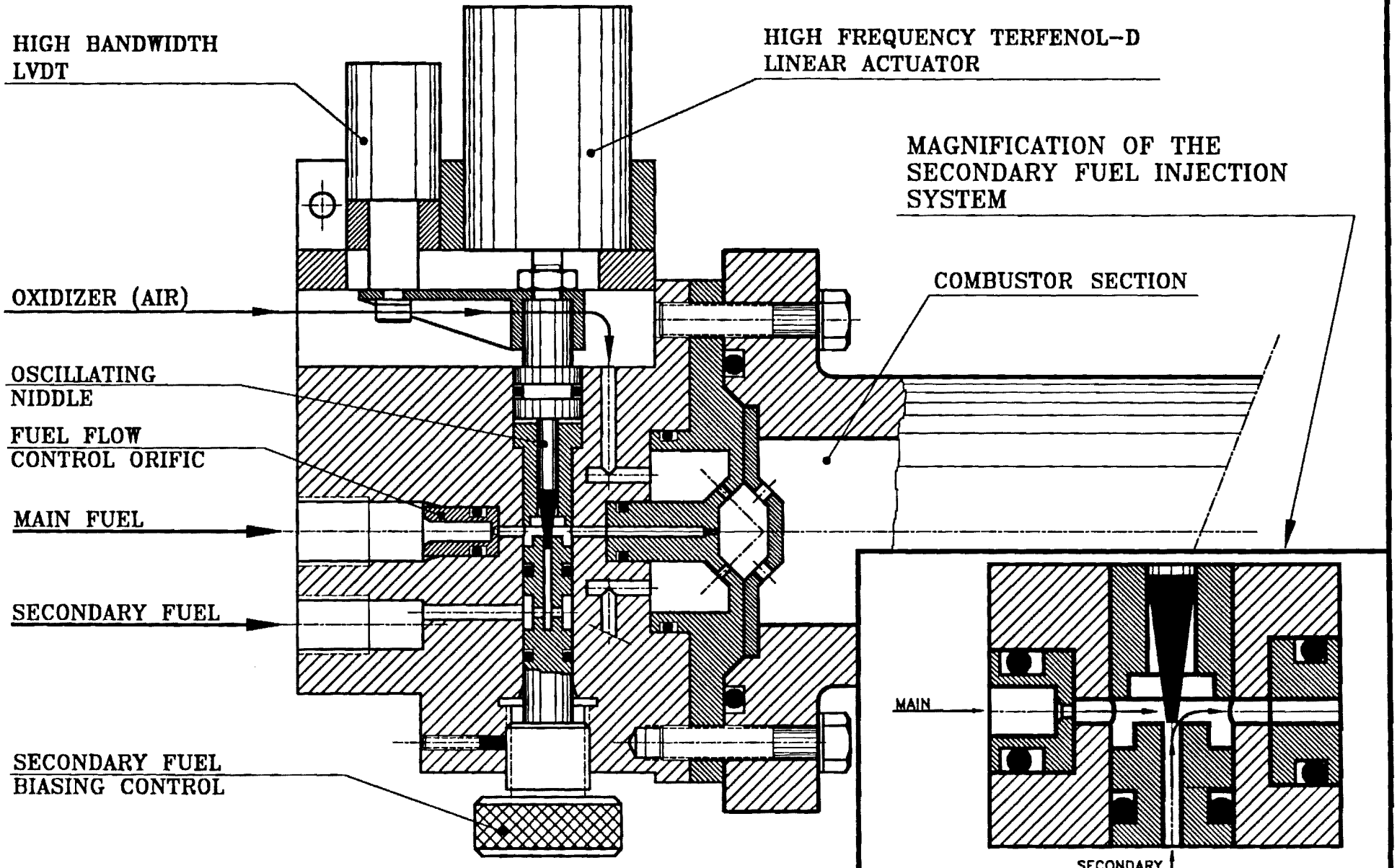

FIGURE 2. A SCHEMATIC OF THE DEVELOPED AIR AND FUEL FEED SYSTEM, INCLUDING A FUEL FLOW RATE MODULATION SYSTEM.

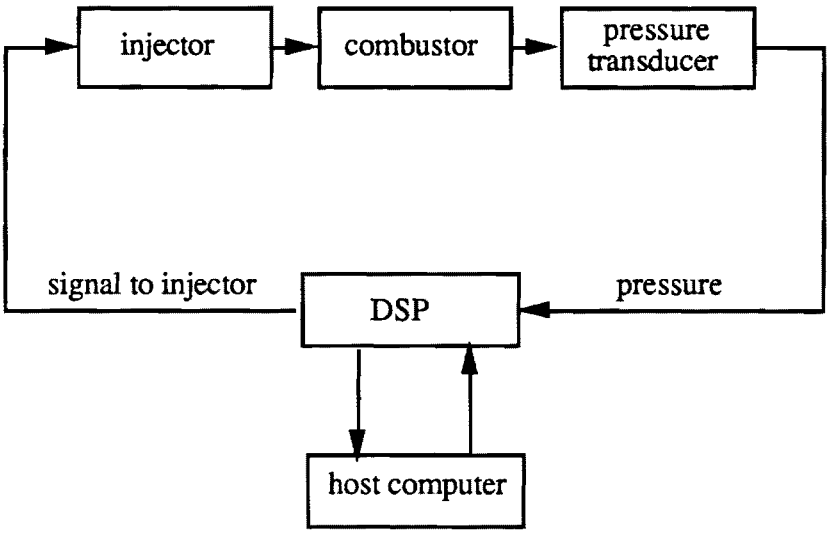

Figure 3: A Schematic of the active control system

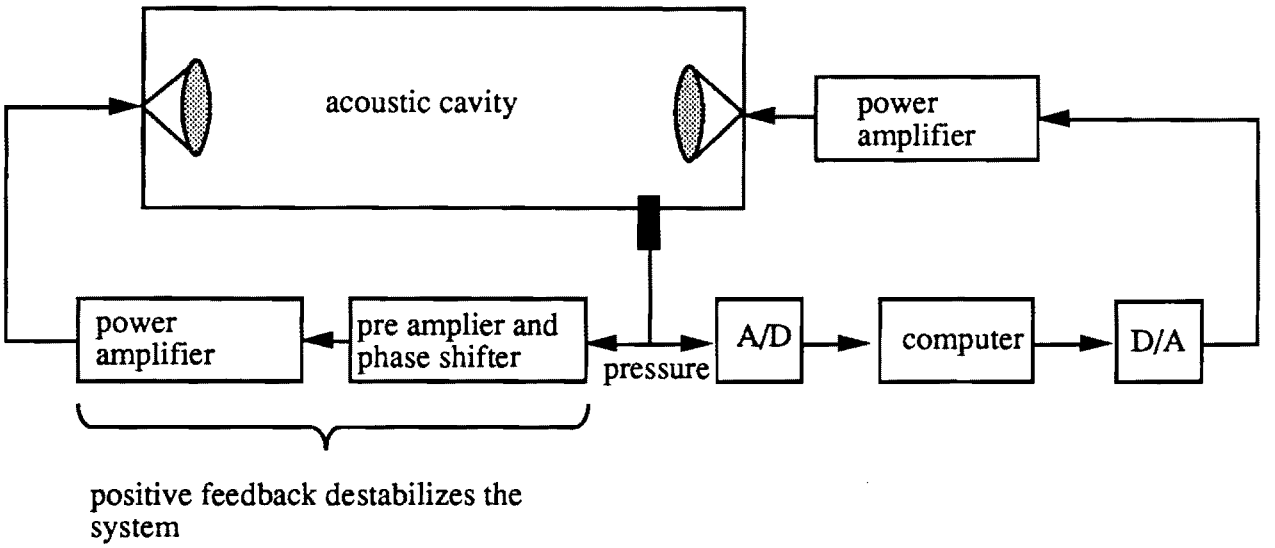

Figure 4: Experimental setup used to investigate the performance of the developed control system.

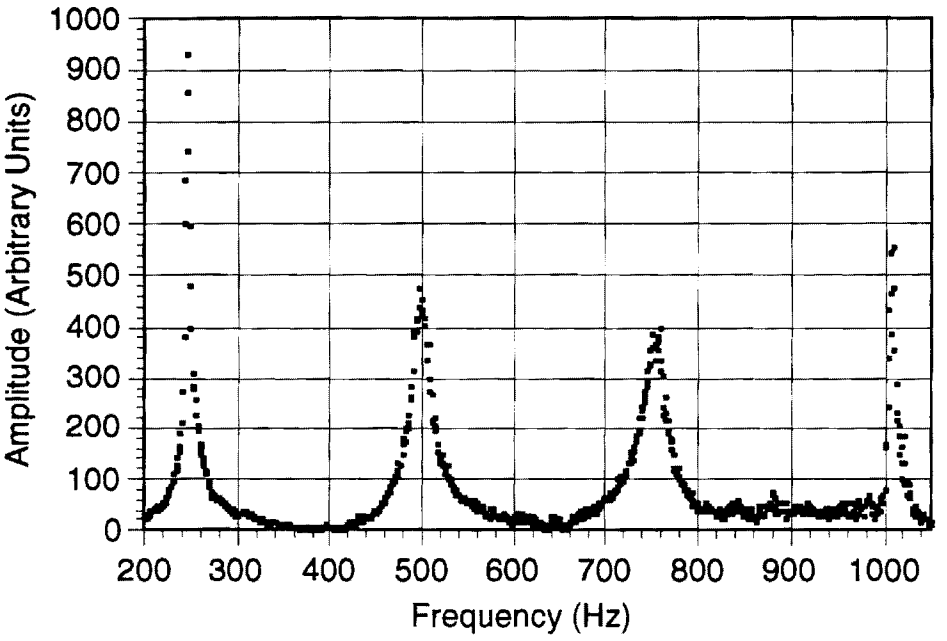

Figure 5.a: Observed pressure amplitude as function of the excitation frequency

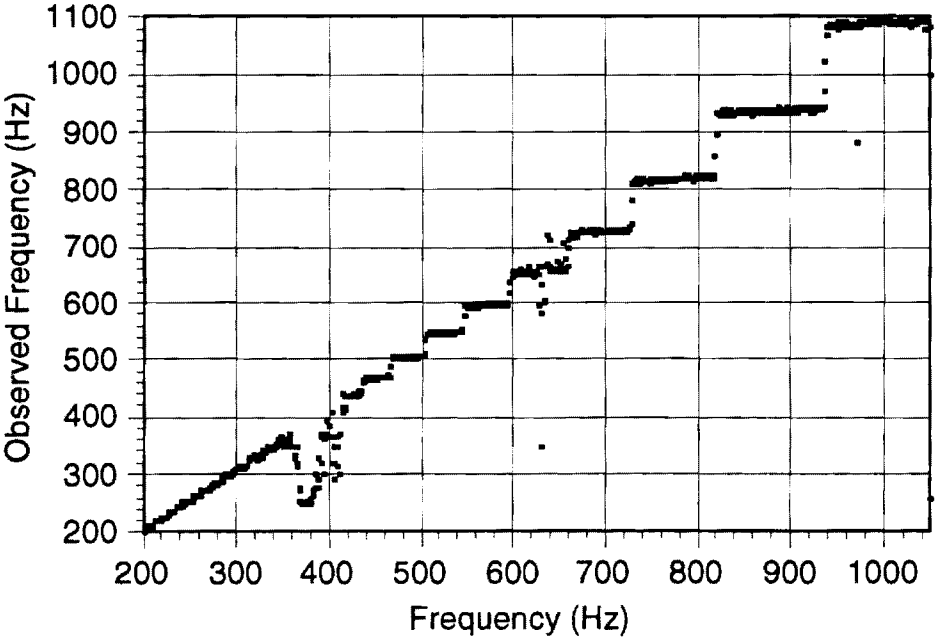

Figure 5b: Observed Vs. real frequency

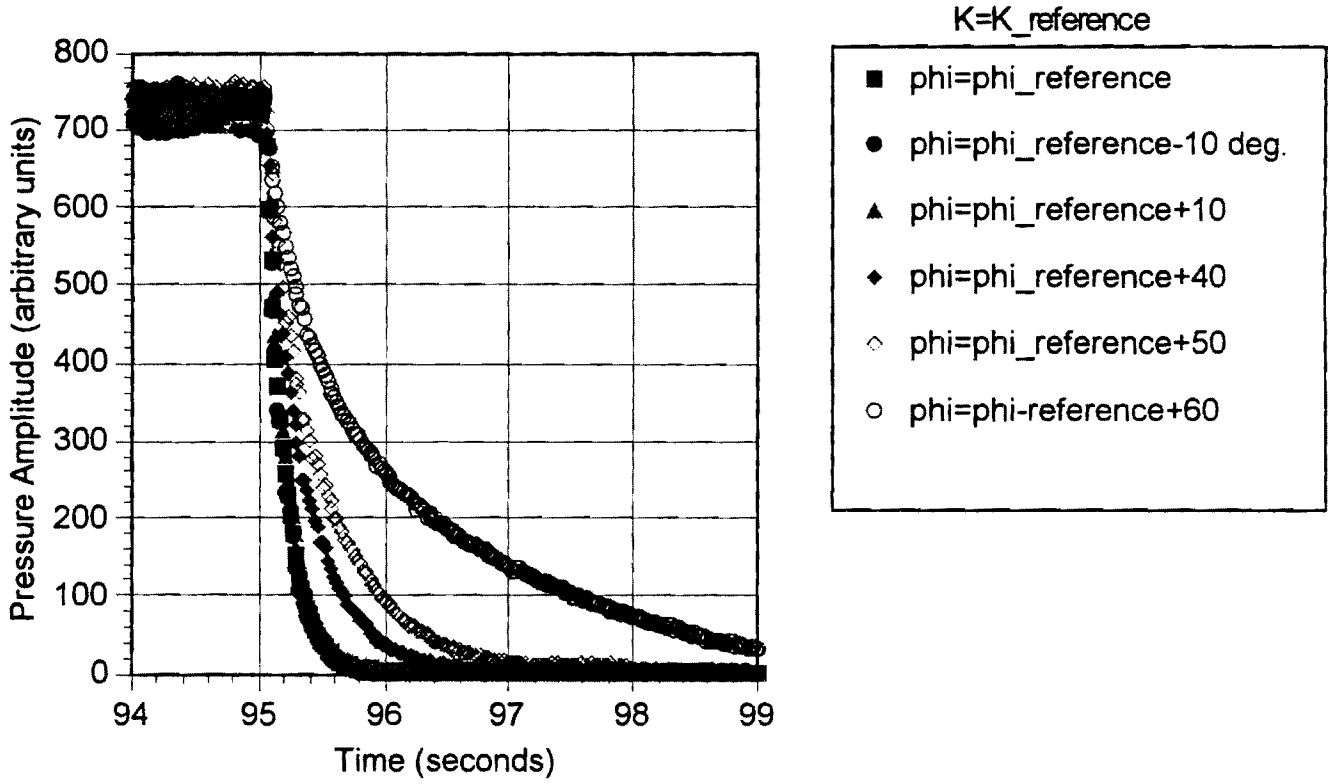

Figure 6.a: Dependance of damping of unstable acoustic oscillations upon the controller phase (active suppression applied at T=95 s)

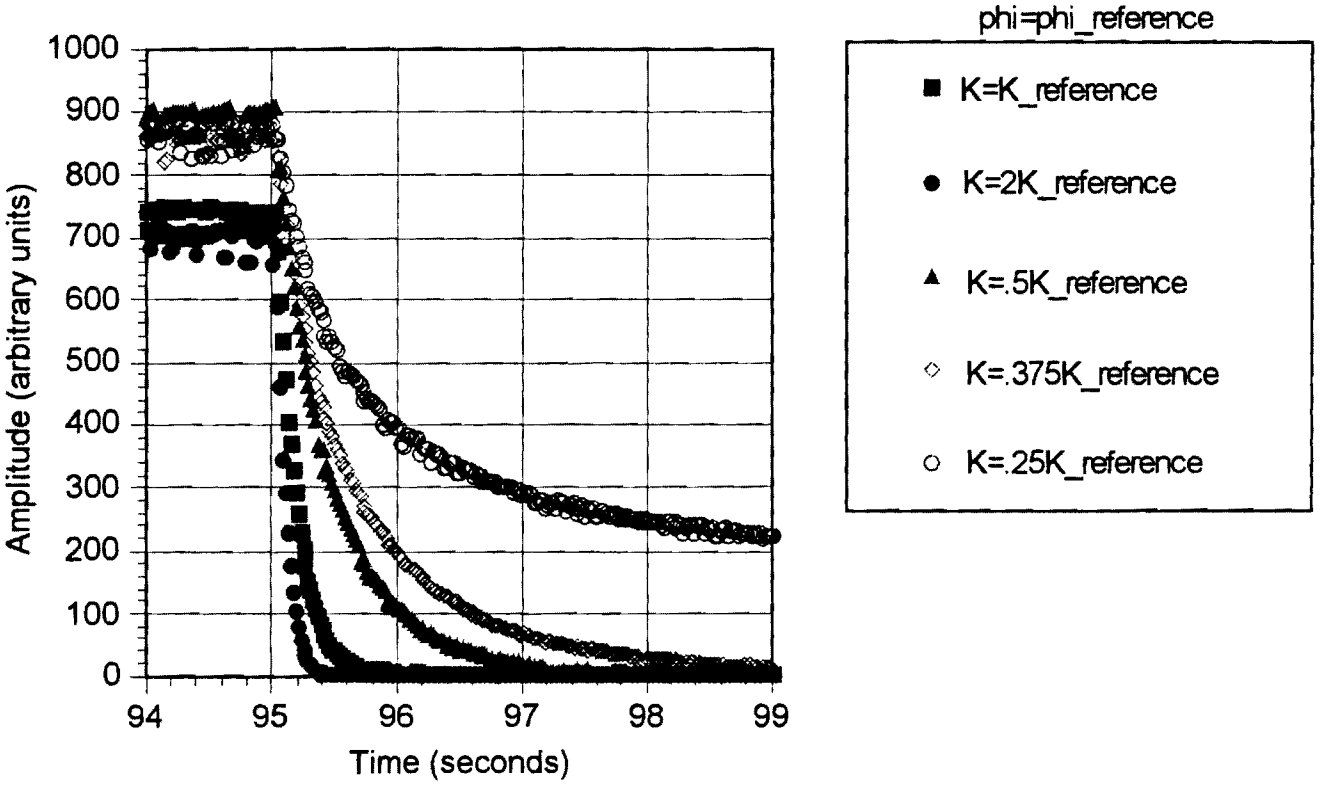

Figure 6.b: Dependance of damping of unstable acoustic oscillations upon the controller gain (active suppression applied at T=95 s)

Appendix

Papers Prepared Under AFOSR Grant No. F49620-93-1-0177 During the Reporting Period

HIGH FREQUENCY NONLINEAR VIBRATIONAL CONTROL

by

Benjamin Shapiro

Undergraduate
Junior Year

Aerospace Engineering Department
Georgia Institute of Technology
Atlanta, Georgia

Presented to

The AIAA Southeastern Regional Student Conference
April 6-10, 1994
Huntsville, Alabama

This paper has been reviewed and approved for presentation by
Dr. Zinn, Faculty Member in Aerospace Engineering

HIGH FREQUENCY NONLINEAR VIBRATIONAL CONTROL

B. Shapiro*

Abstract

In this paper we will discuss the feasibility of high frequency nonlinear vibrational control. Such control has the advantage in that it does not require state measurement and processing capabilities that are required in conventional feedback control. Bellman, Bentsman, and Meerkov investigated nonlinear systems controlled by linear vibrational controllers and proved that vibrational control is not feasible if the Jacobian has a positive trace. Previous work is extended in this paper and it is shown that a nonlinear vibrational controller can stabilize a system even if the Jacobian has a positive trace.

Nomenclature

$(\,)^{(i)}$	i'th time derivative
A_i	i'th order polynomial coefficient
$\mathcal{A}_n$	$1 - A_{n-2}/w^2 + \ldots$
$\mathcal{A}_{n-1}$	$A_{n-1} - A_{n-3}/w^2 + \ldots$
$\vec{f}(\vec{x})$	non-linear state function
$G(\bar{x})$	polynomial modulation function
$\vec{\mathcal{G}}(\vec{x})$	vector modulation function
$h(t)$	periodic, high frequency oscillation
$\mathcal{P}(\bar{x}_s),\mathcal{Q}(\bar{x}_s)$	averaged core terms (Eq. 3.32)
$\vec{\psi}$	$(0,\ldots,0,\psi)$; equilibrium shift (Eq. 4.5)
R^2	$\mathcal{A}_n^2 + \mathcal{A}_{n-1}^2/w^2$
T, w	period, frequency of $h(t)$
$\vec{x}$	state vector variable
x	state scalar variable
x'	shifted equilibrium point variable
x_s	slow mode variable
x_f	fast mode variable
$\bar{x}$	$(x^{(n-1)},\ldots,x)$
$\tilde{x}$	$(x^{(n-1)},\ldots,x')$
z_i	$1/T\int_{t-T}^{t} x_f^{(i)}\sin(w\tau)d\tau$
x_i'	$x_f^{(i)}\sin(wt) - z_i$

*Undergraduate Student, School of Aerospace Engineering, Georgia Institute of Technology, Atlanta, GA 30332. This research was supported by the David S. Lewis Undergraduate Scholarship

1 Introduction

This paper is concerned with the development of effective control for an engineering system, such as an aircraft, rocket or jet engine. In most engineering applications, such a system operates at some equilibrium point; for an aircraft the equilibrium is a trim condition, in the case of the jet engine it is a certain thrust.

It is imperative that this equilibrium point be stable. An equilibrium point is defined to be stable if upon perturbation of the system from equilibrium, the system returns to its equilibrium state. If the equilibrium point is unstable, then a small disturbance will cause the system to depart from that point. Thus, an aircraft operating at an unstable equilibrium point will depart from its trim value and stabilize at a new equilibrium point or it may settle into oscillatory motion known as a limit cycle. Neither option is desirable because an engineering system must remain at the appropriate equilibrium point.

Unstable equilibrium points occur in a wide range of applications, from unsteady combustion in liquid rockets to flutter instabilities in airfoils at high speeds. Generally, a control system is used to alter the stability of such unstable equilibrium points.

There are two distinct principles of applying control; namely, closed and open loop control. In the case of a closed loop control: the system is observed by a sensor; the sensors output is processed by a data processing plant that calculates the necessary correction; and this correction is applied by an actuator to the system (see diagram below).

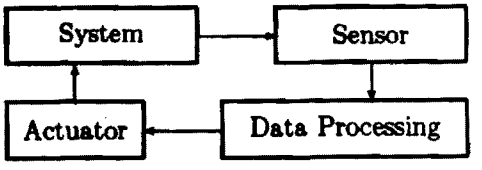

A closed loop is formed by the system, sensor, plant and actuator. Open loop control does not make use of sensors and processing plants. Instead, there is only an actuator. As a result, in an open loop control there is no

feedback loop and the actuator is unaware of the state of the system. Hence, the applied control is independent of the state.

There are obvious advantages to open loop control as opposed to closed loop. It may be applied in cases where closed loop control is impractical. Furthermore, application of open loop control is simpler and is cheaper because it does not require costly sensing and computing capabilities. Clearly, there are also disadvantages; since the actuator is functioning without any knowledge of the state of the system, open loop control is not always feasible. This paper discusses the feasibility of applying open loop control in the form of high frequency vibrational control.

Vibrational control is applied by oscillating an accessible system parameter at high frequency and low amplitude. For example, an inverted pendulum can be stabilized by vertically oscillating the pin of the pendulum at a sufficiently high frequency and low amplitude. This raises the question: under what other circumstances is high frequency vibrational control feasible ?

Vibrational control has found various applications, including lasers [1] and particle beams [2]. Initial work on developing a general theory of vibrational control was carried out by Meerkov [3]. Meerkov presented the principle of vibrational control. He discussed the effect of vibrational control upon stability, transient motion and response of the controlled system to external disturbances. In subsequent publications, several specific nonlinear situations were discussed [4], but no general vibrational control was proposed. Such a theory was outlined in 1986 by Bellman, Bentsman and Meerkov [5] who presented criteria for the control of nonlinear systems by linear vibrational control. In this paper, vibrational control theory is extended to account for the effects of a nonlinear vibrational controller.

2 Theoretical Considerations

Consider a general system of order n described by

$$\dot{\vec{y}} = \vec{f}(\vec{y}) \tag{2.1}$$

where $\vec{y}$ is a state vector of length n. Since we are concerned with the stability of some equilibrium point $\vec{y^*}$, we shift this point to the origin by a change of variables $\vec{x} = \vec{y} - \vec{y^*}$. Thus, Eq. (2.1) becomes

$$\dot{\vec{x}} = \vec{f}(\vec{x}) \tag{2.2}$$

Since we are concerned with small perturbations from equilibrium, only local behaviour around $\vec{x} = 0$ is considered. Suppose the equilibrium point $\vec{x} = 0$ is unstable and we wish to stabilize the system by use of vibratio control. Vibrational control is applied by oscillatin system parameter at high frequency and low amplitu For instance, in the case of a jet engine, the throttle, intake or amount of fuel injected might be vibrated. I $h(t)$ denote the applied high frequency, zero mean, os latory function, and assume that $h(t)$ affects the syst through some modulating function $\vec{G}(\vec{x})$. Furthermo it is assumed that both $\vec{f}(\vec{x})$ and $\vec{G}(\vec{x})$ are continuou differentiable. Thus, we write

$$\dot{\vec{x}} = \vec{f}(\vec{x}) + \vec{G}(\vec{x}) \cdot h(t) \tag{2}$$

where the form of $\vec{G}(\vec{x})$ depends on the state $\vec{x}$ and $h($

Obviously, an oscillating fuel injection rate is not ing to affect the jet engine in the same fashion as oscillating air intake flow rate. Since, for a given $h($ the form of $\vec{G}(\vec{x})$ depends on the system (which is fix and the parameter we vibrate, the only liberty we h is the choice of parameter to oscillate and the functi $h(t)$. This choice will determine the form of $\vec{G}(\vec{x})$. Ot then the choice of parameter and $h(t)$ we have no cont of the form of $\vec{G}(\vec{x})$. This is the reason why vibratio control is not always feasible, in certain cases there ex no functions $\vec{G}(\vec{x})$ which will allow vibrational contr

In order to discuss the results derived in [5], consi Eq. (2.2), suppose the Jacobian matrix $\partial\vec{f}/\partial\vec{x}$ of (2 has a positive trace. A classical theorem in linear gebra states the trace of a matrix is equal to the s of the eigenvalues (see for example [6, p.251]). A consequence, if the trace is positive, then at least o of the eigenvalues must be positive and the equilibri point is unstable. This does not imply, however, tha the trace is negative the equilibrium point is stable. negative trace is a necessary but not sufficient conditi for stability.

Bellman, Bentsman and Meerkov [5] only consider linear vibrational control, which limited the analysis linear functions $\vec{G}(\vec{x})$ in Eq. (2.3). They proved t if the Jacobian $\partial\vec{f}/\partial\vec{x}$ has a positive trace and $\vec{G}(\vec{x})$ linear, then vibrational control is not feasible. In t paper we consider a more general case of vibratio control via a nonlinear, slowly varying, $\vec{G}(\vec{x})$. We sh that in this case, vibrational control is feasible even the trace of the Jacobian Matrix is positive. We a note that a wide variety of engineering systems exhi a positive trace. For instance, the stability of a liq rocket engine can be modeled by a second order d ferential equation that has a positive trace in cert performance regimes [7]. In this case, a positive tr is equivalent to a negative damping, which means t

flow disturbances amplify.

Assume that the functions $\vec{\mathcal{G}}(\vec{x})$ that describe the vibrational excitations resulting from oscillation of various accessible system parameters (see (2.3)) are known. The objective of the theory presented in this paper is to determine a stability criterion for $\vec{\mathcal{G}}(\vec{x})$. Consequently, if a certain $\vec{\mathcal{G}}(\vec{x})$ satisfies the derived stability criterion, then oscillation of the corresponding system parameter will result in vibrational control. Therefore, the above criterion lets us determine if vibrational control is feasible for any accessible system parameter in a given engineering system; (e.g. an unstable rocket motor).

3 General Derivation

Consider once again the forced nonlinear system

$$\dot{\vec{x}} = \vec{f}(\vec{x}) + \vec{\mathcal{G}}(\vec{x}) \cdot h(t) \tag{3.1}$$

where $\vec{x} = 0$ is an equilibrium point of (2.2), but is not necessarily an equilibrium point of the forced system (3.1). If this is the case and $\vec{x} = 0$ is not an equilibrium point of (3.1), then the applied forcing has shifted the equilibrium point. Such an equilibrium shift is undesirable. For instance, it is undesirable for an aircraft to depart from its trim value upon application of vibrational control. Furthermore, our analysis breaks down if this shift from equilibrium is large. Hence, we only consider small and zero equilibrium shifts and state that vibrational control is not feasible if it results in a large equilibrium shift.

To analyze (3.1), we begin by studying the properties of $h(t)$, which describes the high frequency, zero mean, excitation. By definition

$$\begin{aligned} &h(t) = h(t+T) \quad , T \ll 1 \\ &\tfrac{1}{T}\textstyle\int_t^{t+T} h(\tau)d\tau = 0 \end{aligned} \tag{3.2}$$

where T is the period of $h(t)$. When we attempt to vibrationally control a system, we vibrate an accessible parameter at low amplitude. If we were to apply high amplitude vibrations then we would excite high amplitude undesirable oscillations in the system. For convenience, the amplitude of $h(t)$ is taken to equal unity and the low amplitude of the applied vibration is reflected by $\vec{\mathcal{G}}(\vec{x})$. Consequently,

$$\max |h(t)| = 1 \tag{3.3}$$

Expanding $\vec{f}(\vec{x})$ in a Taylor series about the origin, we rewrite (3.1) as

$$\dot{\vec{x}} = \vec{\mathcal{G}}(\vec{x}) \cdot h(t) + \frac{\partial \vec{f}}{\partial \vec{x}}\vec{x} + \frac{1}{2}\frac{\partial^2 \vec{f}}{\partial \vec{x}^2}\vec{x}^2 + \dots \tag{3.4}$$

where $\vec{f}(0) = 0$ because $\vec{x} = 0$ is an equilibrium point of (2.2). Since we are only concerned with small perturbations from equilibrium, $\|\vec{x}\|$ is small and higher order terms in the above series may be neglected. The resulting equation yields an approximation of the system behaviour in a neighbourhood of the origin. It should be noted that $\vec{\mathcal{G}}(\vec{x})$ is not linearized because higher order Taylor terms in $\vec{\mathcal{G}}(\vec{x})$ may produce non-negligible effects through coupling with lower order terms. Hence Eq. (3.4) is simplified to the following form:

$$\dot{\vec{x}} = \frac{\partial \vec{f}}{\partial \vec{x}}\vec{x} + \vec{\mathcal{G}}(\vec{x}) \cdot h(t) \tag{3.5}$$

In expanded form, Eq. (3.5) can be written as

$$\begin{bmatrix} \dot{x}_1 \\ \dot{x}_2 \\ \cdot \\ \cdot \\ \dot{x}_n \end{bmatrix} = \begin{bmatrix} \frac{\partial f_1}{\partial x_1} & \frac{\partial f_1}{\partial x_2} & \cdot & \cdot & \frac{\partial f_1}{\partial x_n} \\ \frac{\partial f_2}{\partial x_1} & \cdot & & & \cdot \\ \cdot & & \cdot & & \cdot \\ \cdot & & & \cdot & \cdot \\ \frac{\partial f_n}{\partial x_1} & \cdot & \cdot & \cdot & \frac{\partial f_n}{\partial x_n} \end{bmatrix} \begin{bmatrix} x_1 \\ x_2 \\ \cdot \\ \cdot \\ x_n \end{bmatrix} + \begin{bmatrix} \mathcal{G}_1(\vec{x}) \\ \mathcal{G}_2(\vec{x}) \\ \cdot \\ \cdot \\ \mathcal{G}_n(\vec{x}) \end{bmatrix} h(t) \tag{3.6}$$

For the purpose of clarity in this discussion we let $h(t) = \sin(wt)$. We note, however, that this analysis can easily be extended to deal with more general periodic functions $h(t)$ such as square or triangular waves. It can be shown that our result will only differ by a constant in such cases.

It is possible to rewrite Eq. (3.6) as an equivalent polynomial whose solution is equivalent to the solution of the matrix equation. The characteristic polynomial of a matrix $\mathcal{M}$ is given by $\det(xI - \mathcal{M})$ where the eigenvalues of $\mathcal{M}$ are the roots of $\det(xI - \mathcal{M}) = 0$. Therefore, we rewrite Eq. (3.6) as its characteristic polynomial

$$\begin{aligned} &x^{(n)} + A_{n-1}x^{(n-1)} + \dots + A_0 x \\ &\quad = G(x^{(n-1)}, \dots, x) \cdot \sin(wt) \end{aligned} \tag{3.7}$$

where x is a linear combination of $x_1, \dots x_n$; $x^{(k)}$ denotes the k'th time derivative of x and G is equivalent to $\vec{\mathcal{G}}$. Note that $-A_{n-1}$ is equal to the sum of the eigenvalues of the Jacobian, which equals the trace of the Jacobian Matrix [9, p.113] & [6, p.251]. This implies that the positive Jacobian trace referred to in [5] equals $-A_{n-1}$.

Since the frequency w of the applied forcing $\sin(wt)$ is high, we assume that the solution $x(t)$ of (3.1) will consist of two modes. A slowly varying mode $x_s(t)$,

which describes the system response to the average of the applied forcing, and a fast mode $x_f(t)$ that describes the system's response to the high frequency component of the forcing function in Eq. (3.7). Therefore, the solution is expressed in the form

$$x(t) = x_s(t) + x_f(t) \tag{3.8}$$

where $x_s(t)$ is the average of $x(t)$ and is defined as

$$x_s(t) = \frac{1}{T}\int_{t-T}^{t} x(\tau)d\tau \tag{3.9}$$

Notice that the average of $x^{(i)}$ is equal to $x_s^{(i)}$ for all i because $x(t)$ is continuous and we can move the differential inside the integral for small T. In view of (3.9), averaging Eq. (3.7) yields the equation

$$\begin{aligned} &x_s^{(n)} + A_{n-1}x_s^{(n-1)} + \ldots + A_0 x_s = \\ &\tfrac{1}{T}\textstyle\int_{t-T}^{t} G(x^{(n-1)}, \ldots, x)\,\sin(w\tau)\,d\tau \end{aligned} \tag{3.10}$$

Eq. (3.10) describes the fundamental assumption of averaging theory; namely, the assumption that the slow mode x_s reacts to the average of the forcing.

By assumption (3.8) we see that Eq. (3.7) minus Eq. (3.10) yields the following equation for x_f

$$\begin{aligned} &x_f^{(n)} + A_{n-1}x_f^{(n-1)} + \ldots + A_0 x_f = \\ &G(\bar{x})\sin(wt) - \tfrac{1}{T}\textstyle\int_{t-T}^{t} G(\bar{x})\,\sin(w\tau)\,d\tau \end{aligned} \tag{3.11}$$

where $\bar{x}$ denotes $(x^{(n-1)}, \ldots, x)$.

Since $\bar{x}_f$ is considered to be a perturbation variable with respect to the average variable $\bar{x}_s$, we expand G in a Taylor series at $\bar{x}_s$. By assumption, the amplitude of the forced vibration is small. Accordingly, the amplitude of the resulting fast solution $\bar{x}_f$ is also small. Consequently, we may neglect higher order terms in $\bar{x}_f$. Thus, Eq. (3.11) becomes

$$\begin{aligned} &x_f^{(n)} + A_{n-1}x_f^{(n-1)} + \ldots + A_0 x_f = \\ &\quad G(\bar{x}_s)\sin(wt) + \tfrac{\partial G}{\partial x}\big|_{\bar{x}_s} x_f \sin(wt) \\ &\quad + \ldots + \tfrac{\partial G}{\partial x^{(n-1)}}\big|_{\bar{x}_s} x_f^{(n-1)} \sin(wt) - \\ &\tfrac{1}{T}\textstyle\int_{t-T}^{t}\left[G(\bar{x}_s)\sin(w\tau) + \tfrac{\partial G}{\partial x}\big|_{\bar{x}_s} x_f \sin(w\tau)\right. \\ &\quad \left. + \ldots + \tfrac{\partial G}{\partial x^{(n-1)}}\big|_{\bar{x}_s} x_f^{(n-1)} \sin(w\tau)\right] d\tau \end{aligned} \tag{3.12}$$

Recall that x_s is slowly varying relative to x_f, it can be assumed constant during one cycle of x_f. As a result, the terms $G(\bar{x}_s), \partial G/\partial x_s, \ldots, \partial G/\partial x_s^{(n-1)}$ in Eq. (3.12) can be treated as constants, and the average $G(\bar{x}_s)\sin(wt)$ is zero. Using the notation

$$\begin{aligned} z_i(t) &= \tfrac{1}{T}\textstyle\int_{t-T}^{t} x_f^{(i)}(\tau)\,\sin(w\tau)\,d\tau \\ z_i'(t) &= x_f^{(i)}\sin(wt) - z_i(t) \end{aligned} \tag{3.}$$

yields

$$\begin{aligned} &x_f^{(n)} + \ldots + A_0 x_f = G(\bar{x}_s)\sin(wt) \\ &+\tfrac{\partial G}{\partial x}\big|_{\bar{x}_s} z' + \ldots + \tfrac{\partial G}{\partial x^{(n-1)}}\big|_{\bar{x}_s} z_{n-1}' \end{aligned} \tag{3.}$$

An order of magnitude analysis is now used to furt simplify Eq. (3.14). In this analysis we only consi slowly varying functions $G(\bar{x}_s)$ as defined below

$$\begin{aligned} |\tfrac{\partial G}{\partial x^{(n-1)}}| &\ll w \\ |\tfrac{\partial G}{\partial x^{(n-2)}}| &\ll w^2 \\ |\tfrac{\partial G}{\partial x^{(n-3)}}| &\ll w^3 \\ \ldots &\quad \ldots \\ \ldots &\quad \ldots \\ |\tfrac{\partial G}{\partial x}| &\ll w^n \end{aligned} \tag{3.}$$

Notice that (3.15) is a mild restriction since w is lar

Consider the order of magnitude of the z_i' terms wh appear in Eq. (3.14). In order to determine the or of magnitude of these z_i' terms, we first consider the terms. Equation (3.13) yields a bound on z_i,

$$|z_i| = \left|1/T\int_{t-T}^{t} x_f^{(i)}(\tau)\,\sin(w\tau)\,d\tau\,\right| \le |x_f^{(i)}| \tag{3.1}$$

Then, using the triangle inequality yields

$$|z_i'| = |x_f^{(i)}\sin(wt) - z_i| \le |x_f^{(i)}| + |z_i| \tag{3.1}$$

Since x_f is periodic in w, it follows that

$$|x_f^{(k+1)}| \approx w|x_f^{(k)}| \tag{3.1}$$

because x_f can be represented as a fourier series th is periodic in w. Consequently, each differentiation i creases the magnitude by a factor of w. As an e ample, consider the time derivative of $\sin(wt)$ which $w\cos(wt)$. Consequently, using Eq.'s (3.16) and (3.1 it follows that

$$|z_i'| \le 2|x_f^{(i)}| \approx 2w^i|x_f| \tag{3.1}$$

and Eq.'s (3.19) and (3.15) yield

$$\begin{array}{ll} \left|\frac{\partial G}{\partial x^{(n-1)}} z'_{n-1}\right| & \ll w^n |x_f| \\ \left|\frac{\partial G}{\partial x^{(n-2)}} z'_{n-2}\right| & \ll w^n |x_f| \\ \left|\frac{\partial G}{\partial x^{(n-3)}} z'_{n-3}\right| & \ll w^n |x_f| \\ \vdots & \vdots \\ \left|\frac{\partial G}{\partial x} z'\right| & \ll w^n |x_f| \end{array} \tag{3.20}$$

In view of Eq. (3.18), it follows that the order of magnitude of the terms in the left side of Eq. (3.14) is given by $w^n|x_f|$. Since the magnitude of the z' terms in Eq. (3.14) is considerably less than $w^n|x_f|$, we assume the z' terms may be neglected. Therefore, Eq. (3.14) becomes

$$x_f^{(n)} + A_{n-1}x_f^{(n-1)} + \ldots + A_0 x_f = G(\bar{x}_s)\sin(wt) \tag{3.21}$$

where $G(\bar{x}_s)$ is constant during one cycle of x_f because $\bar{x}_s$ is a slowly varying quantity. Consequently, Eq. (3.21) can be easily solved by substitution. Letting

$$x_f^{(n)} = \alpha\sin(wt) + \beta\cos(wt) \tag{3.22}$$

then

$$\begin{array}{ll} x_f^{(n-1)} = -(\alpha/w)\cos(wt) + (\beta/w)\sin(wt) \\ x_f^{(n-2)} = -(\alpha/w^2)\sin(wt) - (\beta/w^2)\cos(wt) \\ \vdots \qquad\qquad\qquad\qquad \vdots \end{array} \tag{3.23}$$

Substituting Eq. (3.23) into Eq. (3.21) and collecting the coefficients of the cos and sin terms yields the following linear equations for α and β

$$\begin{array}{ll} \sin(wt): & \alpha + A_{n-1}\beta/w - A_{n-2}\alpha/w^2 + \ldots = G \\ \cos(wt): & \beta - A_{n-1}\alpha/w - A_{n-2}\beta/w^2 + \ldots = 0 \end{array} \tag{3.24}$$

Introducing the definitions

$$\begin{array}{l} \mathcal{A}_n = 1 - A_{n-2}/w^2 + \ldots \\ \mathcal{A}_{n-1} = A_{n-1} - A_{n-3}/w^2 + \ldots \end{array} \tag{3.25}$$

into Eq. (3.24) it follows that

$$\begin{array}{l} \alpha = \frac{GA_n}{(\mathcal{A}_n^2 + \mathcal{A}_{n-1}^2/w^2)} \\ \beta = \frac{GA_{n-1}}{w(\mathcal{A}_n^2 + \mathcal{A}_{n-1}^2/w^2)} \end{array} \tag{3.26}$$

In most cases, w is much larger then A_i (for any i) implying that only the first terms in Eq. (3.25) are significant. Consequently, $\mathcal{A}_n \approx 1$ and $\mathcal{A}_{n-1} \approx A_{n-1}$. By the same argument, $\mathcal{A}_{n-1}^2/w^2 \ll \mathcal{A}_n^2$ indicating that $\alpha \approx G$ and $\beta \approx GA_{n-1}/w$. To simplify the notation, let

$$R^2 = \mathcal{A}_n^2 + \mathcal{A}_{n-1}^2/w^2 \tag{3.27}$$

and note that $R \approx 1$ based upon the arguments above. Even though it is not necessary to assume the above approximations apply throughout the remainder of the analysis, it is useful to keep them in mind because they provide a qualitative appreciation of the formulas that follow.

Substituting Eq. (3.26) and (3.27) into Eq. (3.22) and integrating yields the following expressions for the derivatives $x_f^{(i)}(t)$

$$\begin{array}{ll} x_f^{(n)} & = +\frac{GA_n}{R^2}\sin(wt) + \frac{GA_{n-1}}{wR^2}\cos(wt) \\ x_f^{(n-1)} & = -\frac{GA_n}{wR^2}\cos(wt) + \frac{GA_{n-1}}{w^2R^2}\sin(wt) \\ x_f^{(n-2)} & = -\frac{GA_n}{w^2R^2}\sin(wt) - \frac{GA_{n-1}}{w^3R^2}\cos(wt) \\ \vdots & \vdots \qquad\qquad \vdots \end{array} \tag{3.28}$$

which allows us to compute the right hand side of Eq. (3.10). Expanding G as a Taylor series at $\bar{x}_s$, Eq. (3.10) becomes:

$$\begin{array}{c} x_s^{(n)} + A_{n-1}x_s^{(n-1)} + \ldots + A_0 x_s = \\ \frac{1}{T}\int_{t-T}^{t}\left[G(\bar{x}_s)\sin(w\tau) + \frac{\partial G}{\partial x_s}x_f\sin(w\tau)\right. \\ \left. + \ldots + \frac{\partial G}{\partial x_s^{(n-1)}}x_f^{(n-1)}\sin(w\tau)\right]d\tau \end{array} \tag{3.29}$$

It should be noted that the non-linearities of G are not neglected in Eq. (3.29) since the terms $G(\bar{x}_s), \partial G/\partial x_s, \ldots, \partial G/\partial x_s^{(n-1)}$ are not necessarily linear in $\bar{x}_s$. Substituting Eq. (3.28) into Eq. (3.29) yields

$$\begin{array}{c} x_s^{(n)} + A_{n-1}x_s^{(n-1)} + \ldots + A_0 x_s = \frac{1}{T}\int_{t-T}^{t}\left\{G(\bar{x}_s)\right. \\ + \ldots + \left[-\frac{GA_n}{w^2R^2}\sin(w\tau) - \frac{GA_{n-1}}{w^3R^2}\cos(w\tau)\right]\frac{\partial G}{\partial x_s^{(n-2)}} + \\ \left.\left[-\frac{GA_n}{wR^2}\cos(w\tau) + \frac{GA_{n-1}}{w^2R^2}\sin(w\tau)\right]\frac{\partial G}{\partial x_s^{(n-1)}}\right\}\sin(w\tau)\,d\tau \end{array} \tag{3.30}$$

Evaluating the integral, in Eq. (3.30), and recalling that the average of $\sin^2(wt)$ is a half while the average of $\sin(wt)$ and $\sin(wt)\cos(wt)$ is zero, yields the following equation for the slow mode $x_s(t)$:

$$\begin{array}{c} x_s^{(n)} + A_{n-1}x_s^{(n-1)} + \ldots + A_0 x_s = \left\{\frac{A_{n-1}}{2w^2R^2}G\frac{\partial G}{\partial x_s^{(n-1)}}\right. \\ \left. -\frac{A_n}{2w^2R^2}G\frac{\partial G}{\partial x_s^{(n-2)}} - \frac{A_{n-1}}{2w^4R^2}G\frac{\partial G}{\partial x_s^{(n-3)}} + \ldots\right\} \end{array} \tag{3.31}$$

Equation (3.31) is the averaged equation for the slow dynamics $x_s(t)$ of the forced system (3.1). It is a nonlinear, autonomous (no explicit time dependence), ordinary differential equation. Equation (3.31) is valid in

a small neighbourhood of the point $\vec{x} = 0$ of the forced system (3.1).

Introducing the definitions

$$\mathcal{P}(\bar{x}_s) = \frac{A_{n-1}}{2w^2R^2}G\frac{\partial G}{\partial x_s^{(n-1)}} - \frac{A_{n-1}}{2w^4R^2}G\frac{\partial G}{\partial x_s^{(n-3)}} + \dots$$
$$\mathcal{Q}(\bar{x}_s) = -\frac{A_n}{2w^2R^2}G\frac{\partial G}{\partial x_s^{(n-2)}} + \frac{A_n}{2w^4R^2}G\frac{\partial G}{\partial x_s^{(n-4)}} + \dots \tag{3.32}$$

where we label $\mathcal{P}$ and $\mathcal{Q}$ as the core terms, Eq. (3.31) can be rewritten in the following form

$$x_s^{(n)} + A_{n-1}x_s^{(n-1)} + \dots + A_0x_s = \mathcal{P}(\bar{x}_s) + \mathcal{Q}(\bar{x}_s) \tag{3.33}$$

Next, rewriting Eq. (3.33) in a Taylor series about the origin yields

$$x_s^{(n)} + A_{n-1}x_s^{(n-1)} + \dots + A_0x_s = \mathcal{P}(0) + \mathcal{Q}(0)$$
$$+\frac{\partial \mathcal{P}}{\partial x_s}\bar{x}_s + \frac{\partial \mathcal{Q}}{\partial x_s}\bar{x}_s + \frac{1}{2}\frac{\partial^2 \mathcal{P}}{\partial x_s^2}\bar{x}_s^2 + \frac{1}{2}\frac{\partial^2 \mathcal{Q}}{\partial x_s^2}\bar{x}_s^2 + \dots \tag{3.34}$$

In the above equation, the partials derivatives of $\mathcal{P}$ and $\mathcal{Q}$ are evaluated at the origin to yield constant values. Since we are concerned with local behaviour around $\bar{x}_s = 0$, $\|\bar{x}_s\|$ is small and we may neglect higher order Taylor terms in Eq. (3.34), yielding

$$x_s^{(n)} + (A_{n-1} - \frac{\partial \mathcal{P}}{\partial x_s^{(n-1)}} - \frac{\partial \mathcal{Q}}{\partial x_s^{(n-1)}})x_s^{(n-1)} +$$
$$\dots + (A_0 - \frac{\partial \mathcal{P}}{\partial x_s} - \frac{\partial \mathcal{Q}}{\partial x_s})x_s = \mathcal{P}(0) + \mathcal{Q}(0) \tag{3.35}$$

where we have neglected higher order partials derivatives. Equation (3.35) is a linear differential equation in x_s, which is applicable in a small neighbourhood of the point $\vec{x} = 0$ of the forced system (3.1). Equation (3.35) will allow us to determine whether $\vec{x} = 0$ is still an equilibrium point of (3.1), and if so, the stability of this point. Such a stability analysis is performed in the next section.

Before we begin the stability analysis, we briefly summarize the results of this section. We start with the forced system (3.1). By linearizing $\vec{f}$, but not $\vec{g}$, we derive the polynomial expression (3.7) which is valid in a small neighbourhood of $\vec{x} = 0$. Assuming that the trajectory $x(t)$ is composed of two modes $x_f(t)$ and $x_s(t)$, we obtain an averaged expression (3.10) for the slow mode $x_s(t)$. We restrict ourselves to considering slowly varying functions G as outlined in (3.15). Using assumption (3.8) and Eq. (3.10) we derive Eq. (3.14) for the fast mode $x_f(t)$. An order of magnitude analysis lets us solve Eq. (3.14) to derive the expression (3.28) for the fast mode. Substituting (3.28) into (3.10) yields tl nonlinear, autonomous, averaged equation (3.31) for tl slow mode $x_s(t)$. Linearizing Eq. (3.31) and substitu ing expression (3.32) we derive the final, linear equatic (3.35) for the slow mode $x_s(t)$. It is important to no that Eq. (3.35) only holds in a small neighbourhood the origin. Furthermore, Eq. (3.35) does not discou non-linearities in G because the core terms appearii in Eq. (3.35) are nonlinear functions of G. Eq. (3.3 allows us to perform the stability analysis which follow

4 Stability Analysis

4.1 Equilibrium Shift

When discussing stability, we refer to the stability a given equilibrium point. In this analysis we are co cerned with the equilibrium point $\vec{x} = 0$ of Eq. (2.2 Hence, we must first determine whether $\vec{x} = 0$ is equilibrium point of the forced system (3.1).

Since $x_f(t)$ has a zero average, then any equilibriu shift due to the applied forcing will be reflected by $x_s(t$ Consider Eq. (3.35), it is evident that if $\bar{x}_s = 0$ is remain an equilibrium point, then

$$\mathcal{Q}(0) + \mathcal{P}(0) = 0 \tag{4.}$$

must hold. We define (4.1) to be the zero conditio If the zero condition is not satisfied, then $\bar{x} = 0$ is longer an equilibrium point of Eq. (3.35), which impli $\vec{x} = 0$ is not an equilibrium point of the forced syste (3.1). We can determine the resulting equilibrium sh from Eq. (3.35). Defining

$$x_s' = x_s - \frac{\mathcal{P}(0) + \mathcal{Q}(0)}{(A_0 - \frac{\partial \mathcal{P}}{\partial x_s} - \frac{\partial \mathcal{Q}}{\partial x_s})} \tag{4.}$$

it follows that $x_s'^{(i)} = x_s^{(i)}, [i > 0]$ since x_s' and x diff by a constant. In view of this we let

$$\tilde{x}_s = (x_s^{(n-1)}, \dots, x_s^{(1)}, x_s') \tag{4.}$$

Rewriting Eq. (3.35) in terms of the new variable yields

$$x_s^{(n)} + (A_{n-1} - \frac{\partial \mathcal{P}}{\partial x_s^{(n-1)}} - \frac{\partial \mathcal{Q}}{\partial x_s^{(n-1)}})x_s^{(n-1)}$$
$$+ \dots + (A_0 - \frac{\partial \mathcal{P}}{\partial x_s} - \frac{\partial \mathcal{Q}}{\partial x_s})x_s' = 0 \tag{4.}$$

and we see that $\bar{x}_s = 0$ is an equilibrium point of E (3.35) and the equilibrium shift is given by

$$\psi = -\frac{\mathcal{P}(0) + \mathcal{Q}(0)}{(A_0 - \frac{\delta \mathcal{P}}{\delta x_s} - \frac{\delta \mathcal{Q}}{\delta x_s})} \tag{4.5}$$

Letting $\vec{\psi} = (0, \ldots, 0, \psi)$, it follows that if the equilibrium shift ψ is large, our analysis breaks down since Eq. (3.35) is only valid in a small neighbourhood of the origin. Furthermore, we note that a large equilibrium shift is undesirable in engineering applications. We wish to vibrationally control an existing equilibrium point, not create a new one. Accordingly, we only consider very small equilibrium shifts, since vibrational control is not feasible when the equilibrium shift is large.

In view of Eq. (4.5), $\tilde{x}_s = 0$ is the shifted equilibrium point of Eq. (3.35). It is understood that if the zero condition is satisfied, then $\tilde{x}_s = \bar{x}_s$ and the equilibrium point is not shifted. Notice that the fast mode $\bar{x}_f$ remains unchanged, it is still a perturbation from the average. Consequently, define

$$\tilde{x} = \tilde{x}_s + \bar{x}_f \tag{4.6}$$

It follows that $\tilde{x} = 0$ is the new shifted equilibrium point of the forced system (3.1) and is given by $\tilde{x} = \bar{x} + \vec{\psi}$. Accordingly, we will now concern ourselves with the stability of the equilibrium point $\tilde{x} = 0$.

4.2 Stability Definition

In order to discuss stability, we must rigorously define the concept of stability. The following definition is the classical definition of stability, which can be found in almost any text on differential equations, e.g. [8, p.98].

Definition: Consider the system $\dot{\vec{x}} = \vec{F}(\vec{x}, t)$ with an equilibrium point $\vec{x} = 0$. This equilibrium point $\vec{x} = 0$ is **stable** if for any $\epsilon > 0$ there exists $\delta = \delta(\epsilon)$ such that the initial condition $\|\vec{x}(0)\| < \delta$ implies that the trajectory/solution $\|\vec{x}(t)\| < \epsilon$ for all t. Otherwise, the equilibrium point is **unstable**. The equilibrium point is **asymptotically stable** if it is **stable** and δ can be chosen such that $\|\vec{x}(0)\| < \delta$ implies the

$$\lim_{t \to \infty} \vec{x}(t) = 0$$

Hence, if an equilibrium point is **stable**, we can always find a δ for any given ϵ so that the trajectory never leaves the ϵ neighbourhood. Physically, a **stable** equilibrium point implies that a small perturbation of the initial conditions from equilibrium will result in a small perturbation of the final conditions from equilibrium. In the case of **asymptotic stability**[1], a small perturbation of the initial conditions will result in a zero change of final conditions. Hence, any trajectory that starts sufficiently close to the equilibrium point must decay in time. Consequently, **asymptotic stability** is desirable in most engineering applications because it implies that the system will remain at the equilibrium point.

We are concerned with the stability of the equilibrium point $\tilde{x} = 0$ of the forced system (3.1). Recall that $\tilde{x}$ is composed of two modes, the slow mode $\tilde{x}_s$ and the fast mode $\bar{x}_f$. Since the slow mode is dominant, we first concern ourselves with the stability of $\tilde{x}_s$.

4.3 Slow Asymptotic Stability

Definition: The equilibrium point $\tilde{x}$ of the forced system (3.1) is **slowly asymptotically stable** if the equilibrium point $\tilde{x}_s$ of Eq. (3.35) is **asymptotically stable.**

Hence **slowly asymptotically stable** implies that the slow mode $\tilde{x}_s(t)$ will decay to zero if we perturb the forced system (3.1) from equilibrium. Because the slow mode is dominant, a **slowly asymptotically stable** equilibrium point $\tilde{x} = 0$ of the forced system (3.1) is a definite improvement over an unstable equilibrium point $\vec{x} = 0$ of the unforced system (2.2).

For a linear equations such as (3.35) stability can be determined by the Routh Hurwitz criterion [9, p.113]. The Routh Hurwitz criterion is a necessary and sufficient criterion for stability. One writes a Routh Hurwitz array, this array consists of a schedule of the characteristic polynomial coefficients, and the number of sign changes in the array is equal to the number of unstable poles. If there are no sign changes and the array does not contain zero elements, the equilibrium point is **asymptotically stable** and the linear equation is said to satisfy the Routh Hurwitz criterion. Consequently, if Eq. (3.35) satisfies the Routh Hurwitz criterion then $\tilde{x}_s$ is an **asymptotically stable** equilibrium point and hence (by definition) the equilibrium point $\tilde{x} = 0$ of the forced system (3.1) is **slowly asymptotically stable.**

4.4 Asymptotic Stability

In this section we develop criteria for **asymptotic stability** of the equilibrium point $\tilde{x} = 0$ in the sense of Section (4.2). **Asymptotic stability** implies that the system will return to its equilibrium state upon small perturbations from equilibrium. If application of high

[1] In engineering literature, the concept of asymptotic stability is usually referred to simply as stable.

frequency forcing results in **asymptotic stability**, then we say that vibrational control has been achieved.

Theorem: The equilibrium point $\tilde{x} = 0$ of the forced system (3.1) is **asymptotically stable** if and only if Eq. (3.35) satisfies the Routh Hurwitz criterion and $G(-\vec{\psi}) = 0$, where $\vec{\psi}$ is the small equilibrium shift vector as outlined in Eq. (4.5).

Proof: By the mean value theorem

$$|G(\tilde{x}_s - \vec{\psi}) - G(-\vec{\psi})| < k\|\tilde{x}_s\|$$

for some positive constant k. But $|G(-\vec{\psi})| = 0$, therefore

$$|G(\tilde{x}_s - \vec{\psi})| = |G(\tilde{x}_s)| < k\|\tilde{x}_s\|$$

Eq. (3.28) yields the norm of $\tilde{x}_f$

$$\|\tilde{x}_f\| = \frac{|G(\tilde{x}_s)|}{R^2}\left(\mathcal{A}_n^2 + \frac{\mathcal{A}_{n-1}^2}{w^2} + \ldots\right)^{\frac{1}{2}} = c|G(\tilde{x}_s)| < ck\|\tilde{x}_s\|$$

Hence

$$\|\tilde{x}\| \leq \|\tilde{x}_s\| + \|\tilde{x}_f\| \leq (1 + ck)\|\tilde{x}_s\|$$

Since Eq. (3.35) satisfies the Routh Hurwitz criterion, we can always choose a δ_1 such that $\|\tilde{x}_s(0)\| < \delta_1$ implies that $\|\tilde{x}_s(t)\| < \epsilon_1$ for any ϵ_1 at all t and further

$$\lim_{t\to\infty} \|\tilde{x}_s(t)\| = 0$$

For any ϵ let $\epsilon_1 = \epsilon/(1 + ck)$, then $\|\tilde{x}_s(t)\| < \epsilon_1$ and

$$\|\tilde{x}(t)\| < (1 + ck)\|\tilde{x}_s\| < \epsilon$$

for some δ_1. Consequently we can always choose δ_1 such that the initial conditions $\|\tilde{x}_s(0)\| < \delta_1$ imply the trajectory $\tilde{x}(t)$ will not leave the ϵ neigbourhood, indicating **stability**. Furthermore,

$$\lim_{t\to\infty} \|\tilde{x}(t)\| < (1 + ck) \lim_{t\to\infty} \|\tilde{x}_s(t)\| = 0$$

for $\|\tilde{x}_s(0)\| < \delta_1$ proves **asymptotic stability** since the trajectory $\tilde{x}(t)$ converges to zero as time tends to infinity.

Conversely, if Eq. (3.35) does not satisfy the Routh Hurwitz criterion, then $\tilde{x}_s(t)$ does not converge to zero as time tends to infinity. Since $\tilde{x}_f(t)$ is sinusoidal, if $\tilde{x}_s(t)$ does not converge to zero, then $\tilde{x}_s(t) + \tilde{x}_f(t) = \tilde{x}(t)$ certainly does not converge to zero. Hence, the equilibrium, $\tilde{x} = 0$ is not **asymptotically stable**. If $G(-\vec{\psi}) = 0$ does not hold, then as $\tilde{x}_s(t)$ approaches zero, $G(\tilde{x}_s - \vec{\psi})$ converges to some finite non-zero number q. Hence, $\|\tilde{x}_f(t)\|$ converges to $c|q|$. Consequently, $\|\tilde{x}_s($ $\tilde{x}_f(t)\| = \|\tilde{x}(t)\|$ approaches $c|q|$ as time tends to infi and $\tilde{x} = 0$ is not **asymptotically stable**.

Therefore, the above theorem states necessary sufficient conditions for **asymptotic stability** of equilibrium point $\tilde{x} = 0$. As a physical interpretat we say that the forcing modulation function G n converge to zero as the system approaches equilibri Then as the slow trajectory approach equilibrium excited fast mode decays also since the magnitud the excitation (Eq. (3.1)) decreases to zero. Thu Eq. (3.35) satisfies the Routh Hurwitz criterion $G(-\vec{\psi}) = 0$, then the equilibrium point $\tilde{x} = 0$ of forced system (3.1) is **asymptotically stable**.

4.5 Criteria Summary

We briefly summarize the stability criteria derivec the previous sections.

a) Section (4.1) develops a criterion for an equi rium shift due to forcing. This section shows that if **zero** condition (4.1) is satisfied then there is no e librium shift. If the **zero** condition is not satisfied equilibrium shift ψ is given by Eq. (4.5).

b) Section (4.3) develops a criterion for **slow asyr totic stability** of the shifted or original equilibr point $\tilde{x} = 0$. For **slow asymptotic stability** the lir averaged equation (3.35) must satisfy the Routh H witz criterion.

c) Section (4.4) develops a criterion for **asymptc stability** of the shifted or original equilibrium p $\tilde{x} = 0$. It is shown that for **asymptotic stabil** Eq. (3.35) must satisfy the Routh Hurwitz criteria $G(-\vec{\psi}) = 0$ must hold.

5 Example

In this example we consider a second-order system v a positive trace. As a specific case, we consider second-order equation derived in [7] for the flow pot tial of a liquid rocket engine,

$$\ddot{\Phi} + B\dot{\Phi} + C\Phi = 0 \qquad (5$$

where Φ is the perturbation of the flow potential fr equilibrium. In the case of liquid rockets, unsteady cc bustion provides the negative damping which drives instability. Since the damping is determined by B, n ative damping corresponds to a negative coefficient

Normalization of Eq. (5.1) results in the dimensi less equation

$$\ddot{x} + A_1\dot{x} + A_0 x = 0 \tag{5.2}$$

where x is the normalized flow potential and the time derivatives are taken with respect to a dimensionless time t.

For the purpose of this example, we choose the following constants: $A_1 = -0.2$ and $A_0 = 1$. Notice that $A_1 < 0$ corresponds to a positive trace of the Jacobian matrix. Hence, the equilibrium point $x = 0$ of Eq. (5.2) is unstable. Eq. (5.2) is a second-order linear equation which can be solved analytically. Fig. (1) shows a plot of the trajectory $x(t)$ versus t for initial conditions $x(0) = 0.01, \dot{x}(0) = 0$.

Bellman, Bentsman and Meerkov [5] prove that it is not possible to vibrationally control a system with a positive trace if the function $G(\bar{x}_s)$ is linear. Consequently, we consider a nonlinear function $G(\bar{x}_s)$. Suppose

$$G(\dot{x}, x) = \alpha + \beta x\dot{x} \tag{5.3}$$

describes the effect produced by forcing some accessible system parameter.

This choice of G is not arbitrary. We know that the sign of A_1 creates an instability. Consequently we wish to change the sign of this coefficient by applying vibrational control. Consider the averaged equation (3.35), there are two possibilities for changing the sign of the $\dot{x}$ coefficient; namely, the terms $\mathcal{P}$ or $\mathcal{Q}$. We consider the $\mathcal{Q}$ term, hence,

$$\frac{\partial \mathcal{Q}}{\partial \dot{x}} = -k \Rightarrow \mathcal{Q} = -k\dot{x} \tag{5.4}$$

where $k > |A_1|$. By the definition of the core terms, Eq. (3.32), Eq. (5.4) becomes

$$-\frac{A_2}{2w^2R^2} G \frac{\partial G}{\partial \dot{x}} = -k\dot{x} \tag{5.5}$$

Equation (5.5) can be solved by separation of variables. Unfortunately, the solution to Eq. (5.5) is $G = c\sqrt{|x\dot{x}|}$ which is singular at the origin and violates the assumption that G is continuously differentiable. Hence, we let $G(\dot{x}, x) = \alpha + \beta x\dot{x}$ as an approximation of the square root close to the origin.

Given the above choice of G, let us write the forced equation as

$$\ddot{x} + A_1\dot{x} + A_0 x = (\alpha + \beta x\dot{x}) \sin(wt) \tag{5.6}$$

Let $w = 70$, $\alpha = 15$ and $\beta = 200$. For these values, Eq. (5.6) becomes

$$\ddot{x} - 0.2\dot{x} + x = (15 + 200x\dot{x}) \sin(70t) \tag{5.7}$$

For the analysis in this paper to be valid, the following bounds (see Eq. (3.15)) must hold.

$$\begin{aligned} |\partial G/\partial \dot{x}| &= |200x| \ll 70 \\ |\partial G/\partial x| &= |200\dot{x}| \ll 70^2 \end{aligned} \tag{5.8}$$

These bounds are satisfied if x and $\dot{x}$ are sufficiently small. To check the criterion outlined in the previous section, let us calculate the averaged core terms defined by Eq. (3.32).

$$\begin{aligned} \mathcal{P}(\dot{x}, x) &= \tfrac{-0.2}{2\cdot 70^2}(15 + 200x\dot{x})200x \\ &= -0.061x - 0.816\dot{x}x^2 \\ \mathcal{Q}(\dot{x}, x) &= -\tfrac{1}{2\cdot 70^2}(15 + 200x\dot{x})200\dot{x} \\ &= -.306\dot{x} - 4.082x\dot{x}^2 \end{aligned} \tag{5.9}$$

Eq. (5.9) satisfies the zero condition

$$\mathcal{Q}(0,0) + \mathcal{P}(0,0) = 0 \tag{5.10}$$

indicating that there is no equilibrium shift. In order to determine stability, evaluate the partial derivatives of the slow equation (3.35). Recall that these partials are computed at the origin,

$$\begin{aligned} \tfrac{\partial \mathcal{P}}{\partial x}\big|_{0,0} &= -.061 - 1.632\dot{x}x|_{0,0} = -.061 \\ \tfrac{\partial \mathcal{P}}{\partial \dot{x}}\big|_{0,0} &= -0.816x^2|_{0,0} = 0 \\ \tfrac{\partial \mathcal{Q}}{\partial x}\big|_{0,0} &= -4.082\dot{x}^2|_{0,0} = 0 \\ \tfrac{\partial \mathcal{Q}}{\partial \dot{x}}\big|_{0,0} &= -.306 - 8.164x\dot{x}|_{0,0} = -.306 \end{aligned} \tag{5.11}$$

In view of (5.11), we can write the averaged equation (3.35) for the slow mode $x_s(t)$

$$\ddot{x}_s + 0.1061\dot{x}_s + 1.061x_s = 0 \tag{5.12}$$

For a second-order linear differential equation such as the one above, the Routh Hurwitz criterion is satisfied if all coefficients have the same sign. Clearly, Eq. (5.12) satisfies the Routh Hurwitz criterion. Consequently, by the criteria developed in section (4.3) the equilibrium point $(\dot{x}, x) = 0$ of the forced system (5.6) is slowly asymptotically stable. Finally, $G(0,0) = 12 \neq 0$, hence the equilibrium point $(\dot{x}, x) = 0$ is not asymptotically stable (see section 4.4).

Therefore, if we find an accessible parameter in a liquid rocket engine that can produce a modulating function $G = \alpha + \beta x\dot{x}$ then we can achieve slow asymptotic stability by application of vibrational control.

It is interesting and instructive to compare results obtained by this analysis with a numerical simulation. We can analytically solve the slow mode equation (5.12) to derive the following analytic expression for $x_s(t)$.

$$x_s(t) = e^{-0.053t}[X_{s_0}\cos(1.03t) + \dot{X}_{s_0}\sin(1.03t)] \quad (5.13)$$

where X_{s_0} is the initial displacement and $\dot{X}_{s_0}$ is the initial velocity. Fig. (2) compares $x_s(t)$ of Eq. (5.13) with a $x(t)$ calculated by a numerical simulation. Since the initial conditions for the slow mode are not known, they are matched to the initial conditions shown by the numeric simulation. We can see that the equilibrium point $(\dot{x}, x) = 0$ of the forced system (5.6) is indeed **slowly asymptotically stable** but is not **asymptotically stable**. Furthermore, Fig. (2) shows excellent agreement between the behaviour predicted by the developed theory and that predicted by the numerical simulation.

6 Conclusion

In this paper we present a criterion for the feasibility of vibrational open loop control. Previous work is extended to include analysis of non-linear, vibrational control. Current vibrational control theory proves that linear vibrational control is not feasible if the Jacobian matrix has a positive trace. This paper shows that nonlinear vibrational control is feasible even if the trace of the Jacobian is positive. We note that this result is of significant practical importance because a large number of engineering systems exhibit a positive Jacobian trace: such as rocket motors, jet engines and ramjets.

References

[1] S.M Meerkov and G.I Shapiro. Method of vibrational control in the problem of stabilization of ionization-thermal instability of a powerful continuous CO_2 laser. *Automatic Remote Control*, 1976.

[2] C. McGreavy and J.M Thornton. Stability studies of single catalyst particles. *Chemical Engineering*, 1970.

[3] S.M Meerkov. Principle of vibrational control: theory and applications. *IEEE Transactions on Automatic Control*, 1980.

[4] J. Guckenheimer and P. Holmes. *Nonlinear oscillations, dynamical systems, and bifurcations of vector fields*. Springer and Verlag, 1983.

[5] R.E Bellman, J. Bentsman, and S.M Meerkov. V brational control of nonlinear systems: vibration stabilizability. *IEEE Transactions on Automat Control*, 1986.

[6] G. Strang. *Linear Algebra and its Applications*. Ha court Brace Jovanovich, Inc., 1988.

[7] E. Powell. *Nonlinear combustion instability in l uid propellant rocket engines*. PhD thesis, Georg Institute of Technology, 1970.

[8] H.K Khalil. *Nonlinear Systems*. Macmillan Publis ing Company, 1992.

[9] R.C Dorf. *Modern Control Systems*. Addison-Wesl Publishing Company, 1988.

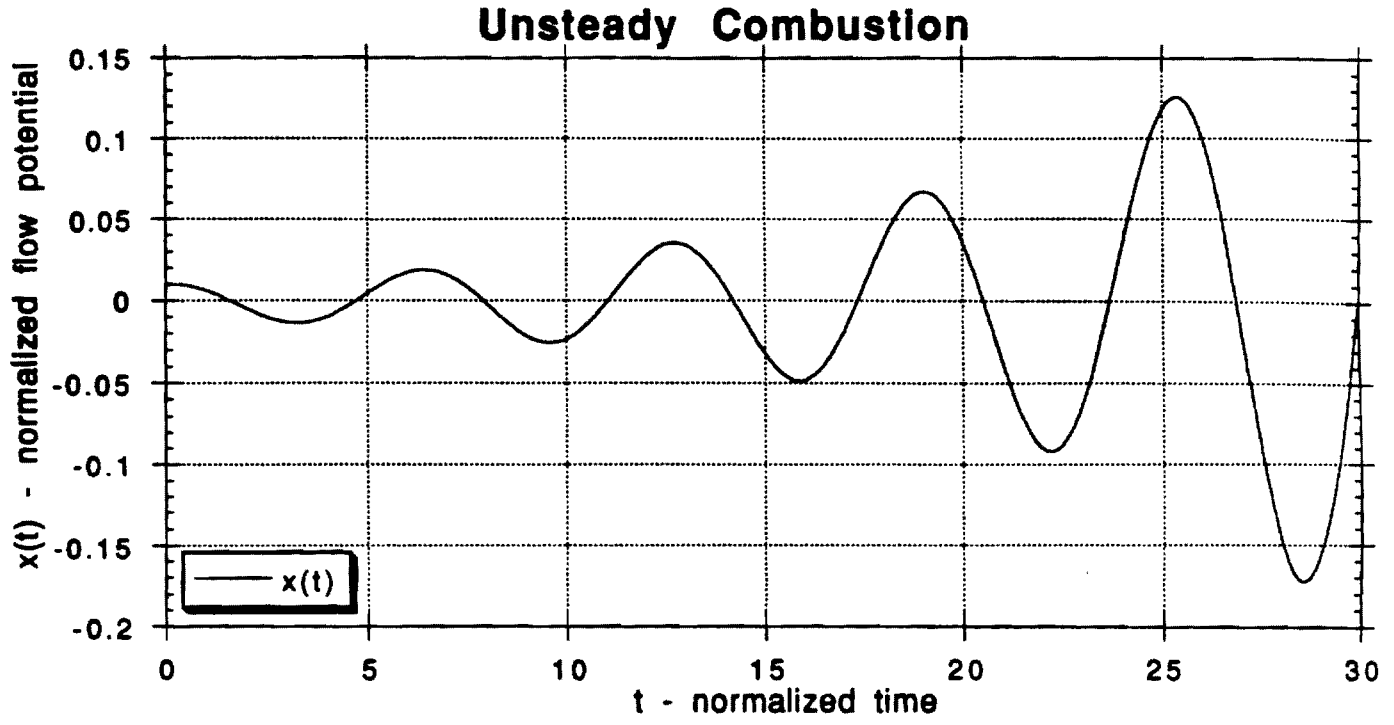

Figure 1: Amplification of a disturbance in an unstable liquid rocket

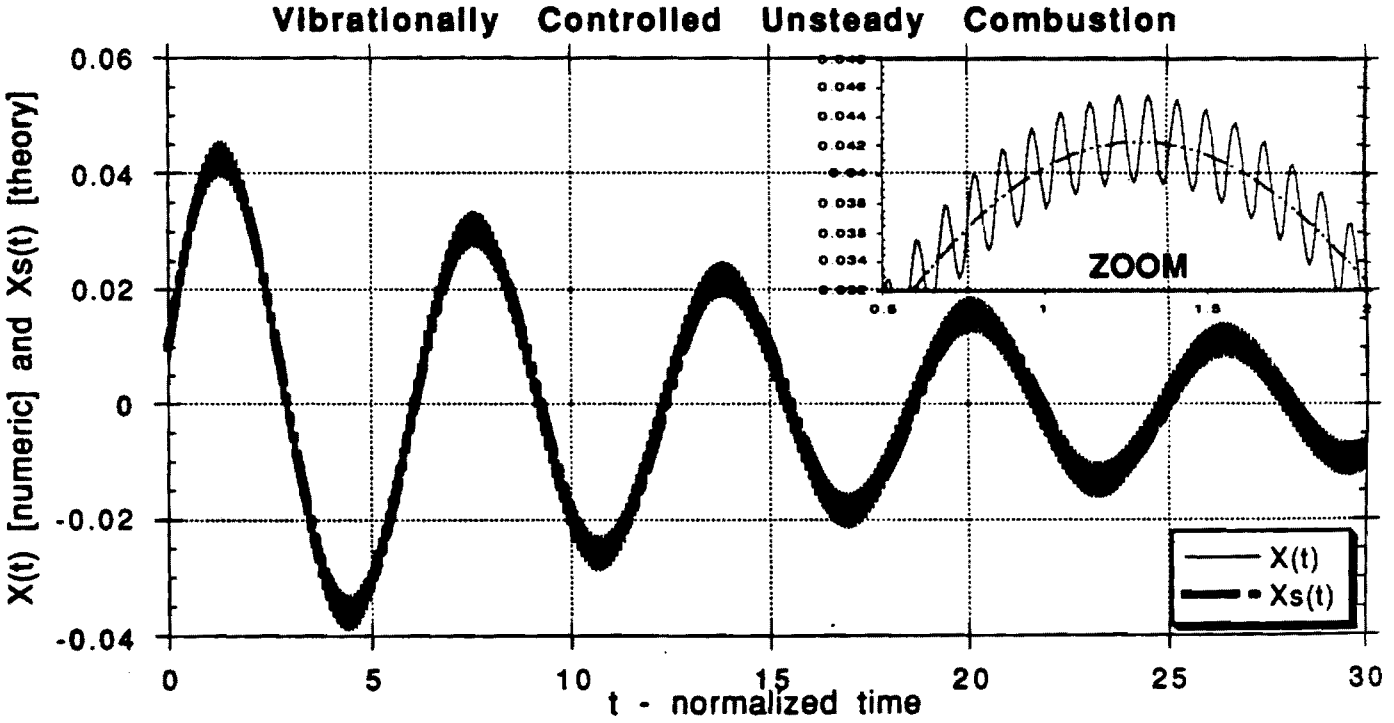

Figure 2: Damping of a liquid rocket instability by high frequency vibrational control

AIAA 94-0099
Theoretical Study of Flow Turning Losses in the Presence of Mean Temperature Gradients

L. M. Matta and B. T. Zinn
Georgia Institute of Technology
Atlanta, GA

32nd Aerospace Sciences Meeting & Exhibit
January 10-13, 1994 / Reno, NV

THEORETICAL STUDY OF FLOW TURNING LOSSES IN THE PRESENCE OF MEAN TEMPERATURE GRADIENTS[†]

L. M. Matta[‡] and B. T. Zinn[*]

School of Aerospace Engineering
Georgia Institute of Technology
Atlanta, GA 30332

Abstract

An understanding of the processes responsible for driving and damping acoustic oscillations in solid rocket motors is necessary for developing practical design methods that eliminate or reduce the occurrence of combustion instabilities. While state of the art solid rocket stability prediction methods generally account for the flow turning loss, the magnitude and characteristics of this loss have never been fully investigated. In this study, an equation for determining the acoustic stability of a duct with axial and transverse temperature gradients was developed and the flow turning loss term identified. The presence of volume integrals in this equation, which reduce to surface flux terms in a previous analysis that did not account for mean temperature gradients, suggests that the presence of these gradients may drive or damp the oscillations. Numerical integration of the governing equations was performed to study the effects of axial temperature gradients in the motor. The presence of an axial temperature gradient was shown to affect the convective terms of the stability equation. The effects of temperature gradients were shown to be most significant in the vicinity of an acoustic pressure antinode in the chamber, where flow turning losses are smallest.

Introduction

The relative magnitudes of the mechanisms within a combustor that drive and damp oscillations determine the acoustic stability of the chamber. When the acoustic energy gains present in the combustor outweigh the losses, small disturbances amplify to levels that can adversely influence motor performance by affecting guidance, thrust, and the structure integrity of the motor[1-4]. Because of the high energy densities and low losses observed in most combustors designed for use in propulsion systems, the possibility of encountering instability is high.

In order to eliminate the occurrence or reduce the severity of combustion instabilities in solid rocket motors, it is necessary to identify and understand the mechanisms by which energy is added to and removed from the acoustic oscillations. It is generally accepted that the energy necessary to initiate and maintain the instability is provided by the interaction of the solid propellant combustion process with acoustic oscillations. Processes that tend to remove energy from the oscillations and, thus, stabilize the motor include energy transmission through the choked nozzle (nozzle losses), viscous dissipation, and flow turning loss. While viscous damping is generally neglected in stability analysis, and much is known about the processes of nozzle damping and combustion driving, relatively little is known about the flow turning loss. Recent studies have investigated the behavior of the flow turning loss in a constant mean temperature environment[5,6]. However, in actual propulsion devices and laboratory combustors used to investigate combustion instabilities, significant mean temperature gradients and heat losses may be present. The goal of this investigation was to develop an understanding of how the flow turning loss and the stability of solid rocket motors are affected by the presence of axial and transverse temperature gradients in the flow field.

The velocity of combustion products leaving the burning solid propellant is generally radial, as shown in Fig. 1. As these gases move away from the propellant and are entrained in the core flow, they turn from radial to axial before exiting the motor through the nozzle. During this turning process, the combustion products acquire axial acoustic energy from the core flow oscillations. This phenomena was first discussed by Culick[7-11] who argued that since the combustion products entering the combustor core flow acquire acoustic energy from the existing axial acoustic core flow oscillations, the axial acoustic field experiences a loss of acoustic energy that tends to stabilize the system.

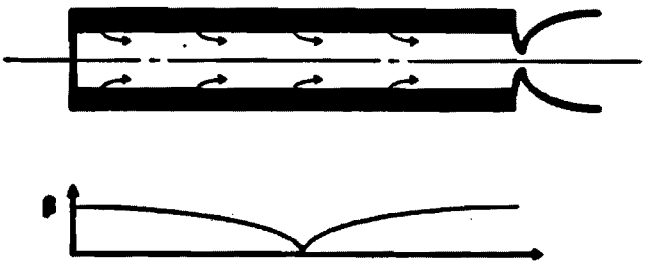

Figure 1. Schematic of a solid rocket motor showing the turning of the flow of combustion products and the pressure distribution characteristic of axial instability.

In earlier constant temperature studies under this program[5,6], a two dimensional expression for the complex growth rate constant α of the oscillations in a constant temperature duct of length L and height H with mean flow

[†] Research supported under AFOSR Contract No. 91-0160; Dr. Mitat A. Birkan contract monitor.
[‡] AIAA Student Member.
[*] Regents Professor, AIAA Fellow.

and mass addition at locations along the side walls was developed. This stability equation can be written as:

$$2\alpha E_m^2 = -\left\langle \left[p'u' + \frac{p'^2 \bar{u}}{\bar{\rho}\bar{a}^2} + \bar{\rho}\bar{u}u'^2 \right]_0^L \right\rangle_{t,y}$$

$$-\left\langle \frac{1}{H}\int_0^L \left(p'[v']_0^H + \frac{p'^2}{\bar{a}^2}\left[\frac{\bar{v}}{\bar{\rho}}\right]_0^H \right.\right.$$

$$\left.\left. + \langle \bar{\rho}u' \rangle_y [v'\bar{u}]_0^H + \langle \bar{\rho}u' \rangle_y [\bar{v}u']_0^H - \langle \bar{\rho}u'^2 \rangle_y [\bar{v}]_0^H \right) dx \right\rangle_t \quad (1)$$

where

$$E_m^2 = \int_0^L \left\langle \frac{p'^2}{2\bar{\rho}\bar{a}^2} + \frac{p'\bar{u}u'}{\bar{a}^2} + \frac{\bar{\rho}u'^2}{2} \right\rangle_{t,y} dx \quad (2)$$

In these equations, u and v are the axial and transverse components of velocity, respectively, ρ is the density, and a is the isentropic speed of sound. The dependent variables have been written as the sum of a time-averaged and a fluctuating component (e.g., $\rho = \bar{\rho} + \rho'$ where $\bar{\rho}$ is the time-average of the instantaneous density ρ). Angle brackets denote averaging with respect to the subscripted variable (e.g., $\langle\ \rangle_t$ represents a time average). The term associated with the flow turning loss is

FLOW TURNING LOSS =

$$\left\langle \frac{1}{H}\int_0^L \langle \bar{\rho}u_i^2 \rangle_y [\bar{v}]_0^H dx \right\rangle_t \quad (3)$$

Cold flow tests conducted earlier under this program have confirmed that the classical flow turning loss term is correctly predicted by the one dimensional acoustic stability equation. Furthermore, in agreement with theoretical predictions, these tests showed that when the mean density is constant throughout the flow field, for a given duct geometry, the flow turning loss is directly proportional to the propellant burning rate and independent of the magnitude of the core flow velocity. Finally, predictions and measurements showed that maximum and minimum flow turning losses occur when the side wall injection occurs at an acoustic pressure node and antinode, respectively.

In the cold flow study, the flow field was assumed isentropic, which greatly simplified the analysis. This assumption restricted application of the developed acoustic stability formulation to flows with uniform mean temperature and density. A problem arises when applying the stability analysis to combustion systems, such as rocket motors, in which mean temperature gradients and heat losses may be significant. To resolve this problem, an investigation of the effects of mean temperature and density gradients in the flow turning region upon the flow turning loss was undertaken.

Theoretical Study

In this analysis, a stability equation that accounts for the mean temperature/density gradients that appear in experimental studies with combustion present was developed from the following conservation equations for mass, axial momentum, and energy:

$$\frac{\partial \rho}{\partial t} + \frac{\partial}{\partial x}(\rho u) + \frac{\partial}{\partial y}(\rho v) = 0 \quad (4)$$

$$\rho\frac{\partial u}{\partial t} + \rho u\frac{\partial u}{\partial x} + \rho v\frac{\partial u}{\partial y} + \frac{\partial p}{\partial x} = 0 \quad (5)$$

$$p\left(\frac{\partial s}{\partial t} + u\frac{\partial s}{\partial x} + v\frac{\partial s}{\partial y}\right) = R\dot{Q} \quad (6)$$

where s is the specific entropy, R is the gas constant and $\dot{Q}$ is the rate of heat addition per volume. The perfect gas equation of state,

$$p = \rho RT \quad (7)$$

where T is the temperature, was also used in this analysis. These equations were written in terms of time averaged and fluctuating quantities. Products of perturbations were neglected (which will be shown to be equivalent to neglecting terms of third order and higher in the result) and the time-invariant forms of the equations were subtracted. Equations 4-7 then became

$$\frac{\partial \rho'}{\partial t} + \frac{\partial}{\partial x}(\bar{\rho}u' + \rho'\bar{u}) + \frac{\partial}{\partial y}(\bar{\rho}v' + \rho'\bar{v}) = 0 \quad (8)$$

$$\bar{\rho}\frac{\partial u'}{\partial t} + \bar{\rho}\frac{\partial}{\partial x}(\bar{u}u') + \rho'\bar{u}\frac{\partial \bar{u}}{\partial x} + \bar{\rho}\bar{v}\frac{\partial u'}{\partial y}$$

$$+\bar{\rho}v'\frac{\partial\bar{u}}{\partial y}+\rho'\bar{v}\frac{\partial\bar{u}}{\partial y}+\frac{\partial p'}{\partial x}=0 \qquad (9)$$

and

$$\bar{\rho}\left(\frac{\partial s'}{\partial t}+\bar{u}\frac{\partial s'}{\partial x}+u'\frac{\partial\bar{s}}{\partial x}+\bar{v}\frac{\partial s'}{\partial y}+v'\frac{\partial\bar{s}}{\partial y}\right)$$

$$+p'\bar{u}\frac{\partial\bar{s}}{\partial x}+p'\bar{v}\frac{\partial\bar{s}}{\partial y}=R\dot{Q}' \qquad (10)$$

Using the following relations,

$$\frac{\partial\bar{s}}{\partial x}=\frac{C_v}{\bar{p}}\frac{\partial\bar{p}}{\partial x}-\frac{C_p}{\bar{\rho}}\frac{\partial\bar{\rho}}{\partial x} \qquad (11)$$

$$s'=C_p\left(\frac{p'}{\gamma\bar{p}}-\frac{\rho'}{\bar{\rho}}\right) \qquad (12)$$

$$\frac{\partial s'}{\partial x}=C_p\left(\frac{1}{\gamma\bar{p}}\frac{\partial p'}{\partial x}-\frac{p'}{\gamma\bar{p}^2}\frac{\partial\bar{p}}{\partial x}-\frac{1}{\bar{\rho}}\frac{\partial\rho'}{\partial x}+\frac{\rho'}{\bar{\rho}^2}\frac{\partial\bar{\rho}}{\partial x}\right) \qquad (13)$$

the acoustic energy equation, Eq. 10, can be rewritten as:

$$\frac{\partial p'}{\partial t}+\bar{u}\frac{\partial p'}{\partial x}+u'\frac{\partial\bar{p}}{\partial x}+\bar{v}\frac{\partial p'}{\partial y}+v'\frac{\partial\bar{p}}{\partial y}$$

$$=a^2\left[\frac{\partial\rho'}{\partial t}+\bar{u}\frac{\partial\rho'}{\partial x}+u'\frac{\partial\bar{\rho}}{\partial x}+\bar{v}\frac{\partial\rho'}{\partial y}+v'\frac{\partial\bar{\rho}}{\partial y}\right.$$

$$+\left(\frac{\bar{u}p'}{\bar{p}}\right)\frac{\partial\bar{\rho}}{\partial x}+\left(\frac{\bar{v}p'}{\bar{p}}\right)\frac{\partial\bar{\rho}}{\partial y}-\left(\frac{\bar{u}\rho'}{\bar{\rho}}\right)\frac{\partial\bar{\rho}}{\partial x}$$

$$\left.-\left(\frac{\bar{v}\rho'}{\bar{\rho}}\right)\frac{\partial\bar{\rho}}{\partial y}+\left(\frac{1}{C_p\bar{T}}\right)\right]\frac{\partial Q'}{\partial t} \qquad (14)$$

where

$$a^2=\frac{\gamma\bar{p}}{\bar{\rho}} \qquad (15)$$

The acoustic continuity equation, Eq. 8, was then used to substitute for the $\partial p/\partial t$ term in Eq. 14. The resulting equation is

$$\frac{1}{a^2}\frac{\partial p'}{\partial t}+\frac{\bar{u}}{a^2}\frac{\partial p'}{\partial x}+\frac{u'}{a^2}\frac{\partial\bar{p}}{\partial x}+\frac{\bar{v}}{a^2}\frac{\partial p'}{\partial y}$$

$$+\frac{v'}{a^2}\frac{\partial\bar{p}}{\partial y}+\bar{\rho}\frac{\partial u'}{\partial x}+\rho'\frac{\partial\bar{u}}{\partial x}+\bar{\rho}\frac{\partial v'}{\partial y}+\rho'\frac{\partial\bar{v}}{\partial y}$$

$$-\left(\frac{\bar{u}p'}{\bar{p}}\right)\frac{\partial\bar{\rho}}{\partial x}-\left(\frac{\bar{v}p'}{\bar{p}}\right)\frac{\partial\bar{\rho}}{\partial y}+\left(\frac{\bar{u}\rho'}{\bar{\rho}}\right)\frac{\partial\bar{\rho}}{\partial x}$$

$$+\left(\frac{\bar{v}\rho'}{\bar{\rho}}\right)\frac{\partial\bar{\rho}}{\partial y}=\left(\frac{1}{C_p\bar{T}}\right)\frac{\partial Q'}{\partial t} \qquad (16)$$

Next, Eq. 16 is multiplied by $\frac{p'}{\bar{\rho}}$, which yields

$$\frac{1}{2\bar{\rho}a^2}\frac{\partial p'^2}{\partial t}+\frac{p'\bar{u}}{\bar{\rho}a^2}\frac{\partial p'}{\partial x}+\frac{p'u'}{\bar{\rho}a^2}\frac{\partial\bar{p}}{\partial x}+\frac{p'\bar{v}}{\bar{\rho}a^2}\frac{\partial p'}{\partial y}+\frac{p'v'}{\bar{\rho}a^2}\frac{\partial\bar{p}}{\partial y}$$

$$+p'\frac{\partial u'}{\partial x}+\frac{p'\rho'}{\bar{\rho}}\frac{\partial\bar{u}}{\partial x}+p'\frac{\partial v'}{\partial y}+\frac{p'\rho'}{\bar{\rho}}\frac{\partial\bar{v}}{\partial y}-\left(\frac{\bar{u}p'^2}{\bar{p}\bar{\rho}}\right)\frac{\partial\bar{\rho}}{\partial x}$$

$$-\left(\frac{\bar{v}p'^2}{\bar{p}\bar{\rho}}\right)\frac{\partial\bar{\rho}}{\partial y}+\left(\frac{\bar{u}\rho'p'}{\bar{\rho}^2}\right)\frac{\partial\bar{\rho}}{\partial x}+\left(\frac{\bar{v}\rho'p'}{\bar{\rho}^2}\right)\frac{\partial\bar{\rho}}{\partial y}$$

$$=\left(\frac{\gamma-1}{\gamma\bar{p}}\right)(p'\dot{Q}') \qquad (17)$$

Using the steady state continuity equation,

$$\frac{\partial}{\partial x}(\bar{\rho}\bar{u})+\frac{\partial}{\partial y}(\bar{\rho}\bar{v})=0 \qquad (18)$$

Eq. 17 can be reduced to

$$\frac{1}{2\bar{\rho}a^2}\frac{\partial p'^2}{\partial t}+\left(\frac{p'}{\bar{\rho}a^2}\right)\left(\bar{u}\frac{\partial p'}{\partial x}+u'\frac{\partial \bar{p}}{\partial x}+\bar{v}\frac{\partial p'}{\partial y}+v'\frac{\partial \bar{p}}{\partial y}\right)$$

$$+p'\frac{\partial u'}{\partial x}+p'\frac{\partial v'}{\partial y}+\left(\frac{p'^2}{\bar{\rho}}\right)\left(\frac{\partial \bar{u}}{\partial x}+\frac{\partial \bar{v}}{\partial y}\right)=\left(\frac{\gamma-1}{\gamma\bar{p}}\right)\left(p'\dot{Q}'\right) \quad (19)$$

Next, Eq. 9 is multiplied by u' and terms of second order and above in mean Mach number are neglected, resulting in

$$\frac{\bar{\rho}}{2}\frac{\partial u'^2}{\partial t}+\bar{\rho}u'\frac{\partial}{\partial x}(\bar{u}u')+\bar{\rho}\bar{v}u'\frac{\partial u'}{\partial y}+\bar{\rho}v'u'\frac{\partial \bar{u}}{\partial y}+u'\frac{\partial p'}{\partial x}=0 \quad (20)$$

Equations 19 and 20 are then added, giving the following equation:

$$\frac{\partial}{\partial t}\left(\frac{p'^2}{2\bar{\rho}a^2}+\frac{\bar{\rho}u'^2}{2}\right)+\left(\frac{p'}{\bar{\rho}a^2}\right)\left(\bar{u}\frac{\partial p'}{\partial x}+u'\frac{\partial \bar{p}}{\partial x}+\bar{v}\frac{\partial p'}{\partial y}+v'\frac{\partial \bar{p}}{\partial y}\right)$$

$$+\frac{\partial}{\partial x}(p'u')+p'\frac{\partial v'}{\partial y}+\bar{\rho}u'\frac{\partial}{\partial x}(\bar{u}u')+\bar{\rho}\bar{v}u'\frac{\partial u'}{\partial y}+\bar{\rho}v'u'\frac{\partial \bar{u}}{\partial y}$$

$$+\left(\frac{p'^2}{\bar{\rho}}\right)\left(\frac{\partial \bar{u}}{\partial x}+\frac{\partial \bar{v}}{\partial y}\right)=\left(\frac{\gamma-1}{\gamma\bar{p}}\right)\left(p'\dot{Q}'\right) \quad (21)$$

Next, the acoustic continuity equation, Eq. 8, is multiplied by $(\bar{u}u')$ and again terms of the order of mean Mach number squared and higher are neglected,

$$(\bar{u}u')\frac{\partial \rho'}{\partial t}+(\bar{u}u')\frac{\partial}{\partial x}(\bar{\rho}u')+(\bar{u}u')\frac{\partial}{\partial y}(\bar{\rho}v')=0 \quad (22)$$

and to this is added Eq. 9 multiplied by $\left(\frac{\bar{u}\rho'}{\bar{\rho}}\right)$ (again neglecting terms of second order and above in mean Mach number),

$$\bar{u}\rho'\frac{\partial u'}{\partial t}+\frac{\bar{u}\rho'}{\bar{\rho}}\frac{\partial p'}{\partial x}=0 \quad (23)$$

which results in

$$\frac{\partial}{\partial t}(\bar{u}u'\rho')+\bar{u}u'\frac{\partial}{\partial x}(\bar{\rho}u')+\frac{\bar{u}\rho'}{\bar{\rho}}\left(\frac{\partial p'}{\partial x}\right)+\bar{u}u'\frac{\partial}{\partial y}(\bar{\rho}v')=0 \quad (24)$$

Now Eq. 24 is added to Eq. 21, which results in an equation for a quantity with units of acoustic energy. This equation is

$$\frac{\partial}{\partial t}\left(\frac{p'^2}{2\bar{\rho}a^2}+\rho'u'\bar{u}+\frac{\bar{\rho}u'^2}{2}\right)+\frac{\partial}{\partial x}\left(p'u'+\overline{\rho u}u'^2\right)+p'\frac{\partial v'}{\partial y}$$

$$+\left(\frac{p'}{\bar{\rho}a^2}\right)\left(\bar{u}\frac{\partial p'}{\partial x}+u'\frac{\partial \bar{p}}{\partial x}+\bar{v}\frac{\partial p'}{\partial y}+v'\frac{\partial \bar{p}}{\partial y}\right)$$

$$+\bar{\rho}\bar{v}u'\frac{\partial u'}{\partial y}+\bar{\rho}v'u'\frac{\partial \bar{u}}{\partial y}+\left(\frac{p'^2}{\bar{\rho}}\right)\left(\frac{\partial \bar{u}}{\partial x}+\frac{\partial \bar{v}}{\partial y}\right)$$

$$+\frac{\bar{u}\rho'}{\bar{\rho}}\left(\frac{\partial p'}{\partial x}\right)+\bar{u}u'\frac{\partial}{\partial y}(\bar{\rho}v')=\left(\frac{\gamma-1}{\gamma\bar{p}}\right)\left(p'\dot{Q}'\right) \quad (25)$$

It is assumed that $\bar{p}$ is constant throughout the duct and that p' is constant over the cross-section of the duct. Using these assumptions, Eq. 25 is averaged across the duct from $y = 0$ to H.

$$\frac{\partial}{\partial t}\left\langle\frac{p'^2}{2\bar{\rho}a^2}+\rho'u'\bar{u}+\frac{\bar{\rho}u'^2}{2}\right\rangle_y=-\frac{\partial}{\partial x}\left(\langle p'u'\rangle_y+\langle\overline{\rho u}u'^2\rangle_y\right)$$

$$-\left\langle\frac{\bar{u}p'}{\bar{\rho}a^2}\left(\frac{\partial p'}{\partial x}\right)+\frac{\bar{u}\rho'}{\bar{\rho}}\left(\frac{\partial p'}{\partial x}\right)+\frac{p'^2}{\bar{p}}\left(\frac{\partial \bar{u}}{\partial x}\right)\right\rangle_y$$

$$-\left\langle p'\frac{\partial v'}{\partial y}\right\rangle_y-\left\langle\frac{p'^2}{\bar{p}}\frac{\partial \bar{v}}{\partial y}\right\rangle_y-\frac{1}{H}\left[\overline{\rho v'}\overline{u}u'\right]_0^H+\left\langle\overline{\rho v'}\frac{\partial}{\partial y}(\bar{u}u')\right\rangle_y$$

$$-\left\langle\overline{\rho v'}u'\frac{\partial \bar{u}}{\partial x}\right\rangle_y-\left\langle\overline{\rho v}u'\frac{\partial u'}{\partial y}\right\rangle_y+\left(\frac{\gamma-1}{\gamma\bar{p}}\right)\left\langle p'\dot{Q}'\right\rangle_y \quad (26)$$

This equation must be massaged into a form that is comparable to the previous versions of the acoustic stability formulation. The following three equations are used in the manipulation procedure.

$$\bar{\rho}v'\frac{\partial}{\partial y}(\bar{u}u') - \bar{\rho}v'u'\frac{\partial \bar{u}}{\partial y} = \bar{\rho}v'\bar{u}\frac{\partial u'}{\partial y} \qquad (27)$$

$$-\bar{\rho}\bar{v}u'\frac{\partial u'}{\partial y} = \bar{\rho}u'^2\frac{\partial \bar{v}}{\partial y} - \bar{\rho}u'\frac{\partial}{\partial y}(u'\bar{v}) \qquad (28)$$

$$-\frac{\partial}{\partial y}(\bar{\rho}v'\bar{u}u') = -\bar{\rho}u'\frac{\partial}{\partial y}(\bar{u}v') - \overline{\rho u}v'\frac{\partial u'}{\partial y} - \bar{u}u'v'\frac{\partial \bar{\rho}}{\partial y} \qquad (29)$$

After some manipulations using the relations given in Eqs. 27-29, Eq. 26 is written in the form

$$\frac{\partial}{\partial t}\left\langle \frac{p'^2}{2\bar{\rho}a^2} + \rho'u'\bar{u} + \frac{\bar{\rho}u'^2}{2}\right\rangle_{y,s} = -\frac{\partial}{\partial x}\left\langle p'u' + \overline{\rho u}u'^2\right\rangle_{y,s}$$

$$-\left\langle \frac{\bar{u}p'}{\bar{\rho}\bar{a}^2}\left(\frac{\partial p'}{\partial x}\right) + \frac{\bar{u}\rho'}{\bar{\rho}}\left(\frac{\partial p'}{\partial x}\right) + \frac{p'^2}{\bar{p}}\left(\frac{\partial \bar{u}}{\partial x}\right)\right\rangle_{y,s}$$

$$-\left\langle \frac{1}{H}\int_0^L \left\{ p'[v']_0^H + \frac{p'^2}{\bar{p}}[\bar{v}]_0^H + \langle\bar{\rho}u'\rangle_y[\bar{u}v']_0^H \right.\right.$$

$$+\langle\bar{\rho}u'\rangle_y[u'\bar{v}]_0^H - \langle\bar{\rho}u'^2\rangle_y[\bar{v}]_0^H$$

$$\left.\left. +\langle\bar{u}u'v'\rangle_y[\bar{\rho}]_0^H - \left(\frac{\gamma-1}{\gamma\bar{p}}\right)\langle p'\dot{Q}'\rangle_y \right\} dx \right\rangle_t \qquad (30)$$

The resulting acoustic stability equation, which can account for the presence of mean temperature and density gradients in the region, is:

$$2\alpha E_m^2 = -\left\langle \left[p'u' + \bar{\rho}\bar{u}u'^2\right]_0^L \right\rangle_{t,y}$$

$$-\int_0^L \left\langle \frac{\bar{u}p'}{\bar{\rho}\bar{a}^2}\left(\frac{\partial p'}{\partial x}\right) + \frac{\bar{u}\rho'}{\bar{\rho}}\left(\frac{\partial p'}{\partial x}\right) + \frac{p'^2}{\bar{p}}\left(\frac{\partial \bar{u}}{\partial x}\right)\right\rangle_{y,s} dx$$

$$-\left\langle \frac{1}{H}\int_0^L p'[v']_0^H + \frac{p'^2}{\bar{p}}[\bar{v}]_0^H + \langle\bar{\rho}u'\rangle_y[\bar{u}v']_0^H + \langle\bar{\rho}u'\rangle_y[u'\bar{v}]_0^H \right.$$

$$\left. -\langle\bar{\rho}u'^2\rangle_y[\bar{v}]_0^H + \langle\bar{u}u'v'\rangle_y[\bar{\rho}]_0^H - \left(\frac{\gamma-1}{\gamma\bar{p}}\right)\langle p'\dot{Q}'\rangle_y \right] dx \Bigg\rangle_t \qquad (31)$$

where,

$$E_M^2 = \int_0^L \left\langle \frac{p'^2}{2\bar{\rho}\bar{a}^2} + \rho'\bar{u}u' + \frac{\bar{\rho}u'^2}{2}\right\rangle_{t,y} dx \qquad (32)$$

The most important differences to recall between this acoustic stability equation and Eq. 1 is that, in Eq. 31, $\bar{\rho}$ is not constant and $\bar{a}^2 = \frac{\gamma\bar{p}}{\bar{\rho}} \neq \frac{p'}{\rho'}$ in the new formulation. The term

$$\left\langle \frac{1}{H}\int_0^L \langle\bar{\rho}u'^2\rangle_y[\bar{v}]_0^H dx \right\rangle_t$$

was identified as the flow turning loss term in this version of the stability equation, and is similar in form to the corresponding flow turning loss term in the constant temperature case, as shown in Eq. 3.

Eq. 31 contains the following term

$$\left\langle \frac{1}{H}\int_0^L \langle\bar{u}u'v'\rangle_y[\bar{\rho}]_0^H dx \right\rangle_t$$

that does not appear in Eq. 1, because in the previous analysis $[\bar{\rho}]_0^H = 0$. Comparison of the equations shows that the term

$$\int_0^L \left\langle \frac{\bar{u}p'}{\bar{\rho}\bar{a}^2}\left(\frac{\partial p'}{\partial x}\right) + \frac{\bar{u}\rho'}{\bar{\rho}}\left(\frac{\partial p'}{\partial x}\right) + \frac{p'^2}{\bar{p}}\left(\frac{\partial \bar{u}}{\partial x}\right)\right\rangle_{y,t} dx$$

in the variable mean temperature formulation, Eq. 31, relates to the term

$$\left\langle \left[\frac{p'^2\bar{u}}{\bar{\rho}\bar{a}^2}\right]_0^L \right\rangle_{t,y}$$

in Eq. 1. In the constant mean temperature analysis, this term represents fluxes of potential energy convected through the axial boundaries of the control volume, while the term from Eq. 31 cannot be reduced to a surface flux term, and represents volumetric effects. This difference is due to the inclusion of density gradients in Eq. 31, and suggests that the interaction of acoustic oscillations with mean density gradients in the presence of a mean flow may drive or damp the acoustics.

Computational Study

In the second phase of this study, the relevant acoustic equations were numerically integrated to investigate the behavior of the various terms that appear in the derived acoustic stability equation. The two dimensional forms of the equations were averaged over the cross-section of the duct and then integrated along the axis of the experimental setup. In this analysis, a mean temperature gradient was imposed upon the flow, and the effects of the temperature gradient upon an imposed harmonic oscillation was studied. Oscillating heat addition was not included in this analysis. In order to solve the equations, initial conditions for the acoustic variables were set at the upstream wall of the duct, and it was assumed that the amplitude of the oscillations was kept constant by an acoustic driver. The computed solutions for the dependent variables were then substituted into the acoustic stability equation to determine the effects of the mean temperature gradient upon terms that affect the stability of the system.

A series of "numerical tests" was performed using the quasi-one dimensional numerical solver to determine how axial temperature gradients affect the acoustic energy balance in a duct with a low Mach number mean flow. The first investigated configuration consisted of a duct with mean flow injection at the head end and no injection through the walls. A mean temperature gradient was imposed at a given axial location, and the resulting mean density and velocity profiles are shown in Fig. 2.

The effect of the temperature gradient upon the acoustic pressure, velocity and density when the gradient

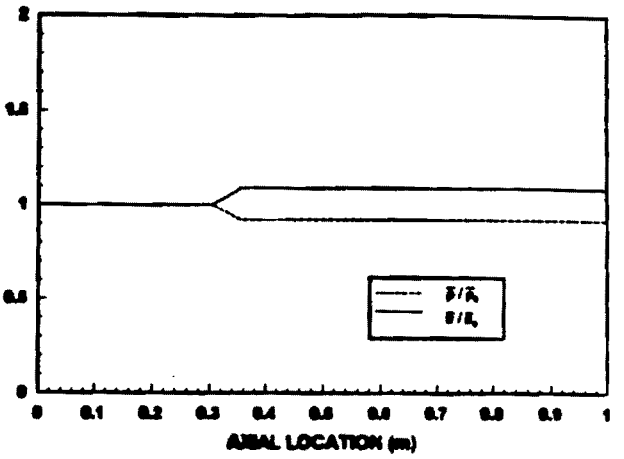

Figure 2. Axial distribution of the mean density and axial velocity used in the numerical procedure without wall injection.

occurs near an acoustic pressure node is shown in Fig. 3. The oscillatory pressure and density are not linearly dependent downstream of the injection due to entropy wave generation.

In this configuration, $\overline{v}$ and v' (the y-direction components of the mean and acoustic velocity) are zero. Neglecting terms involving these quantities, Eq. 31 can be reduced to the following equation

$$2\alpha E_M^2 = -\left\langle \left[p'u' + \overline{\rho}\,\overline{u}\,u'^2 \right]_0^L \right\rangle_{t,y}$$

$$-\int_0^L \left\langle \frac{\overline{u}p'}{\overline{\rho}\overline{a}^2}\left(\frac{\partial p'}{\partial x}\right) + \frac{\overline{u}\rho'}{\overline{\rho}}\left(\frac{\partial p'}{\partial x}\right) + \frac{p'^2}{\overline{p}}\left(\frac{\partial \overline{u}}{\partial x}\right) \right\rangle_{y,t} dx \quad (33)$$

where, with the exception of the first term on the right side,

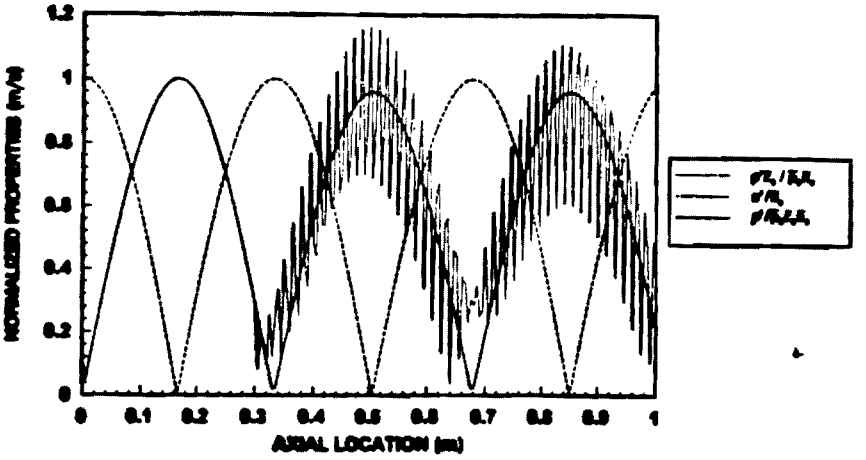

Figure 3. Normalized values of the acoustic pressure, axial velocity, and density calculated without wall injection.

all the terms depend upon the mean axial velocity , which represent convective losses. Since $\overline{u}$ increases as $\overline{\rho}$ decreases, it is expected that a mean temperature gradient will modify the terms in the above equation that are proportional to $\overline{u}$, which is indeed confirmed by the results of the calculations. In order to investigate this effect, the sum of the terms in Eq. 33 that are proportional to $\overline{u}$ were evaluated and subtracted from the sum of the corresponding terms for the case where the mean duct temperature is constant, to obtain the increase (or decrease) in convective energy losses. Such calculations were performed for a duct with the temperature gradient located at different positions relative to the standing acoustic wave and the results are presented in Fig. 4. An examination of this figure shows that the convective losses are maximum when the temperature gradient occurs near a pressure antinode.

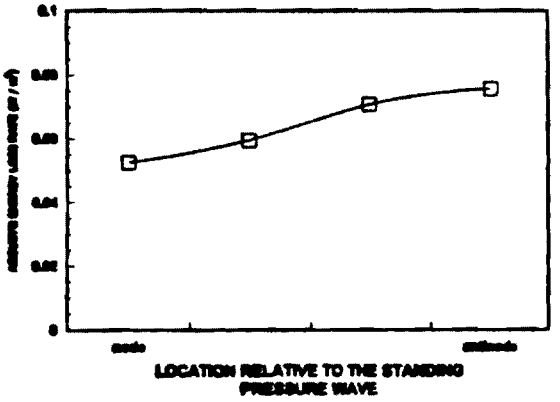

Figure 4. Dependence of the increased convective losses due to an axial temperature gradient upon the location of the gradient relative to the pressure oscillation.

The above computations were repeated for the same duct configuration but with flow injection through the side wall. The investigated model is not realistic because the cross duct density gradients were not modeled, but the results provide some insight into the behavior of the flow turning loss in the presence of a mean axial temperature gradient. In this series of computations, it was assumed that flow was injected through the side wall into the previously investigated duct with a velocity of 1 m/s. The assumed axial distributions of the mean density and velocity are shown in Fig. 5, and the calculated acoustic pressure, velocity and density are shown in Fig. 6. These computations reveal that a purely axial density gradient has little effect upon the behavior of the flow turning loss. A comparison between the flow turning loss and the increase (relative to the case where no temperature gradient is present) convective loss due to the axial temperature gradient for the test conditions is shown in Fig. 7. This figure shows that the increase in convective losses are maximum and the flow turning losses are minimum when flow injection and temperature gradient occur at an acoustic pressure antinode, and vice versa.

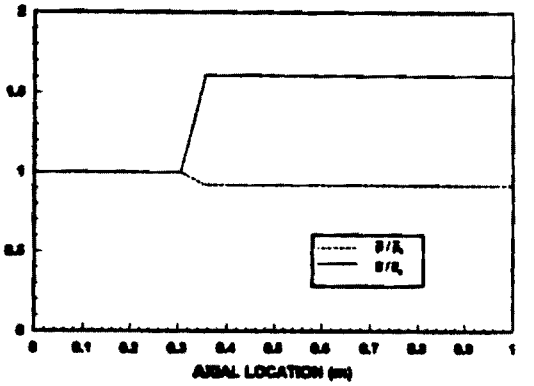

Figure 5. Axial distribution of the mean density and axial velocity used in the numerical procedure with wall injection in the temperature gradient region.

Concluding Remarks

An equation for determining the acoustic stability of a duct with axial and transverse temperature gradients was developed. The flow turning loss term of this equation is similar in form and function to that of the constant

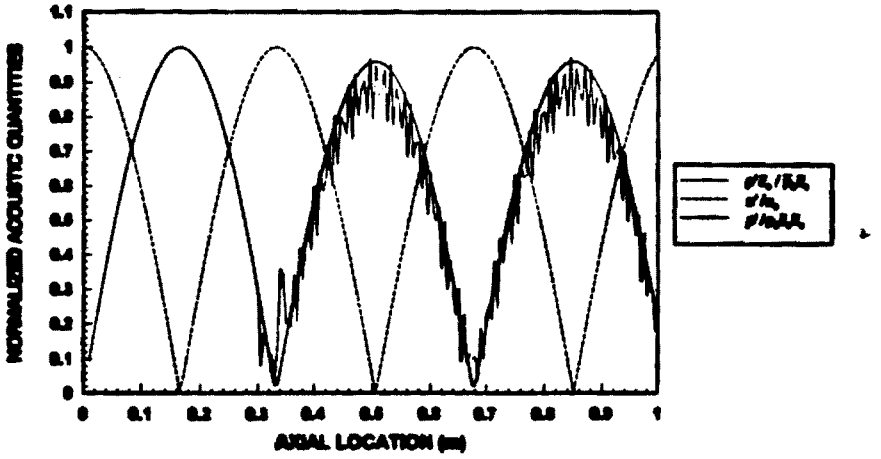

Figure 6. Normalized values of the acoustic pressure, axial velocity, and density calculated with wall injection in the temperature gradient region.

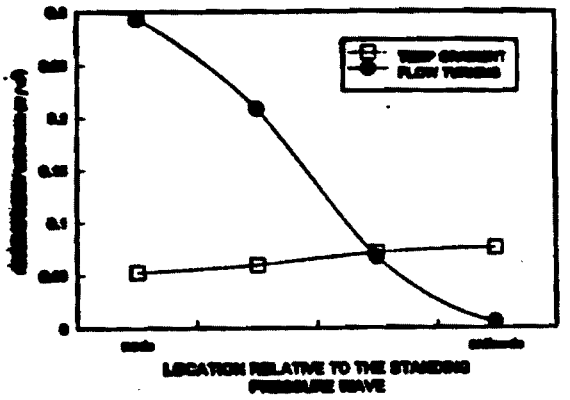

Figure 7. Comparison of the increase in convective losses due to the temperature gradient and the flow turning loss for injection/temperature change at various locations relative to the acoustic pressure.

temperature stability equation, except that the mean density must be treated as a function of position. The developed stability equation contains a term that is directly related to the presence of transverse temperature gradients that does not appear in the constant temperature equation and a heat addition term corresponding to Rayleigh's criterion. The presence of volume integrals in this equation, which appear as surface flux terms in previous analyses that did not account for mean temperature gradients, suggests that the presence of these gradients may drive or damp the oscillations.

Numerical integration of the governing equations provided some insight into the behavior of the various terms that appear in the developed stability equation. The numerical integration, however, shows only the effects of axial temperature gradients, because transverse gradients could not be adequately handled by this method. The presence of an axial temperature gradient was shown to affect the convective terms of the stability equation. The effects of temperature gradients were shown to be most significant in the vicinity of an acoustic pressure antinode in the chamber, where flow turning losses are smallest, and the effects were least significant in the vicinity of an acoustic pressure node, where flow turning losses are greatest.

References

1) McClure, F. T., Hart, R. W., and Cantrell, R. H., "Interaction Between Sound and Flow: Stability of T-Burners," *AIAA Journal*, Vol. 1, No. 3, March 1963.

2) Derr, R. L., Mathes, H. B., and Crump, J. E., "Application of Combustion Instability Research to Solid Rocket Motor Problems," *Proceedings of the 53rd Meeting of the NATO AGARD Propulsion and Energetics Panel*, Oslo, Norway, April 2-5, 1979.

3) Baum, J. D., "Acoustic Energy Exchange Through Flow Turning," AIAA Paper No. 87-0217, presented at the 25th Aerospace Sciences Meeting, Jan. 12-15, 1987, Reno, NV.

4) Sutton, G. P., *Rocket Propulsion Elements*, 5th Ed., pp. 310-312, John Wiley and Sons, Inc., 1986.

5) L. M. Matta, B. T. Zinn, and B. R. Daniel, "Theoretical Investigation of Flow Turning Losses in an Experimental Setup Which Simulates Instabilities in Solid Propellant Rocket Motors", AIAA Paper No. 92-0780, AIAA 30th Aerospace Sciences Meeting, Reno, NV, Jan 6-9, 1992.

6) L. M. Matta and B. T. Zinn, "Investigation Of Flow Turning Loss In A Simulated Unstable Solid Propellant Rocket Motor", AIAA Paper No. 93-0115, AIAA 31st Aerospace Sciences Meeting, Reno, NV, Jan 11-14, 1993.

7) Culick, F. E. C., "The Stability of One Dimensional Motions in a Rocket Motor", *Combustion Science and Technology*, Vol. 7, 1973, pp. 165-175.

8) Culick, F. E. C., "Stability of Three-Dimensional Motions in a Combustion Chamber," *Combustion Science and Technology*, Vol. 10, 1975, pp. 109-124.

9) Culick, F. E. C., "Remarks on Entropy Production in the One Dimensional Approximation to Unsteady Flow in Combustion Chambers," *Combustion Science and Technology*, Vol. 15, 1977.

10) Culick, F. E. C., Magiawala, K., Wat, J., Awad, E., and Kubota, T., "Measurements of Energy Losses Associated with Interactions Between Acoustic Waves and Non-Uniform Steady Flow," AFRPL-TR-81-22, 1981.

11) Culick, F. E. C., "Combustion Instabilities in Propulsion Systems," presented at The Winter Annual Meeting of the Society of Mechanical Engineers, San Francisco, CA December 10-15, 1989.

AIAA 94-0359

Exact Solution for One-Dimensional Acoustic Fields in Ducts with Axial Temperature Gradient

R. I. Sujith, G. A. Waldherr and B. T. Zinn
Department of Aerospace Engineering
Georgia Institute of Technology
Atlanta, GA 30332

32nd Aerospace Sciences Meeting & Exhibit
January 10-13, 1994 / Reno, NV

EXACT SOLUTION FOR ONE-DIMENSIONAL ACOUSTIC FIELDS IN DUCTS WITH AXIAL TEMPERATURE GRADIENT

R. I. Sujith, G. A. Waldherr and B. T. Zinn
Department of Aerospace Engineering
Georgia Institute of Technology
Atlanta, Georgia 30332

Abstract

In this study exact analytical solutions are developed for sound propagation in ducts with an axial mean temperature gradient. The one-dimensional wave equation for ducts with an axial mean temperature gradient is derived. The derived wave equation is then transformed to the mean temperature space. It is shown that by use of suitable transformations, the derived wave equation can be reduced to analytically solvable equations (e.g., Bessel's differential equation). The applicability of the developed technique is demonstrated by obtaining solutions for ducts with linear and exponential temperature profiles. These solutions are then applied to investigate the dependance of sound propagation in a quarter wave tube upon the mean temperature profile. Furthermore, the developed analytical solution is also used to extend the classical impedance tube technique to the determination of admittances of high temperature systems (e.g., a flame). The results obtained using the developed analytical solution are in excellent agreement with experimental as well as numerical results.

Nomenclature

English alphabets

a	constant in Eq. (17)
b, c	constants in Eq. (31)
c_0	speed of sound
c_1, c_2	constants of integration in Eq. (16) and Eq. (35)
C_p	specific heat at constant pressure
i	imaginary number, $\sqrt{-1}$
J_n	Bessel function of the n^{th} order
m	mean temperature gradient in Eq. (12)
$\dot{m}$	mass Flow rate
p'	acoustic pressure
P'	acoustic pressure amplitude
R	specific gas constant
s	transformation variable in Eq. (14)
t	time
T	temperature
$\bar{T}$	mean temperature
u	velocity
U	acoustic pressure amplitude
x	distance
w	transformation variable in Eq. (33)
Y_n	Neumann Function of the n^{th} order
z	transformation variable in Eq. (33)

Greek Alphabets

ρ	density
γ	ratio of specific heats (C_p/C_v)
ω	angular frequency
δ	constant in Eq. (37)
ϕ	phase of the standing wave pressure distribution

Subscripts

r	real
im	imaginary

Superscripts

$'$	oscillating quantity
$-$	time averaged quantity
$*$	complex conjugate

Introduction

The behavior of one dimensional acoustic fields in ducts with a mean temperature gradient is a problem of considerable scientific and practical interest. For instance, there is a need to develop an understanding of the manner in which a mean axial temperature gradient (caused, for example, by heat transfer to or from the walls) affects the propagation of sound waves and the stability of small amplitude disturbances in a duct. Such understanding will improve existing capabilities for controlling combustion instabilities in propulsion and power generating systems, designing pulse combustors and automotive mufflers, analyzing the behavior of resonating thermal systems, and measuring impedances of high temperature systems (e.g., flames). Consequently, there exists a need for obtaining exact analytical solutions that describe one dimensional wave systems in ducts with axial temperature gradients.

A physical description of the effect of a mean temperature gradient upon wave propagation in a duct may be obtained by assuming that the gas in the duct consists of infinitesimally thin gas layers, each at a different (constant) temperature, that are in contact with one another. In this case, propagation of sound from one layer to another is accompanied by wave transmission and reflection, which modifies the wave structure in the duct. To date, considerable efforts have been expended on the development of an understanding of wave propagation in such ducts and improving existing capabilities for controlling the behavior of practical systems where such phenomena occur.

The behavior of one dimensional waves in ducts with an axial temperature gradient is described by the solutions of a second order wave equation with variable coefficients [1]. Cummings [1] has developed an approximate analytical solution for ducts with arbitrary temperature gradients, while Munjal and Prasad [2] and K. S. Peat [3] have developed approximate solutions for ducts with small temperature gradients. Also, Kapur, Cummings and Munjur [4] solved this problem by numerically integrating the wave equation using a Runge-Kutta method. The same approach was followed by Zinn and his students [5-7] who developed the impedance tube technique for high temperature systems. While these numerical methods yield accurate answers, they often do not provide adequate insight into the physics of the problem. Moreover, since they cannot be implemented without the availability of an efficient computer, it is often difficult to incorporate these solution approaches into practical design procedures. These difficulties would be alleviated if analytical solutions of the equations that describe one dimensional acoustic oscillations in ducts with a temperature gradient were available.

Robins [8] developed an approach for obtaining analytical solutions of a related problem that is of interest in underwater acoustics; that is, wave propagation in water whose density and speed of sound vary with distance due to changes in water depth. Robins used an inverse approach to obtain density profiles that reduce the wave equation to a standard differential equation whose exact solutions are known. A significantly different analytical approach for solving such problems is presented in this paper.

A method for obtaining an exact solution that describes the behavior of one dimensional oscillations in a duct with an arbitrary axial temperature is outlined in this paper. The developed analytical solution procedure consists of several steps. First, the one-dimensional wave equation for a constant area duct with an arbitrary axial temperature gradient is derived for a perfect, inviscid and non heat conducting gas. Next, assuming periodic solutions, the derived wave equation is reduced to a second order ordinary differential equation with variable coefficients. Since the equation has variable coefficients, exact solutions of this equation for an arbitrary temperature profile cannot be obtained. To obtain an exact solution, the derived differential equation is transformed from the physical, x, space to the mean temperature, $\bar{T}$, space. Using appropriate transformations the resulting equation is then reduced to a standard differential equation (e.g., Bessel's differential equation), whose form depends upon the specific mean temperature profile in the duct. The application of the developed solution technique is demonstrated in this paper by obtaining analytical solutions for wave propagation in ducts with linear and exponential temperature profiles, and utilizing the developed solution in high temperature admittance measurements.

Derivation of the wave equation

The analysis begins with the development of the wave equation for a constant area duct with a mean temperature gradient. Assuming a perfect, inviscid and non heat conducting gas, the one dimensional momentum, energy and state equations can be expressed in the following form:

Momentum: $$\rho\frac{\partial u}{\partial t} + \rho u\frac{\partial u}{\partial x} + \frac{\partial p}{\partial x} = 0 \qquad (1)$$

Energy: $$\frac{\partial p}{\partial t} + u\frac{\partial p}{\partial x} + \gamma p\frac{\partial p}{\partial x} = 0 \qquad (2)$$

State: $$p = \rho RT \qquad (3)$$

Expressing each of the dependent variables as the following sums of steady and time dependent, small amplitude solutions:

$$u = \bar{u}(x) + u'(x,t)\ , p(x,t) = \bar{p}(x) + p'(x,t),$$
$$\rho(x,t) = \bar{\rho}(x) + \rho'(x,t) \qquad (4)$$

and substituting these expressions into the conservation equations yields systems of steady and wave equations. Assuming that the magnitude of the mean velocity is much smaller than the speed of sound, the solution of the steady momentum equation shows that the mean pressure, $\bar{p}$, is constant in the duct.

The wave equation is derived from the first order acoustic momentum and energy equations:

Momentum: $$\frac{\partial u'}{\partial t} + \frac{1}{\bar{\rho}}\frac{\partial p'}{\partial x} = 0 \qquad (5)$$

Energy: $$\frac{\partial p'}{\partial t} + \gamma\bar{p}\frac{\partial u'}{\partial x} = 0 \qquad (6)$$

Differentiating the momentum equation with respect to x and the energy equation with respect to t and eliminating the cross derivative term yields the following wave equation with variable coefficients.

$$\frac{\partial^2 p'}{\partial x^2} - \frac{1}{\bar{\rho}}\frac{d\bar{\rho}}{dx}\frac{\partial p'}{\partial x} - \frac{\bar{\rho}}{\gamma\bar{p}}\frac{\partial^2 p'}{\partial t^2} = 0 \qquad (7)$$

Differentiating the steady equation of state and recalling that the steady pressure is constant in the duct yields the following relationship between the steady temperature and density:

$$\frac{1}{\bar{\rho}}\frac{d\bar{\rho}}{dx} + \frac{1}{\bar{T}}\frac{d\bar{T}}{dx} = 0 \qquad (8)$$

Using Eq. (8), Eq. (7) can be reduced to the following form.

$$\frac{\partial^2 p'}{\partial x^2} + \frac{1}{\bar{T}}\frac{d\bar{T}}{dx}\frac{\partial p'}{\partial x} - \frac{1}{\gamma R\bar{T}}\frac{\partial^2 p'}{\partial t^2} = 0 \qquad (9)$$

Assuming that the solution has a periodic time dependance (i.e., $p'(x,t) = P'(x)\,e^{i\omega t}$), Eq. (9) reduces to the following second order ordinary differential equation for the complex amplitude $P'(x)$:

$$\frac{d^2P'}{dx^2} + \frac{1}{\bar{T}}\frac{d\bar{T}}{dx}\frac{dP'}{dx} + \frac{\omega^2}{\gamma R\bar{T}}P' = 0 \qquad (10)$$

Equation (10) has variable coefficients. Therefore, exact solutions of this equation for a general temperature profile $\bar{T}(x)$ cannot be obtained. An exact solution is obtained herein by first transforming Eq. (10) to the mean temperature space. Assuming that the mean temperature profile $\bar{T}(x)$ is known, Eq. (10) is transformed from the x to the $\bar{T}(x)$ space yielding the following differential equation:

$$\left(\frac{d\bar{T}}{dx}\right)^2\frac{d^2P'}{d\bar{T}^2} + \frac{1}{\bar{T}}\frac{d}{dx}\left(\bar{T}\frac{d\bar{T}}{dx}\right)\frac{dP'}{d\bar{T}} + \frac{\omega^2}{\gamma R}\frac{P'}{\bar{T}} = 0 \qquad (11)$$

In order to solve Eq. (11), the temperature profile, $\bar{T}(x)$, whose shape depends upon the physics of the problem, must be known. There are many mean temperature distributions $\bar{T}(x)$ for which Eq. (11) can be reduced to a standard differential equation whose solution is known. The manner in which this is accomplished is demonstrated in the remainder of this paper by considering two special cases; a duct with a linear temperature distribution and a duct with an exponential temperature distribution.

Acoustic behavior of a duct with a linear temperature distribution

This section investigates the acoustic characteristics of a duct with a linear mean temperature distribution that is given by the expression

$$\bar{T} = T_0 + mx \qquad (12)$$

where T_0 and m are constants that describe the temperature at $x = 0$ and the temperature gradient, respectively. Using Eq. (12), Eq. (11) can be reduced to the following form:

$$\frac{d^2P'}{d\bar{T}^2} + \frac{1}{\bar{T}}\frac{dP'}{d\bar{T}} + \frac{\omega^2/m^2}{\gamma R\bar{T}}P' = 0 \qquad (13)$$

To further simplify Eq. (13), a new independent variable s is introduced:

$$\bar{T} = \frac{m^2\gamma R}{4\omega^2}s^2, \qquad (14)$$

Transforming Eq. (13) from the $\bar{T}$ to the s space yields the following ordinary differential equation

$$\frac{d^2P'}{ds^2} + \frac{1}{s}\frac{dP'}{ds} + P' = 0 \qquad (15)$$

which is a zeroeth order Bessel's differential equation [9, 10]. The solution to Eq. (15) is well known [9,10] and given by

$$P' = c_1 J_0(s) + c_2 Y_0(s)$$

$$= c_1 J_0\left[\frac{\omega}{a}\sqrt{\bar{T}}\right] + c_2 Y_0\left[\frac{\omega}{a}\sqrt{\bar{T}}\right] \qquad (16)$$

where c_1 and c_2 are, in general, complex constants, J_0 and Y_0 are the Bessel and Neumann functions of order zero and the constant a is given by

$$a = \frac{|m|}{2}\sqrt{\gamma R} \qquad (17)$$

Using the derived solution for the acoustic pressure and the acoustic momentum equation, (i.e., Eq. (5)) the following expression for acoustic velocity can also be derived.

$$U'(x) = -\frac{1}{i\omega\rho}\frac{dP'}{dx} = -\frac{1}{i\omega\rho}\frac{dP'}{d\bar{T}}\frac{d\bar{T}}{dx}$$

$$= -\frac{m}{|m|}\frac{i}{\rho\sqrt{\gamma R\bar{T}}}\left(c_1 J_1\left[\frac{\omega}{a}\sqrt{\bar{T}}\right] + c_2 Y_1\left[\frac{\omega}{a}\sqrt{\bar{T}}\right]\right) \tag{18}$$

To determine the effect of a linear temperature gradient upon the acoustic properties of a duct, the developed solutions are used to investigate the acoustic characteristics of a duct closed at one end and open at the other (i.e., a quarter wave tube). Determination of the solution requires that the unknown constants c_1 and c_2 and the eigenvalue ω in Eq. (16) be determined by requiring that the solutions (i.e., Eq. (16) and (18)) satisfy the boundary conditions of the problem. The acoustic velocity U' is zero at the closed end of the duct (i.e., at $x = 0$, where $\bar{T} = T_1$), and the acoustic pressure P' is zero at the open end of the duct (i.e., at $x = L$ where $\bar{T} = T_2$). Requiring that U' and P' equal zero at the closed and open ends of the duct, respectively, yields the following set of two homogeneous algebraic equations:

$$c_1 J_1\left[\frac{\omega}{a}\sqrt{T_1}\right] + c_2 Y_1\left[\frac{\omega}{a}\sqrt{T_1}\right] = 0 \tag{19}$$

$$c_1 J_0\left[\frac{\omega}{a}\sqrt{T_2}\right] + c_2 Y_0\left[\frac{\omega}{a}\sqrt{T_2}\right] = 0 \tag{20}$$

Since these equations are homogenous, their solution requires that their determinant vanish, which yields the following relationship for the eigenfrequency ω.

$$J_0\left[\frac{\omega}{a}\sqrt{T_2}\right] Y_1\left[\frac{\omega}{a}\sqrt{T_1}\right] - J_1\left[\frac{\omega}{a}\sqrt{T_1}\right] Y_0\left[\frac{\omega}{a}\sqrt{T_2}\right] = 0 \tag{21}$$

Requiring that the acoustic pressure be a real quantity with a magnitude of P_1 at the closed end (i.e., $x = 0$) and that it equal zero at the other end (i.e., $x = L$), yields the following expressions for the unknown constants c_1 and c_2.

$$c_1 = -\frac{\pi\omega\sqrt{T_1}}{2a} P_1 Y_1\left[\frac{\omega}{a}\sqrt{T_1}\right]$$

$$c_2 = \frac{\pi\omega\sqrt{T_1}}{2a} P_1 J_1\left[\frac{\omega}{a}\sqrt{T_1}\right] \tag{22}$$

The dependence of the eigenfrequency ω upon the properties of the temperature distribution in the duct was investigated by solving Eq. (21) for different values of T_1, the temperature at the closed end and m, the temperature gradient (see Eq. (12)), for fixed values of T_2 = 300 K and L= 4 meters. The calculated eigenfrequencies are given in Table I.

T_1 (K)	c (K/m)	1st (Hz)	2nd (Hz)	3rd (Hz)	4th (Hz)	5th (Hz)
300	0	21.72	65.16	108.6	152.04	195.48
500	0.13	23.61	74.23	124.15	173.97	223.77
700	0.21	25.15	81.61	136.8	191.81	246.78
900	0.27	26.48	88	147.74	207.24	266.67
1,100	0.32	27.67	93.7	157.51	221.03	284.46

Table I: The variation of eigenvalues of a duct closed at one end and open at the other for different values of T_1, the temperature at the closed end. The temperature distribution in the tube in linear.

Table I shows that when there is a temperature gradient the higher harmonics are no longer integral multiples of the fundamental frequency as is the case in a duct with uniform temperature.

The effect of temperature gradient upon the distributions of the amplitudes of the acoustic pressure and velocity distributions was also investigated. Using the relationships

$$|P'|^2 = P'P'^*, \; |U'|^2 = U'U'^* \tag{23}$$

where P'^* and U'^* are the complex conjugates of P' and U' respectively, the amplitude distributions for two different values of m, are calculated, see Figs. (1) and (2). In these calculations, T_1 was varied while the values of T_2 and L were kept constant at 300 K and 4 m, respectively. The figures present the results for the cases m = 50 K/m, T_1 = 500 K and m = 200 K/m and T_1 = 1100 K. The eigenfrequencies are 136.8 Hz and 157.51 Hz respectively. The results show that the pressure and velocity nodes and anti-nodes are unevenly spaced, undoubtedly due to the spatial dependence of the speed of sound.

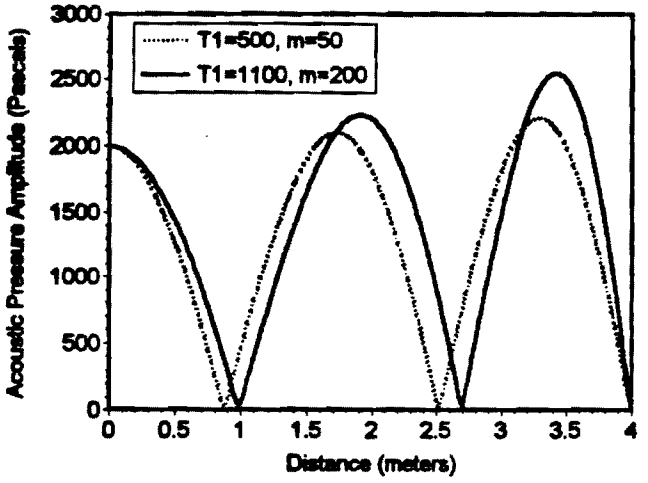

Figure 1 The variation of acoustic pressure with axial distance in a duct closed at one end and open at the other, for different linear mean temperature profiles.

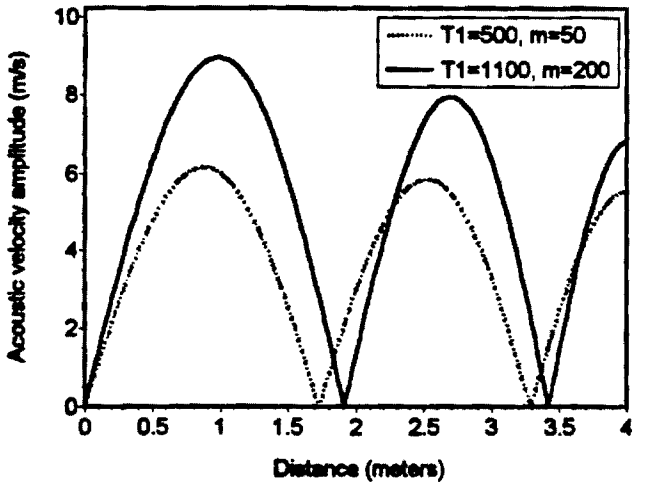

Figure 2 The variation of acoustic velocity with axial distance in a duct closed at one end and open at the other, for different linear mean temperature profiles.

To further check the validity of the results, the same problem was solved numerically by integrating the original conservation equations using a fourth order Runge-Kutta scheme. The axial mean temperature distribution was chosen to be $\bar{T} = 1100 - 200x$ K. The computed spatial dependence of the pressure amplitude is plotted in Fig. (3) for a frequency of 157.51 Hz, which is one of the eigenfrequencies of the problem. Examination of the figure shows that the analytical and numerical solutions are virtually identical; the difference is too small to be observed on the plots.

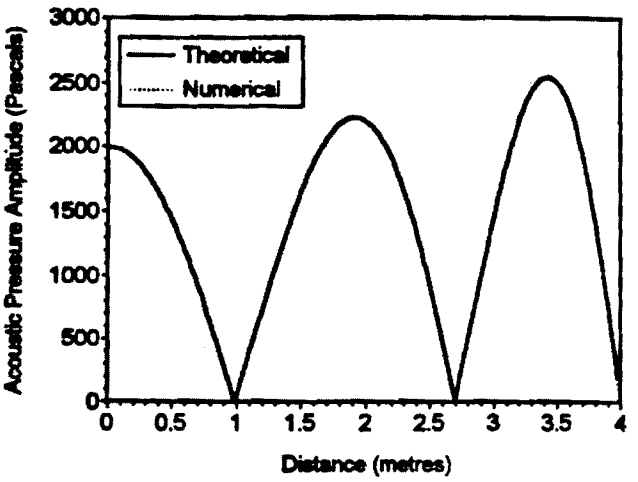

Figure 3 Comparison of analytical and numerical solutions of the acoustic pressure amplitude distribution in a duct closed at one end and open at the other end. (Frequency = 157.51 Hz, $\bar{T} = 1100 - 200x$ K.)

Impedance tube application

In this section, the application of the developed analytical solutions to the determination of unknown acoustic admittances in high temperature systems is presented. The acoustic properties of various systems or components are often described by specifying the acoustic admittances at their interface with other components. This acoustic admittance, y, is defined as the complex ratio of the local velocity perturbation normal to the interface and the local pressure perturbation; that is,

$$y = y_r + i\, y_{im} = \frac{\mathbf{u}' \bullet \mathbf{n}}{P'} \qquad (24$$

where $\mathbf{u}'$, $\mathbf{n}$, P', y_r and y_{im} represent the velocity perturbation vector, the unit normal vector pointing outwards from the interface, the pressure perturbation and the real and imaginary part of admittance, respectively. The admittance can be non-dimensionalized with respect to the mean pressure and the speed of sound yielding the following non-dimensionalized admittance Y:

$$Y = \frac{(\mathbf{u}' \bullet \mathbf{n})/c}{P'/(\gamma \bar{P})} \qquad (25$$

The magnitude and sign of the real part of admittance are directly related to the magnitude and direction of the acoustic energy flow at the measurement plane. When the real part of admittance is positive the component is driving, producing a net acoustic energy flux out of the component. On the other hand, when the real part of admittance is negative, the component is damping, producing a net acoustic energy flux into the component. The imaginary part of the admittance provides information about the time delay between the instants at which a wave is incident and reflected at an interface.

The classical impedance tube technique [11] is often used to determine unknown admittances. The impedance tube set-up consists of a tube with a driver at one end and the component whose admittance is measured at the other end. The driver excites an acoustic wave of specific frequency in the tube and the unknown admittance is determined from measurements of acoustic pressure amplitudes and phase distributions in the tube. When the mean temperature along the impedance tube is constant, analytical solutions that describe the dependance of the tube oscillations upon the unknown admittance can be readily obtained. Using these analytical solutions, the acoustic admittance can be determined from the measurements of maximum and minimum pressure amplitudes and the distance of the first acoustic pressure minimum from the interface whose admittance is being measured.

The classical impedance tube technique cannot be applied in high temperature situations, such as the measurement of a flame admittance. In this case, heat transfer from the hot combustion products to the walls of the impedance tube results in an axial mean temperature gradient along the tube. This complicates the determination of the unknown flame admittance. To date, in the absence of analytical solutions for acoustic waves in the presence of a temperature gradient, investigators [5-7] resorted to numerical solutions in their determination of the unknown flame admittance from the acoustic pressure measurements. This required an iterative solution technique in which pressure amplitudes and phase distributions along the impedance tube were predicted using assumed admittance boundary conditions and numerical integration of the acoustic conservation equations along the impedance tube. The predicted pressure distribution was then compared with the measured pressure distribution of the standing wave. The correct admittance was determined from the boundary condition that provided the best agreement between measured and the calculated acoustic pressure distributions. In order to accurately determine the admittance using numerical data reduction techniques, pressure measurements are required at a number (as many as possible) of locations along the impedance tube. To alleviate the difficulties associated with this procedure, an analytical expression for the admittance was obtained that enables the calculation of the acoustic admittance by measuring only the maximum and minimum pressure amplitudes and their locations, as in the classical impedance tube technique.

Substituting Eqs. (16) and (18) in Eq. (25), the following expression for the non-dimensional acoustic admittance at some location x, with a mean temperature $\bar{T}$ can be obtained:

$$Y = -i\,\frac{m}{|m|}\left[\frac{c_1 J_1\left[\frac{\omega}{a}\sqrt{\bar{T}}\right] + c_2 Y_1\left[\frac{\omega}{a}\sqrt{\bar{T}}\right]}{c_1 J_0\left[\frac{\omega}{a}\sqrt{\bar{T}}\right] + c_2 Y_0\left[\frac{\omega}{a}\sqrt{\bar{T}}\right]}\right] \qquad (26)$$

Using the conditions that P' is a real quantity at a pressure maximum (i.e., $|P'| = P_{max}$), where $\bar{T} = T_1$, that a minimum pressure amplitude, $|P'| = P_{min}$, occurs where $\bar{T} = T_2$, and $\frac{d|P'|}{dx} = \frac{d|P'|}{d\bar{T}}\frac{d\bar{T}}{dx} = 0$ at the pressure maximum, the following algebraic expressions for coefficients c_1 and c_2 can be derived from Eq. (16) and (18).

$$c_1 = -\frac{\pi\omega\sqrt{T_1}}{2a} P_{max}\, Y_1\left[\frac{\omega}{a}\sqrt{T_1}\right] + i\; Y_0\left[\frac{\omega}{a}\sqrt{T_1}\right] H$$

$$c_2 = \frac{\pi\omega\sqrt{T_1}}{2a} P_{max}\, J_1\left[\frac{\omega}{a}\sqrt{T_1}\right] - i\; J_0\left[\frac{\omega}{a}\sqrt{T_1}\right] H \qquad (27)$$

where

$$H = \pm\frac{1}{\Phi}\sqrt{P_{min}^2 - \left(\frac{\pi\omega}{2a}\right)^2 T_1 \Psi^2}$$

$$\Psi = Y_1\left[\frac{\omega}{a}\sqrt{T_1}\right] J_0\left[\frac{\omega}{a}\sqrt{T_2}\right] - J_1\left[\frac{\omega}{a}\sqrt{T_1}\right] Y_0\left[\frac{\omega}{a}\sqrt{T_2}\right]$$

$$\Phi = J_0\left[\frac{\omega}{a}\sqrt{T_2}\right] Y_0\left[\frac{\omega}{a}\sqrt{T_1}\right] - J_0\left[\frac{\omega}{a}\sqrt{T_1}\right] Y_0\left[\frac{\omega}{a}\sqrt{T_2}\right] \qquad (28)$$

The choice of sign for H depends upon whether the investigated system is driving or damping. This information can be obtained from the slope of the measured spatial dependence of the phase, which is given by

$$\tan\phi = q\frac{Y_1\left[\frac{\omega}{a}\sqrt{T_1}\right]J_0\left[\frac{\omega}{a}\sqrt{\bar{T}}\right]-J_1\left[\frac{\omega}{a}\sqrt{T_1}\right]Y_0\left[\frac{\omega}{a}\sqrt{\bar{T}}\right]}{J_0\left[\frac{\omega}{a}\sqrt{T_1}\right]Y_0\left[\frac{\omega}{a}\sqrt{\bar{T}}\right]-Y_0\left[\frac{\omega}{a}\sqrt{T_1}\right]J_0\left[\frac{\omega}{a}\sqrt{\bar{T}}\right]} \tag{29}$$

where

$$q = \frac{\pi\omega\sqrt{T_1}}{2a}\frac{P_{max}}{H} \tag{30}$$

Therefore, the sign of the slope of the phase distribution depends upon whether H was chosen to be positive or negative; H is chosen to be positive when the slope of the experimentally determined phase distribution is positive and vice versa. Salikuddin [12] has shown that the slope of the phase curve is positive when the measured component is damping and vice versa.

To check the validity of the developed solution approach, data obtained in an impedance tube study [13] of the driving of a mixing section of a Helmholtz combustor that burned natural gas and air were compared with the theoretical results of this study. The schematic of the set up used in reference [13] is shown in Fig. (4). A Helmholtz pulse combustor mixing chamber that burns natural gas was attached to one end of the tube. A standing wave pattern of a desired frequency and amplitude was established in the impedance tube using an electro-pneumatic acoustic driver installed at the opposite end of the tube. A piezo-electric pressure transducer was permanently attached to the tube wall at the interface of the mixing chamber and the impedance tube. A water cooled microphone was translated along the tube in order to measure the acoustic pressure distribution in the tube. Thermocouples were used to measure the radial temperature distributions at preselected axial locations, which were numerically integrated to obtain local bulk temperatures.

A linear temperature profile was fitted to the measured axial temperature distribution using the method of least squares, yielding $\bar{T} = 1253 - 235x$ K. The coefficients c_1 and c_2 of Eq. (16) were determined from the measured maximum and minimum acoustic pressure amplitudes and the mean temperature profile using Eq (27). The acoustic pressure amplitude distribution was then calculated using Eq. (23).

A comparison of the distributions of the experimental and predicted acoustic pressure amplitude for the measured temperature profile and a frequency of 34 Hz is shown in Fig. (5). An excellent agreement

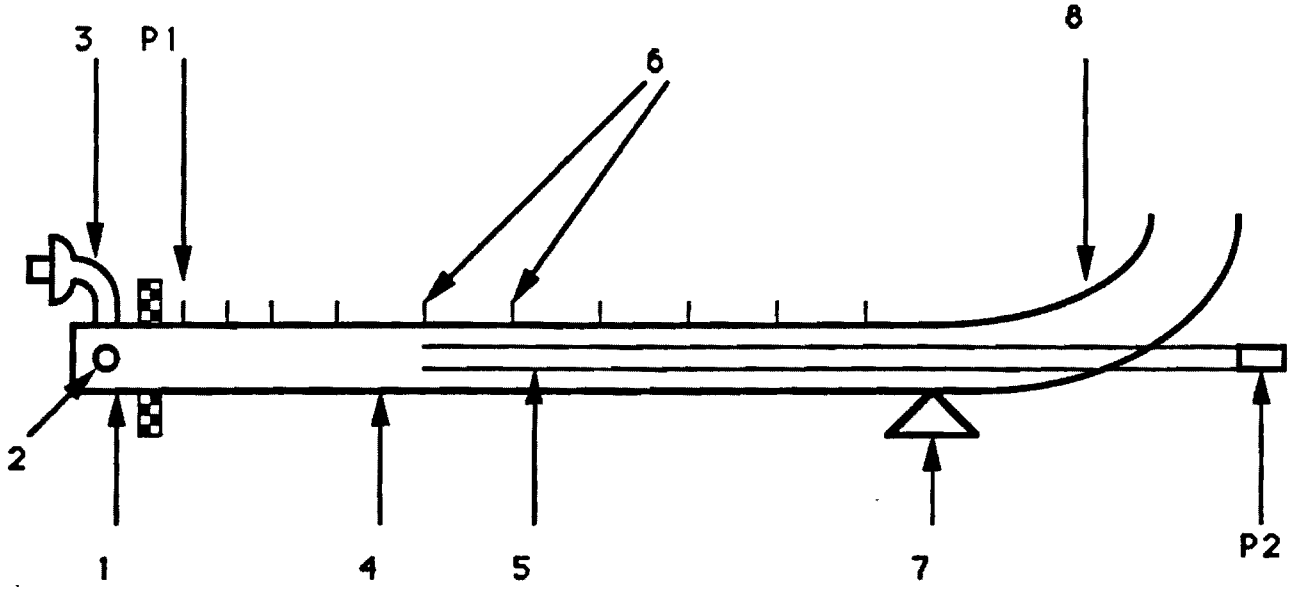

Figure 4 A schematic of the impedance tube set-up.
1-Mixing chamber, 2-Fuel flapper valve, 3-Air flapper valve, 4-Impedance tube, 5-Water cooled tube, 6-Thermocouples, 7-Driver, 8-Exhaust, P1 and P2- Pressure transducers

between the theoretical and the experimental values is observed. This agreement demonstrates that using the developed analytical technique, the unknown admittances of "high temperature" systems can be determined without resorting to the use of iterative and time consuming numerical solution techniques as has been done to date.

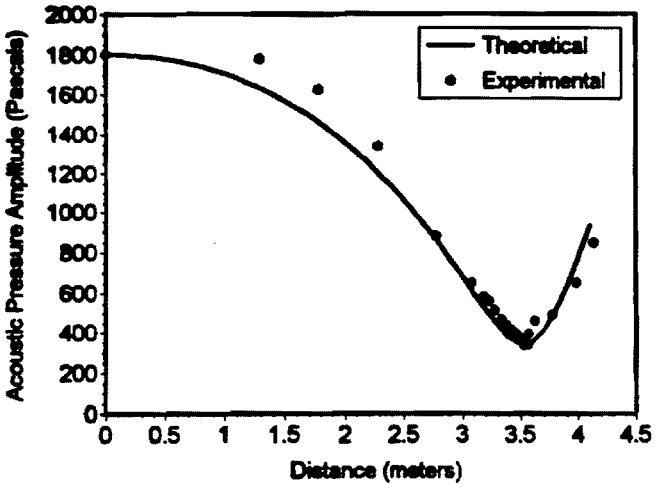

Figure 5 Comparison of the experimental and theoretical acoustic pressure amplitudes. (Frequency = 34 Hz, $\bar{T} = 1253 - 253x$ K.)

Acoustic behavior of a duct with an exponential temperature distribution

In the final part of the study, the developed solution technique was used to obtain a solution for wave propagation in a duct which has an exponential temperature profile which is given by the expression

$$\bar{T} = be^{-cx} \tag{31}$$

where b and c are constants. Using Eq. (31), Eq. (11) can be reduced to the following form:

$$\bar{T}^2 \frac{d^2P'}{d\bar{T}^2} + 2\bar{T} \frac{dP'}{d\bar{T}} + \frac{\omega^2}{\gamma Rc^2} \frac{P'}{\bar{T}} = 0 \tag{32}$$

To further simplify Eq. (32), the following variables w and z which replace P' and $\bar{T}$ respectively in Eq. (32) are introduced:

$$w = P'\sqrt{\bar{T}}\,, \quad z^2 = \frac{4\omega^2}{\gamma Rc^2}\frac{1}{\bar{T}}, \tag{33}$$

Transforming Eq. (32) from the P'-$\bar{T}$ space to the w-z space yields the following ordinary differential equation

$$\frac{d^2w}{dz^2} + \frac{1}{z}\frac{dw}{dz} + \left(1 - \frac{1}{z^2}\right) w = 0 \tag{34}$$

which is a first order Bessel's differential equation. The solution to Eq. (34) is given by [9, 10]

$$w = c_1 J_1(z) + c_2 Y_1(z) \tag{35}$$

where c_1 and c_2 are, in general, complex constants and J_1 and Y_1 are the Bessel and Neumann functions of first order. Therefore, the acoustic pressure P' can be expressed as

$$P' = \frac{1}{\sqrt{\bar{T}}}\left(c_1 J_1\left[\frac{\omega\delta}{\sqrt{\bar{T}}}\right] + c_2 Y_1\left[\frac{\omega\delta}{\sqrt{\bar{T}}}\right]\right) \tag{36}$$

where

$$\delta = \frac{2}{\sqrt{\gamma Rc^2}} \tag{37}$$

Analytical solutions can also be obtained for Eq. (11) when the temperature distribution has a quadratic or square root profile. It is also possible that analytical solutions for other temperature profiles may be determined by the described method.

To determine the effect of an exponential temperature gradient upon the acoustic properties of a duct, the developed solutions are used to investigate the acoustic characteristics of a duct closed at one end and open at the other (i.e., a quarter wave tube). To determine the unknown constants c_1 and c_2 and the eigenvalue ω in Eq. (36), the solution must satisfy the boundary conditions of the problem; that is, the acoustic velocity U' is zero at the closed end of the duct (i.e., at $x = 0$ where $\bar{T} = T_1$), and the acoustic pressure P' is zero at the open end of the duct (i.e., at $x = L$ where $\bar{T} = T_2$). Satisfying these boundary conditions yields the following set of two homogeneous algebraic equations.

$$c_1 J_1\left[\frac{\omega\delta}{\sqrt{T_1}}\right] + c_2 Y_1\left[\frac{\omega\delta}{\sqrt{T_1}}\right] = 0 \tag{38}$$

$$c_1 J_0\left[\frac{\omega\delta}{\sqrt{T_1}}\right] + c_2 Y_0\left[\frac{\omega\delta}{\sqrt{T_1}}\right] = 0 \tag{39}$$

Since these equations are homogeneous, their solution requires that their determinant vanish, which

yields the following relationship that must be satisfied by the eigenfrequencies.

$$J_0\left[\frac{\omega\delta}{\sqrt{T_1}}\right]Y_1\left[\frac{\omega\delta}{\sqrt{T_2}}\right]-J_1\left[\frac{\omega\delta}{\sqrt{T_2}}\right]Y_0\left[\frac{\omega\delta}{\sqrt{T_1}}\right]=0 \tag{40}$$

Requiring that the acoustic pressure be a real quantity with a magnitude of P_1 at the closed end (i.e., $x = 0$) and that it equal zero at the open end (i.e., $x = L$) yields the following expressions for the constants c_1 and c_2 in Eq. (36).

$$c_1 = \frac{\pi}{2}\omega\delta P\, Y_0\left[\frac{\omega\delta}{\sqrt{T_1}}\right]$$

$$c_2 = -\frac{\pi}{2}\omega\delta P\, J_0\left[\frac{\omega\delta}{\sqrt{T_1}}\right] \tag{41}$$

The dependance of the eigenfrequency ω upon the properties of the temperature distribution in the duct was investigated by solving Eq. (40) for different values of T_1, the temperature at the closed end and c in Eq. (31), for fixed values of T_2 =300 K and L = 4 meters. The calculated eigenfrequencies are given in table II. It can be seen that these eigenfrequencies are slightly different from those obtained for the same duct with a linear temperature gradient, but the same end temperatures. As in the case of a linear temperature gradient, the frequencies of the higher harmonics are not integral multiples of the fundamental frequency.

T_1 (K)	c (K/m)	1st (Hz)	2nd (Hz)	3rd (Hz)	4th (Hz)	5th (Hz)
300	0	21.72	65.16	108.6	152.04	195.48
500	0.13	23.35	73.4	122.81	172.1	221.35
700	0.21	24.42	79.22	132.79	186.2	239.55
900	0.27	25.2	83.72	140.56	197.18	253.72
1,100	0.32	25.82	87.42	146.95	206.22	265.39

Table 2 The variation of eigenvalues of a duct closed at one end and open at the other for different values of T_1, the temperature at the closed end. The temperature distribution in the tube in exponential.

The effect of temperature gradient upon the acoustic pressure and velocity distributions was also investigated. The acoustic pressure and the velocity amplitude distributions, calculated using Eq. (23), for two different values of c are presented in Figs. (6) and (7). In these calculations, T_1 was varied while the values of T_2 and L were kept constant at 300 K and 4 meters, respectively. The figures present results for the cases c = 0.13 K/m, T_1 = 500 K and c = 0.32 K/m and T_1 = 1100 K. The eigenfrequencies are 132.79 Hz and 146.95 Hz, respectively. As in the case of a linear temperature profile, these figures show that the acoustic pressure and velocity nodes and anti-nodes are unevenly spaced.

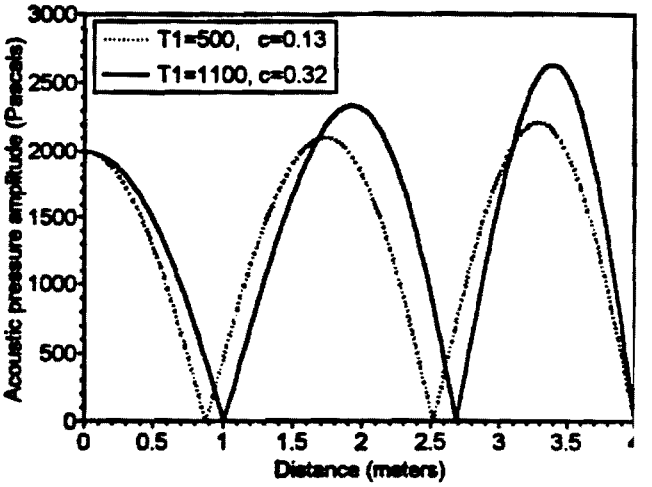

Figure 6 The variation of acoustic pressure with axial distance in a duct closed at one end and open at the other, for different exponential temperature profiles.

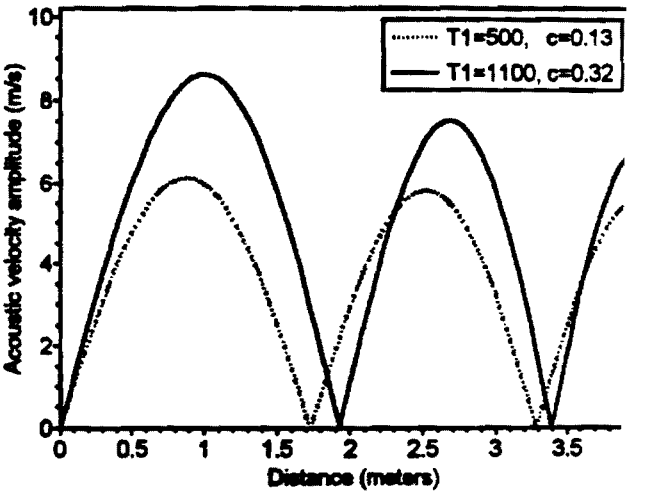

Figure 7 The variation of acoustic velocity with axial distance in a duct closed at one end and open at the other, for different exponential temperature profiles.

In order to validate the results, the problem was solved numerically by integrating the original conservation equations using a fourth order Runge-Kutta scheme. The axial mean temperature distribution was chosen to be $\bar{T} = 1100e^{-0.324821x}$ K. The acoustic pressure amplitude $|P|$ was obtained using Eq. (23) and its spatial dependence is presented in Fig. (8) for a frequency of 146.95 Hz, which is one of the eigenfrequencies of the problem. Examination of the figure shows that the analytical and numerical solutions are virtually identical; the difference is too small to be observed on the plots.

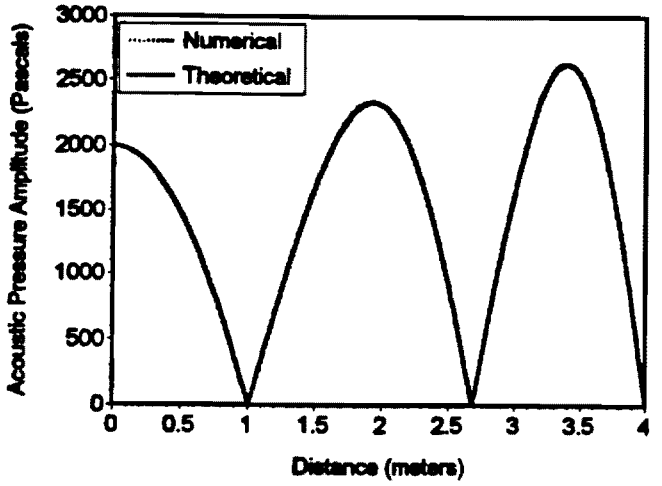

Figure 8 Comparison of analytical and numerical solutions of the acoustic pressure amplitude distribution in a duct which is closed at one end and open at the other end. (Frequency = 157.51 Hz, $\bar{T} = 1100e^{-0.324821x}$ K.)

Conclusions

A new approach for obtaining exact, analytical solutions of the behavior of one-dimensional acoustic oscillations in ducts with an axial temperature gradient was obtained by transforming the wave equation to the mean temperature space. Solutions were obtained for two special cases; a duct with a linear temperature profile and a duct with an exponential temperature profile. The developed solutions were then used to investigate the problem of sound propagation in a quarter wave tube, and to extend the classical impedance tube technique to the determination of admittances of combustion and other high temperature processes. The new analytical technique for solving the wave equation in the mean temperature space promises to considerably simplify the analysis of systems where one dimensional acoustic waves interact with axial mean temperature gradients, often encountered in problems related to combustion instabilities and pulse combustion.

Acknowledgment

This work was supported by the Gas research Institute under contract Number 5089-260-1839, for which Mr. James Kezerle was the contract monitor and AFOSR under contract number 91-0160, for which Dr. Mitat Birkam was the contract monitor.

References

1. A. CUMMINGS 1977 *J. Sound and Vibration* **51**, 55-67. Ducts with Axial Temperature Gradients: An Approximate Solution for Sound Transmission and Generation.

2. M. L. MUNJAL and M. G. PRASAD 1986 *J. Acoust. Soc. Am.* **80**, 1501-1506. On Plane-Wave Propagation in a Uniform Pipe in the Presence of a Mean Flow and a Temperature Gradient.

3. K. S. PEAT 1988 *J. Sound and Vibration* **123**, 43-53. The Transfer Matrix of a Uniform Duct with a Linear Temperature Gradient.

4. A. KAPUR, A. CUMMINGS, and P. MUNGUR 1972 *J. Sound and Vibration* **25**, 129-138. Sound Propagation in a Combustion Can with Axial Temperature and Density Gradients.

5. M. SALIKUDDIN and B. T. ZINN 1980 J. Sound and Vibration 68, 119-132. Adaptation of the Impedance Tube Technique for the Measurement of Combustion Process Admittances.

6. J. D. BAUM, B. R. DANIEL and B. T. ZINN 1980 *AIAA paper* No. **80-0281**. Determination of Solid Propellant Admittances by the Impedance Tube Technique.

7. B. T. ZINN, and L. NARAYANASWAMI 1982 *ACTA Astronautica* **9**, 303-315 Application of Impedance tube Technique in the Measurement of Driving Provided by Solid Propellants During combustion Instabilities.

8. A. ROBINS 1993 *J. Acoust. Soc. Am.* **93**, 1347-1352. Exact Solutions of the Helmholtz equation for Plane Wave Propagation in a Medium with Variable Density and Sound Speed.

9. M. HUMI and W. MILLER 1988 *Second Course in Ordinary Differential Equations for Scientists and Engineers*, Springer-Verlag.

10. M. ABRAMOWITZ and I. A. STEGUN 1970 Handbook of Mathematical Functions, 503-514. Newyork: Dover.

11. R. A. SCOTT 1946 An Apparatus for Accurate Measurement of the Acoustic Impedance of Sound Absorbing Materials, The Proceedings of the Physical Society, **58**, pp. 235-239

12. M. SALIKUDDIN 1978 *PhD Thesis, Georgia Institute of Technology*. Application of the Impedance Tube Technique in the Measurement of Burning Solid Propellent Admittances.

13. R.I. SUJITH, F. CHEN, B. R. DANIEL, J. I. JAGODA and B. T. ZINN 1992 Acoustic Characteristics of Pulse Combustor Mixing Chambers. *24th Symposium (International)* of Combustion/ The Combustion Institute, pp.1315-1321.

Active Control of Combustion Instabilities Using Real Time Identification of Unstable Combustor Modes

Y. Neumeier* and B. T. Zinn**
School of Aerospace Engineering
Geogia Institute of Technology
Atlanta, Georgia 30332-0150

* Post Doctoral Fellow
** David S. Lewis, Jr. Chair of Aerospace Engineering and Regents' Professor

Submitted to the Twenty-Fifth Symposium (International) on Combustion, The Combustion Institute, Pittsburgh, PA

Abstract

The theoretical foundation and performance of an active control system that rapidly characterizes and damps combustor instabilities whose characteristics are not known in advance are presented. The heart of this control system is an observer that uses, for example, a measured combustor pressure to determine the frequencies and amplitudes of the combustor modes in real time. This information is input into a controller that provides each mode with a gain and a phase shift prior to sending a signal to an actuator that injects an oscillating fuel stream into the combustor. The paper uses numerical simulations to demonstrate the capabilities of the developed controller. First, it is shown that the developed observer can determine the frequencies and amplitudes of oscillating modes without having any prior knowledge about their characteristics. Next, it is shown that this controller can identify and control instabilities involving several modes in linearly unstable systems. Finally, the ability of the developed controller to rapidly damp a nonlinear, shock-wave like, instability in a rocket combustor by controlling the fundamental mode and its harmonics is demonstrated.

Introduction

Instabilities in combustion systems in general and propulsion devices in particular occur when the combustion process excites one or more natural acoustic modes of the system [1]. Utilized approaches for eliminating these instabilities generally consist of one or more of the following: changing the magnitude and frequency of the driving provided by the combustion process, increasing the combustor's damping, preventing the excitation of unstable combustor modes, and shifting the frequencies of the combustor's unstable modes away from the range where the combustion process driving is maximized. Unfortunately, these passive control approaches are generally costly and time consuming, and often fail to adequately damp the instability. Consequently, interest in developing active control systems for stabilizing propulsion systems has increased in recent years. These efforts started with theoretical considerations of the subject in the 1950s [2-4], and the eventual demonstration of the potential of active control of combustion instabilities in the 1980s [5-15].

A typical actively controlled propulsion system consists of the combustor, a sensor that detects the instability, an observer that determines the state of the system, a controller that modifies the observer's output to provide a signal for the actuator, and an actuator that perturbs the system in a controlled manner. Ideally, such a controller must offer flexibility that will permit its application in

different systems, and it should perform effectively as the system's operating conditions change. In addition, such a controller should be capable of controlling the performance of systems whose behavior is not fully understood. Finally, it must be significantly less expensive and more dependable than existing approaches for suppressing combustion instabilities. While the development of such controllers was not possible in the past due to unavailability of needed components and appropriate control algorithms, recent developments of powerful microprocessors provide the computing power needed for the development of effective active controllers for unstable combustors. To complete the development of such active controllers, needed software must be developed. This paper presents a theoretical development that can serve as a foundation for the development of such software.

Reported active control systems have been designed to suppress instabilities consisting of one or two modes [14] whose characteristics are generally known in advance. These controllers utilize a pressure transducer and/or a photo-multiplier to measure the dynamic pressure and/or reaction rate, respectively. The sensor's signal is filtered, phase shifted, amplified and fed to the actuator, which may be a speaker [6, 16], an oscillating valve [17], or a fuel injector [11]. The design of these controllers is based upon the application of classical filtering and transfer function techniques. Consequently, these controllers can only damp instabilities consisting of a finite number of natural acoustic modes whose frequencies are sufficiently removed from one another. Such behavior is not always demonstrated by unstable combustors where the frequencies of the unstable modes may be close to one another. In fact, the differences between the frequencies of natural combustor acoustic modes relative to the magnitudes of the frequencies become smaller as the frequencies of the modes increase. Consequently, if the combustor experiences a high frequency mode instability, it becomes more difficult to filter its adjacent modes from the measured signal. This, in turn, may produce an interaction between the controller and stable system modes, which could result in the destabilization of stable combustor modes [12,15]. Such problems can be corrected by use of filters with a high rejection ratio whose performance is very sensitive to the frequency; that is, a small variation in the frequency of the controlled mode may cause significant changes in the gain and phase of the controller.

Billoud [12] proposed to overcome these difficulties by use of an adaptive control system. It uses an iterative scheme to optimize the controller parameters that stabilize a specific mode. While the performance of this controller is superior to those exhibited by fixed-parameter controllers, it has also, on occasion, destabilized stable system modes. It is also important to note that most known active controllers cannot identify the frequencies and amplitudes of the excited instability

modes. Instead, these controllers rely on previous knowledge of the characteristics of the instability to determine the mode(s) that needs to be controlled.

In an effort to provide a theoretical background needed for developing effective active controllers for unstable combustors, Fung et al. [18, 19] have proposed an active controller that is based upon a state feedback theory. This controller describes the unstable combustor behavior using solutions consisting of series of natural acoustic modes of the combustor [20, 21]. Fung modeled the unstable combustor as a linear system, and used a classical observer to estimate the state of the system from pressure measurements. This observer requires knowledge of the driving (by the combustion process), damping, and frequency of each controlled mode, to estimate the state of the system. These parameters are generally not known in advance, and capabilities for determining these parameters will have to be developed before this observer could be applied in actual propulsion systems.

This paper presents an approach for active control of combustion instabilities that overcomes some of the critical shortcomings of existing active control systems. It is based upon a novel observer that can rapidly identify the frequencies and amplitudes of the excited combustor modes, which are generally not known in advance. Furthermore, this observer can rapidly respond to (i.e., follow) changes in the characteristics of the instability. The information acquired by this observer is then used by the controller to optimally attenuate each unstable mode without destabilzing other combustor modes. The presentation of the developed active control system starts with a discussion of the theoretical foundation of the observer and a demonstration of its performance capabilities. Next, the manner in which this observer is applied in active control of an unstable rocket combustor is demonstrated in numerical simulations.

The Observer

Theory The proposed observer assumes that the oscillations in the combustor can be described in terms of a time varying frequency spectrum. The time dependence of such a spectrum can be studied by wavelet analysis, as recently demonstrated by Gutmark [22] who applied this technique to evaluate the temporal dependence of the pressure oscillations in a controlled combustor. The implementation of wavelet analysis involves, however, an analysis of a continuous spectrum between set frequency limits, which requires a considerable numerical effort. This, in turn, limits the practicality of using wavelet analysis as a real time observer in a closed loop controller. The developed observer uses an alternate approach to reduce the required

numerical efforts. It identifies the finite number of modes that significantly contribute to the investigated oscillations, and only analyzes the behavior of these modes.

The developed observer assumes that the combustor oscillations are quasi-periodic, consisting of several acoustic modes and their harmonics. Accordingly, a measured unstable combustor pressure, $p'(t)$, is expressed in the following series solution form:

$$p'(t) = \sum_{i=1}^{i=K} p_i(t); \text{ where } p_i(t) = \sum_{n=1}^{n=M} A_{n,i}(t)\sin(n\omega_i t + \phi_{n,i}(t)) \qquad (1)$$

where $p_i(t)$ is one of the K modes present in the combustor. Each of the modes $p_i(t)$ is expressed as a series solution consisting of M terms whose "instantaneous" amplitudes, $A_{n,i}$, and phases, $\phi_{n,i}$, are obtained by use of the following expressions that are similar to those used in Fourier series analysis:

$$A_{n,i}(t) = (S_{n,i}(t)^2 + C_{n,i}(t)^2)^{.5}; \quad S_{n,i}(t) = \frac{2}{T}\int_{t-T}^{t} p_i'(t)\sin(n\omega_i t)dt \text{ and } C_{n,i}(t) = \frac{2}{T}\int_{t-T}^{t} p_i'(t)\cos(n\omega_i t)dt$$

$$\phi_{n,i}(t) = \tan^{-1}(C_{n,i}(t) / S_{n,i}(t)) \qquad (2)$$

Because of the required numerical effort, utilization of Eqs. 2 may not be practical for real time processing. Consequently, the above equations are replaced by the following relationships:

$$S_{n,i}(t+dt) = \frac{2}{T}\int_{t-T+dt}^{t+dt} p_i'(t)\sin(n\omega_i t)dt = S_{n,i}(t) + \frac{2}{T}[p_i(t+dt) - p_i(t-T+dt)]\cdot\sin(n\omega_i t)\cdot dt \qquad (3)$$

$$C_{n,i}(t+dt) = \frac{2}{T}\int_{t-T+dt}^{t+dt} p_i'(t)\cos(n\omega_i t)dt = C_{n,i}(t) + \frac{2}{T}[p_i(t+dt) - p_i(t-T+dt)]\cdot\cos(n\omega_i t)\cdot dt \qquad (4)$$

that enable the observer to "follow" the state of the combustor in real time.

The observer starts the calculations assuming that the measured combustor oscillation $p'(t)$ consists of a single mode $p(t)$ that is oscillating with a frequency ω_1, ignoring (initially) the possible presence of additional modes. Calculations for an oscillation consisting of a single mode have shown that when the assumed frequency ω_1 is wrong, the calculated pressure $p'(t)$ (using Eqs. 1 and 2) nevertheless oscillates with the correct frequency ω_2 of the measured pressure signal, but the phase $\phi_1(t)$ of the first term in the series expansion varies with time (these results are

not shown here due to paper length limitations). Examination of the calculated pressure showed that the time rate of change of the phase $\phi_1(t)$ can be expressed in the following form

$$\dot{\phi}_1 = \bar{\dot{\phi}}_1 + \tilde{\dot{\phi}}_1 \tag{5}$$

where $\bar{\dot{\phi}}_1$ is a mean value and $\tilde{\dot{\phi}}$ is an oscillating quantity. The fact that the calculated (using an incorrect frequency ω_1) and input pressures oscillate with the correct frequency ω_2 implies that $\bar{\dot{\phi}}_1$ satisfies the following relationship:

$$\bar{\dot{\phi}}_1 = \omega_1 - \omega_2 \tag{6}$$

where ω_1 and ω_2 are the assumed and correct frequencies, respectively. Equation 6 was then used to develop an iterative procedure that converges to the correct frequency ω_2.

When several modes $p_i(t)$ are present in the measured pressure $p(t)$, the above discussed solution procedure yields the frequency of the dominant mode, which is the one with the largest amplitude. Simultaneously, the observer uses the determined characteristics of the dominant mode to calculate $p_1(t)$, which is subtracted from the measured pressure signal $p(t)$. The observer then proceeds to determine the characteristics of the next dominant mode in the "remaining" pressure signal. This procedure is continued until the characteristics of all the modes that need to be controlled are identified at a given instant. This procedure is repeated, at each time step, to determine the temporal variation of the characteristics of the controlled modes.

Observer Performance. To demonstrate the ability of the observer to identify the hierarchy of modes in the input signal, it has been provided with an oscillation consisting of two modes whose frequencies and amplitudes slightly differ from one another; that is,

$$p'(t) = 1.3\sin(270 \bullet 2\pi t) + \cos(200 \bullet 2\pi t)$$

The observer's performance is described in Figs. 1-a, b. The calculation started assuming that all modes oscillated with an assumed frequency of 120 Hz. Figure 1-a shows that the observed frequencies rapidly converged to the correct values of 270 and 200 Hz. The calculated 270 Hz. frequency is modulated by a 70 Hz. oscillation due to the presence of the second mode in the input signal that used in the initial identification of the "first" dominant mode. Such a modulation is not

superimposed upon the calculated 200 Hz. frequency because it was calculated using a signal primarily consisting of second mode oscillations.

In the above example, the observer expressed each of the modes as a series solution consisting of five harmonics (i.e., M=5 in Eq. 5). A comparison of the pressure computed by the observer, using the series solutions for each of the two modes, with the input pressure over a .05 seconds time interval is presented in Fig. 1-b. It clearly shows that the observer can "reproduce" the input pressure with high fidelity.

Active Control of Unstable Combustors

Control of Linear Instabilities. Demonstrations of the capabilities of the developed active control system start with a numerical simulation of the control of a linearly unstable system, see Fig. 2. The investigated combustor behavior is described by the collective response of six oscillators [20,21] whose frequencies equal 100, 220, 350, 430, 600 and 800 Hz. The instability is introduced by assuming that the 430 and 800 Hz. modes have negative damping, while the remaining modes have small positive damping. The active control system consists of a sensor that measures the combustor's pressure, transfers it to the observer that determines the combustor pressure using the observed state of the modes and transfers its output to the controller. The latter modifies its input signal by a prescribed gain and a phase shift, and transmits its output to the actuator, which introduces a heat addition oscillation $\dot{q}$ into the combustor. Fig. 2

While the developed observer provides the active control system with a capability to simultaneously identify and control all the modes that significantly contribute to the instability, its capabilities are demonstrated in this example by controlling one mode at a time. This, in turn, produces an interesting system behavior in which the control system attenuates the instability by alternate damping of the two unstable modes.

The simulation starts with the controller off and the observer starting its search for the dominant combustor mode with an assumed frequency of 1000 Hz. Since two of the modes are unstable, the combustor pressure initially increases exponentially with time, see Fig. 3-a. At time t=.05, the controller is activated, resulting in subsequent damping of the oscillations. It should be noted that after activating the controller, the combustor pressure amplitude increases and decreases in an oscillatory fashion as it approaches zero. The cause of this behavior can be understood by considering Fig. 3-b where the frequency of the dominant mode of the instability, as determined by Figs 3-a,b

the observer, during different time periods is described. It shows that the observer initially identifies the 800 Hz. oscillation as the dominant combustor mode. Activation of the controller at t=.05 results in rapid attenuation of this mode. As this mode is attenuated, the observer identifies the 430 Hz. mode as the dominant mode of the instability. Consequently, the active control system switches control to this mode, resulting in its rapid attenuation. While the 430 Hz. mode is attenuated, the 800 Hz. mode, which is not controlled during this period, starts amplifying again. As this occurs, the controller switches control again to the 800 Hz. mode. The continuous switching of the control action between the two unstable modes eventually leads to their attenuation. The switching of the controller action between these two modes is responsible for the observed oscillatory variation of the combustor pressure amplitude as it decays towards zero, see Fig. 3-a.

Control of an Unstable Rocket Motor. This section demonstrates the application of the developed active control system to stabilize an unstable rocket combustor, see Fig. 4. The rocket is supplied with reactants through an upstream injector and the instability is driven by a feedback process between the pressure and combustion process heat addition oscillations that is characterized by a time delay τ_c. The active control system consists of an observer, a controller and an actuator that supplies the combustor with a periodic fuel flow rate. Following Rayleigh's criterion [23], the active control system attenuates the instability by producing an oscillatory heat addition that is 180° out of phase with the combustor pressure oscillations. To accomplish this goal, the controller must account for the "inherent" time delay, τ_d, introduced by the actuator, mixing, and reaction processes associated with the combustion of the secondary fuel stream.

The behavior of the unstable combustor was numerically simulated by the solution of the following one dimensional conservation equations:

Continuity: $$\frac{\partial \rho}{\partial t} + \frac{\partial (\rho u A)}{\partial x} = 0 \qquad (7)$$

Momentum: $$\frac{\partial (\rho u A)}{\partial t} + \frac{\partial (\rho u^2 A + pA)}{\partial x} = 0 \qquad (8)$$

Energy: $$\frac{\partial (\rho A (e + \frac{u^2}{2}))}{\partial t} + \frac{\partial (\rho u A (h + \frac{u^2}{2}))}{\partial x} = \dot{q} \cdot A \qquad (9)$$

where ρ, A, u, p, e, h, $\dot{q}$, x, *and* t are the density, area, velocity, pressure, internal energy, enthalpy, volumetric heat addition, axial location and time, respectively. The state variables are

related to one another by appropriate perfect gas equations of state. The heat addition $\dot{q}$ is described by

$$\dot{q} = \bar{q} + \dot{q}_i + \dot{q}_c \tag{10}$$

where $\bar{q}$, $\dot{q}_i$, *and* $\dot{q}_c$ are the mean heat addition, oscillatory heat addition that drives the instability, and the controller heat addition. In this simulation, the oscillatory heat addition that drives the instability, $\dot{q}_i$, has been assumed to be governed by the following first order differential equation:

$$\frac{d\dot{q}_i}{dt} + \tau_c \dot{q}_i = p \tag{11}$$

where τ_c is the time delay between the $\dot{q}_i$ and p oscillations.

Equations 7 through 9 were solved numerically using the MacCormack predictor-corrector algorithm [24]. The effect of the mean heat addition $\bar{q}$ was accounted for by assuming that the mean temperature of the injected reactants is the adiabatic flame temperature. The boundary conditions at the injector plane required that the flow rate and stagnation temperature of the incoming flow be constant. The nozzle was assumed to be compact (and, thus, quasi-steady), and its boundary condition was given by the relationship between the pressure and flow rate at the nozzle entrance. Finally, it was assumed that the heat addition process was confined to the second spatial element of the numerical grid.

The presence of a time delay τ_d between the actuator's input and actual heat addition indicates that these oscillations are related to one another by the following relationship:

$$\dot{q}_c(t) = \dot{q}_{input}(t - \tau_d) \tag{12}$$

where $\dot{q}_{input}$ is the actuator input signal. In order for $\dot{q}_c$ to be 180° out of phase with the combustor pressure oscillations, the controller must compensate for this time delay by introducing an appropriate phase shift.

In this example, the instability was controlled by only observing the five harmonics that describe the behavior of the most dominant combustor mode. Control was accomplished by multiplying each observed harmonic by a negative constant $-k_n$ and adding a phase shift that cancels the effect of the inherent time delay τ_d. Thus, the actuator input signal becomes:

$$\dot{q}_{comp}(t) = \sum_{n=1}^{n=N} -k_n A_n(t) \sin(n\omega(t)t + \phi_n(t) + \phi_m(t)) \qquad (13)$$

where

$$\phi_m(t) = n\omega(t)\tau_d \qquad (14)$$

It should be pointed out that the frequency $\omega(t)$ is expressed as a function of time in Eqs. 13-14 because it varies with time while the observer computes the frequency of the dominant mode of the instability.

The numerical simulation of the controlled rocket motor behavior was initiated with the control element off, which required that $\dot{q}_c$ be zero in Eq. 10. To save computation time, the simulation was initiated using a known steady state solution as an initial condition. The combustor oscillations were initiated by adding a perturbation to the steady pressure in one of the spatial grid elements. The simulation assumed that the calculated pressure at the injector face was the "measured" observer input. The observer then analyzed the input pressure signal using a five mode series expansion. The calculated modes amplitudes and phases were then used as an input for the controller.

Figure 5-a shows a comparison of the measured and calculated (by the observer) combustor pressure before and after the activation of the control system, and Fig. 5-b shows the variations of the amplitudes of the calculated modes during the same time period. These figures show that the amplitudes of the combustor pressure and its five harmonics increase with time, apparently reaching a limit cycle behavior, before the controller is activated. It is interesting to note that the predicted combustor pressure oscillations exhibit a highly nonlinear, shock-wave like, behavior prior to activating the controller. Figure 5-c presents the time dependence of the ratio of the observed frequency and the frequency of the fundamental mode of the combustor. It demonstrates that in spite of the large error in the initially assumed frequency, the observer rapidly converged to the correct frequency prior to activation of the controller. Figures 5-a and 5-b show that activation of the controller, at t=.04 seconds, resulted in rapid damping of the instability; the pressure and the observed amplitudes of the dominant mode and its harmonics decreased to a small fraction of their initial values .02 seconds after activating the controller.

It is also important to note that the developed controller did not destabilized any stable combustor modes in any of the examples in this section.

Summary

The theoretical foundation and performance of an active control system that can rapidly identify and damp combustion instabilities are presented. This control system is based upon a novel observer that can characterize the modes that contribute to the instability in real time without any prior knowledge about the instability. Unlike classical observers, the one presented in this paper only requires a measured signal. This, in turn, provides the developed control system with flexibility that permits its application to variety of systems, including those whose behavior is not fully understood.

Acknowledgment

This research was supported by an AFOSR Grant No. F49620-93-1-0177, monitored by Dr. Mitat Birkan.

References

1. Harjee, D. and Reardon, F. (Eds.), "Liquid Propellant Rocket Combustion Instability", NASA SP 194, 1972.

2. Tsien, H. S., ARS Journal. 22, 256, 1952.

3. Marble, F. E. and Cox, D. W., Jr., ARS Journal. 23, 63, 1953.

4. Crocco, L. and Cheng, S. I. (1956). "Theory of Combustion Instability in Liquid Propellant Rocket Motors", AGARDograph No. 8, Butterworths Scientific Publications, London.

5. McManus, K. R., Poinsot, T. and Candel, S. M., Prog. Energy Combust. Sci. 1993, Vol. 19, pp. 1-29

6. Dines, P. J., "Active Control of Flame Noises," Ph.D. Thesis, Cambridge University, Cambridge, England, 1984.

7. Bloxside, G. J., Dowling, A. P., Hooper, N. and Langhorne, P. J., AIAA J. 26, p. 783 (1988)

8. Lang, W., Poinsot, T. and Candel, S, Combustion and Flame, 70, 281, 1987.

9. Poinsot, T., Bourienne, F., Candel, S., Esposito, E. and Lang, W., Journal of Propulsion and Power, 5 (1), 14, 1987.

10. Poinsot, T., Veynante, d., Bourienne, F., Candel, S., Esposito, E. and Surget, J., "Initiation and Suppression of Combustion Instabilities by Active Control," Proceedings of the 22nd Symposium (International) on Combustion, 1363, 1988.

11. Langhorne, P. J., Dowling, A. P. and Hooper, N., Journal of Propulsion and Power, 6 (3), 324, 1990.
12. Billoud, G., Galland, M. A., Huynh Huu, C. and Candel, S., Combust. Sci. and Tech., 1992, Vol. 81, pp. 257-283.
13. Gutmark, E., Parr, T. P., Parr, D. M. and Schadow, K. C., The 7th Symposium on Turbulent Shear Flows, Stanford University, Calif., Aug. 1989
14. Gutmark, E., Wilson, K. J., Parr, T. P. and Schadow, K. C., AIAA Paper 92-0778, 30th Aerospace Sciences Jan. 1992, Reno, Nevada.
15. Gulati, A. and Mani, R., AIAA Paper 90-0270, 28th Aerospace Science Meeting 1990, Reno, Nevada.
16 Heckl, M. A., IUTAM Symposium on Aero and Hydro-Acoustics, Springer Verlag, pp. 211-216, 1985
17 Hendricks, E. W., Sivasegaram, S. and Whitelwa, J. H., "Control of Oscillations in Ducted Premixed Flames", Paper presented in the IUTAM Meeting, Taipei, Taiwan, June 1991.
18. Fung, Y. (1991). "Active Control of Linear and Nonlinear Pressure Oscillations in Combustion Chambers," Ph.D. Thesis, The Pennsylvania State University, University Park, Pennsylvania.
19. Fung, Y. and Yang, V. (1991). "Active Control of Nonlinear Pressure Oscillations in Combustion Chambers," to be presented at the 27th AIAA/ASME/SAE/ASEE Joint Propulsion Conference, Sacramento, CA, June 1991.
20. Zinn, B. T. and Lores, M. E., Combustion Science and Technology. 4, 269, 1972.
21. Culick, F. E. C., "Combustion Instabilities in Liquid Fueled Propulsion Systems-An Overview." California Institute of Technology Report, 1988.
22. Gutmark, E., Parr, T. P., Hanson, D. M., Shadow, K. C. and Hewer, G. A. "Wavelet Analysis of a Controlled Pulsating Flame," Proceedings of the International Symposium on Pulsating Combustion Volume II Monterey Calif., Aug. 1991
23 Rayleigh, L., "The Theory of Sound", Dover Pub., New York, 1945.
24 MacCormack, R. W., AIAA Paper 69-354, 1969.

Figure 1-a. Observed frequencies of the first and second dominant combustor modes.

Figure 1-b. Comparison of observer input and output signals.

Figure 2. A schematic of the linear model of an actively controlled combustor.

Figure 3-a. Time dependence of the pressure in linearly unstable combustor pressure prior and after controller activation.

Figure 3-b. Time dependence of the observed frequency of the dominant mode of the combustor pressure oscillations.

Figure 4. A block diagram of the simulated, actively controlled, rocket combustor

Figure 5-a. Time dependence of the measured and observed pressure oscillations in the rocket combustor prior and after controller activation.

Figure 5-b. Time dependence of the amplitudes of the observed fundamental pressure oscillation and its harmonics.

Figure 5-c. Time dependence of the observed fundamental mode frequency.

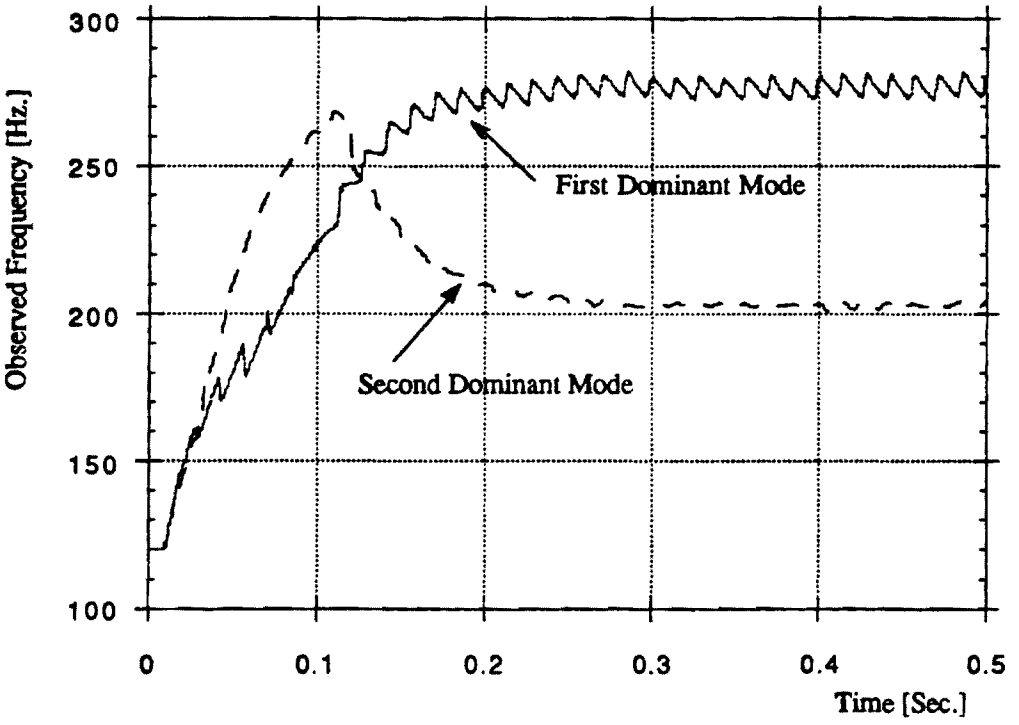

Neumeier, Zinn, Figure 1-a.

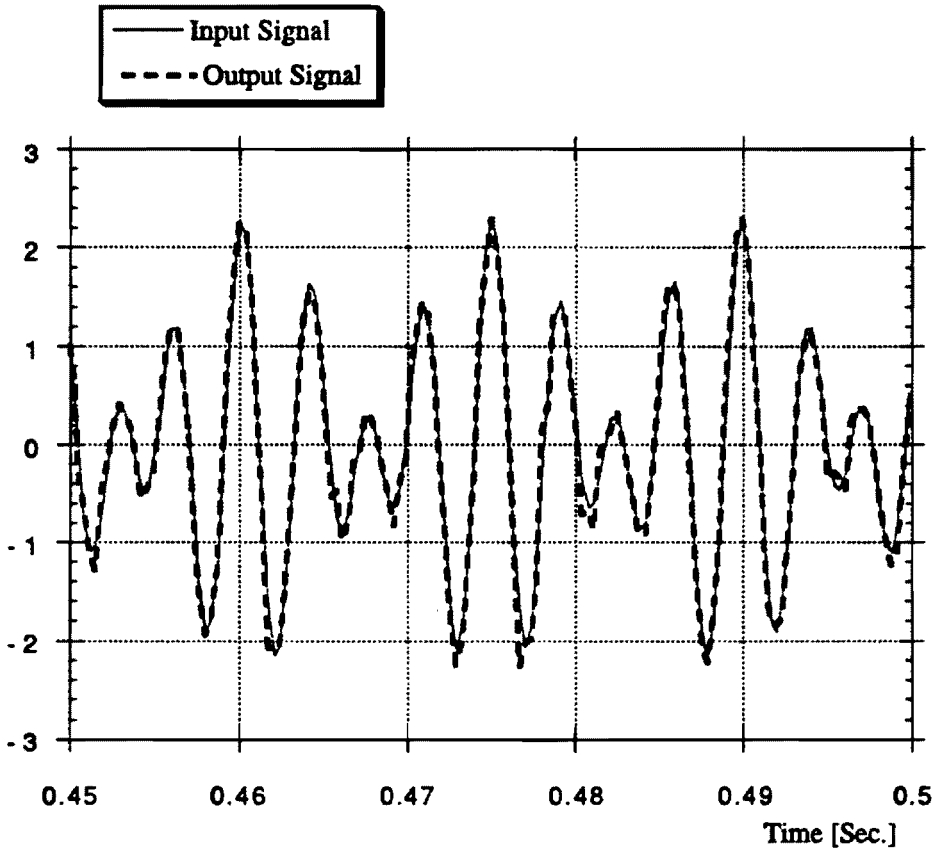

Neumeier, Zinn, Figure 1-b.

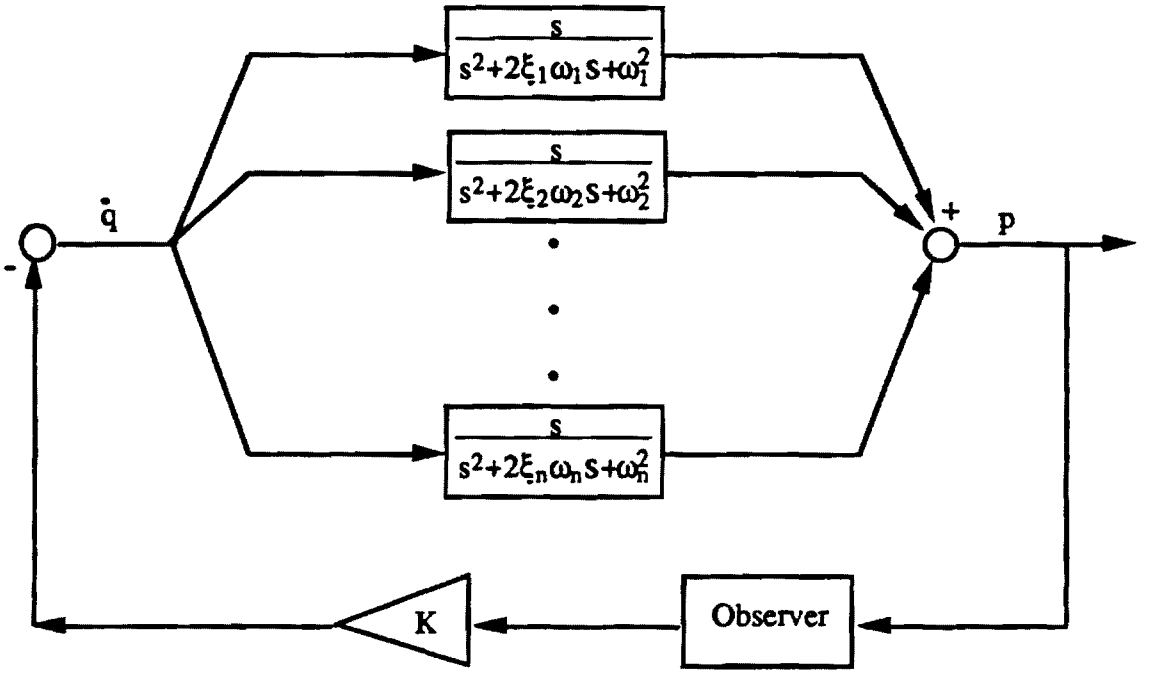

Neumeier, Zinn, Figure 2.

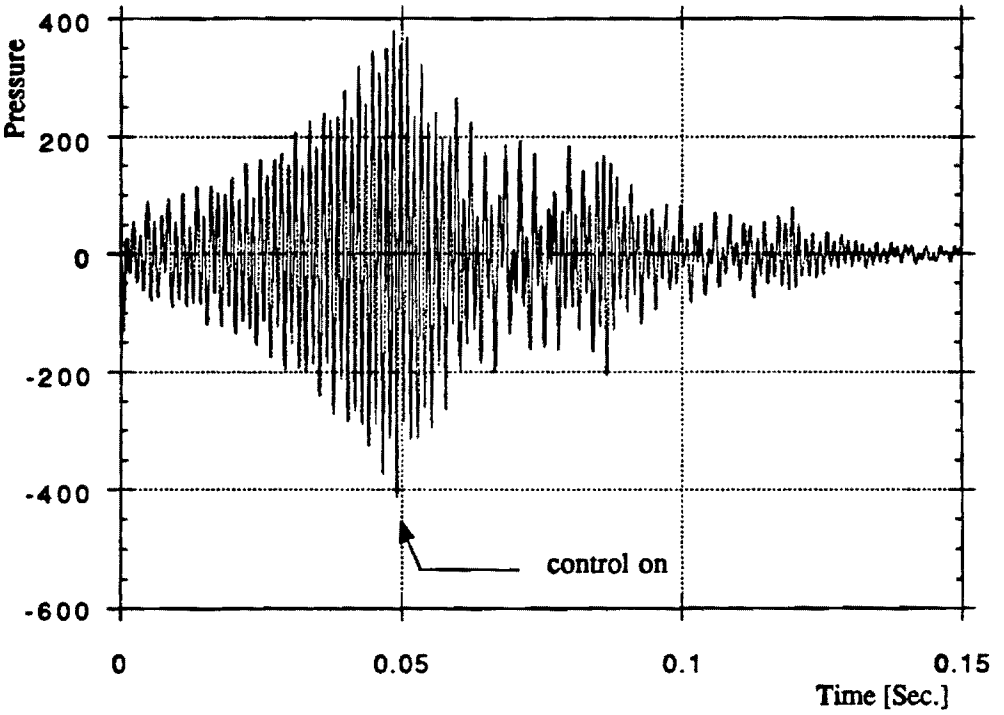

Neumeier, Zinn, Figure 3-a.

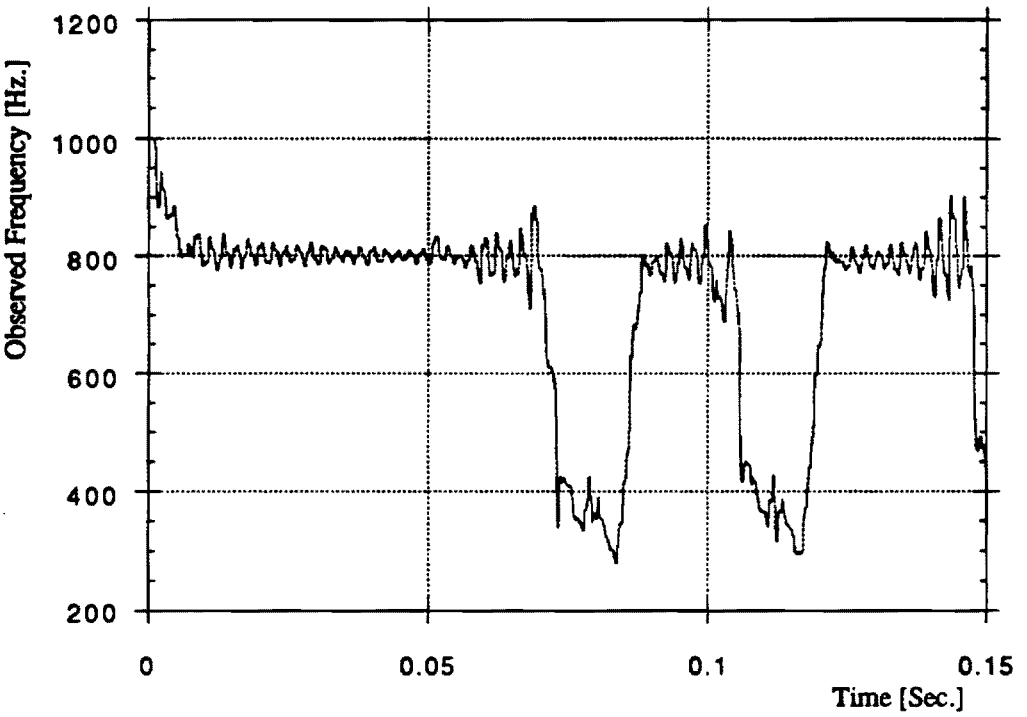

Neumeier, Zinn, Figure 3-b.

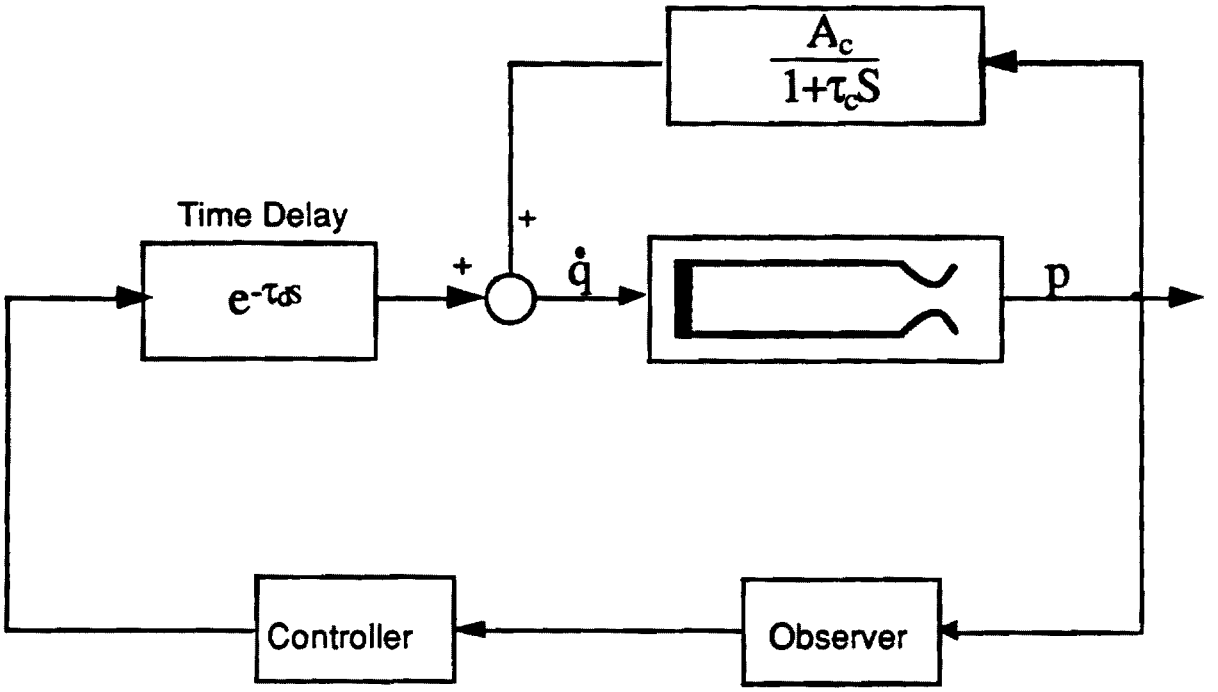

Neumeier, Zinn, Figure 4.

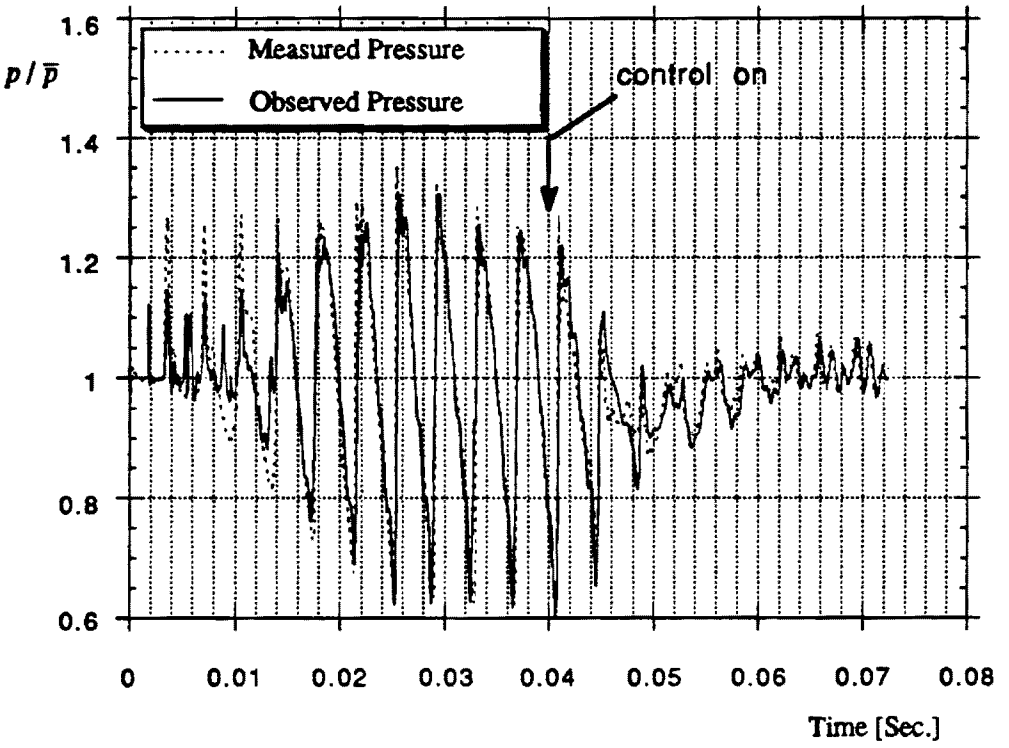

Neumeier, Zinn, Figure 5-a.

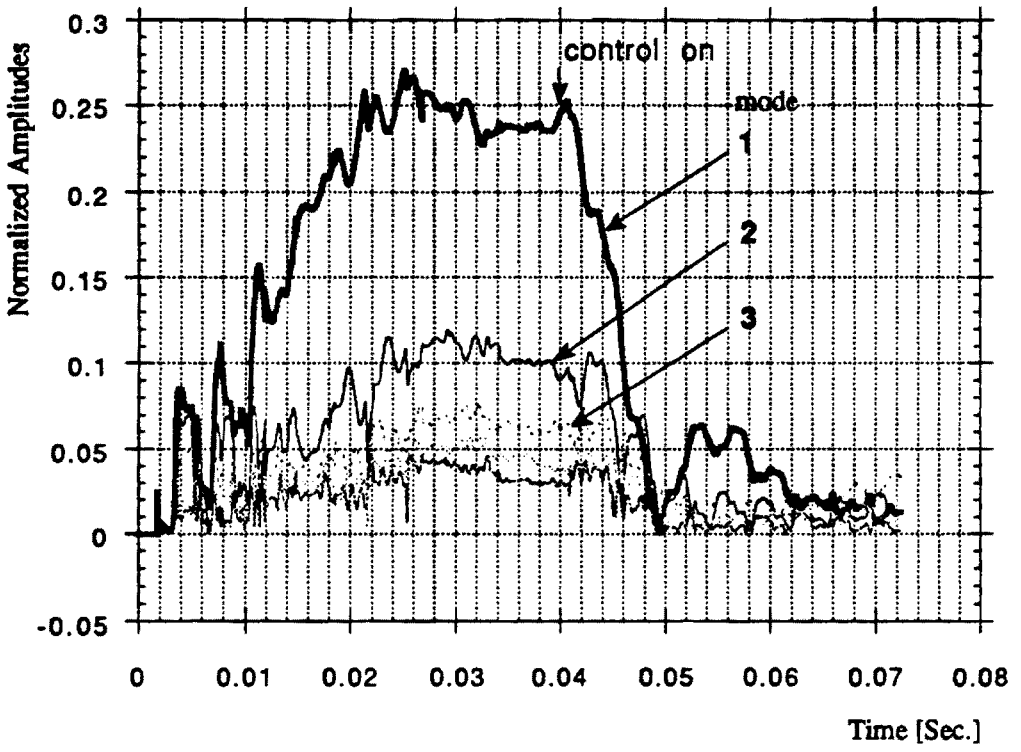

Neumeier, Zinn, Figure 5-b.

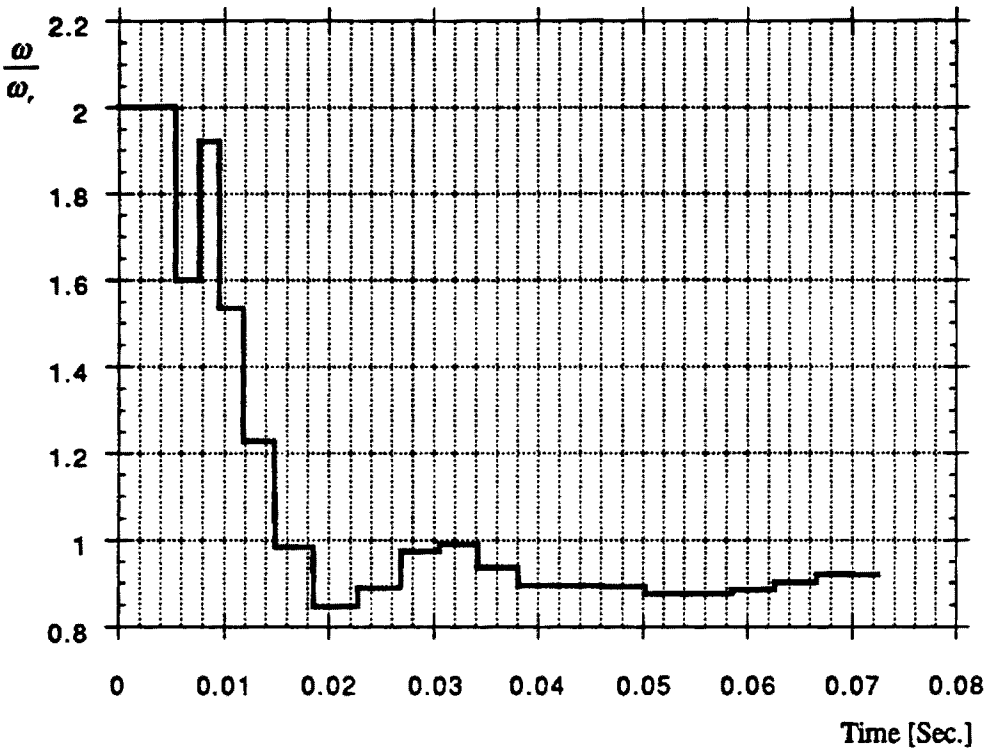

Neumeier, Zinn, Figure 5-c.

INVESTIGATION OF ACTIVE CONTROL OF COMBUSTION INSTABILITIES IN CHEMICAL ROCKETS

AFOSR Grant No. F49620-93-1-0177

Principal Investigators

Dr. Ben T. Zinn Regent's Professor
Mr. Brady R. Daniel, Senior Research Engineer
Dr. Yedidia Neumeier, Research Engineer

School of Aerospace Engineering
Georgia Institute of Technology
Atlanta, GA 30332

Summary/Overview

Parallel theoretical and experimental investigations of active control of detrimental combustion instabilities in chemical rockets have been conducted with the objective of developing a control system that can simultaneously damp several unstable combustor modes. The studied controller incorporates a novel observer that identifies, in virtually real time, the characteristics of the unstable combustor modes, a controller that modifies each unstable mode separately by the addition of appropriate gain and phase shift, and a fuel injector that modulates the fuel flow rate into the combustor to produce heat release oscillations that damp the instability. Experimental and theoretical studies have shown that the developed observer, which utilizes a unique wavelet transformer, can identify the characteristics of complex instabilities in virtually real time. Another significant accomplishment was the development a fuel injector actuator that can modulate a fuel jet with frequencies in the 0-2,000 Hz. range. The effectiveness of this fuel injector actuator was demonstrated in open loop control tests in which it excited reaction rate and pressure oscillations within the developed combustor in the 0-1,000 Hz. frequency range, indicating that it can serve as an actuator in an active control system for unstable rocket motors.

Technical Discussion

This program consists of parallel theoretical and experimental investigations whose goal is to develop the knowhow needed for effective active control of combustion instabilities in chemical rockets. Such instabilities are generally driven by a periodic combustion process whose oscillations are in phase with the combustor pressure oscillations, in accordance with Rayleigh's criterion. The operation of a rocket motor becomes unstable if the driving provided by the combustion process is larger than the damping inherently present within the system due to, for example, viscous dissipation and nozzle flow. The processes responsible for the establishment of a periodic combustion process generally involve complex interactions between the combustion process, flow and acoustic oscillations within the combustor, which depend upon the rocket motor design and operating conditions. Due to their detrimental effects, there is an urgent need for dependable engineering solutions for stabilizing chemical rockets in particular and combustors in general. To date, passive approaches have been primarily used to damp combustion instabilities with limited success. The present study investigates whether a practical active control system for stabilizing rocket motors, which is based upon recent progress in electronics, computers, sensors and actuators, can be developed.

Rayleigh's criterion indicates that acoustic oscillations are driven or suppressed when heat is added in or out of phase with the local combustor pressure oscillations, respectively. This suggests that combustion instability oscillations could be suppressed if effective means for generating heat addition oscillations that are out of phase with the combustor pressure oscillations

could be developed. Active control of combustion instabilities investigated to date[1] utilized a time domain control approach and focused on the damping of combustion instabilities consisting of the fundamental longitudinal mode or, at most, a combination of low frequency longitudinal modes. Moreover, the application of these methods required apriori knowledge of the characteristics of the unstable modes. In reality, the characteristics of the excited instability are not known in advance, and they often change with time in response to changes in rocket motor operating conditions.

A new approach for active control of rocket motor combustion instabilities that overcomes the limitations of previous active control systems has been developed under this program. The developed system consists of a sensor (a pressure transducer), an observer, a controller and an actuator. The sensor monitors the combustor performance by measuring its pressure, which is continuously transmitted to the observer. The observer analyzes the measured pressure to determine, in virtually real time, the frequencies, amplitudes and phases of the excited combustor modes. These data are sent to the controller where each of the identified modes is provided with an appropriate phase shift and an amplitude gain. The modified modes are then synthesized and the resulting signal sent to an actuator consisting of a fuel injector capable of injecting a secondary, oscillatory, fuel flow rate into the combustor. The novel components of this system are: 1. the observer whose task is to identify in real time the characteristics of modes that contribute to the instability, 2. the controller whose task is to provide each mode with an appropriate phase shift and a gain that will produce oscillatory heat release oscillations within the combustor out of phase with the unstable pressure modes oscillations, thus resulting in their attenuation, and 3. an actuator that can inject an oscillatory fuel flow rate into the combustor over a wide frequency range and with significant amplitudes.

The feasibility and performance of the developed active control method were initially investigated theoretically assuming that the flow in the combustor can be modeled by one dimensional, nonlinear, Euler equations. The driving of the instability by the combustion process was modeled by means of a simple linear feedback between the pressure and combustion process heat addition oscillations. The unstable combustor model was then "equipped" with the developed active control system and the resulting system of equations was used to investigate the effectiveness of active control system. Numerical simulations showed that the developed active control system can damp a variety of instabilities including, for example, combustor acoustic mode oscillations with amplitudes equaling twenty five percent of the mean combustor pressure, which were damped out within a few milliseconds of "activating" the controller.

Continued theoretical studies led to the development of a heuristic unstable combustor model and an improved numerical scheme for solving the resulting combustor conservation equations. Since the investigated flow is assumed to be one dimensional and inviscid, and it does not account for turbulent mixing, a mixing model that can account for some of the "missing" mixing processes has been incorporated into the combustor conservation equations. It accounts for the mixing of the fuel and air as well as the mixing of hot combustion products with the reactants. When a combustible mixture is formed, the combustion process heat rate is controlled by Arrhenius type kinetics. The improvement in the numerical solution scheme consists of a novel numerical representation of the boundary conditions at the injector face and nozzle entrance. This model is now being used to theoretically investigate the performance of the developed active control system.

The experimental efforts led to the development of an actively controlled, small scale, gas rocket motor set up, see Fig. 1. This setup is being used to investigate various active control approaches. It consists of a reactants feed system, a combustor section with windows for observations and optical diagnostics, and an active control system. During testing, the combustor is immersed in a water bath to provide needed cooling. The combustor has a large length to diameter ratio to prevent excitation of transverse and three dimensional instabilities. The combustor length can be changed, by adding or removing combustor sections, to permit investigation of active

1. Gutmark, E., Wilson, K. J., Parr, T. P. and Schadow, K. C., Feedback Control of Multi-Mode Combustion Instability, AIAA Paper 92-0778, 30th Aerospace Sciences Jan. 1992, Reno, Nevada.

control of different frequency axial mode instabilities; high frequency instabilities are excited in short combustors and vice versa.

Figure 1 also includes elements of the active control system. It includes a piezoelectric pressure transducer that "senses" the combustor pressure. The measured pressure signal is sampled by Analog Devices RT-800/802 I/O interface boards and is fed to the PC 486 processor on the host computer. The digital control signal that is generated by the 486 processor is converted into an analog signal, amplified by a power amplifier, and fed to the actuator. The data acquisition system consists of a Data Translation board that contains a TX320C40 DSP and a 3801-G I/O interface. The board is installed in the host IBM PC personal computer and the DSP communicates with the host 486 PC through a DMA channel. This configuration provides a compact and powerful control and data acquisition system in which the host computer can synchronize the data acquisition process with the controller processes during an experiment. The state of the system is continuously displayed on the host screen and commands to the controller and DSP are sent by the user from the host keyboard.

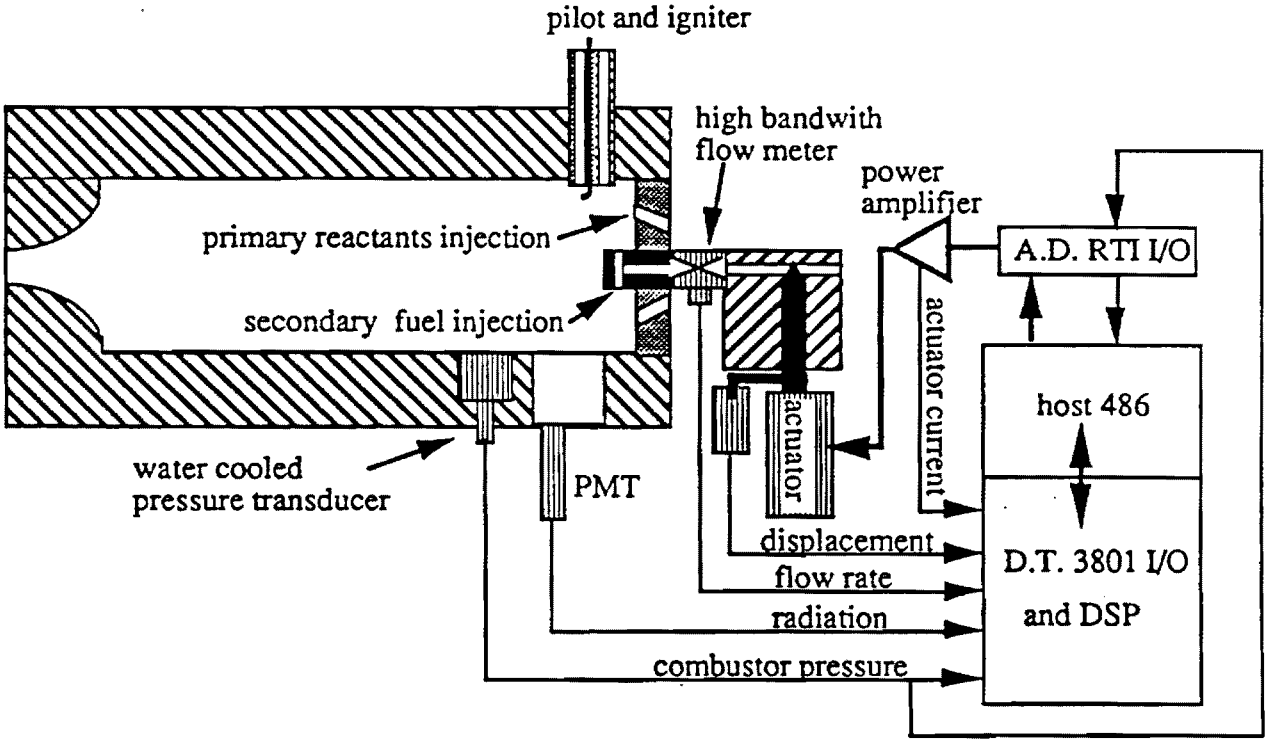

Figure 1: A Schematic of the Actively Controlled Gas Rocket Experimental Setup

In the first phase of testing, the onset of combustion instabilities in the developed gas rocket was investigated. These tests revealed that large amplitude instabilities involving excitation of different combinations of natural combustor acoustic modes with frequencies in the 200-850 Hz. range may be excited under different operating conditions. Follow up tests investigated whether the developed fuel injector could modulate the injected fuel jet at a desired frequency. For this purpose, a special low resistance flow meter capable of sensing flow rate oscillations at frequencies well above a 1,000 Hz. was developed. These tests showed that the developed fuel injector performs properly in the 0-2,300 Hz. frequency range that will be investigated in this study.

Before attempting closed loop active control of an unstable combustor, it was necessary to assure that the conditions within the rocket combustor can be controlled with the developed fuel injector. Specifically, it was necessary to demonstrate that oscillatory fuel injection produces periodic combustion and heat release rates within the combustor that oscillate with the frequency of the fuel injection. Consequently, the effect of modulating the developed fuel injector's flow rate

upon the combustion process and combustor pressure was investigated in open loop tests. These were conducted in a short combustor whose natural fundamental acoustic mode frequency was around 1,800 Hz., which was higher than the frequency range of the investigated fuel flow rate oscillations. In a typical experiment, the frequency of the fuel injection rate was set a given value and the combustor response was determined from measured combustor pressure and flame radiation spectra. The effect of modulating the fuel flow rate at 800 Hz. is shown in Fig. 2 where combustor pressure and radiation spectra measured in tests with steady and oscillatory secondary fuel injection rates are presented. The spectra measured in the absence of fuel modulation does not exhibit any peaks at the 800 Hz. driving frequency. In contrast, distinct 800 Hz. peaks are present in both the pressure and radiation spectra obtained when the fuel flow was modulated at 800 Hz., indicating that oscillating the fuel injection rate produces a heat release oscillation that excites a corresponding pressure oscillation. Similar results were obtained in tests with other frequencies in the 0-1,000 Hz., indicating that the developed fuel injector actuator can control conditions within the developed rocket combustor setup.

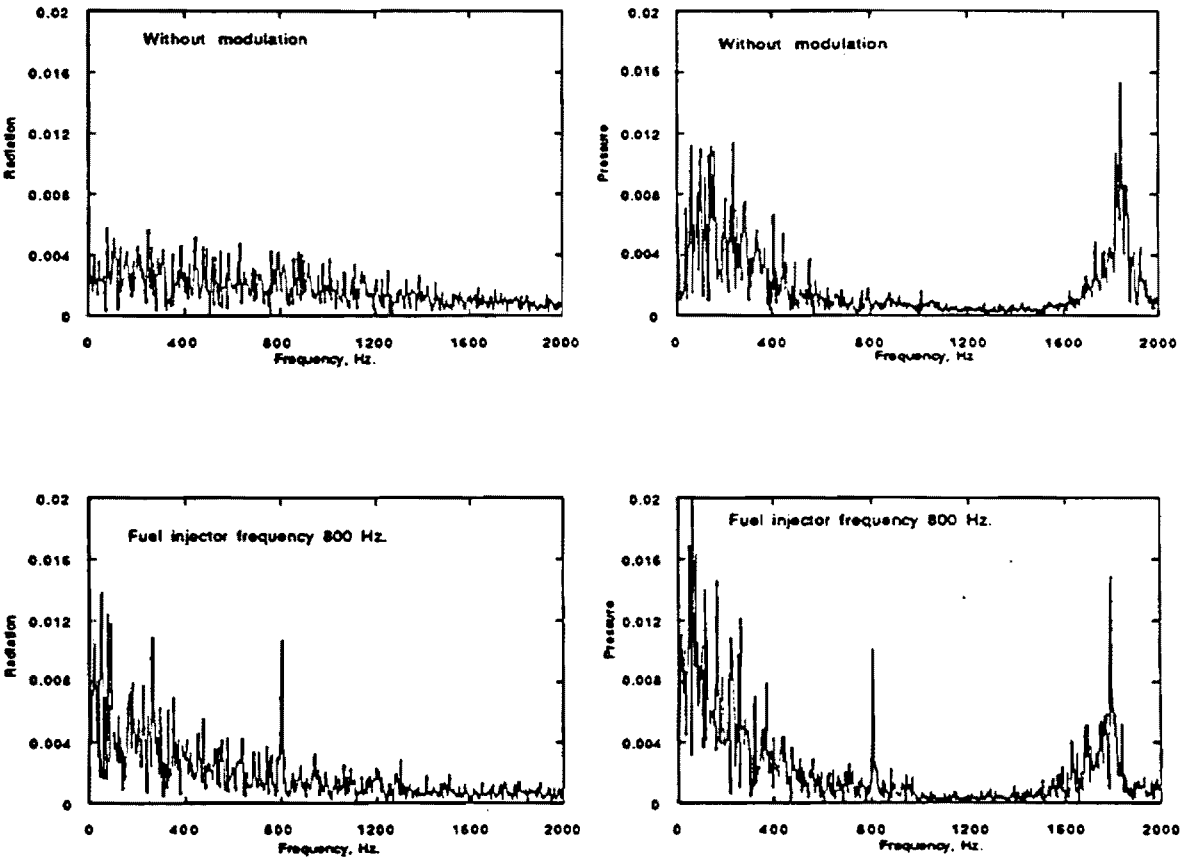

Figure 2: Radiation and Pressure Spectra with and Without Open Loop Driving at 800 Hz.

Current research is focused upon obtaining qualitative relationships between the characteristics of the fuel flow rate oscillations and resulting oscillatory pressure and heat release processes, which will be required for implementing a closed loop active control in the developed rocket combustor.

Principal Investigator Annual Data Collection- FY 95 ATCH 4

(From 1 May 1994 to 31 July 1995)

(Please Mail this form by 31 July 1995)

NAME (Last, First, MI): ZINN, BEN T.

INSTITUTION: GEORGIA INSTITUTE OF TECHNOLOGY

GRANT NUMBER: F49620 - 9 3 - 1 - 0 1 7 7

AFOSR NUMBER: AFOSR - __ __ - __ __ __ __

(Obtain the grant numbers above from your University Contracts and Grants Office)

Please Answer the questions below with the total numbers for the Period 1 May 1994 to 31 July 1995 related to the above grant :

How Many Facuty members are involved in the above grant/contract? TOTAL 1

How Many Post-Doctorates? US Cit __ __ Non-US __ __ TOTAL 0

How Many Graduate Stud. ? US Cit __ __ Non-US ✓ TOTAL 1

Others? ..(RESEARCH ENGINEERS)..... TOTAL 4

Number of Publications in the Peer Reviewed Journals TOTAL (SEE ATTACHMENT "a")

Books or Book Chapters Published TOTAL 0

Number of Awards Received in general TOTAL 1

In a second page(use additional pages if necessary), please give detail answers to the following questions :

1) List all your publications in Peer Reviewed Journals for the period 1 May 94 to 31 July 95 as a product of the above grant/contract(Authors, Title, Journal, Vol, Nr, Year, pp)

2) Books or Book Chapters published in the period 1 May 94 to 31 July 95

3) List all the awards you received in detail during the period 1 May 94 to 31 July 95

4) Participation/presentations at meetings, conferences etc.

5) Consultative and advisory functions to other laboratory and agencies, especially Air Force and other DoD laboratories

Attachment "a"

1) Publications:

"Study of the Flow Turning Loss in a Simulated Solid Rocket Motor," co-authored with L. M. Matta. *Journal of Propulsion and Power*, Vol. 11, No. 2, pp. 278-284, March-April 1995.

"Exact Solution for One Dimensional Acoustic Fields in Ducts with an Axial Temperature Gradient," R. I. Sujith, G. A. Waldherr and B. T. Zinn. Accepted for publication in the *Journal of Vibration and Acoustics*. (1995)

(NOTE: Although we have done a significant amount of work under this contract the past year, our patent attorneys asked us to withhold publications of papers describing our work on active control of instabilities until after filing a patent to protect the developed active control system. Since filing a patent application in March 1995, we have had a paper accepted for presentation in a September 1995 IEEE Controls Meeting, and another was submitted for presentation at the 1996 AIAA Aerospace Sciences Meeting. We would also like to point out that due to conflicts with our patent application, we were forced to withdraw papers on active control of instabilities that were accepted for presentation at the 1994 and 1995 AIAA Aerospace Sciences Meeting.)

2) Books or Book Chapters:

None

3) Patents:

"Methods, Apparatuses and Systems for Real Time Identification and Control of Modes of Oscillations," applied for March 1995.

4) Awards:

Ben T. Zinn, elected to the National Academy of Engineering, June 1, 1995

5) Participations/Presentations:

Seminar (Invited) Workshop on "Combustion Instability," for Westinghouse Electric Corporation, Orlando, FL, May 12 & 13, 1994.

"Active Control of Combustion Instabilities," presentation for the Westinghouse Research & Development Center, Pittsburgh, PA, November 21, 1994.

"Active Control of Combustion Instabilities," presentation for United Technology Research Center, Georgia Institute of Technology, School of Aerospace Engineering, Atlanta, Georgia, July 17, 1995.

6) Consultative and Advisory Functions:

Westinghouse Electric Corporation, Orlando, Florida

7) Other Professional Activities:

Session Chairman, 25th International Symposium on Combustion, University of CA-Irvine, Irvine, CA, July 31-August 5, 1994.

Participant/Invited Lecturer DOE Workshop on "Fundamental Research in Support of Industrial Combustion Needs," Irvine, CA, August 8-9, 1995.

SPACE PROPULSION and POWER/2308AS/BIRKAN/TECHNOLOGY TRANSFER and TRANSITION

ATTACHMENT 5

	Performer	Customer	Results	Application
1.	B. T. Zinn	Westinghouse Elec. Corp.	Westinghouse is investigating the feasibility of	Magnetostrictive actuator fuel injection system
	Georgia Tech	David Amos	using the results of our research in controlling	to stabilize low NOx gas turbines for power
	Ph: (404) 894-3033	Ph: (407) 281-3263	instabilities in their gas turbines.	generation
2.	B. T. Zinn	Pratt & Whitney/UTRC	Observer for real time determination of the	Unstable jet engines and compressor systems.
	Georgia Tech	C. N. Nett	characteristics of the Instability	
	Ph: (404) 894-3033	Ph: (203) 727-7957		
3.	B. T. Zinn	United Technology Rsch. Ctr.	Cooperation with UTRC project on active	Control of instabilities in the low NOx FT8
	Georgia Tech	Thomas S. Rosfjord	control of combustion instabilities.	gas turbine.
	Ph: (404) 894-3033	Ph: (203) 727-7418		

REPORT OF INVENTIONS AND SUBCONTRACTS

(Pursuant to "Patent Rights" Contract Clause) (See Instructions on Reverse Side.)

Form Approved
OMB No. 0704-0297
Expires Jun 30, 1992

1a. NAME OF CONTRACTOR / SUBCONTRACTOR	c. CONTRACT NUMBER	2a. NAME OF GOVERNMENT PRIME CONTRACTOR	c. CONTRACT NUMBER	3. TYPE OF REPORT (X one)
Georgia Institute of Tech.	F49620-93-1-0177			a. INTERIM [ ] b. FINAL [X]
b. ADDRESS (Include ZIP Code)	d. AWARD DATE (YYMMDD)	b. ADDRESS (Include ZIP Code)	d. AWARD DATE (YYMMDD)	4. REPORTING PERIOD (YYMMDD)
School of Aerospace Eng. Atlanta, GA 30332-0150	3/1/93			a. FROM 3/1/93 b. TO 2/29/96

SECTION I – SUBJECT INVENTIONS

5. "SUBJECT INVENTIONS" REQUIRED TO BE REPORTED BY CONTRACTOR / SUBCONTRACTOR (If "None," so state)

a. NAME(S) OF INVENTOR(S) (Last, First, MI)	b. TITLE OF INVENTION(S)	c. DISCLOSURE NO., PATENT APPLICATION SERIAL NO. OR PATENT NO.	d. ELECTION TO FILE PATENT APPLICATIONS				e. CONFIRMATORY INSTRUMENT OR ASSIGNMENT FORWARDED TO CONTRACTING OFFICER	
			(1) United States		(2) Foreign			
			(a) Yes	(b) No	(a) Yes	(b) No	(1) Yes	(2) No
Neumeier, Yedidia Zinn, Ben T.	Methods, Apparatuses & Systems for Real Time Identificatin & Control of Modes of Oscillation	Patent Docket No: 6T02-1-430	X					

f. EMPLOYER OF INVENTOR(S) NOT EMPLOYED BY CONTRACTOR / SUBCONTRACTOR		g. ELECTED FOREIGN COUNTRIES IN WHICH A PATENT APPLICATION WILL BE FILED	
(1) (a) Name of Inventor (Last, First, MI)	(2) (a) Name of Inventor (Last, First, MI)	(1) Title of Invention	(2) Foreign Countries of Patent Application
(b) Name of Employer	(b) Name of Employer	NONE	
(c) Address of Employer (Include ZIP Code)	(c) Address of Employer (Include ZIP Code)		

SECTION II – SUBCONTRACTS (Containing a "Patent Rights" clause)

6. SUBCONTRACTS AWARDED BY CONTRACTOR / SUBCONTRACTOR (If "None," so state)

a. NAME OF SUBCONTRACTOR(S)	b. ADDRESS (Include ZIP Code)	c. SUBCONTRACT NO.(S)	d. OFAR "PATENT RIGHTS"		e. DESCRIPTION OF WORK TO BE PERFORMED UNDER SUBCONTRACT(S)	f. SUBCONTRACT DATES (YYMMDD)	
			(1) Clause Number	(2) Date (YYMM)		(1) Award	(2) Estimated Completion
					NONE		

SECTION III – CERTIFICATION

7. CERTIFICATION OF REPORT BY CONTRACTOR / SUBCONTRACTOR (Not required if [ ] Small Business or [X] Non-Profit organization.) (X appropriate box)

a. NAME OF AUTHORIZED CONTRACTOR / SUBCONTRACTOR OFFICIAL (Last, First, MI)	c. I certify that the reporting party has procedures for prompt identification and timely disclosure of "Subject Inventions," that such procedures have been followed and that all "Subject Inventions" have been reported.	
Zinn, Dr. Ben T.		
b. TITLE David S. Lewis, Jr. Chair and Regents' Professor	d. SIGNATURE	e. DATE SIGNED

DD Form 882, OCT 89 — *Previous editions are obsolete.* — 971284

ATCH 6

REPORT DOCUMENTATION PAGE

1. AGENCY USE ONLY (Leave blank)	2. REPORT DATE	3. REPORT TYPE AND DATES COVERED
	04/28/96	Final Tech. Rpt. 3/01/93 - 2/29/96

4. TITLE AND SUBTITLE
Investigation of Active Control of Combustion Instabilities in Chemical Rockets

5. FUNDING NUMBERS
F-49620-93-1-0177

6. AUTHOR(S)
Ben T. Zinn
Brady R. Daniel
Yedidia Neumeier

7. PERFORMING ORGANIZATION NAME(S) AND ADDRESS(ES)
Georgia Institute of Technology
School of Aerospace Engineering
Atlanta, Georgia 30332-0150

8. PERFORMING ORGANIZATION REPORT NUMBER

9. SPONSORING/MONITORING AGENCY NAME(S) AND ADDRESS(ES)
AFOSR/NA
110 Duncan Avenue, Sutie B115
Bolling AFB, DC 20332-0001

10. SPONSORING/MONITORING AGENCY REPORT NUMBER

11. SUPPLEMENTARY NOTES

12a. DISTRIBUTION/AVAILABILITY STATEMENT
Approved for public release; distribution is unlimited

12b. DISTRIBUTION CODE

13. ABSTRACT *(Maximum 200 words)*

This report summarizes the main accomplishments of a three-year research program supported under AFOSR Grant No. F49620-93-1-0177. The main objective of this program was to investigate active suppression of detrimental combustion instabilities in chemical rockets by a controlled, secondary, combustion process. The program consisted of parallel theoretical and experimental efforts; the former developed the theoretical foundation of the investigated control approach and the latter developed a small scale, actively controlled, gas rocket setup that was used to guide the development of the investigated active control system and demonstrate its effectiveness.

14. SUBJECT TERMS

15. NUMBER OF PAGES 65

16. PRICE CODE

17. SECURITY CLASSIFICATION OF REPORT	18. SECURITY CLASSIFICATION OF THIS PAGE	19. SECURITY CLASSIFICATION OF ABSTRACT	20. LIMITATION OF ABSTRACT
unclassified	unclassified	unclassified	unlimited

AFOSR FINAL REPORT

on

INVESTIGATION OF ACTIVE CONTROL OF COMBUSTION INSTABILITIES IN CHEMICAL ROCKETS

Prepared for

Air Force Office of Scientific Research
Aerospace Sciences Directorate
Bolling Air Force Base

by

Ben T. Zinn
Brady R. Daniel
Yedidia Neumeier

School of Aerospace Engineering
Georgia Institute of Technology
Atlanta, GA 3032

March 1996

Approved for public release; distribution unlimited
AFOSR Grant No. F49620-93-1-0177

Summary

This report summarizes the main accomplishments of a three-year research program supported under AFOSR Grant No. F49620-93-1-0177. The main objective of this program was to investigate active suppression of detrimental combustion instabilities in chemical rockets by a controlled, secondary, combustion process. The program consisted of parallel theoretical and experimental efforts; the former developed the theoretical foundation of the investigated control approach and the latter developed a small scale, actively controlled, gas rocket setup that was used to guide the development of the investigated active control system and demonstrate its effectiveness.

The developed active control system (ACS) consists of a pressure transducer that continuously measures the combustor's pressure, an observer that analyzes the measured pressure and determines the amplitudes, phases and frequencies of the unstable combustor modes in real time, a controller that provides each identified mode (by the observer) with a phase shift and a gain and generates a control signal that is sent to a fuel injector actuator that modulates the injection rate of a secondary fuel stream into the combustor. This control system is based upon Rayleigh's criterion and designed to produce a secondary, oscillatory, combustion process within the combustor that is out of phase with the combustor pressure oscillations, thus resulting in their attenuation.

The theoretical efforts investigated the performance of an actively controlled rocket motor that is prone to axial instabilities. Two models that investigated the control of axial instabilities were developed. The first used an approximate, Galerkin type, approach to study the control of linear instabilities and the second used a heuristic model and a numerical solution approach to investigate the performance of an actively controlled rocket. The latter used a phenomenological model to describe combustor mixing processes and global, Arrhenius type, global kinetics to describe the combustion processes. These models were used to predict the conditions within the combustor with the ACS on and off. The control of both linear and nonlinear instabilities was investigated. These studies demonstrated that the developed ACS can identify the characteristics of severe instability in practically real time and effectively damp each unstable mode. Furthermore, numerical predictions of the combustor response to open loop control were found to be in good agreement with experimental results. Finally, these studies developed improved means for the numerical representation of the injector face boundary condition and the handling of various sources (e.g., heat and mass addition, area change and friction) in Roe's Rieman scheme, which was used to numerically solve the model equations.

The experimental efforts developed an actively controlled gas rocket that was subsequently used to investigate the performance of the ACS in open and closed loop control modes. The open loop studies developed two approaches for determining the frequency dependence of the fuel injector actuator-combustor system response. The results of these studies were stored in the ACS' controller and used to determine the phase shift and gain that controller must add to the unstable combustor modes in closed loop control. Subsequent, closed loop, control studies showed that the investigated ACS can effectively damp large amplitude, highly nonlinear, instabilities in periods of the order of 40 milliseconds, which are considerably shorter than the times reported by other investigators.

The main contributions of this study are:

1. the development of an active control approach based upon Rayleigh's criterion,

2. the development and demonstration of an observer that determines the amplitudes, phases and frequencies of a prespecified number of unstable, combustor modes in real time,

3. the development of theoretical models for investigating active control of linear and nonlinear instabilities in rocket motors,

4. the development of a fuel injector actuator that utilizes a magnetostrictive material to modulate a secondary fuel injection rate over a 0-1,200 Hz. range, which is wider than that of any known injector,

5. the demonstration that the developed fuel injector actuator can excite significant reaction rate heat release oscillations within the combustor,

6. the development of two different approaches for determining the frequency dependence of the response of the secondary combustion process generated by the fuel injector actuator, and

7. the demonstration that closed loop application of the investigated ACS significantly (e.g., by 26 dB.) and rapidly (e.g., within 40 milliseconds) damps a rocket motor instability without destabilizing any stable modes.

It is believed that these findings provide a foundation for guiding the development of ACS for unstable rockets and other combustors. The results of this program have been demonstrated to a number of companies. A major gas turbine manufacturer is currently working on adapting the developed ACS technology for application in unstable gas turbines, and a fuel injector actuator based upon the one developed under this program is being investigated by the Navy for application in active control of shipboard incinerators.

Introduction

This report describes the results of a three-year investigation of active control of combustion instabilities in chemical rockets. Such instabilities are generally driven by a feedback-type interaction between flow and combustion process oscillations; energy supplied by an oscillatory combustion process produces oscillatory heat release that excites one or more natural acoustic modes of the combustor whose oscillations are responsible for the periodicity of the combustion process. The condition for driving an instability in a combustor can be expressed by the following modified form of Rayleigh's criterion:

$$\int_V \int_T p'(x,t)Q'(x,t)dtdV \geq \int_V \int_T \sum_i L_i(x,t)dtdV \qquad (1)$$

where p', Q', L_i, t, x, T and V are the combustor pressure oscillation, heat addition oscillation, i-th loss process (e.g., viscous dissipation, acoustic energy transmission through the nozzle), time, location within the combustor, period of the oscillation and combustor volume, respectively. The integral on the left and right hand side of Eq. 1 describes the total driving and damping experienced by the combustor oscillations, respectively. An instability occurs when the inequality in Eq. 1 is satisfied; that is, the overall driving within the combustor is larger than the overall combustor damping. It is noteworthy that driving occurs at a given location x when the time integral on the left side of Eq. 1 is positive at that location. This condition is satisfied when magnitude of the phase difference ϕ between the pressure and heat addition oscillations is less than 90 degrees. It follows that at locations where the magnitude of this phase difference is larger than 90 degrees, the oscillatory heat addition process damps the oscillations.

An examination of Eq. 1 suggests that instabilities could be prevented by decreasing the magnitude of the integral on the left and/or increasing the magnitudes of various loss terms on the right. The former can be attained by modifying the characteristics of the combustion process and/or its interaction with the flow oscillations. The characteristics of the combustion process could be changed by, for example, modifying the propellants' feed system, fuel injectors and propellants' composition. On the other hand, the loss terms on the right hand side of the Eq. 1 could be increased by, for example, changing the characteristics of the nozzle and/or adding mechanical elements (e.g., an acoustic liner) that dissipate acoustic energy in the combustor. These control approaches are generally referred to as passive, and their effective implementation requires understanding of the mechanisms that drive the instability, the characteristics of the excited oscillations, and the losses produced by various system elements.

Unfortunately, passive control approaches have generally not been satisfactory. Lack of adequate understanding of the fundamental processes that control the instability resulted in "solutions" there were only applicable to a specific combustor design over a limited range of operating conditions. Consequently, different passive control approaches had to be developed for different unstable combustors. Since these passive control approaches were generally developed in costly and lengthy trial-and-error development programs, it became apparent that new approaches for controlling combustion instabilities are needed.

The considerable progress in the areas of computers, electronics, sensors, actuators and control theory in recent years has renewed interest in the development of active control systems (ACS) for preventing combustion instabilities. An ACS can prevent the onset and/or damp an instability by one or more of the following actions:

1. production of heat addition oscillations in the combustor that are 180 degrees out of phase relative to the unstable pressure oscillations, thus resulting in their attenuation (based upon Rayleigh's criterion; see Eq. 1 above), and/or

2. interference with the mechanisms that drive the instability in a way that reduces their driving effectiveness, and/or

3. modification of the system's boundary condition(s) in a way that produces one or all the following: (i) increase in the system's damping, (ii) modification of the modes that can be excited within the system, and (iii) destructive interference with the mechanisms that drive the instability.

A typical ACS generally consists of a sensor, an observer, a controller, and an actuator, see Fig. 1. The sensor (e.g., a pressure transducer or a photo-multiplier) continuously "senses" the conditions inside the unstable combustor. The signal measured by the sensor is transmitted to the observer that determines the state of the system. This information is sent to the controller where it is modified, using a specific control approach, and sent to the actuator that "perturbs" the combustor in a controlled manner. The latter prevents the onset or damps the instability via one or more of the actions described in Items 1-3 above.

The main advantages of a given ACS are:

1. it can prevent the onset and/or rapidly attenuate combustion instabilities,

2. it can rapidly respond to changes in the combustor operating conditions and, thus, the characteristics of the instability, and

3. it is expected to be applicable (perhaps with some modifications) to different unstable combustors, thus providing a capability for effective control of instabilities in a variety of combustion systems.

While prior investigations of active control of combustion instability had demonstrated the considerable promise of this approach, a close examination of the results of these studies revealed that much remained to be done in several areas before active control can be implemented in practical combustors. For example, past investigations generally filtered the measured signal before sending it to the controller where it was amplified and phase shifted before being sent to the actuator. The use of a filter requires, however, apriori knowledge of the frequency of the instability. While this frequency can be readily determined in advance in experimental combustors, it is generally not known apriori in practical combustors, and may vary in response to changes in combustor operating conditions. Consequently, a practical ACS should possess capabilities for determining in real time the frequencies of the unstable combustor modes. Another problem is the shortcomings of actuators such as loudspeakers, mechanical valves and fuel injectors that had been utilized by other investigators. For example, loudspeakers generally don't have the power required for stabilizing practical combustors, capabilities for continuous operation without failure, and "hardware" that can survive in hostile combustor environments. Similarly, mechanical valves are complex, heavy and limited to low frequency applications. It, thus, became apparent at the outset of this program that a fuel injector that can supply an oscillatory fuel flow rate into the combustor to drive pressure oscillations at a desired frequency and phase and/or modify the primary combustion process in a manner that reduces its driving effectiveness should be used as the actuator in an ACS for damping combustion instabilities. The automotive fuel injectors that were utilized in past studies are limited, however, to low frequencies and low fuel flow rates and, consequently, are not suitable for use in practical ACS.

In an effort to advance the state of the art and develop capabilities that would lead to the development of practical active control systems for unstable rocket (and other) combustors, efforts under this program focused on developing the following capabilities:

1. an observer that can analyze the sensor's signal and determine in the amplitudes, frequencies and phases of up to five unstable combustor modes in virtually real time,

2. a fuel injector actuator that can modulate the flow rate of a gaseous fuel with significant amplitudes over a 0-1,200 Hz. frequency range, whose upper limit is considerably higher than the maximum frequency of any known (e.g., automotive) fuel injector,

3. a small scale, actively controlled, variable length, gas rocket that exhibits axial instabilities, similar to those observed in full scale rocket motors, over a wide range of frequencies (e.g., 100-1800 Hz.), and

4. a model of an actively controlled gas rocket that can be used to theoretically investigate the performance of various ACS and control strategies.

The research activities and accomplishments of this program are described in the remainder of this report. These are described in the following order: 1. the principles of operation of the investigated ACS, 2. theoretical investigations of the performance of unstable rocket motors actively controlled with the investigated ACS, 3. the developed experimental setup, 4. open loop active control performance of the investigated ACS, 5. closed loop active control of combustion instabilities with the investigated ACS, and 6. summary and conclusions of the results of this program.

The Investigated Active Control System

At the onset of this program it was recognized that an ACS capable of preventing detrimental rocket motor instabilities will require capabilities for:

1. identification of the characteristics of all the unstable combustor modes in virtually real time (i.e., before the instability results in rocket malfunction) using limited sensor data about the combustor performance,

2. determination of the appropriate phase and gain that must be "added" by the controller to each unstable mode and generation of an appropriate control signal for the actuator, and

3. means for introducing controlled "perturbations" into the combustor that will attenuate the unstable combustor modes.

To provide these capabilities, the developed ACS uses a pressure transducer installed near the combustor's injector as its sensor, because the anti-nodes of most potentially unstable axial pressure oscillations are likely to occur near this location. This maximizes the likelihood that the measured pressure will include contributions from all unstable combustor modes. The measured pressure is then transmitted to an observer whose task is to determine, in virtually real time, the amplitudes, frequencies and phases of all combustor modes that significantly contribute to the instability. The identified characteristics of the unstable modes are transmitted to a controller where each mode is provided with a gain and a phase shift that will result in the attenuation of the corresponding mode within the combustor. The controller combines the modified modes into a single signal that is sent to a fuel injector actuator that can modulate the injection rate of a gaseous fuel into the combustor over a 0-1,200 Hz. frequency range. The fuel injection modulations produce reaction rate and heat addition oscillations within the combustor at the frequency of the fuel flow rate modulation. These heat addition oscillations should, according to Rayleigh's criterion, damp the instability if the magnitude of the phase difference between these heat addition and combustor pressure oscillations is smaller than ninety degrees.

The Observer

Since the developed observer plays a key role in the investigated ACS and it is repeatedly referred to in the remainder of this report, its principles of operation are presented in this section.

The observer analyzes the measured pressure to determine in real time the amplitudes, phases, and frequencies of the unstable combustor modes. It assumes that the measured combustor

pressure p(t) can be expressed as the following sum of combustor modes that may not be harmonics of one another and may have frequencies, amplitudes and phases that slowly vary with time.

$$p(t) = \sum_{n=1}^{n=k} S_n \sin(\omega_n t) + C_n \cos(\omega_n t) \qquad (2)$$

The observer determines the characteristics of the dominant (i.e., largest amplitude) mode by solving the integrals

$$S_n(t) = \frac{2}{T_n} \int_{t-T_n}^{t} \sin(\omega_n t) p(t) dt; \; C_n(t) = \frac{2}{T_n} \int_{t-T_n}^{t} \cos(\omega_n t) p(t) dt \qquad (3)$$

where the oscillation period T_n and frequency ω_n are related by $T_n = 2\pi / \omega_n$ and are not known apriori. It can be shown that the above integrals can replaced by following recursive formulae:

$$S_n(t + \Delta t) = S_n(t) + \frac{2}{T_n}\left(p(t + \Delta t) - p(t - T_n + \Delta t)\right) \cdot \sin(\omega_n t) \cdot \Delta t \qquad (4\text{-a})$$

$$C_n(t + \Delta t) = C_n(t) + \frac{2}{T_n}\left(p(t + \Delta t) - p(t - T_n + \Delta t)\right) \cdot \cos(\omega_n t) \cdot \Delta t \qquad (4\text{-b})$$

whose solution requires little computational effort[1]

The unknowns $S_n(t)$, $C_n(t)$ and ω_n are determined in a rapidly converging iterative solution procedure. Initially, a value for ω_n (and, thus, T_n) is assumed and substituted into Eqs. 4, which are then solved for the "corrected" coefficients of $S_n(t+Dt)$ and $C_n(t+Dt)$. The calculated coefficients are then substituted into the following relationship[1] that determines a corrected value of the frequency:

$$\left[(\omega)^2\right]^{t+\Delta t} = \left[\omega^2 + \frac{\omega\left(\frac{ds}{dt}\sin(\omega t) + \frac{dc}{dt}\cos(\omega t)\right)}{S \bullet \cos(\omega t) - C \bullet \sin(\omega t)} \right]^{t} \qquad (5)$$

where the subscript 'n' has been omitted for simplicity. The values of ω on the left and right sides of Eq. 5 are the "corrected" and "previous calculated" values of the frequency, respectively. Once a corrected value of ω is obtained from Eq. 5, the corresponding period T is substituted into Eqs.

4 to obtain improved values of S(t) and C(t). This procedure rapidly converges into the "final" values of the unknowns ω, S and C, which are then used to determine he amplitude, phase and frequency of the dominant mode. This procedure can also track "slow" variations of these quantities. Once the characteristics of the dominant mode are known, the expression describing its time dependence is subtracted from the measured pressure p(t) and the above procedure is repeated to determine the characteristics of the "next" dominant mode within the remaining signal.

The above described procedure can be repeated to determine the characteristics of as many modes as desired. Clearly, the need to attain real time identification of the characteristics of an instability would limit the number (e.g., two or three) of modes that can be identified. This is not, however, a problem as most instabilities are generally dominated by one or two modes.

Figures 2-a through 2-e demonstrate the ability of the observer to identify in real time the hierarchy of modes in an unstable combustor. The observer was provided with the pressure signal shown in Fig. 2-a, which was measured in the gas rocket motor that was developed under this program when it experienced combustion instability. Figure 2-a shows that the instability "switches" from low to high frequency oscillations between .05 and .064 seconds. This signal was analyzed by the observer and the computed frequencies and amplitudes were used to determine the time dependence of the two most dominant combustor modes, see Figs. 2-b through 2-e. Figures 2-b shows that the frequency of the nearly sinusoidal, dominant, mode abruptly increases around .065 seconds to that of the second mode, while Fig. 2-c shows that the second mode oscillates with a higher frequency and its amplitudes decreases to practically zero around .065 seconds. Figures 2-b,c also show that the observer can simultaneously track the behavior of both modes in real time. Figure 2-d presents the calculated time dependence of the frequencies of the two observed modes. It shows that the observed frequency of the dominant mode changed from 650 to 1250 Hz. within only three milliseconds. Finally, Fig. 2-e compares the measured pressure p(t) with that obtained by synthesis of the two observed modes. It clearly shows that the observer can "reproduce" the input pressure in real time and with high fidelity.

During the last year of this program a theoretical study aimed to extend the initially developed observer approach to provide a capability for simultaneous identification of several unstable modes was undertaken. This study is presented in Appendix A. While the current observer determines the characteristics of the unstable modes in a hierarchical manner (i.e., the most dominant mode is identified first, then the next mode dominant mode is identified and so on), the new approach simultaneously identifies the characteristics of several unstable combustor modes. It is expected that the results of this study will increase the accuracy and robustness of the observer and increase the likelihood that its output will converge to the correct results.

Theoretical Studies

The performance of the investigated ACS, see Fig. 1, was initially theoretically studied by solving the system of one dimensional, unsteady, conservation equations that modeled the flow in an unstable combustor[2]. The model assumed that the instability is driven by a simple linear feedback between the pressure and combustion process heat addition oscillations. The unstable combustor model was then "equipped" with the developed ACS and used to theoretically investigate the effectiveness of the developed ACS. Numerical simulations showed that the developed ACS can rapidly damp a variety of instabilities including, for example, combustor acoustic mode oscillations with amplitudes equaling twenty-five percent of the mean combustor pressure, which were damped within a few milliseconds after activating the ACS.

Subsequent studies developed a heuristic model of an unstable gaseous rocket combustor and an improved numerical approach for solving the model equations. The conservation equations solved by this model are summarized in Fig. 3. Since the model assumes that the combustor flow is one dimensional and inviscid, and, thus, cannot account for turbulent mixing, a phenomenological mixing model that describes the mixing of the premixed reactants with the hot combustion products has been incorporated into the conservation equations (i.e., see terms proportional to $1/\tau_{mix}$). This model also accounts for the mixing of the secondary fuel, injected by the fuel injector actuator, with the combustor flow before its reaction. The magnitude of the spatial dependence of the mixing process is controlled by the function W(x), see Fig. 3, which depends upon a prespecified mixing length l_{mix}. Once a combustible mixture is formed, the combustion process heat release rate is controlled by global, Arrhenius type, methane kinetics, which is the fuel used in the experimental phase of the program.

Once it had been shown that the heuristic model predicts unstable rocket operation of ranges of design and operating parameters, the model was "equipped" with the investigated ACS and the resulting model was used to investigate the behavior of an actively controlled rocket motor. Typical results obtained in this study are presented in Figs. 4 and 5. Figure 4 shows predictions of the motor's performance under open loop control excitation. It shows predicted time dependence of pressure and heat release oscillations within the rocket combustor when the fuel injector actuator modulated the secondary fuel injection rate at specific frequency. The results show that the actuator can excite significant pressure and heat release oscillations within the combustor, indicating that it could serve as an actuator in closed loop control of rocket motor combustion instabilities. An analysis of the time dependence of the results shows that the heat release oscillations lead the pressure oscillations and that the magnitude of the phase difference is always

smaller than ninety degrees, in agreement with Rayleigh's criterion. This phase difference decreases as the amplitude of the excited oscillations increases, and it approaches ninety degrees as the growth grate of the oscillations decreases, indicating that less driving is needed when the amplitude growth rate goes to zero.

Figure 5 presents predictions of the effect of closed loop control upon the oscillations in an unstable rocket combustor. The two top plots show the onset, growth and decay of the instability before and after the activation of the ACS at t≈.03 seconds. These plots show that the ACS significantly attenuated the instability. The middle plot compares the predicted and "observed" (by the ACS' observer) pressure oscillations. It shows that the developed observer can indeed "identify" the characteristics of the combustor pressure oscillations in practically real time. The second plot in the middle demonstrates the observer's ability to "follow" in real time the variations in the frequency of the instability. The plot on the bottom left presents an "amplified" view of the oscillations shown in the top left plot after activating the ACS. It shows that the amplitude of the "damped" combustor oscillations is negligible. Finally, the plot on the bottom right shows the time dependence of the control signal o the actuator. In summary, the results presented in Fig. 5 predict that the investigated ACS will effectively attenuate rocket motor combustion instabilities.

In a parallel study, Roe's Rieman Solver[3] was modified for applications in numerical simulations of unstable combustors. Specifically, Roe's Rieman scheme was modified to properly account for the presence of source terms (e.g., the combustion process heat addition, friction) in the numerical solution of the conservation equations. Furthermore, numerical schemes that improve the representation of the injector face and nozzle boundary conditions were developed for incorporation into the numerical solution scheme.

Finally, the feasibility of applying open loop, nonlinear, high frequency, vibrational control to damp instabilities in mechanical systems was theoretically investigated[4]. Such control has the advantage that it does not require accurate determination of the state of the controlled system and the data processing capabilities required in conventional feedback control. This paper extends previous linear investigations of this type of control to include nonlinear vibrational controllers. It shows that a nonlinear vibrational controller can stabilize a system even if the Jacobian matrix has a positive trace. A copy of this paper, which was submitted for publication in the IEEE Journal, is provided in Appendix.B.

Experimental Setup

The experimental efforts led to the development of an actively controlled, small scale, gas rocket motor setup shown in Fig. 6. It consists of a reactants feed system, a combustor section, a

nozzle, a secondary fuel injection system (i.e., the fuel injector actuator), a main control panel, and a computer-based controller of the secondary fuel actuator. The setup also includes transducers and photomultipliers that measure the combustor pressure and reaction rate, respectively, and a computer-based data acquisition system.

A primary reactants stream, consisting of premixed air and methane, enters the combustor through the injector orifices. The air and methane are separately introduced into a mixing port through calibrated, choked, orifices that provide means for measuring the flow rate of each reactant. These flow rates are manually controlled by setting the pressure upstream of each orifice to a desired value. The flows through the injector orifices are choked to prevent feedback between the combustor and reactants supply lines. The injected reactants jets are oriented twenty degrees relative to the combustor axis, which forces the primary combustion process to stabilize near the combustor walls.

The combustor's exhaust nozzle is choked at all test conditions. Under typical operating conditions, the combustor pressure, premixed reactants line pressure and fuel and air supply lines pressures are 45, 90 and 200 psi, respectively. The combustor pressure was always sufficient for choking the exhaust nozzle. The supply pressure to the secondary fuel injector is 450 psi. Under this operating condition, the flow rates of the primary stream of premixed fuel and oxidizer and secondary fuel stream are 10 and 0.1 gram/sec., respectively, resulting in a total combustor power output of 55 kW.

The combustor has a large length to diameter ratio to prevent excitation of transverse modes. The combustor length can be changed by adding or removing pipe sections. This capability permits the investigation of axial mode instabilities having different frequencies; high frequency instabilities are excited in short combustors and vice versa. At its shortest length, the combustor's fundamental mode frequency is around 1800 Hz. while at its longest configuration the fundamental mode frequency is 200 Hz. During operation, the combustor is immersed in a bath with running water to cool the combustor.

As shown in Fig. 6, the axis of the investigated combustor is "broken" to provide a location for installing the window, optics and photomultiplier required to measure the total (integrated) combustion zone radiation. This system measures the total CC or CH radicals radiation from the combustion region, which is proportional to the combustion process heat release rate. A second, side view, window, which is installed near the injector, is used for optical measurements and visualization of the combustion zone.

The actively controlled secondary fuel injector actuator introduces an oscillatory fuel flow into the combustion zone. High pressure fuel is supplied to the actuator and forced through an annular orifice between the outer wall of a needle's wider diameter base and its seat. A magnetostrictive actuator is attached to the needle and used to change the needle's base position relative to its seat in response to changes in an electric control signal. The acoustic impedance and pneumatic resistance of the actuator's cavities that carry the fuel from the supply line to the combustor were sized to maximize the fuel flow rate oscillations at the injector's exit and minimize the effect of the combustor pressure oscillations upon the actuator's performance over a wide frequency range. As a result, this actuator can modulate the fuel flow rate over a 0-1,200 Hz. frequency range when pressure oscillations are present in the combustor without a significant attenuation or a phase delay. Furthermore, this actuator can produce fuel flow rate amplitudes of the order of 0.2 grams/sec., which, in principle, can produce 20 kW peak to peak heat release rate oscillations.

The electric signal to the actuator consists of a steady and an oscillating component, which control the magnitudes of the steady and oscillating flow rates through the fuel injector actuator, respectively. Both signals are generated in the control computer, separately amplified, and then combined into a single control signal that is fed to the actuator.

Two different actuators and injection systems were developed and tested during this study. Each injection system, see Figs. 7-a,b, supplied the combustor with a primary stream of premixed reactants and a secondary fuel stream. The latter was used to control the instability by generating a secondary, oscillatory, combustion process within the combustor. The actuators were similar in design, but the annular cross sectional area of the second actuator was between two to three times larger than that in the first actuator. For further reference, the small and large actuators will be denoted as ACT1 and ACT2, respectively, and the injection systems shown in Figs. 7-a,b will be denoted by INJ1 and INJ2, respectively. The investigated injector/actuator configurations, whose performance is described later in this report, will be described by the notation INJi/ACTi where the index i=1,2 describes the injector and actuator used in the study. It should be pointed out that the ACT2 actuator, which was developed later in the program, could be retrofitted to both injection systems while the ACT1 actuator could be only installed on the INJ1 injector.

The second injector, INJ2, and actuator, ACT2, were developed and investigated in a cooperative effort with a major gas turbine manufacturer that is interested in developing capabilities for active control of instabilities in large scale gas turbines.

Open Loop Studies

As stated above, effective application of the investigated ACS in closed loop control of combustion instabilities requires knowledge of the gain and phase shift that the controller must add to each combustor unstable mode. Since each unstable mode oscillates at a different frequency and these frequencies may span a wide range, the frequency dependence of the phase shift and gain that the controller must add to the unstable modes must be known over a wide frequency range. Since, unfortunately, the characteristics of the secondary combustion processes cannot be accurately modeled to predict the frequency dependence of its phase shift and gain, these quantities must be experimentally determined in open loop tests. The objective of the open loop tests is to measure the phase delay between the combustion process heat release and actuator control signal oscillations and the ratio of the amplitudes of the combustion process heat release and control signal oscillations, which is referred to as the gain. Together, the measured phase shift and gain describe the secondary combustion process response (SCPR).

Another critically important reason for investigating the SCPR is to determine whether the developed fuel injector actuator can excite combustion process heat release and pressure oscillations within the combustor of sufficient magnitude (i.e., capable of affecting the unstable combustor oscillations) . If the developed fuel injector actuator could not excite heat addition oscillations of sufficient magnitude within the combustor, it would not be suitable for application in closed loop control of combustion instabilities. In this case, a different fuel injector (or another type of actuator) will have to be developed and/or investigated.

Two approaches for determining the SCPR frequency dependence were developed and investigated under this program. The first used a very short combustor whose fundamental, longitudinal, acoustic mode frequency was around 1800 Hz., which was significantly above the upper limit of the frequency range of the open loop studies. Consequently, the operation of the combustor was "quiet" over the investigated frequency range and the magnitudes of driven disturbances (by the fuel injector actuator) were significantly above the combustor noise level. When tests were conducted in this short combustor, high frequency reaction rate and pressure oscillations driven by a combustor instability could be readily observed in the measured pressure and radiation data and clearly distinguished from the "single" frequency oscillations driven by the fuel injector actuator. Using this combustor, the characteristics of the SCPR were determined from the measured pressure* and a relationship between these pressure oscillations and reaction rate

* Global radiation measurements could not be used with this combustor because the available sideview window, see Fig. 6, could not "view" the whole combustion zone.

oscillations, which was provided by a model of the combustor oscillations (which is derived below). The "short" combustor also included a side view window, similar to the one shown in Fig. 6, which was used to measure CH radicals radiation from the combustion region. Unfortunately, this window could not "view" the whole combustion region, and the measured radiation could only provide qualitative description of the characteristics of the secondary combustion process oscillations.

The following analysis describes the derivation of a model that predicts the behavior of small amplitude (i.e., linear) oscillations in the short combustor. This model was used to determine the SCPR from measured pressure data.

Neglecting kinetic energy terms, the energy equation for a combustor with uniform properties can be expressed in the following form:

$$\frac{d}{dt}\int_V \rho e dV = \dot{q}_{comb.} + \dot{m}_a h_a + \dot{m}_f h_f - \dot{m}_e h_e \qquad (6)$$

where the terms from left to right are the rate of change of the combustor internal energy, oscillatory heat release supplied by the secondary combustion process, the air and fuel enthalpy fluxes into the combustor and the enthalpy flux exiting through the choked nozzle, respectively. Assuming a perfect gas behavior and that the flow through the choked nozzle is quasi steady, the following relationships can be derived:

$$\frac{d}{dt}\int_V \rho e dV = (VC_v / R)\frac{dp}{dt}; \quad \dot{m}_e h_e = (K_N p / \sqrt{T})C_p T \qquad (7)$$

Substituting Eqs. (7) into Eq. (6), assuming that each dependent variable consists of a steady component and a small amplitude perturbation (e.g., $p = \overline{p} + p'$), and linearizing the resulting energy equation yields the following linear form of the energy equation

$$\frac{\dot{q}'}{\dot{m}C_p\overline{T}} = \frac{p'}{\overline{p}} + \frac{\tau}{\overline{p}}\frac{dp}{dt} + \frac{T'_e}{2\overline{T}}; \quad \tau = \frac{VT_a\overline{p}}{\overline{T}C_a^2\dot{m}} \qquad (8)$$

where τ is a characteristic time, C_a is the speed of sound and the subscript 'a' denotes the state of the incoming air. Since the temperature perturbations generated within the combustion process are expected to decay before they reach the nozzle entrance at high frequencies, the term involving T'_e is neglected in Eq. (8), yielding the following relationship

$$\frac{\dot{q}'}{\bar{m}C_p\bar{T}} = \frac{p'}{\bar{p}} + \frac{\tau}{\bar{p}}\frac{dp}{dt} \qquad (9)$$

for determining the heat release $\dot{q}'$ oscillations from measured pressure oscillations at high frequencies.

In the second approach for determining the SCPR, the combustor shown in Fig. 6 was employed. Since this combustor is considerably longer than the "short" combustor that was used in the first study, several natural longitudinal acoustic modes of the combustor could be excited in the range of investigated SCPR frequencies. For example, the fundamental mode frequency of this combustor was 370 Hz. Consequently, small heat addition oscillations at one of the natural acoustic mode frequencies of the combustor could produce significant pressure oscillations at this frequency. Consequently, when the fuel injector actuator is operated at a non-resonant frequency of this combustor, it excites significant secondary combustion process oscillations within the combustor but only small amplitude pressure oscillations. Thus, the phase and amplitude of the secondary combustion process heat release oscillations can be determined at non-resonant frequencies of the combustor by direct measurements of the characteristics of the total radiation from the combustion region. These were directly measured with a photomultiplier through the window on the slanted combustor section in Fig. 6.

Figure 8 shows an example of the time dependence and spectra of pressure and CH radiation signals measured in the combustor shown in Fig. 8 when the secondary fuel injection rate oscillated at 610 Hz. Figure 8-a shows that the pressure spectrum is dominated by spikes representing three unstable combustor modes at 370, 740 and 1110 Hz. In general, if a single mode is driven by an unstable combustion process, the amplitudes of its harmonics, which are excited by nonlinear processes, are smaller than the amplitude of the most unstable lowest frequency mode. The pressure spectrum in Fig. 8-a indicates that this was not the case in this experiment as the amplitudes of the higher frequency spikes are larger than the amplitude of the fundamental mode. This suggests that each of the observed pressure oscillations was independently driven by the combustion process.

An examination of the pressure spectrum in Fig. 8 also shows a small, but clearly visible, spike at 610 Hz., the frequency of the actuator. In contrast, only one, large amplitude, spike is present in the spectrum of the CH radiation signal at 610 Hz. The dominance of the spike of the driven heat release oscillations in the CH radiation spectrum indicates that the fuel injector actuator could readily excite heat release oscillations in this combustor that are significantly larger than any

other heat release oscillation when the frequency of the fuel flow rate modulation was not close to any natural acoustic mode frequency of the combustor.

Figure 8 shows that FFT can be used to identify a small amplitude, periodic, pressure signal in the neighborhood of large amplitude spikes. It was found, however, that an FFT analysis cannot accurately determine the phase of such a small signal. Unlike the FFT determination of the amplitude, the FFT determination of the phase is highly sensitive to the frequency at which the FFT integral is evaluated. Since the FFT evaluation is performed at a discrete number of frequencies, it may not be performed at the exact frequency of the secondary combustion oscillations, thus increasing the likelihood of inaccurate phase determination.

To overcome the shortcomings of the FFT, a MATLAB-based software that employs an ensemble averaging technique was developed to accurately determine the amplitude and phase of the secondary heat release oscillations. The basic steps of this approach are:

1. The input to the actuator, (usually a current) is chosen as a reference signal.

2. Measured data points are correlated with the reference signal by referencing the time of each data point to a specific phase in the period of the reference signal, thus "collapsing" all the measured data points into one period.

3. A "moving" narrow-width window is used to obtain the ensemble average of the time dependence of the collected data over the period of the reference signal. It should be noted that the time dependence of the calculated average does not necessarily assume a sinusoidal shape.

4) The ensemble-averaged line is curve-fitted with a sinusoidal signal to obtain the corresponding amplitude and phase of the measured data.

Figure 9 presents typical results obtained with this data reduction approach, using the data presented in Fig. 8. The top to bottom plots on the left side of Fig. 9 show measured data points describing, respectively, the actuator control signal (current), actuator needle displacement, combustor pressure and combustion process CH radiation. The corresponding plots on the right side of Fig. 9 show the determined averages of the collected data points (solid lines) and the sinusoidal curves that were fitted to the ensemble-averaged curves (dashed lines).

The actuator current, pressure and CH radiation are measured by sensors with practically no time delay. In contrast, the proximity sensor that measures the actuator's needle displacement introduces a significant phase lag and attenuation to the measured data. This phase lag and attenuation, which are determined in advance by comparing known input signals at various

frequencies to the sensor's output, are accounted for in the data reduction procedure by providing the determined sinusoidal signal with a phase lead and a gain relative to the calculated "average" curve.

Figure 9 shows that the measured CH radiation and pressure data form "clouds" of points. While the CH radiation "cloud" exhibits a sine-like shape, such a pattern is not readily apparent in the thick "cloud" of pressure data points. This difference between the pressure and radiation data is reflected in the presence of high frequency components in the ensemble average of the pressure data, and the practically sinusoidal shape of the ensemble average of the CH radiation data, which nearly coincides with its sinusoidal curve fit.

The above described data reduction procedure was applied to the data measured in the open loop tests to obtain the frequency dependence of the phase and gain of the above described variables and, in particular, the transfer function between the needle displacement, which closely resembles the fuel injection modulation, and secondary combustion process heat release oscillations.

The frequency dependence of the gain and phase delay of the secondary combustion process heat release oscillations generated by the fuel injector actuator were measured by the two, above discussed, methods and the results are compared in Figs. 10-a,b. The excellent agreement between the two sets of data that were determined using different approaches in two different combustors strongly suggests that the frequency response of the heat addition oscillations generated by the developed fuel injector actuator is practically independent of the acoustic properties of the combustor.

Figures 11-a,b show the measured frequency dependence of the phase and gain of the secondary combustion process heat release of two different injector/actuator configurations that consisted of each of the developed injectors, see Figs. 7-a,b, and the larger fuel injector actuator (i.e., configurations INJ1/ACT2 and INJ1/ACT2). The frequency dependence of the SCPR of the INJ1/ACT2 configuration was determined for various magnitudes of the actuator's needle displacement. Figure 11-a shows that all the measured phase data can be closely correlated by a single curve that describes a nearly linear dependence of the phase upon the frequency. This nearly linear frequency dependence of the phase suggests the presence of a pure time delay between the fuel injection rate modulation and the corresponding secondary combustion process heat release oscillations. This is a surprising result as it was not expected that an identical, pure, time delay will be produced by different injectors and excitation levels.

Figure 11-b shows the frequency dependence of the ratio of the amplitudes of the combustion process heat release the actuator's needle displacement oscillations. Since these results apparently depend upon the amplitude of the needle's displacement, this amplitude is indicated next to some of the data points to provide means for determining the dependence of the data upon the needle's amplitude. Figure 11-b indicates that the INJ2 injector has a larger gain at frequencies below 300 Hz. and smaller gain at higher frequencies. It also shows that the gain depends upon the needle's displacement and is larger for smaller displacements. This result suggests that the SCPR is controlled by nonlinear processes whose potential origin is discussed below.

The developed fuel injector actuator provides the combustor with a fuel flow consisting of a mean and an oscillatory component. To maintain the mean flow rate at a set value, it is measured and compared with the set value. If the two are not equal, the mean flow rate controller sends a slowly varying signal to the actuator that changes the mean position of the needle and, thus, the mean area of the actuator's orifice, in an effort to provide the desired mean fuel flow rate. In addition to the slowly varying signal from the mean flow controller, the actuator receives a high frequency signal that sets the needle into high frequency, back-and-forth, axial oscillations that periodically vary the actuator's orifice cross sectional area, resulting in a periodic secondary fuel injection rate. As long as the periodic variation of the orifice's area is small and does not change its mean area, the periodic change in the orifice's cross sectional area does not interfere with the mean flow rate through the actuator. As the amplitude of the actuator's needle displacement oscillations increases, a threshold amplitude that forces the actuator's orifice to momentarily close (at the instant of maximum" upward" needle displacement, see Fig. 6) is reached. As the amplitude of the needle's displacement oscillations increases beyond this threshold value, the mean values of the actuator's needle displacement and mean flow rate increase, see Fig. 12. This forces the actuator's mean flow rate controller to further close the actuator orifice, resulting in additional "truncation" of the needle's oscillations. Since it can be shown that the amplitude of the actuator's orifice area variation oscillations cannot be larger than the magnitude the orifice's mean area, the amplitude of the fuel flow rate modulation cannot exceed that of the mean fuel flow rate.

Figure 13 shows the dependence of the ratio of the amplitude of the combustion process CH radiation oscillations and the mean CH radiation on the needle's displacement amplitude at a frequency of 540 Hz. for three different injector/actuator configurations. The behavior exhibited by the three plots is in agreement with the above discussion. They show that the amplitude of the CH radiation oscillations reaches a limiting value at a given needle displacement amplitude and cannot increase beyond this limiting value as the needle displacement is further increased.

To further understand the results of Fig. 13, we should consider the two main processes that control the interaction between the secondary combustion process heat release and needle displacement oscillations. First, consider the variation in the cross sectional area of the actuator's orifice, see Fig. 6, in response to the needle's displacement oscillations. As discussed above, the amplitude of the cross sectional area oscillations cannot exceed the mean magnitude of the cross sectional area of the orifice. Consequently, to increase the amplitude of the fuel flow rate modulation would require increasing the magnitude of its mean flow rate. The difference between the behavior of the two actuators that were used in this study is qualitative described in Fig. 14 where the expected dependence of the amplitude of the secondary fuel injection rate modulation upon the amplitude of the actuator's needle displacement is plotted for the large and small actuators operating with two different mean flow rates. Figure 14 shows that since the orifice of the larger ACT2 actuator has a larger cross sectional area than that of the ACT1, the ACT2 actuator provides larger amplitude fuel flow rate modulations for a given amplitude of the needle's displacement oscillations than the ACT1 actuator. It also shows that both actuators can provide the same maximum fuel flow rate oscillations amplitudes as long as they can provide the same fuel mean flow rate.

Another factor affecting the amplitude of the combustion process heat release oscillations is the "efficiency" of converting the secondary fuel injection rate modulations into combustion process heat release oscillations. Intuitively, one would expect that the ratio of the amplitudes of the combustion process heat release and secondary fuel injection rate oscillations would depend upon the injector design. Examining the configurations of the two investigated injectors, see Figs. 7-a,b, shows that injector INJ1 supplies the secondary fuel stream directly into the "center" of the primary combustion zone whereas injector INJ2 apparently injects the secondary fuel upstream of the primary combustion region, possibly enabling the secondary fuel to fully or partially mix with the premixed, primary, reactants before reaching the combustion zone. This pre-mixing process apparently tends to decrease the magnitude of the attained secondary combustion heat release oscillations. Consequently, injector INJ1 is expected to provide a more "efficient" conversion of the fuel injection rate modulation into combustion process heat release oscillations than injector INJ2.

On the basis of the above discussion, one would expect that configurations INJ1/ACT2 and INJ2/ACT1 will produce the largest and smallest secondary combustion process heat release oscillations for a given needle displacement, respectively, while configurations INJ1/ACT1 and INJ2/ACT2 will produce heat release oscillations that fall between these limits. These expectations are supported by the results in Fig. 13, where it is shown that for a given amplitude of the

actuator's needle displacement the amplitude of the secondary heat release oscillations decreased in the following order: INJ1/ACT2, INJ1/ACT1 and INJ2/ACT2.

The above discussion and Figs. 13 and 14 indicate that the smaller ACT1 actuator could provide the same maximum fuel flow rate and heat release oscillations as the larger ACT2 actuator if it could be provided with a larger maximum needle displacement amplitude. This explains why the two configurations INJ1/ACT1 and INJ1/ACT2 that used the same injector but different actuators attained the same maximum secondary heat release magnitudes, see Fig. 13. It is also interesting to note in Fig. 13 that the maximum amplitude of heat release oscillations that can be excited by the INJ2 injector is significantly smaller than those excited with the INJ1 injector even though INJ2 used the larger ACT2 actuator.

Closed Loop Active Control of Instabilities

As stated earlier, the investigated ACS is guided by Rayleigh's criterion and its objective is to generate heat addition oscillations within an unstable combustor 180 degrees out of phase with the unstable pressure oscillations. This mode of control will be discussed assuming that the instability can be damped by controlling its dominant mode only. In this case, the observer only identifies the dominant mode and the control signal to the actuator, y_c, is given by:

$$y_c = G(\omega) \bullet \left(S \cdot \sin(\omega t + \phi(\omega)) + C \cdot \cos(\omega t + \phi(\omega))\right) \qquad (10)$$

where S, C and ω are the observed amplitudes and frequency of the dominant mode while $G(\omega)$ and $\phi(\omega)$ are the gain and phase that are added by the controller using data (in the form of plots or tables) obtained in the above discussed open loop experiments. Since Fig. 10-b shows that the gain of the heat addition oscillations decreases with increasing frequency, the magnitude of G(w) should increase with frequency to assure that the ACS generates heat addition oscillations of adequate magnitude at higher frequencies.

Closed loop control of the rocket motor setup shown in Fig. 6 was investigated. Combustor pressure, control signal and observed frequency measured in a typical test before and after activation of the ACS are described in Fig. 15. In this experiment, the development of a large amplitude instability was "monitored" by the observer before activating the control system at t=0.1 seconds. The ACS was "conditionally" activated by requiring the gain $G(\omega)$ in Eq. 10 to satisfy the following conditions

$$G(\omega) = \begin{cases} 0 & when \ \ |\omega_{observed} - \omega_0| > d_1 = 100 Hz. \\ & \\ G_{table} & when \ |\omega_{observed} - \omega_0| < d_2 = 50 Hz. \end{cases} \qquad (11)$$

where ω_0 is the observed frequency of the instability before activating the controller (see Fig. 15) while d_1 and d_2 are specified parameters. These conditions require the controller to "remember" the frequency of the dominant unstable mode before activating the ACS and to respond only when this mode becomes dominant, thus leaving other modes uncontrolled. This mode of operation demonstrates the high flexibility of the developed control approach.

Figure 15-a shows that this ACS practically damped the instability in 40 milliseconds, indicating that it could damp rocket instabilities before they could seriously damage the engine and/or result in mission failure. FFT analysis of the combustor pressure oscillations before and after the activation of the ACS showed that the amplitude of the dominating mode was reduced by 26 dB., which exceeds the performance of ACS investigated elsewhere (see survey of results in Table 1 in Ref. 5). Figure 15-b describes the time dependence of the control signal to the actuator, which is proportional to the magnitude of $G(\omega)$ (see Eqs. 10 and 11) and, thus, depends upon the observed frequency, see Fig. 15-c. Figures 15-b,c show that the control signal goes to zero when the 370 Hz. dominant mode is damped by the ACS. When this occurs, the observer identifies the 740 Hz. harmonic as the dominant mode and stops controlling the 370 Hz. mode, see Fig. 15-b. Consequently, the unstable 370 Hz. mode starts growing again. When its amplitude exceeds that of other unstable combustor modes (e.g., the 740 Hz. mode), the observer identifies this mode again as the dominant mode and turns on the actuator. As shown in Figs. 15-b,c, this sequence of events continuously repeats itself, resulting in effective control of the dominant 370 Hz. mode, while not destabilzing other modes of the combustor.

Additional closed loop experiments, not reported herein, have demonstrated that the investigated ACS can effectively control multi-mode instabilities.

Summary and Conclusions

In closing, this report presents a novel active control approach for damping detrimental rocket instabilities. The main contributions of this study are:

1. the development of an active control approach based upon Rayleigh's criterion,

2. the development and demonstration of an observer that can determine the amplitudes, phases and frequencies of a prespecified number of unstable, combustor modes in real time,

3. the development of theoretical models for investigating active control of linear and nonlinear instabilities in rocket motors,

4. the development of a fuel injector actuator that utilizes a magnetostrictive material to modulate a secondary fuel injection rate over a 0-1,200 Hz. range, which is wider than that of any known injector,

5. the demonstration that the developed fuel injector actuator can excite significant reaction rate heat release oscillations within the combustor,

6. the development of two different approaches for determining the frequency dependence of the response of the secondary combustion process generated by the fuel injector actuator, and

7. the demonstration that closed loop application of the investigated ACS significantly (e.g. by 26 dB.) and rapidly (e.g., within 40 milliseconds) damps a rocket motor instability without destabilization of any stable modes.

It is believed that these findings provide a foundation for guiding the development of ACS for unstable rockets and other combustors.

References

1) Neumeier, y. and Zinn, B. T. Active Control of Combustion Instabilities Using Real Time Identification of Unstable Combustor Modes. Proceeding of 4th IEEE Confeerence on Control Aplication. Sept. 28-29, 1995, Albany, N.Y.

2) Neumeier, y. and Zinn, B. T. Active Control of Combustion Instabilities With Real Time Observation of Unstable Combustor Modes. AIAA 96-0758, 34th Aerospace Sciences Meeting, Jan. 15-18, 1996, Reno, NV. (submitted to AIAA Journal of Propulsion and Power)

3) Mohanraj, R., Neumeier, Y. and Zinn, B. T., Modification of Roe's Riemann Solver for the Euler Equations with Source Terms. AIAA 96-0766, 34th Aerospace Sciences Meeting, Jan. 15-18, 1996, Reno, NV.

4) Shapiro, B. and Zinn B. T. High Frequency Nonlinear Vibrational Control. Submitted to IEEE Transaction on Automatic Control.

5) Sivasegaram, S., Tsai, R. F. and Whitelaw, J. H. Control of Combustion oscillations by Forced Oscillation of Part of the Fuel Supply. Combust. Sci. and Tech. 1995 Vol. 105, pp. 67-83

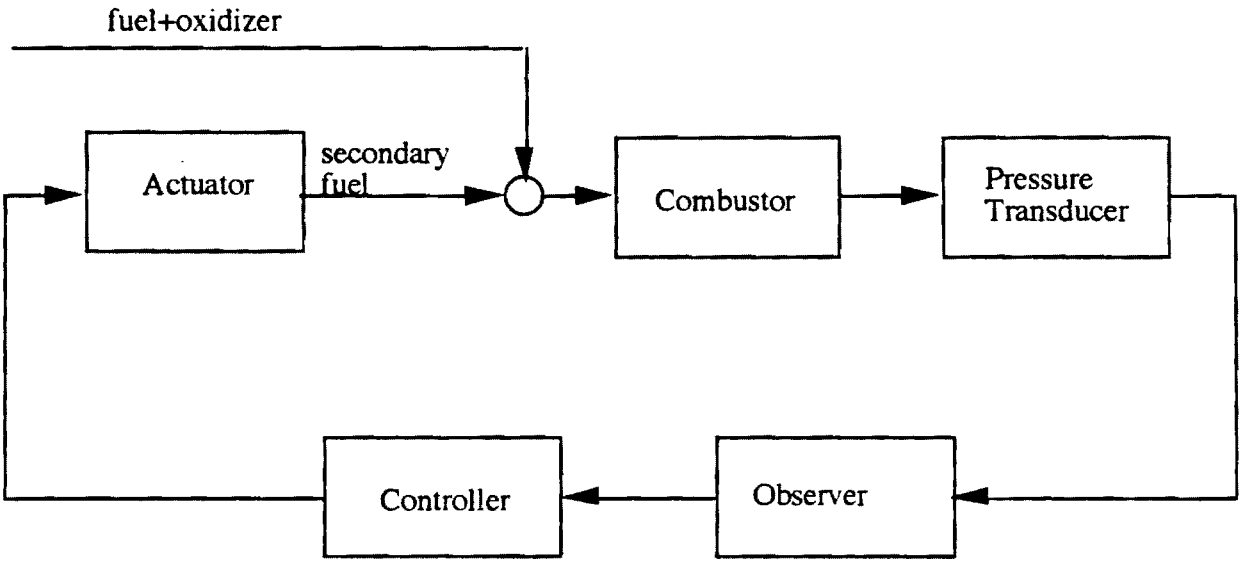

Figure 1. A schematic of the developed ACS.

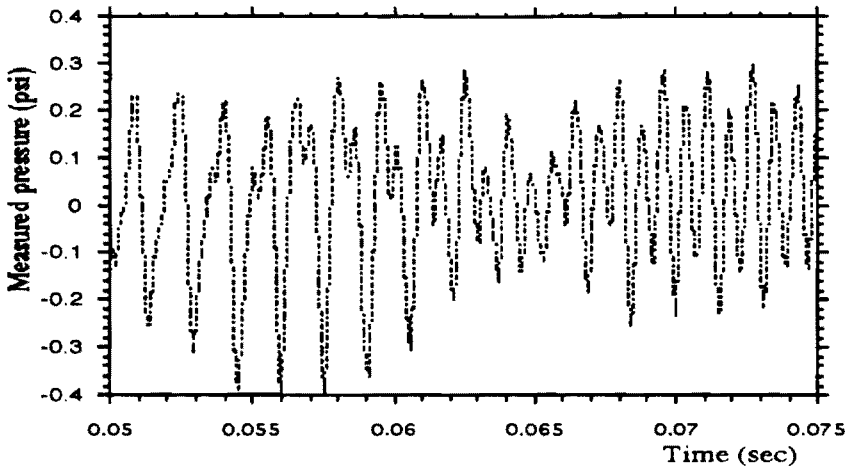

Figure 2-a. Unstable pressure oscillations measured in the developed gas rocket motor.

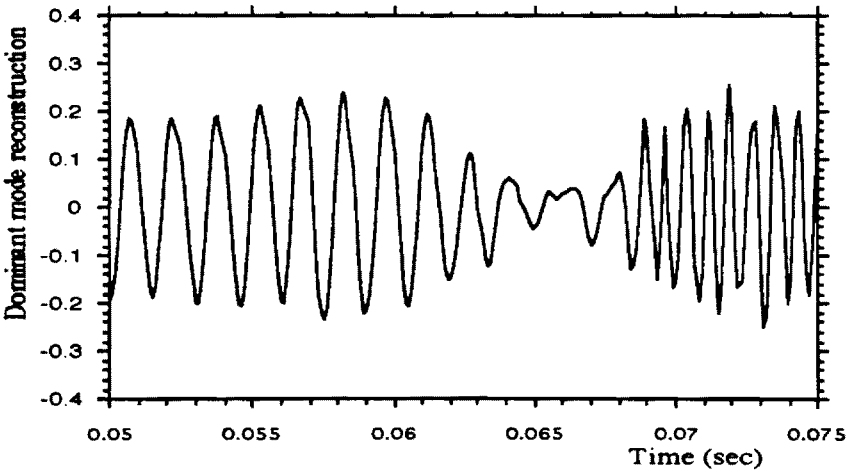

Figure 2-b. Observed time dependence of the dominant mode of the instability.

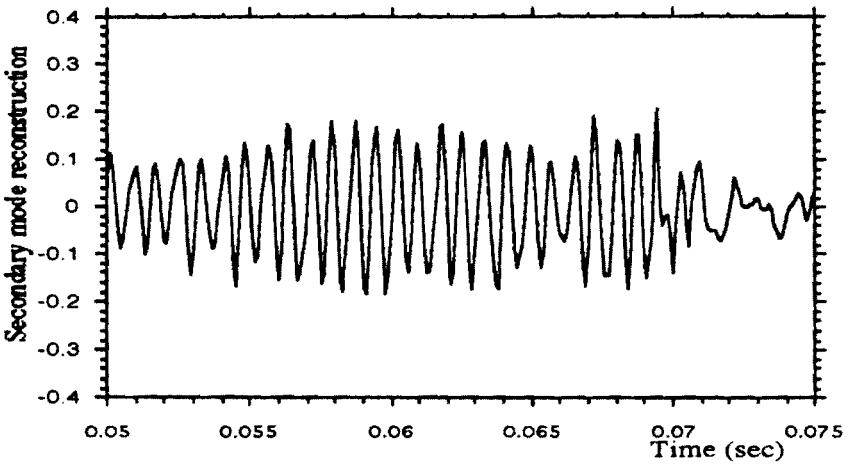

Figure 2-c. Observed time dependence of the secondary mode of the instability.

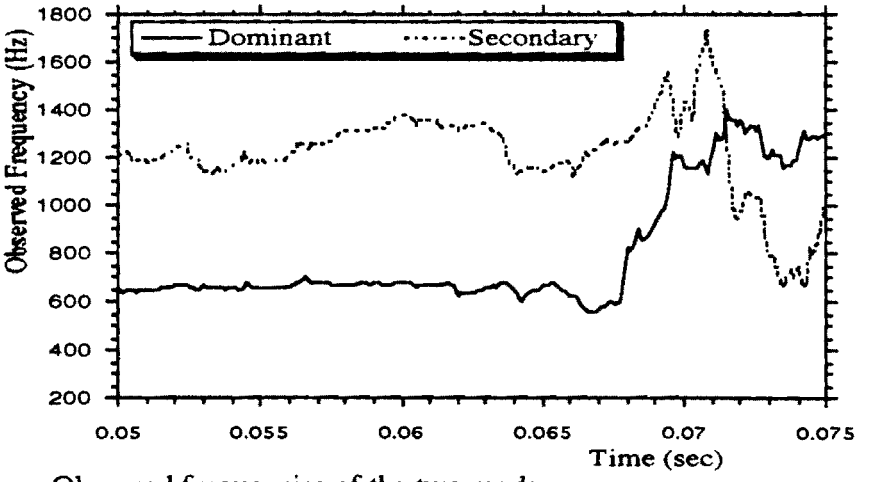

Figure 2-d. Observed frequencies of the two modes.

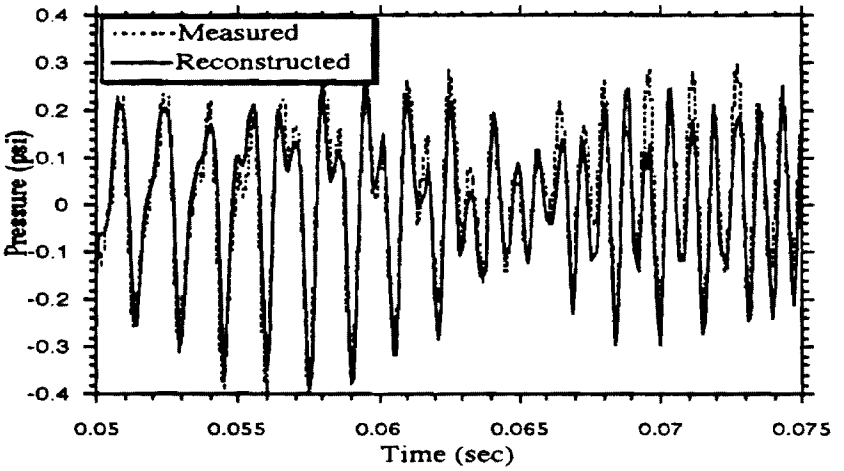

Figure 2-e. Comparison of the measured pressure and that synthesized from two observed modes.

$$\frac{\partial U}{\partial t} = -\frac{\partial F}{\partial x} + \eta(x)\left(\frac{U_{mix} - U}{\tau_{mix}}\right) + S \qquad U = \left\{\rho, \rho u, \rho\left(e + \frac{u^2}{2}\right)\right\}^T$$

$$F = \left\{\rho u, \rho u^2 + p, \rho u\left(h + \frac{u^2}{2}\right)\right\}^T \qquad e = \frac{p}{(\gamma - 1)\rho} \qquad h = \frac{\gamma p}{(\gamma - 1)\rho}$$

$$U_{mix} = \frac{\int_{V_{mix}} U\eta dV}{\int_{V_{mix}} \eta dV} \qquad S = (s_1, s_2, s_3)^T$$

$$\frac{\partial \rho_f}{\partial t} = -\frac{\partial[\rho_f u]}{\partial x} + \eta(x)\left(\frac{\rho_{f,mix} - \rho_f}{\tau_{mix}}\right) + \omega_f + s_f$$

$$\frac{\partial \rho_{ox}}{\partial t} = -\frac{\partial[\rho_{ox} u]}{\partial x} + \eta(x)\left(\frac{\rho_{ox,mix} - \rho_{ox}}{\tau_{mix}}\right) + \omega_{ox}$$

Reaction rate model (Global Kinetics)

$$\omega_f = \omega_{CH_4} = -2.15 \times 10^{16}\left[\rho_{CH_4}\right]^{0.2}\left[\rho_{O_2}\right]^{1.3} e^{\left[\frac{-24,368}{T}\right]}$$

Heat release

$$\dot{q} = -Q_{cal}\omega_f$$

Weighting function

$$\eta(x) = e^{-(x - x_f)/l_{mix}} \qquad x \geq x_f$$
$$= 0 \qquad x < x_f$$

U_{mix}	Weighted average of the state vector
s_1, s_2, s_3	Source terms due to secondary mass, momentum and heat addition
s_f	Source term due to secondary (controller) fuel addition
$\dot{q}$	Heat release due to chemical reaction (s_3 contains $\dot{q}$)
Q_{cal}	Calorific value of the fuel (methane)
x_f	Flame holder location
l_{mix}	Characteristic mixing length

Figure 3. Conservation equations used to model the behavior of an unstable gaseous rocket motor.

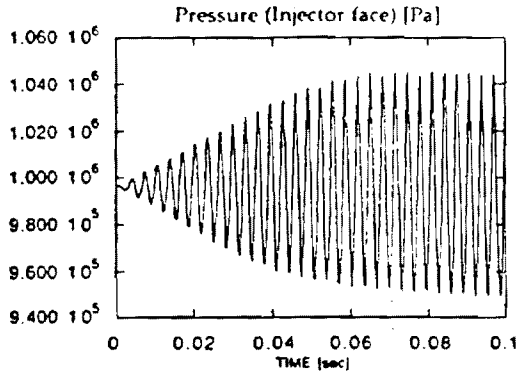

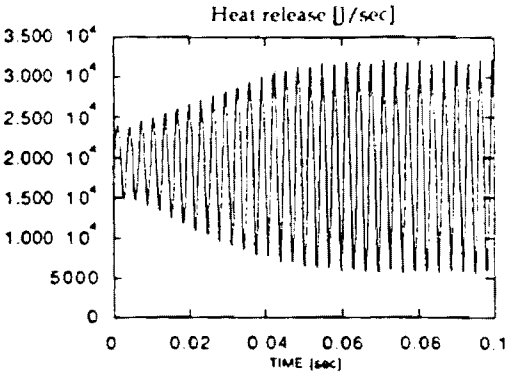

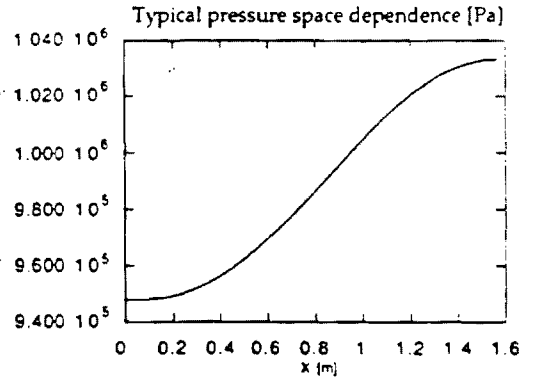

$L_{chamber}$=1.57 m
τ_{mix}=0.3 ms
l_{mix}=4 cm
x_f=2 cm
x_{secf}=2 cm
ϕ=0.7 (equivalence ratio)
Secondary fuel constitutes 40% of the total fuel.

Phase difference between heat release and pressure (heat release leading pressure)
28^0 (around t=0) and 71^0 (around t=0.1sec)

Figure 4. Prediction of the combustor response to open loop excitation by oscillatory fuel injection.

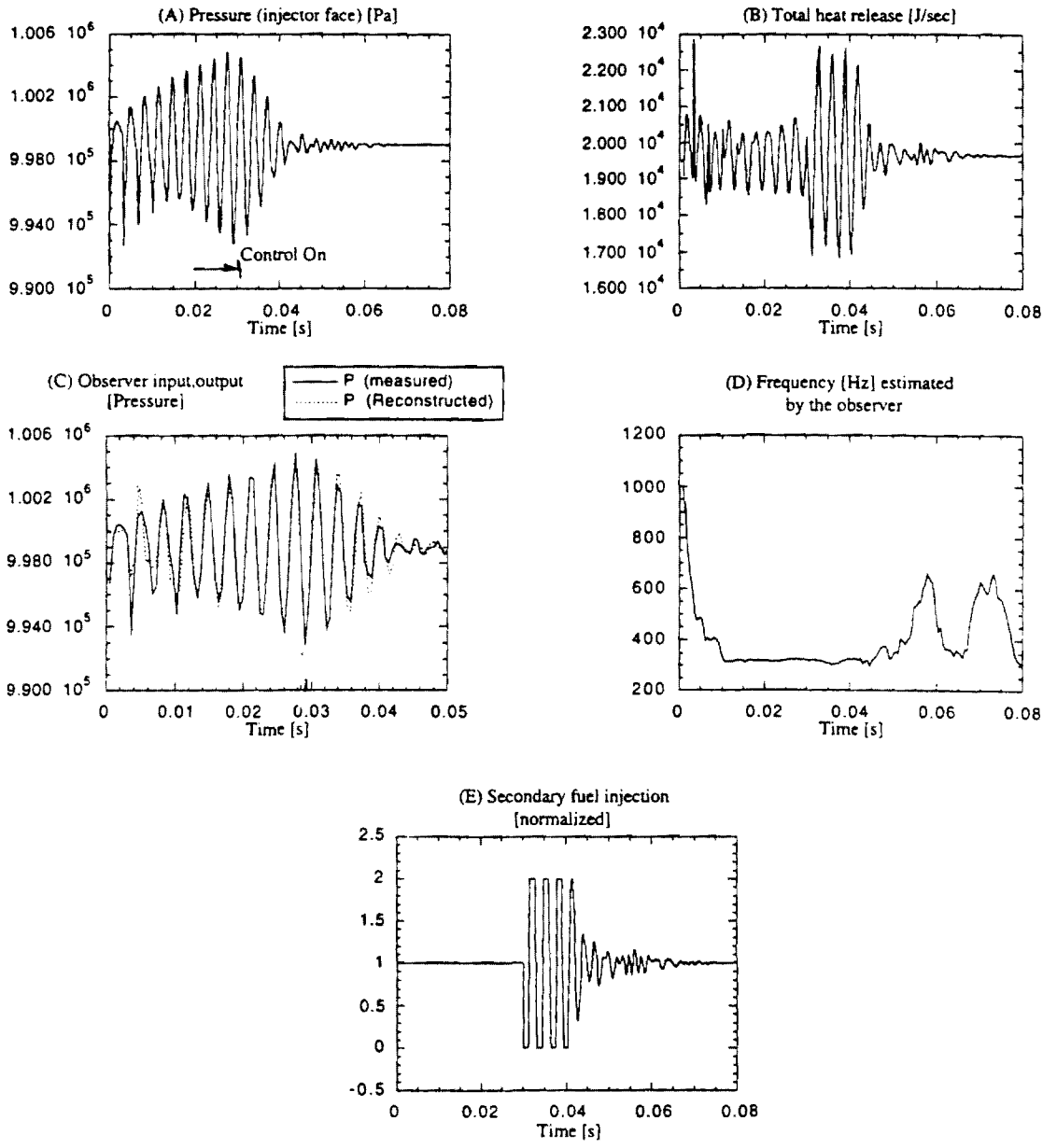

Figure 5. Results of numerical simulation of an unstable combustor response to closed loop active control by means of an oscillatory secondary fuel injection using real time observation of the dominant mode.

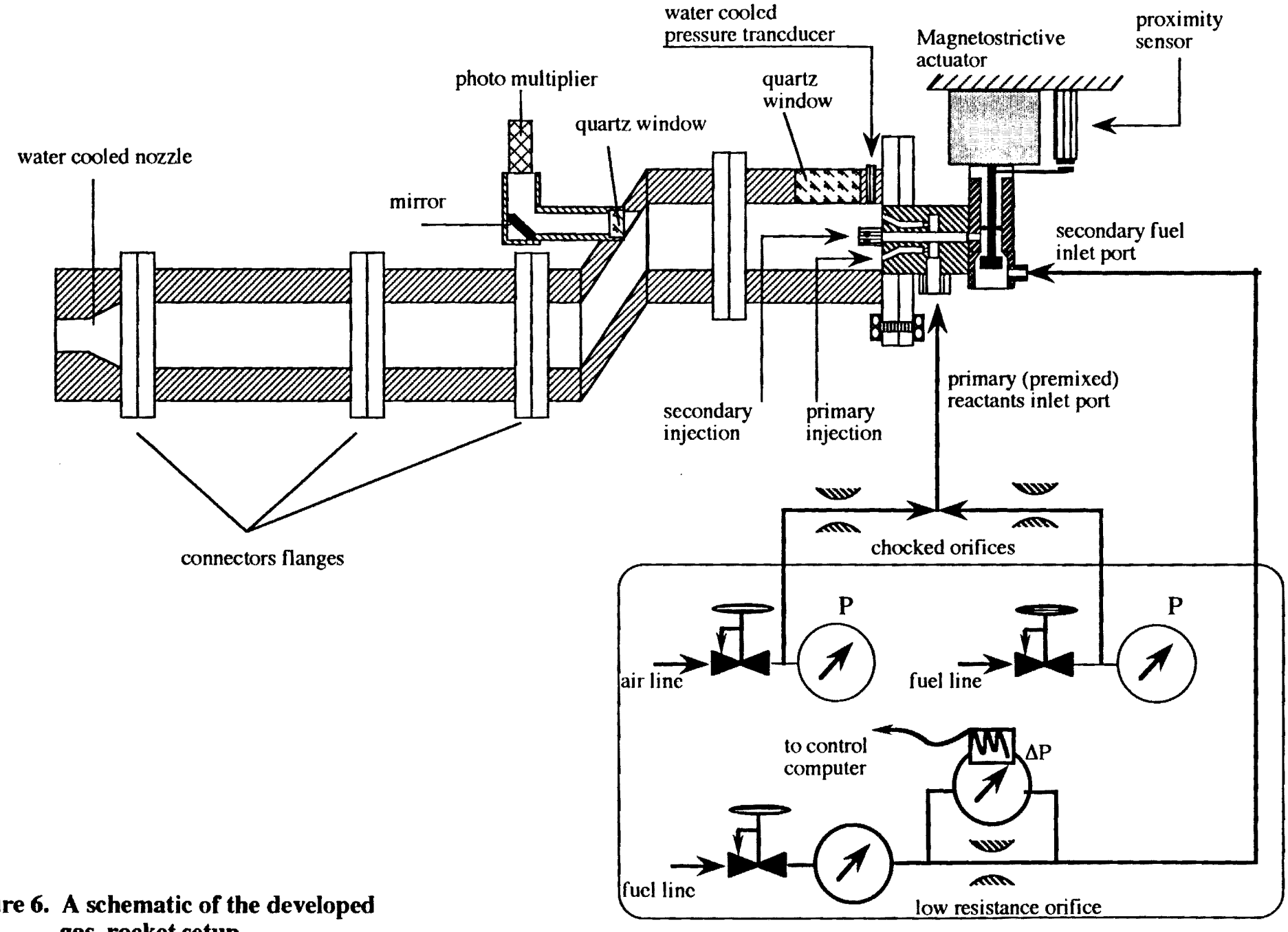

Figure 6. A schematic of the developed gas rocket setup

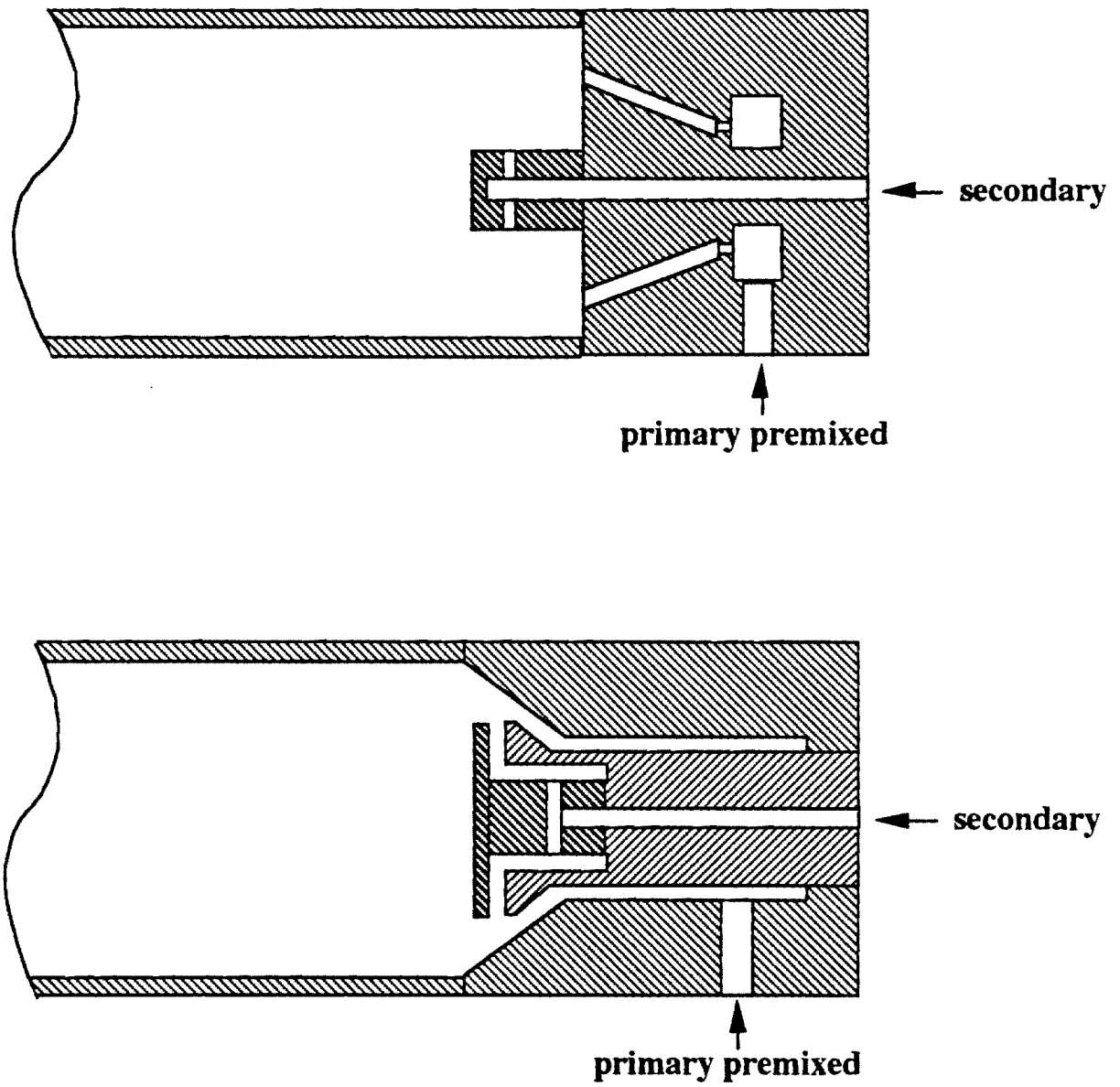

Figure 7. A schematic of the investigated, INJ1 (above) and INJ2 (below), injectors.

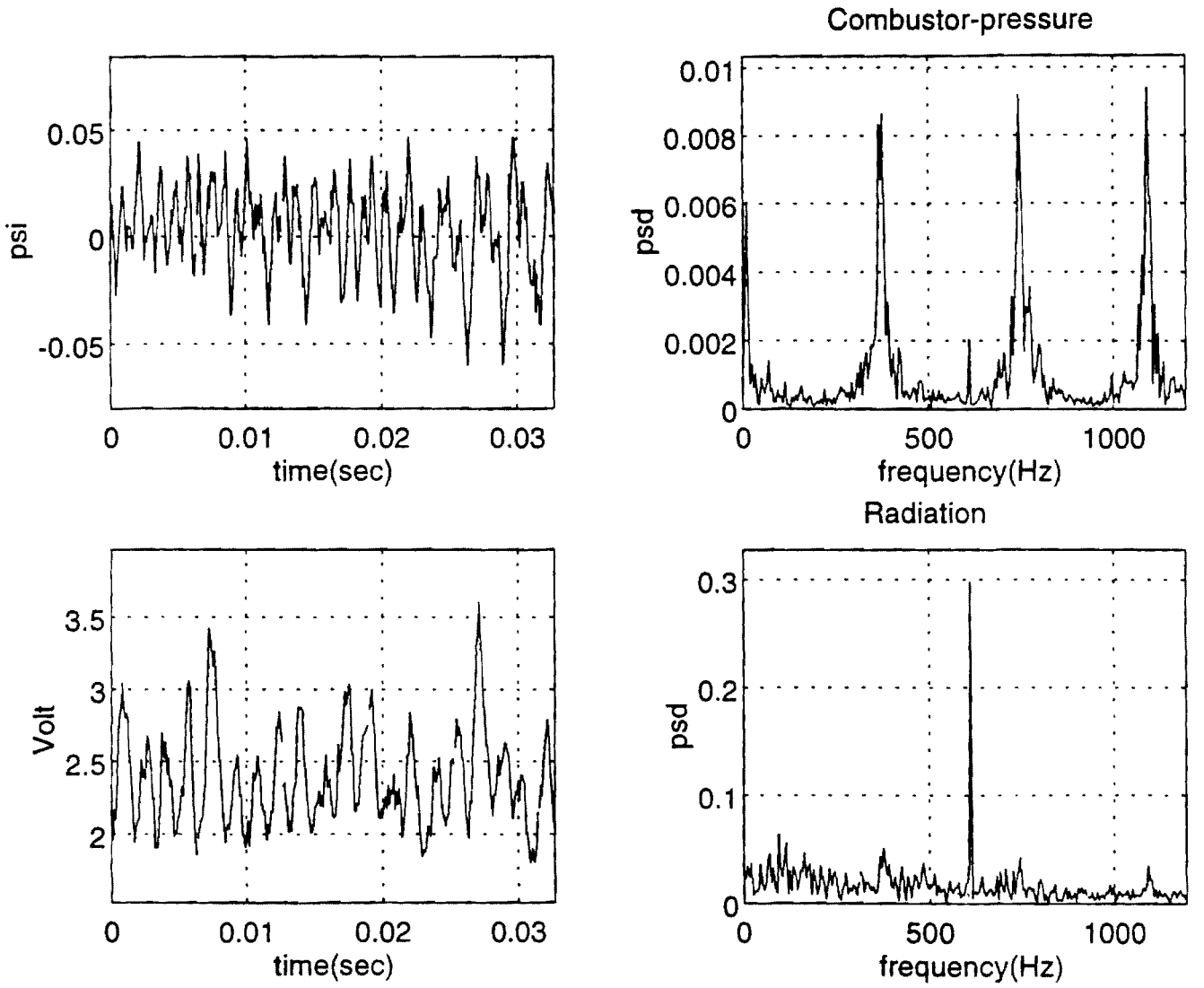

Figure 8. Time dependence and spectra of the combustor pressure and combustion region CH radicals radiation measured in an open loop experiment.

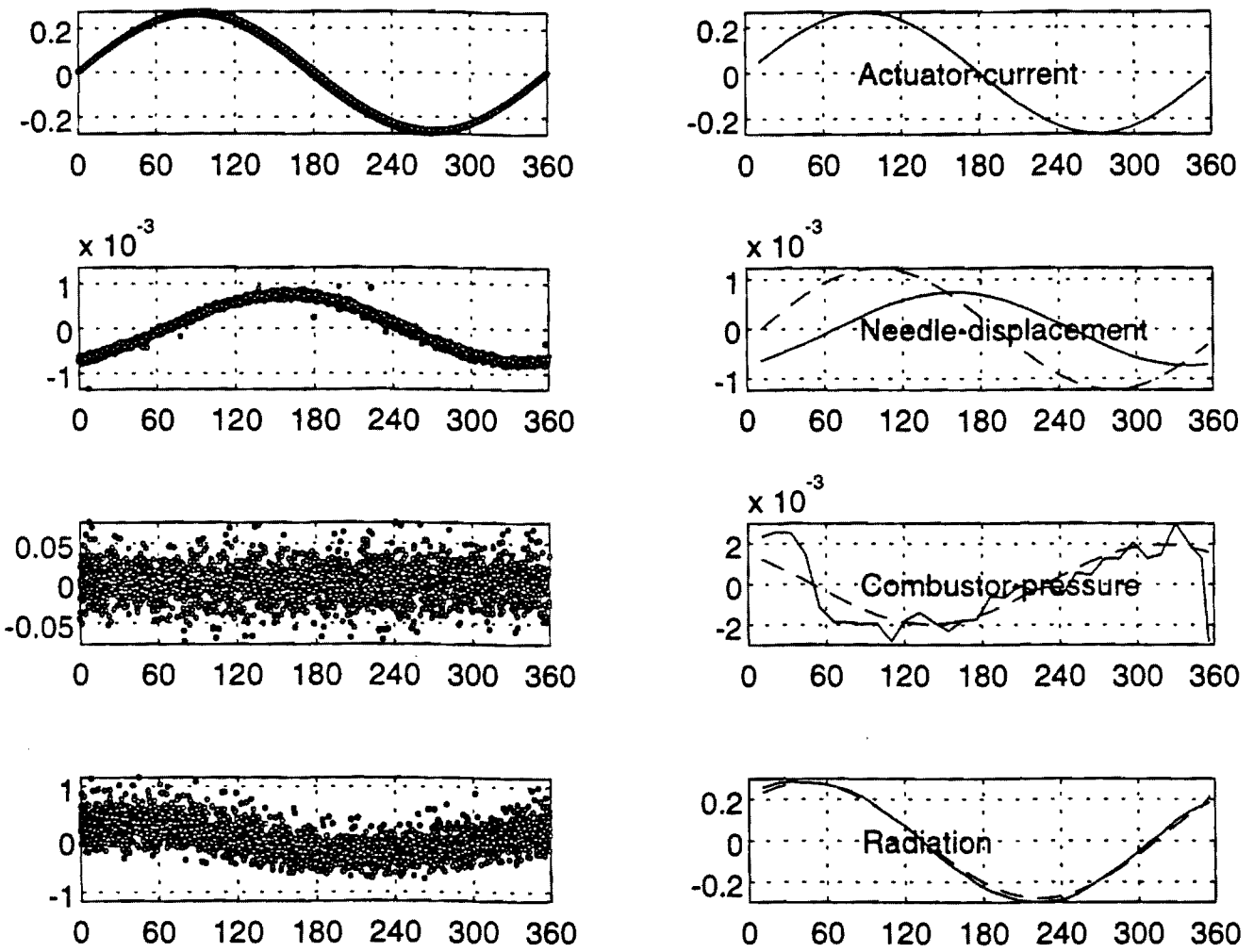

Figure 9. Measured and ensemble averaged data describing the actuator current, needle displacement, combustor pressure and CH radicals radiation obtained in the open loop experiment whose results are presented in Fig. 8.

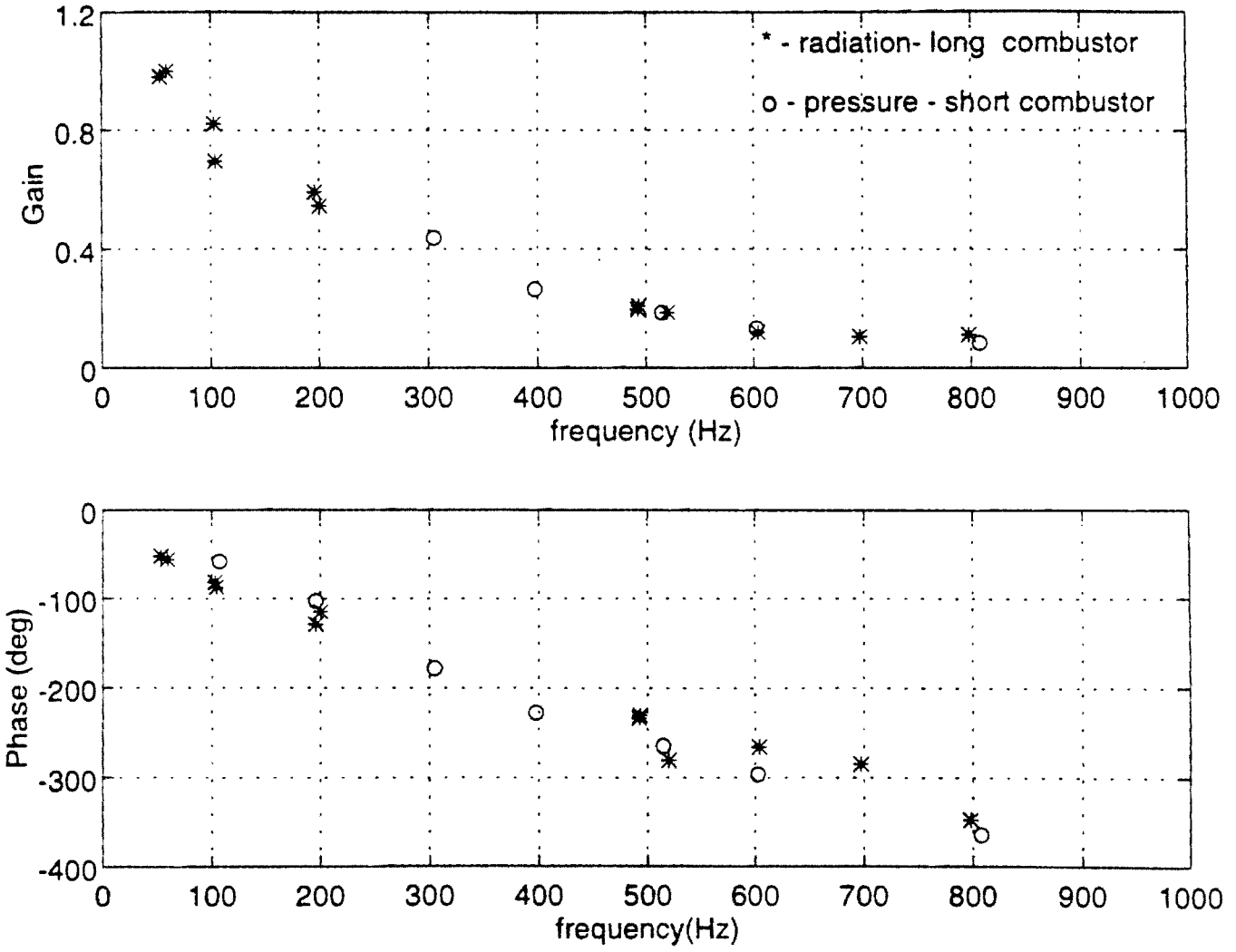

Figure 10. Comparisons of the frequency dependence of the amplitude and phase of the heat release oscillations produced by the fuel injector actuator obtained using pressure data measured in the short combustor and direct CH radiation measurements in the long combustor.

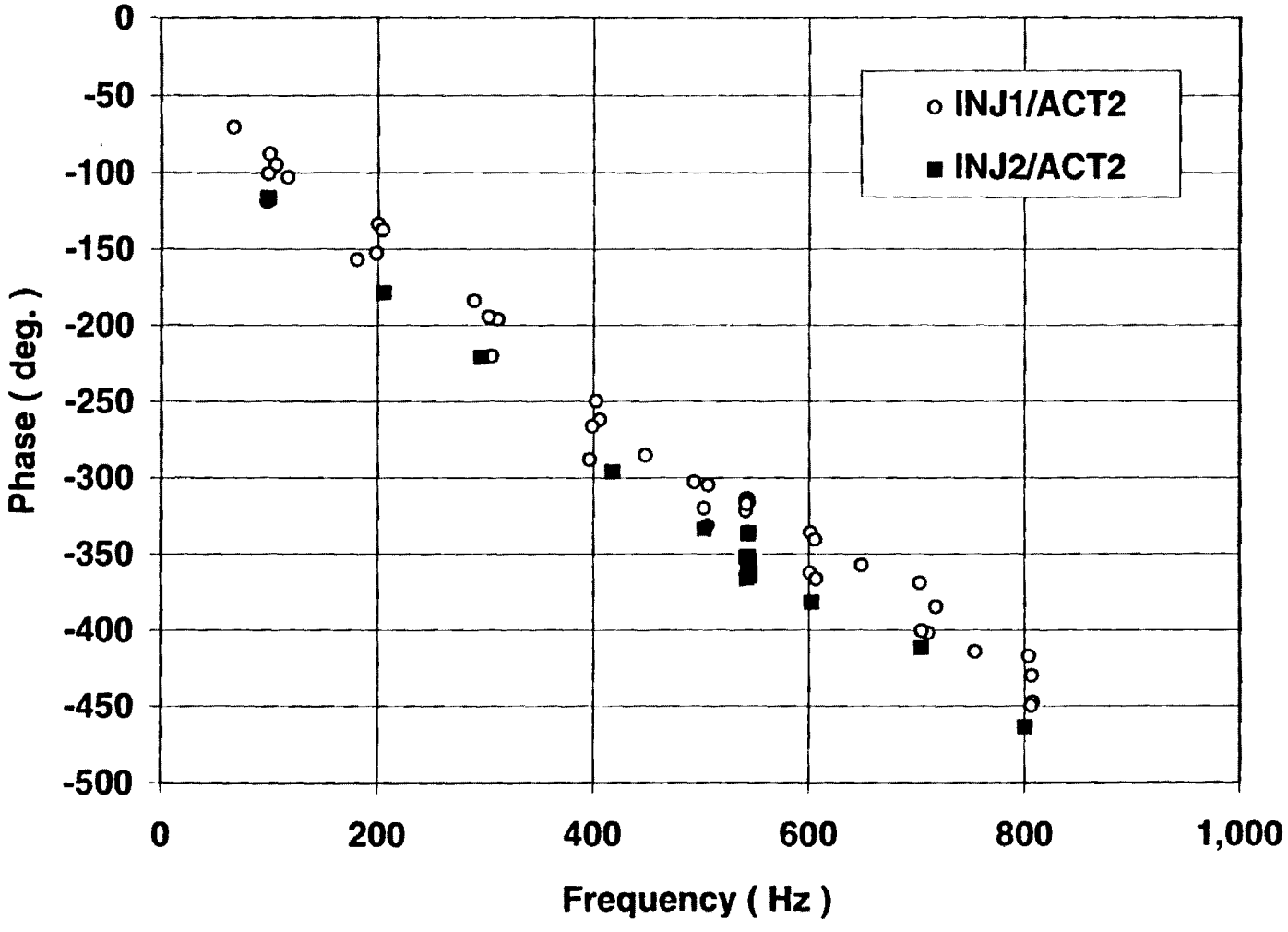

Figure 11-a. Phase difference between heat release and actuator displacement oscillations for two different injector/actuator configurations.

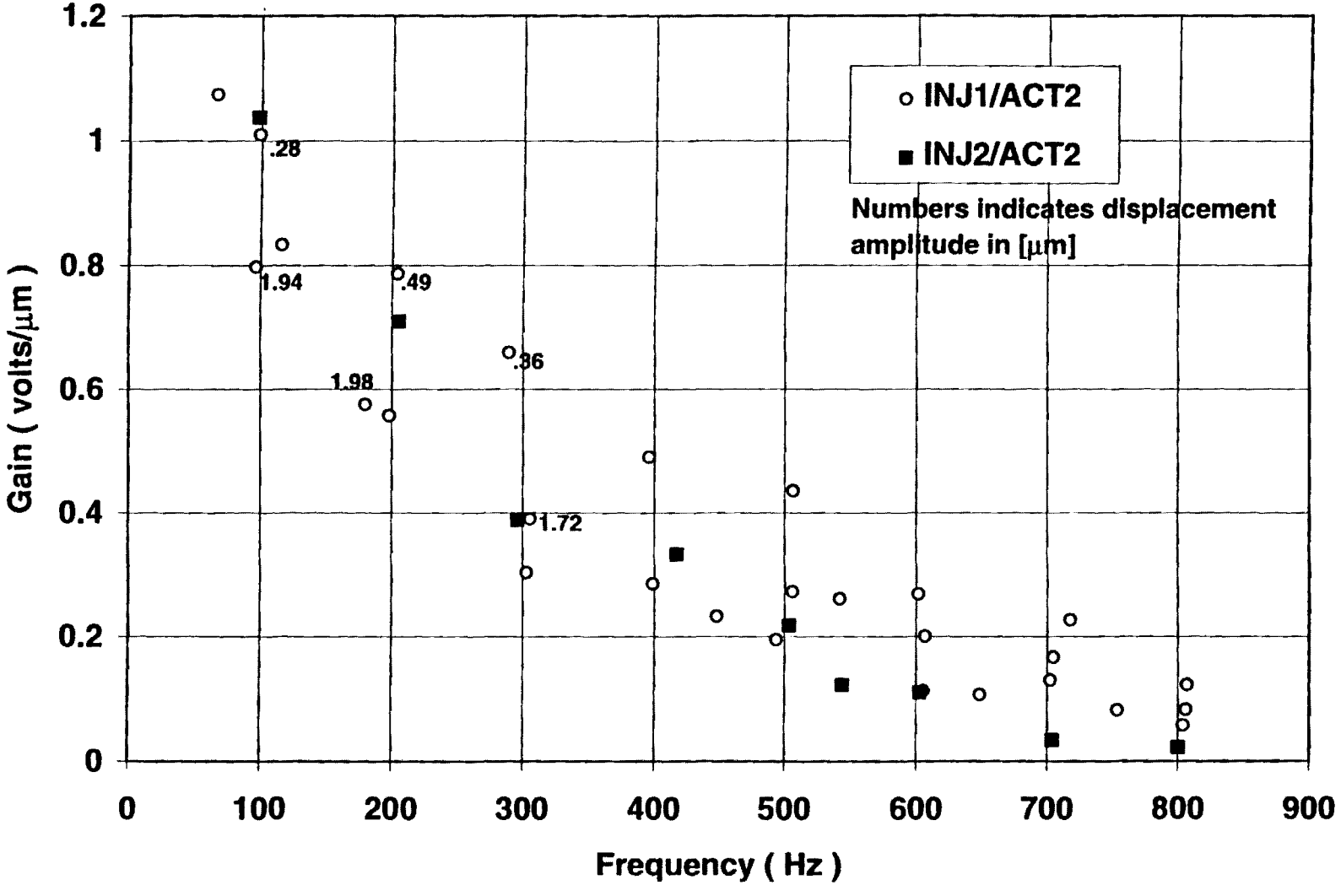

Figure 11-b. Gain of heat release with respect to actuator displacement oscillations for two different injector/actuator configurations.

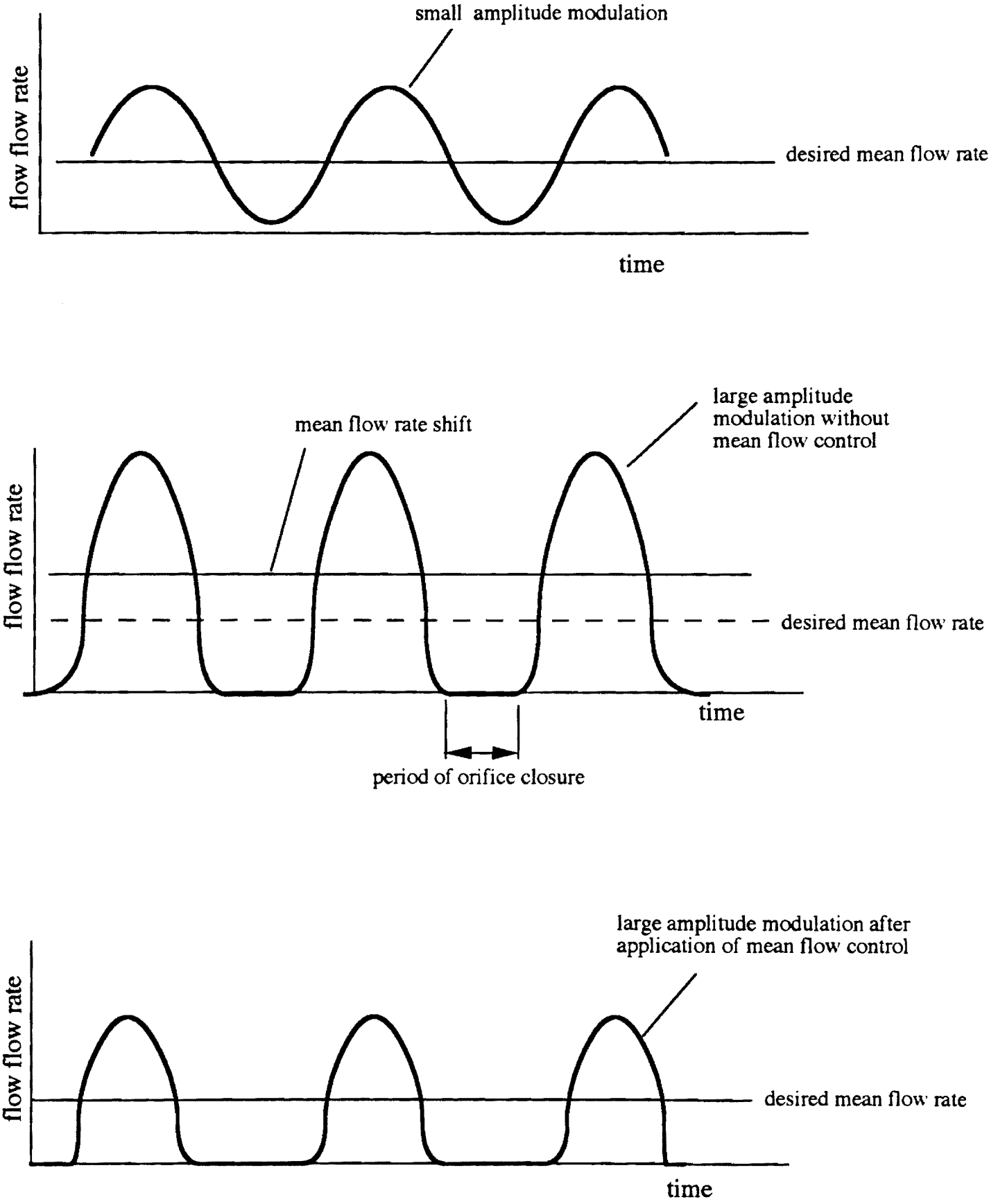

Figure 12. Qualitative description of the effect of mean flow control upon fuel flow modulation

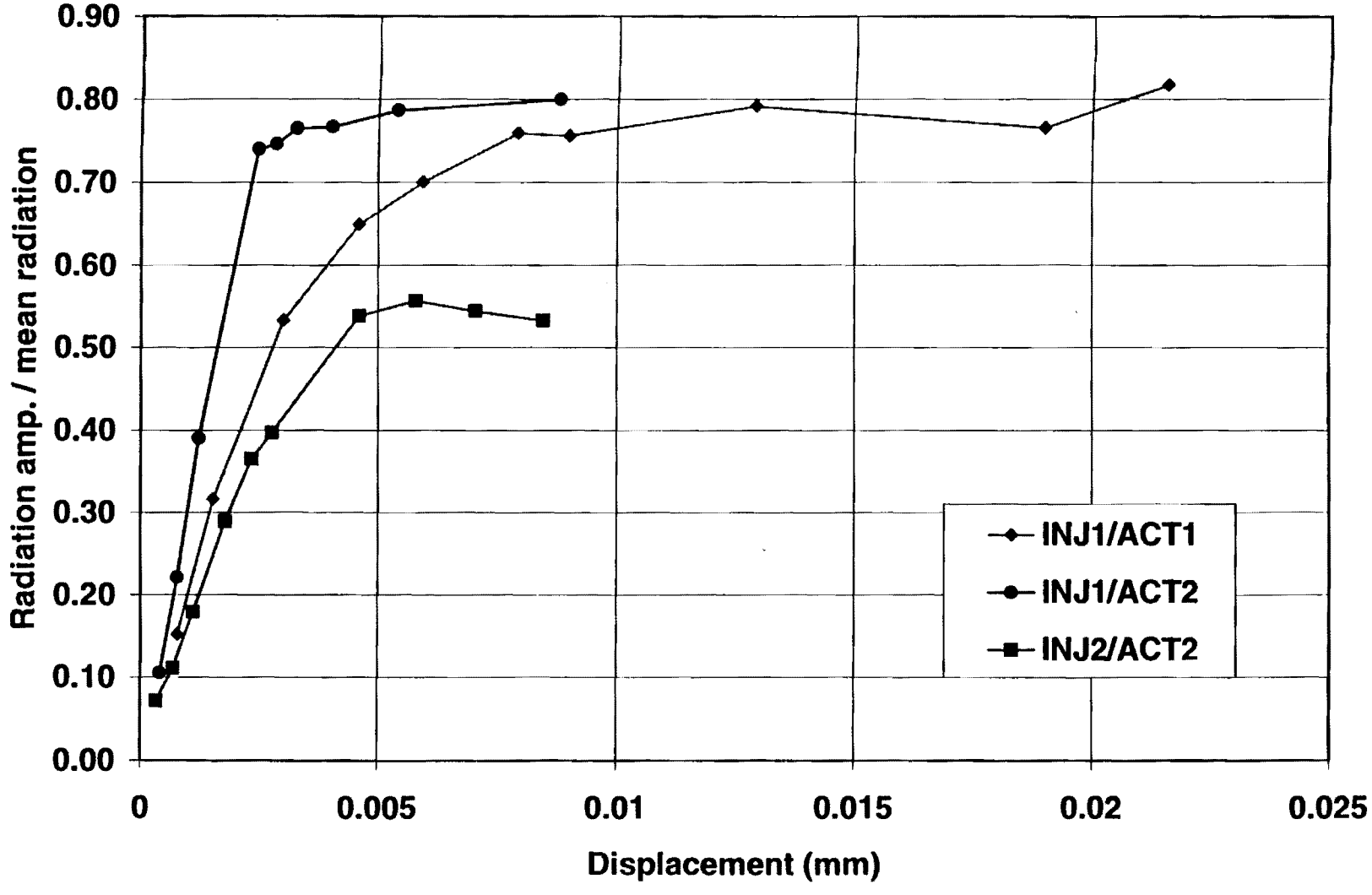

Figure 13. The dependence of the ratio of oscillating to mean heat release radiation upon the displacement of the actuator's needle amplitude.

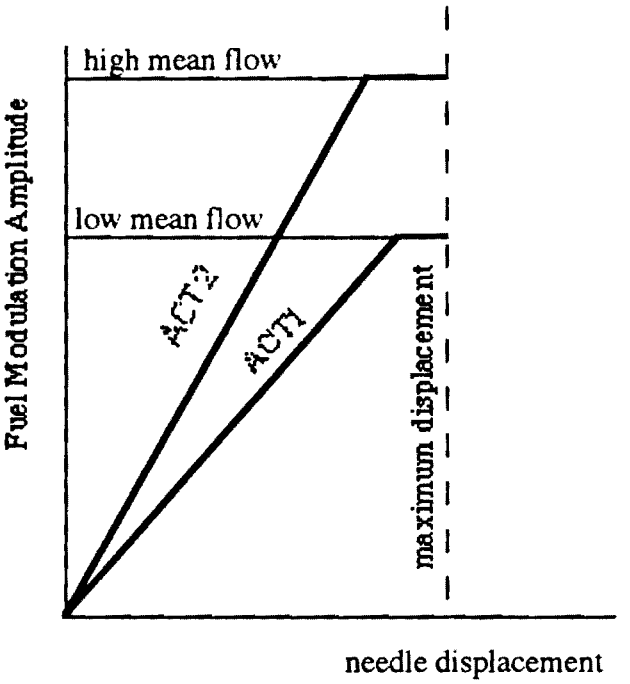

Figure 14-a. Qualitative description of the dependence of the fuel modulation amplitude upon the needle displacement amplitude for two different actuators and mean flows.

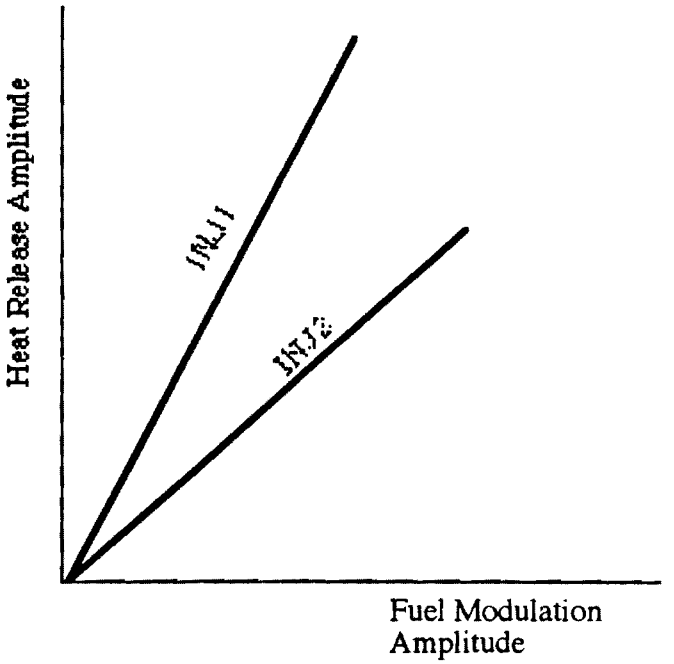

Figure 14-b. Qualitative description of the dependence of the heat release amplitude upon the amplitude of the fuel flow modulation for two different injectors.

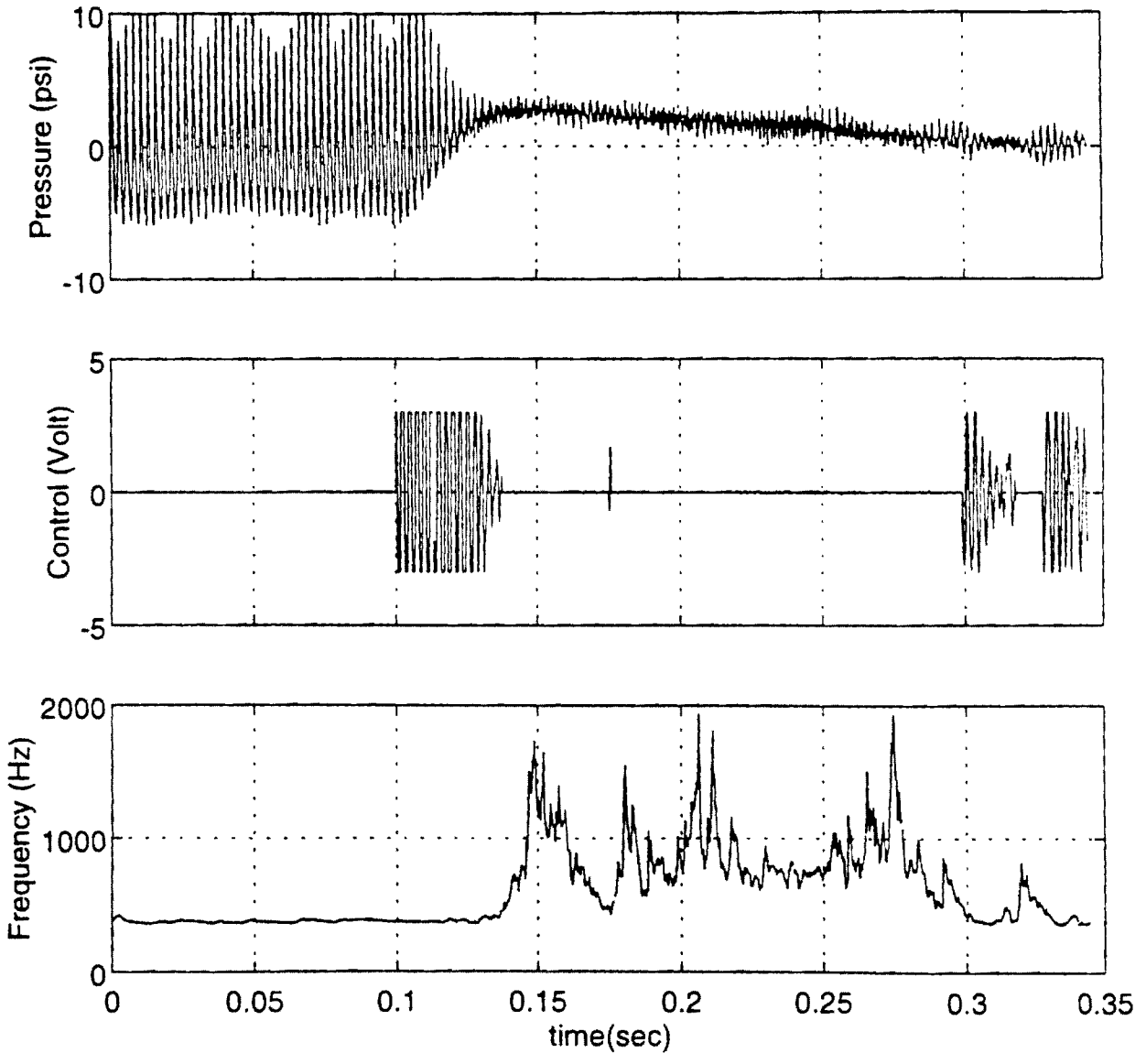

Figure 15. Time dependence of the pressure, control signal and observed frequency before and after the activation of the ACS in the gas rocket .

Appendix A

Extension of the Theory of the Observer for Simultaneous Identification of an Arbitrary Number of Modes in the Input Signal

Prepared by

Nikos Markopoulos and Yedidia Neumeier

1. Introduction

The frequency adaptation formula used so far in our observer is based on a single, sinusoidal input. If we know a signal at each instant of time, and if we also know that the signal is indeed a sinusoid, then, this frequency adaptation formula supplies us with the exact frequency of the sinusoid, without the need for any iterations. In practice, the need for iterations arises because of at least two reasons. First, the real pressure signals that we encounter in a combustion chamber vary with time in a manner that is far more complex than that of a single sinusoid. Second, the frequency domain characteristics of such signals are not stationary, but change, at best slowly, with time. We may be able to improve this situation at least partially by generalizing our frequency adaptation formula, so that it is accurate for input signals that are composed of an arbitrary number of sinusoids. Then, by accounting for a large enough number of sinusoids, we hope to increase the accuracy and ease with which we capture the characteristics of real signals exhibiting a discrete energy spectrum. This in turn may make our observer more robust and reduce some of our worries about convergence. This generalization of the frequency adaptation formula is given here in two steps. First, in Section 2, the formula is generalized to an input signal that is equal to a sum of two sinusoids. Then, with the insights gained in Section 2, the formula is generalized in Section 3 to an input signal that is equal to a sum of an arbitrary number of sinusoids.

2. Extending the Theory of the Observer to two modes

2.1 The input signal

Consider a signal f(t) given by:

$$f(t) = f_1(t) + f_2(t) \tag{1}$$

where $f_1(t)$ and $f_2(t)$ are two sinusoids:

$$f_1(t) = C_1 \sin \Omega_1 t + D_1 \cos \Omega_1 t \tag{2}$$

$$f_2(t) = C_2 \sin \Omega_2 t + D_2 \cos \Omega_2 t \tag{3}$$

Assume that:

(i) We know f(t) at each instant of time t.

(ii) We know that f(t) is a sum of two sinusoids.

The problem that we will try to solve is the following: Based on the information given in (i), (ii), determine the characteristics of f(t), that is, the frequencies Ω_1 and Ω_2, and the amplitudes C_1, D_1, C_2, and D_2.

2.2 The observer

To solve the problem, in analogy with the one-mode case, we set up an "observer" signal F(t) in the following way: F(t) is equal to the sum:

$$F(t) = F_1(t) + F_2(t) \tag{4}$$

with $F_1(t)$ and $F_2(t)$ given by:

$$F_1(t) = A_1(t)\sin\omega_1 t + B_1(t)\cos\omega_1 t \tag{5}$$

$$F_2(t) = A_2(t)\sin\omega_2 t + B_2(t)\cos\omega_2 t \tag{6}$$

Here ω_1 and ω_2 are two arbitrary frequencies that we select in advance for our observer. The time functions $A_1(t)$, $B_1(t)$, $A_2(t)$, and $B_2(t)$ are given by:

$$A_1(t) = \frac{2}{T_1}\int_{t-T_1}^{t}[f(\tau) - F_2(\tau)]\sin\omega_1\tau\, d\tau \tag{7}$$

$$B_1(t) = \frac{2}{T_1}\int_{t-T_1}^{t}[f(\tau) - F_2(\tau)]\cos\omega_1\tau\, d\tau \tag{8}$$

$$A_2(t) = \frac{2}{T_2}\int_{t-T_2}^{t}[f(\tau) - F_1(\tau)]\sin\omega_2\tau\, d\tau \tag{9}$$

$$B_2(t) = \frac{2}{T_2}\int_{t-T_2}^{t}[f(\tau) - F_1(\tau)]\cos\omega_2\tau\, d\tau \tag{10}$$

In Eqs. (7-10) $T_1=2\pi/\omega_1$ and $T_2=2\pi/\omega_2$ are the periods corresponding to the observer frequencies. Using some well-known trigonometric identities, we can completely eliminate $A_1(t)$, $B_1(t)$, $A_2(t)$, and $B_2(t)$ and work directly with $F_1(t)$ and $F_2(t)$. Combining Eqs. (5), (7), and (8) one obtains:

$$F_1(t) = \frac{2}{T_1}\int_{t-T_1}^{t}[f(\tau) - F_2(\tau)]\cos\omega_1(t-\tau)\, d\tau \tag{11}$$

Similarly, combining Eqs. (6), (9), and (10) results in:

$$F_2(t) = \frac{2}{T_2}\int_{t-T_2}^{t}[f(\tau) - F_1(\tau)]\cos\omega_2(t-\tau)\, d\tau \tag{12}$$

Our observer is completely described by Eqs. (4), (11), and (12). If one thinks of $F_1(t)$ and $F_2(t)$ as the estimates of $f_1(t)$ and $f_2(t)$ respectively, then, from Eq. (11), the input for evaluating the estimate of $f_1(t)$ is f(t) minus the estimate of $f_2(t)$. Likewise, from Eq. (12), the input for evaluating the estimate of $f_2(t)$ is f(t) minus the estimate of $f_1(t)$. The symmetry is complete.

For the particular f(t) given by Eqs. (1-3), the solution of Eqs. (11-12) can be expressed as:

$$F_1(t) = F_{11}(t) + F_{12}(t) \tag{13}$$

where $F_{11}(t)$ and $F_{12}(t)$ are two sinusoids:

$$F_{11}(t) = K_{11}\sin\Omega_1 t + L_{11}\cos\Omega_1 t \tag{14}$$

$$F_{12}(t) = K_{12}\sin\Omega_2 t + L_{12}\cos\Omega_2 t \tag{15}$$

and:

$$F_2(t) = F_{21}(t) + F_{22}(t) \tag{16}$$

where $F_{21}(t)$ and $F_{22}(t)$ are the two sinusoids:

$$F_{21}(t) = K_{21}\sin\Omega_1 t + L_{21}\cos\Omega_1 t \tag{17}$$

$$F_{22}(t) = K_{22}\sin\Omega_2 t + L_{22}\cos\Omega_2 t \tag{18}$$

The amplitudes K_{ij} and L_{ij} are independent of t. They depend in quite a complex manner on the frequencies Ω_1 and Ω_2 and amplitudes C_1, D_1, C_2, and D_2 of the input signal f(t), plus the frequencies ω_1 and ω_2 of our observer. To find this dependence one can substitute from Eqs. (13-18) into Eqs. (11-12) and determine K_{ij}, L_{ij} by equating the coefficients of terms in $\sin\Omega_1 t$, $\cos\Omega_1 t$, $\sin\Omega_2 t$, and $\cos\Omega_2 t$. This step is very tedious and time consuming and won't be given here explicitly.

2.3 Perfect reconstruction of the input

When our observer operates at the "correct" frequencies, that is, when $\omega_1=\Omega_1$ and $\omega_2=\Omega_2$, then, one can show that the cross-coupling sinusoids $F_{12}(t)$ and $F_{21}(t)$ are identically zero, while $F_1(t)=F_{11}(t)=f_1(t)$, and $F_2(t)=F_{22}(t)=f_2(t)$. In this case $f_1(t)$ is perfectly reproduced by $F_1(t)$, $f_2(t)$ is perfectly reproduced by $F_2(t)$, and the input signal f(t) is perfectly reproduced by the observer signal F(t). Thus, in order to find the amplitudes, phase shifts, and frequencies of the input signal f(t), all we have to do is determine first, in some way, the frequencies Ω_1 and Ω_2. After that, we can simply update the frequencies of our observer to Ω_1 and Ω_2. Then, the signals $F_1(t)$ and $F_2(t)$ produced by our observer will be the same as the sinusoids $f_1(t)$ and $f_2(t)$ respectively.

2.4 Determining the correct frequencies

The reason that the determination of Ω_1 and Ω_2 is not straightforward is that our observer supplies us only with the signals $F_1(t)$ and $F_2(t)$. That is, we have no knowledge of the components $F_{11}(t)$, $F_{12}(t)$,

$F_{21}(t)$, and $F_{22}(t)$ individually. Similarly, we have no knowledge of the components $f_1(t)$ and $f_2(t)$ of f(t) individually. All we know is their sum f(t). Keeping this in mind, the frequencies Ω_1 and Ω_2 can be found by extending the method applied previously to a one-mode signal f(t) in the following way: First, one can examine the explicit expressions for the amplitudes Kij and Lij (not given here) and show that the time derivatives of the functions $F_{ij}(t)$ can be written as:

$$\dot{F}_{11}(t) = \frac{\omega_1 \Omega_1^2}{\pi\left(\Omega_1^2 - \omega_1^2\right)} \left[f_1(t) - F_{21}(t) - f_1(t-T_1) + F_{21}(t-T_1)\right] \tag{19}$$

$$\dot{F}_{12}(t) = \frac{\omega_1 \Omega_2^2}{\pi\left(\Omega_2^2 - \omega_1^2\right)} \left[f_2(t) - F_{22}(t) - f_2(t-T_1) + F_{22}(t-T_1)\right] \tag{20}$$

$$\dot{F}_{21}(t) = \frac{\omega_2 \Omega_1^2}{\pi\left(\Omega_1^2 - \omega_2^2\right)} \left[f_1(t) - F_{11}(t) - f_1(t-T_2) + F_{11}(t-T_2)\right] \tag{21}$$

$$\dot{F}_{22}(t) = \frac{\omega_2 \Omega_2^2}{\pi\left(\Omega_2^2 - \omega_2^2\right)} \left[f_2(t) - F_{12}(t) - f_2(t-T_2) + F_{12}(t-T_2)\right] \tag{22}$$

Then, combining Eqs. (19-20), and using Eqs. (1), (16) one obtains:

$$\left(\frac{\Omega_1^2 - \omega_1^2}{\Omega_1^2}\right)\dot{F}_{11}(t) + \left(\frac{\Omega_2^2 - \omega_1^2}{\Omega_2^2}\right)\dot{F}_{12}(t) = \frac{\omega_1}{\pi}\left[f(t) - F_2(t) - f(t-T_1) + F_2(t-T_1)\right] \tag{23}$$

Similarly, combining Eqs. (21-22), and using Eqs. (1), (13) results in:

$$\left(\frac{\Omega_1^2 - \omega_2^2}{\Omega_1^2}\right)\dot{F}_{21}(t) + \left(\frac{\Omega_2^2 - \omega_2^2}{\Omega_2^2}\right)\dot{F}_{22}(t) = \frac{\omega_2}{\pi}\left[f(t) - F_1(t) - f(t-T_2) + F_1(t-T_2)\right] \tag{24}$$

Denoting the terms in the brackets above by $M_1(t)$ and $M_2(t)$:

$$M_1(t) = f(t) - F_2(t) - f(t-T_1) + F_2(t-T_1) \tag{25}$$

$$M_2(t) = f(t) - F_1(t) - f(t-T_2) + F_1(t-T_2) \tag{26}$$

and using Eqs. (13), (16), one can write Eqs. (23), (24) as:

$$\frac{\omega_1^2}{\Omega_1^2}\dot{F}_{11}(t)+\frac{\omega_1^2}{\Omega_2^2}\dot{F}_{12}(t)=\dot{F}_1(t)-\frac{\omega_1}{\pi}M_1(t) \tag{27}$$

$$\frac{\omega_2^2}{\Omega_1^2}\dot{F}_{21}(t)+\frac{\omega_2^2}{\Omega_2^2}\dot{F}_{22}(t)=\dot{F}_2(t)-\frac{\omega_2}{\pi}M_2(t) \tag{28}$$

Defining two auxiliary variables by:

$$N_1(t)=\dot{F}_1(t)-\frac{\omega_1}{\pi}M_1(t), \qquad N_2(t)=\dot{F}_2(t)-\frac{\omega_2}{\pi}M_2(t) \tag{29}$$

and using again Eqs. (13), (16), one can further manipulate Eqs. (27) and (28) into the form:

$$\frac{1}{\Omega_1^2}\dot{F}_1(t)+\left(\frac{1}{\Omega_2^2}-\frac{1}{\Omega_1^2}\right)\dot{F}_{12}(t)=\frac{N_1(t)}{\omega_1^2} \tag{30}$$

$$\left(\frac{1}{\Omega_1^2}-\frac{1}{\Omega_2^2}\right)\dot{F}_{21}(t)+\frac{1}{\Omega_2^2}\dot{F}_2(t)=\frac{N_2(t)}{\omega_2^2} \tag{31}$$

We want to solve Eqs. (30-31) for Ω_1, Ω_2, but the problem is that we don't know the cross-components $F_{12}(t)$, $F_{21}(t)$ (see Eqs. (13-18)). If the observer frequencies ω_1, ω_2 are close enough to the input frequencies Ω_1, Ω_2 respectively, then, by examining the corresponding expressions for the amplitudes K_{ij}, L_{ij}, of $F_{ij}(t)$ (not given here explicitly), one can show that K_{12}, L_{12}, and K_{21}, L_{21}, are much smaller compared to K_{11}, L_{11}, and K_{22}, L_{22}, respectively. In such a case, it is safe to neglect the time derivatives of $F_{12}(t)$, $F_{21}(t)$ in Eqs. (30-31), and solve these equations approximately for Ω_1, Ω_2 as:

$$\Omega_1^2=\frac{\pi\,\omega_1^2\,\dot{F}_1(t)}{\pi\,\dot{F}_1(t)-\omega_1\left[f(t)-F_2(t)-f(t-T_1)+F_2(t-T_1)\right]} \tag{32}$$

$$\Omega_2^2=\frac{\pi\,\omega_2^2\,\dot{F}_2(t)}{\pi\,\dot{F}_2(t)-\omega_2\left[f(t)-F_1(t)-f(t-T_2)+F_1(t-T_2)\right]} \tag{33}$$

2.5 Comparison with the old frequency adaptation scheme

Before proceeding further, it is interesting to see the connection between Eqs. (32-33) and the frequency adaptation used in our present day observer. To make this connection, consider first an input signal f(t) which is a single sinusoid with frequency Ω. If F(t) is the corresponding (single) observer signal that we use to reproduce f(t), and if ω is the frequency of our observer, then Ω can be found from

the old adaptation formula, derived by Dr. Neumeier, who worked with the quantities A(t) and B(t) rather than F(t). Using our notation this old adaptation formula can be written as:

$$\Omega^2 = \frac{\pi\,\omega^2\,\dot{F}(t)}{\pi\,\dot{F}(t) - \omega\,[f(t) - f(t-T)]} \tag{34}$$

Eq. (34) supplies us with the exact value of Ω, as long as f(t) is a single sinusoid. If we now consider an input signal f(t) which is a sum of n sinusoids, the intuitive way to generalize Eq. (34) would be:

$$\Omega_i^2 = \frac{\pi\,\omega_i^2\,\dot{F}_i(t)}{\pi\,\dot{F}_i(t) - \omega_i \left\{ f(t) - f(t-T_i) - \sum_{j=1,\,j\neq i}^{n} \left[F_j(t) - F_j(t-T_i) \right] \right\}} \qquad i = 1,2,\ldots,n \tag{35}$$

Clearly, Eqs. (32-33) correspond to the special case n=2 in Eq. (35). What is done in our present day observer corresponds basically to using Eq. (35) in an iterative scheme to determine the frequencies Ω_i of an input signal. The iterations are needed partly because Eq. (35) is only approximate, since it ignores the coupling terms $F_{ij}(t)$, and partly because real signals may have characteristics that change with time, like component frequencies, amplitudes, phase shifts, etc.

2.6 Accurate frequency adaptation for two modes

We can try to improve this situation by obtaining a more accurate way of determining the component frequencies Ω_i for input signals composed of n sinusoids. We will first do this for the case n=2, then generalize it to an arbitrary n.

For n=2 we have to reconsider the exact Eqs. (30-31). These equations are valid at any instant of time t, in particular, they are valid for the time instants t-Δt, and t+Δt, where Δt can be taken as a known, strictly positive, and apart from that arbitrary time increment. Explicitly, at t-Δt one has:

$$\frac{1}{\Omega_1^2}\dot{F}_1(t-\Delta t) + \left(\frac{1}{\Omega_2^2} - \frac{1}{\Omega_1^2}\right)\dot{F}_{12}(t-\Delta t) = \frac{N_1(t-\Delta t)}{\omega_1^2} \tag{36}$$

$$\left(\frac{1}{\Omega_1^2} - \frac{1}{\Omega_2^2}\right)\dot{F}_{21}(t-\Delta t) + \frac{1}{\Omega_2^2}\dot{F}_2(t-\Delta t) = \frac{N_2(t-\Delta t)}{\omega_2^2} \tag{37}$$

and, at t+Δt one similarly has:

$$\frac{1}{\Omega_1^2}\dot{F}_1(t+\Delta t)+\left(\frac{1}{\Omega_2^2}-\frac{1}{\Omega_1^2}\right)\dot{F}_{12}(t+\Delta t) = \frac{N_1(t+\Delta t)}{\omega_1^2} \tag{38}$$

$$\left(\frac{1}{\Omega_1^2}-\frac{1}{\Omega_2^2}\right)\dot{F}_{21}(t+\Delta t)+\frac{1}{\Omega_2^2}\dot{F}_2(t+\Delta t)= \frac{N_2(t+\Delta t)}{\omega_2^2} \tag{39}$$

From Eqs. (15), one can now show that:

$$\dot{F}_{12}(t-\Delta t) = \dot{F}_{12}(t)\cos(\Omega_2\Delta t) + \Omega_2 F_{12}(t)\sin(\Omega_2\Delta t) \tag{40}$$

$$\dot{F}_{12}(t+\Delta t) = \dot{F}_{12}(t)\cos(\Omega_2\Delta t) - \Omega_2 F_{12}(t)\sin(\Omega_2\Delta t) \tag{41}$$

Similarly, from Eqs. (17), one can show that:

$$\dot{F}_{21}(t-\Delta t) = \dot{F}_{21}(t)\cos(\Omega_1\Delta t) + \Omega_1 F_{21}(t)\sin(\Omega_1\Delta t) \tag{42}$$

$$\dot{F}_{21}(t+\Delta t) = \dot{F}_{21}(t)\cos(\Omega_1\Delta t) - \Omega_1 F_{21}(t)\sin(\Omega_1\Delta t) \tag{43}$$

Substituting back from Eqs. (40-43) into Eqs. (36-39) we get:

$$\frac{1}{\Omega_1^2}\dot{F}_1(t-\Delta t)+\left(\frac{1}{\Omega_2^2}-\frac{1}{\Omega_1^2}\right)\left[\dot{F}_{12}(t)\cos(\Omega_2\Delta t) + \Omega_2 F_{12}(t)\sin(\Omega_2\Delta t)\right] = \frac{N_1(t-\Delta t)}{\omega_1^2} \tag{44}$$

$$\left(\frac{1}{\Omega_1^2}-\frac{1}{\Omega_2^2}\right)\left[\dot{F}_{21}(t)\cos(\Omega_1\Delta t) + \Omega_1 F_{21}(t)\sin(\Omega_1\Delta t)\right]+\frac{1}{\Omega_2^2}\dot{F}_2(t-\Delta t)= \frac{N_2(t-\Delta t)}{\omega_2^2} \tag{45}$$

$$\frac{1}{\Omega_1^2}\dot{F}_1(t+\Delta t)+\left(\frac{1}{\Omega_2^2}-\frac{1}{\Omega_1^2}\right)\left[\dot{F}_{12}(t)\cos(\Omega_2\Delta t) - \Omega_2 F_{12}(t)\sin(\Omega_2\Delta t)\right] = \frac{N_1(t+\Delta t)}{\omega_1^2} \tag{46}$$

$$\left(\frac{1}{\Omega_1^2}-\frac{1}{\Omega_2^2}\right)\left[\dot{F}_{21}(t)\cos(\Omega_1\Delta t) - \Omega_1 F_{21}(t)\sin(\Omega_1\Delta t)\right]+\frac{1}{\Omega_2^2}\dot{F}_2(t+\Delta t)= \frac{N_2(t+\Delta t)}{\omega_2^2} \tag{47}$$

Equations (44-47), together with Eqs. (30-31) constitute a set of six equations in six unknowns. The unknowns are the four quantities Ω_1, Ω_2, $F_{12}(t)$, $F_{21}(t)$, and the time derivatives of $F_{12}(t)$ and $F_{21}(t)$. From Eqs. (30), (44), and (46), eliminating $F_{12}(t)$ and its time derivative one obtains:

$$\Omega_1^2 = \omega_1^2\left[\frac{2\dot{F}_1(t)\cos(\Omega_2\Delta t) - \dot{F}_1(t+\Delta t) - \dot{F}_1(t-\Delta t)}{2N_1(t)\cos(\Omega_2\Delta t) - N_1(t+\Delta t) - N_1(t-\Delta t)}\right] \tag{48}$$

Similarly, from Eqs. (31), (45), and (47), eliminating $F_{21}(t)$ and its time derivative results in:

$$\Omega_2^2 = \omega_2^2\left[\frac{2\dot{F}_2(t)\cos(\Omega_1\Delta t) - \dot{F}_2(t+\Delta t) - \dot{F}_2(t-\Delta t)}{2N_2(t)\cos(\Omega_1\Delta t) - N_2(t+\Delta t) - N_2(t-\Delta t)}\right] \tag{49}$$

Equations (48-49) must now be solved for the two unknown frequencies Ω_1 and Ω_2. In general, this requires the application of a numerical iterative scheme. If we select a very small time increment Δt, say, equal to the integration time step for the observer signals $F_1(t)$ and $F_2(t)$, then, we can presumably approximate the cosines in Eqs. (48-49) as:

$$\cos(\Omega_1\Delta t) \approx 1 - \frac{\Omega_1^2\Delta t^2}{2}, \qquad \cos(\Omega_2\Delta t) \approx 1 - \frac{\Omega_2^2\Delta t^2}{2} \tag{50}$$

In this case Eqs. (48-49) can be solved analytically. If Δt is small enough so that the cosines can be approximated by unity, then, Eqs. (48-49) decouple and supply us with the solution:

$$\Omega_1^2 = \omega_1^2\left[\frac{2\dot{F}_1(t) - \dot{F}_1(t+\Delta t) - \dot{F}_1(t-\Delta t)}{2N_1(t) - N_1(t+\Delta t) - N_1(t-\Delta t)}\right], \qquad \text{as } \Delta t \to 0 \tag{51}$$

$$\Omega_2^2 = \omega_2^2\left[\frac{2\dot{F}_2(t) - \dot{F}_2(t+\Delta t) - \dot{F}_2(t-\Delta t)}{2N_2(t) - N_2(t+\Delta t) - N_2(t-\Delta t)}\right], \qquad \text{as } \Delta t \to 0 \tag{52}$$

for the frequencies Ω_1 and Ω_2. This solution tends to the exact solution as Δt tends to zero. In practice, for a finite, small Δt the solution expressed in Eqs. (51-52) is either close enough to the exact solution, or if not, it can be used as a first guess for the iterative solution (at a fixed t) of Eqs. (48-49).

3. Extending the Theory of the Observer to n modes

3.1 The input signal

With the two-mode case in the background, the general case of n modes now becomes more transparent. Consider again a signal f(t) given by:

$$f(t) = \sum_{i=1}^{n} f_i(t) \tag{53}$$

where $f_i(t)$ are individual sinusoids:

$$f_i(t) = C_i \sin\Omega_i t + D_i \cos\Omega_i t\,, \qquad i = 1,2,....,n \tag{54}$$

Assume again that:

(i) We know f(t) at each instant of time t.

(ii) We know that f(t) is a sum of n sinusoids, where, n is known.

Again, based on the information given in (i), (ii), we would like to determine the frequencies Ω_i, and the amplitudes C_i, D_i of f(t).

3.2 The observer

To solve the problem, we set up again an observer signal F(t) which is equal to the sum:

$$F(t) = \sum_{i=1}^{n} F_i(t) \tag{55}$$

where, in analogy with Eqs. (11-12), $F_i(t)$ are given by:

$$F_i(t) = \frac{2}{T_i} \int_{t-T_i}^{t} \left[f(\tau) - \sum_{j=1,\, j\neq i}^{n} F_j(\tau) \right] \cos\omega_i(t-\tau)\, d\tau\,, \qquad i = 1,2,....,n \tag{56}$$

For the particular f(t) given by Eqs. (53-54), the solution of Eqs. (56) can be expressed as:

$$F_i(t) = \sum_{j=1}^{n} F_{ij}(t)\,, \qquad i = 1,2,.....,n \tag{57}$$

where $F_{ij}(t)$ are individual sinusoids:

$$F_{ij}(t) = K_{ij} \sin\Omega_j t + L_{ij} \cos\Omega_j t\,, \qquad i = 1,2,..,n, \qquad j = 1,2,..,n \tag{58}$$

The amplitudes K_{ij} and L_{ij} are independent of t. As in the two-mode case, they depend on the frequencies Ω_i and amplitudes C_i, D_i, of the input signal f(t), plus the frequencies ω_i of the observer. To guess this dependence one substitutes from Eqs. (57-58) into Eqs. (56) and determines K_{ij}, L_{ij} by equating the coefficients of terms in $\sin\Omega_i t$ and $\cos\Omega_i t$.

3.3 Perfect reconstruction of the input

In analogy with the two-mode case, one can show that an observer operating at the frequencies $\omega_i = \Omega_i$ reproduces the input signal perfectly. In this case all the cross-coupling sinusoids $F_{ij}(t)$, $i \neq j$, are identically zero, while $F_{ii}(t) = f_i(t)$. Thus, to find the characteristics of the input signal, we must again first determine the input frequencies Ω_i.

3.4 Determining the correct frequencies

Before determining the frequencies Ω_i we have to note that we know only f(t) and the signals $F_i(t)$ supplied to us by our observer. We have no knowledge of the individual components $F_{ij}(t)$ of the observer, or the individual components $f_i(t)$ of the input. Luckily, Eqs. (19-22) which led to the determination of Ω_i in the two-mode case afford a straightforward generalization for the present case. By examining the explicit expressions for the amplitudes Kij and Lij (not given here) one can show that the time derivatives of the functions $F_{ij}(t)$ can be written as:

$$\dot{F}_{ij}(t) = \frac{\omega_i \Omega_j^2}{\pi\left(\Omega_j^2 - \omega_i^2\right)} \left\{ f_j(t) - f_j(t-T_i) - \sum_{k=1,k\neq i}^{n} \left[F_{kj}(t) - F_{kj}(t-T_i) \right] \right\} \tag{59}$$

Rearranging the above expression and summing over the index j one obtains:

$$\sum_{j=1}^{n} \left(\frac{\Omega_j^2 - \omega_i^2}{\Omega_j^2} \right) \dot{F}_{ij}(t) = \frac{\omega_i}{\pi} \left\{ \sum_{j=1}^{n} \left[f_j(t) - f_j(t-T_i) \right] - \sum_{j=1}^{n} \sum_{k=1,k\neq i}^{n} \left[F_{kj}(t) - F_{kj}(t-T_i) \right] \right\} \tag{60}$$

The sum on the left-hand-side can be simplified by using Eq. (57). The first sum on the right-hand-side can be simplified by using Eq. (53). For the double sum on the right-hand-side one first uses Eq. (57) and sums with respect to j, then the dummy index k is changed to j. After rearranging terms, Eq. (60) can be written in the equivalent form:

$$\sum_{j=1}^{n} \left(\frac{\omega_j^2}{\Omega_j^2} \right) \dot{F}_{ij}(t) = \dot{F}_i(t) - \frac{\omega_i}{\pi} \left\{ f(t) - f(t-T_i) - \sum_{j=1,j\neq i}^{n} \left[F_j(t) - F_j(t-T_i) \right] \right\} \tag{61}$$

Just as in Eqs. (25-26), defining the auxiliary quantities $M_i(t)$ by:

$$M_i(t) = f(t) - f(t-T_i) - \sum_{j=1,j\neq i}^{n} \left[F_j(t) - F_j(t-T_i) \right], \qquad i = 1,2,\ldots\ldots,n \tag{62}$$

one can write Eq. (61) as (see Eqs. (27-28)):

$$\sum_{j=1}^{n} \left(\frac{\omega_j^2}{\Omega_j^2} \right) \dot{F}_{ij}(t) = \dot{F}_i(t) - \frac{\omega_i}{\pi} M_i(t) \tag{63}$$

Then, using the definitions (see Eqs. (29)):

$$N_i(t) = \dot{F}_i(t) - \frac{\omega_i}{\pi} M_i(t), \qquad i = 1,2,.....,n \tag{64}$$

and Eq. (57), one can write Eq. (64) in a form completely analogous to Eqs. (30-31):

$$\frac{1}{\Omega_i^2}\dot{F}_i(t) + \sum_{j=1, j\neq i}^{n}\left(\frac{1}{\Omega_j^2} - \frac{1}{\Omega_i^2}\right)\dot{F}_{ij}(t) = \frac{N_i(t)}{\omega_i^2}, \qquad i = 1,2,.....,n \tag{65}$$

To solve the above n equations for Ω_i we first need to have sufficient information to determine the cross-coupling sinusoids $F_{ij}(t)$. Extending the procedure followed in section 2.6, we can select an integer m, and write equations identical to Eqs. (65), valid at the 2m instants of time t-kΔt, t+kΔt, with k=1,2,.....,m. We thus obtain an additional 2mn equations (just like Eqs. (36-39) in the two-mode case). In each one of these equations, just as in Eqs. (40-42), we use the identities:

$$\dot{F}_{ij}(t - k\Delta t) = \dot{F}_{ij}(t)\cos(k\Omega_j\Delta t) + \Omega_j F_{ij}(t)\sin(k\Omega_j\Delta t) \tag{66}$$

$$\dot{F}_{ij}(t + k\Delta t) = \dot{F}_{ij}(t)\cos(k\Omega_j\Delta t) - \Omega_j F_{ij}(t)\sin(k\Omega_j\Delta t) \tag{67}$$

Then, we have a total of $2n^2$-n unknowns. The unknowns are the n frequencies Ω_i, the n^2-n quantities $F_{ij}(t)$, and the n^2-n derivatives of $F_{ij}(t)$. We also have 2mn+n equations, n of them given by Eqs. (65), and 2mn of them given by (see Eqs. (44-47)):

$$\frac{1}{\Omega_i^2}\dot{F}_i(t - k\Delta t) + \sum_{j=1, j\neq i}^{n}\left(\frac{1}{\Omega_j^2} - \frac{1}{\Omega_i^2}\right)\left[\dot{F}_{ij}(t)\cos(k\Omega_j\Delta t) + \Omega_j F_{ij}(t)\sin(k\Omega_j\Delta t)\right] = \frac{N_i(t - k\Delta t)}{\omega_i^2} \tag{68}$$

$$\frac{1}{\Omega_i^2}\dot{F}_i(t + k\Delta t) + \sum_{j=1, j\neq i}^{n}\left(\frac{1}{\Omega_j^2} - \frac{1}{\Omega_i^2}\right)\left[\dot{F}_{ij}(t)\cos(k\Omega_j\Delta t) - \Omega_j F_{ij}(t)\sin(k\Omega_j\Delta t)\right] = \frac{N_i(t + k\Delta t)}{\omega_i^2} \tag{69}$$

Sufficient information for a solution is thus provided when 2mn+n=$2n^2$-n. This determines the value of m as m=n-1. Adding Eqs. (68-69) one obtains:

$$\sum_{j=1, j\neq i}^{n}\left(\frac{1}{\Omega_j^2} - \frac{1}{\Omega_i^2}\right)\dot{F}_{ij}(t)\cos(k\Omega_j\Delta t) = \frac{N_i(t + k\Delta t) + N_i(t - k\Delta t)}{2\omega_i^2} - \frac{\dot{F}_i(t + k\Delta t) + \dot{F}_i(t - k\Delta t)}{2\Omega_i^2} \tag{70}$$

For m=n-1, Eqs. (70) constitute a set of $mn=n^2-n$ equations that can be used to eliminate the n^2-n time derivatives of $F_{ij}(t)$. The resulting expressions for these time derivatives can then be substituted into Eqs. (65), supplying us with a system of n equations in the n frequencies Ω_i. Just as in the two-mode case, a complete solution for the frequencies Ω_i can be obtained when the time increment Δt tends to zero. In this case all the cosines can be safely replaced by unity, and Eq. (70) becomes:

$$\sum_{j=1,\, j\neq i}^{n}\left(\frac{1}{\Omega_j^2}-\frac{1}{\Omega_i^2}\right)\dot{F}_{ij}(t) = \frac{N_i(t+k\Delta t)+N_i(t-k\Delta t)}{2\omega_i^2}-\frac{\dot{F}_i(t+k\Delta t)+\dot{F}_i(t-k\Delta t)}{2\Omega_i^2}, \quad \text{as } \Delta t\to 0 \qquad (71)$$

Substituting from Eq. (71) into Eq. (65), and taking k=1, results in a set of n decoupled equations which can be solved for the frequencies Ω_i as:

$$\Omega_i^2=\omega_i^2\left[\frac{2\dot{F}_i(t)-\dot{F}_i(t+\Delta t)-\dot{F}_i(t-\Delta t)}{2N_i(t)-N_i(t+\Delta t)-N_i(t-\Delta t)}\right], \quad \text{as } \Delta t\to 0, \quad i=1,2,.....,n \qquad (72)$$

This solution is qualitatively identical to the one obtained for the two-mode case (compare with Eqs. (51-52)), and tends to the exact solution for Ω_i as Δt tends to zero. In practice, for a finite, small Δt the solution expressed in Eqs. (72) is either close enough to the exact solution, or if not, it can be used as a first guess for the iterative solution (at a fixed t) of Eqs. (65), (70).

Appendix B

High Frequency Nonlinear Vibrational Control

B. Shapiro and B. T. Zinn

Submitted for publication to the IEEE Transaction on Automatic Control.

HIGH FREQUENCY NONLINEAR VIBRATIONAL CONTROL

B. Shapiro* and B. T. Zinn†

Abstract

This paper discusses the feasibility of high frequency nonlinear vibrational control. Such control has the advantage that it does not require state measurement and processing capabilities that are required in conventional feedback control. Bellman, Bentsman, and Meerkov (1986) investigated nonlinear systems controlled by linear vibrational controllers and proved that vibrational control is not feasible if the Jacobian matrix has a positive trace. This paper extends previous work to include nonlinear vibrational controllers. A stability criteria is derived for nonlinear systems with nonlinear controllers, and it is shown that a nonlinear vibrational controller can stabilize a system even if the Jacobian matrix has a positive trace.

Preferred Address
B. Shapiro, P.O. 38176, Georgia Tech Station, Atlanta GA, 30332, (before September 3rd).
B. Shapiro, Control and Dynamical Systems, Mail Code 104-44, California Institute of Technology, Pasadena, CA 91125, (after September 3rd).

Acknowledgment
This work benefited from many helpful discussions with Dr. J. Hale; and was supported by funds provided by the Davis S. Lewis Jr. Chair and AFOSR contract number F49620-93-1-0177, Dr. Mitar Birkan, contract monitor.

*School of Aerospace Engineering, Georgia Institute of Technology, Atlanta, GA 30332. Email: gt8176b@prism.gatech.edu Tel: (404) 325-4714.

†School of Aerospace Engineering, Georgia Institute of Technology, Atlanta, GA 30332. Email: ben.zinn@aerospace.gatech.edu Tel: (404) 894-3033

1 Introduction

This paper discusses the feasibility of applying open loop control in the form of high frequency vibrational control to engineering systems. Such control may be applied in cases where closed loop control is impractical and has the advantage that it does not require costly sensing and computing capabilities. Vibrational control is applied by oscillating an accessible system component at low amplitude and high frequency (relative to the natural frequency of the system). For example, an inverted pendulum can be stabilized by vertically oscillating the pendulum pin at a sufficiently high frequency and low amplitude. Let us examine the case of the pendulum in more detail. The vertically oscillated pendulum is described by the following nonlinear differential equation,

$$\dot{x}_1 = x_2, \tag{1.1}$$

$$\dot{x}_2 = C\sin(x_1) - Bx_2 + aw^2 D\sin(x_1)\sin(wt), \tag{1.2}$$

where x_1 is the angular displacement measured from the inverted equilibrium point, x_2 is the angular velocity. B, C and D are positive physical constants, and a and w are the amplitude and frequency of the applied vibration, respectively. In this example, the control input is the applied vibration, which is given by $a\sin(wt)$. Note that the amplitude and frequency of the control input are constant and, therefore, independent of the state of the system. Since there is no sensing or computation involved, this is a form of open loop control. However, (1.2) involves a feedback-like term $w^2 D\sin(x_1)$, which occurs naturally as a result of the moment arm $\sin(x_1)$ between the vertically oscillating pendulum pin and the center of mass of the pendulum. Consequently, the feedback $w^2 D\sin(x_1)$ is *naturally occurring*.

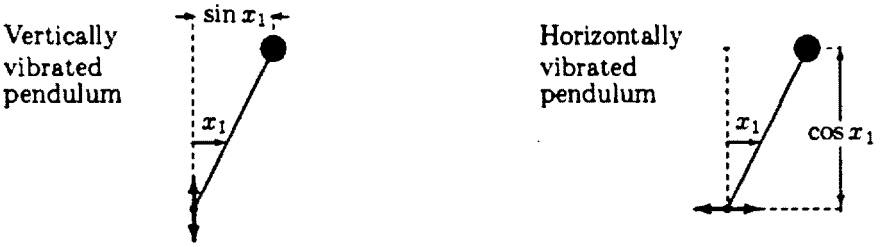

Since the naturally occurring feedback $w^2 D\sin(x_1)$ in (1.2) is of the same form as $C\sin(x_1)$, we can view this form of control as a variation of the parameter C; that is,

$$\dot{x}_1 = x_2, \tag{1.3}$$

$$\dot{x}_2 = [C + aw^2 D\sin(wt)]\sin(x_1) - Bx_2. \tag{1.4}$$

Linearization of the above system yields

$$\begin{bmatrix} \dot{x}_1 \\ \dot{x}_2 \end{bmatrix} = \begin{bmatrix} 0 & 1 \\ C + aw^2 D\sin(wt) & -B \end{bmatrix} \begin{bmatrix} x_1 \\ x_2 \end{bmatrix}, \tag{1.5}$$

which is of the form

$$\dot{x} = [A + B(t)]x, \tag{1.6}$$

where x is a vector, A is a constant matrix and $B(t)$ is a time-varying matrix. In the linear model (1.6), vibrational control appears as a variation of parameters, where the parameters of the matrix A are varied by $B(t)$. This is the model investigated by Bellman, Bentsman and Meerkov [1]. However, there is no reason to assume that vibrational control can always be viewed as a variation of parameters as in the above example. In fact, there are examples where the above model does not apply.

Consider the pendulum once again. Suppose we oscillate the pin of the pendulum horizontally instead of vertically, producing motions that are described by

$$\dot{x}_1 = x_2, \tag{1.7}$$

$$\dot{x}_2 = C\sin(x_1) - Bx_2 + aw^2 D\cos(x_1)\sin(wt). \tag{1.8}$$

Instead of the moment arm $\sin(x_1)$ we now have a moment arm $\cos(x_1)$ and the naturally occurring feedback is $w^2 D\cos(x_1)$. Linearization of this system of equations yields

$$\begin{bmatrix} \dot{x}_1 \\ \dot{x}_2 \end{bmatrix} = \begin{bmatrix} 0 & 1 \\ C & -B \end{bmatrix} \begin{bmatrix} x_1 \\ x_2 \end{bmatrix} + \begin{bmatrix} 0 \\ aw^2 D\sin(wt) \end{bmatrix}, \tag{1.9}$$

which cannot be written in the form of (1.6). Consequently, we cannot view the above case as a variation of parameters.

The above example demonstrates that vibrating a system component does not always produce "variation of parameters" as in the vertically vibrated pendulum. Consequently, we adopt a more general approach that permits the analysis of problems where a vibrated system component may result in nonlinear functions in the governing equations. Consider a nonlinear system

$$\dot{x} = f(x), \tag{1.10}$$

with an equilibrium point at the origin (i.e., $f(0) = 0$). Vibrational control is applied by oscillating a system component or process at high frequency and low amplitude. For instance, in the case of a jet engine, the air-throttle or amount of fuel injected might be vibrated. Let $h(wt) = \sin(wt)$ denote the applied high frequency vibration. It is assumed that the vibration affects the system $f(x)$ through some naturally occurring feedback function $g(x, w, a)$, which depends on the vibrated component. The vibrationally controlled system is described by

$$\dot{x} = f(x) + h(wt)g(x, w, a). \tag{1.11}$$

For convenience, the amplitude of $h(wt)$ is taken to equal unity and the amplitude of the applied vibration is accounted for by $g(x, w, a)$. In the case of the pendulum,

$$f(x) = [x_2, C\sin(x_1) - Bx_2]^T \tag{1.12}$$

and $g(x, w, a) = [0, aw^2 D\sin(x_1)]^T$ for the vertically vibrated pin, or $g(x, w, a) = [0, aw^2 D\cos(x_1)]^T$ for the horizontally vibrated pin. We emphasize once again that $g(x, w, a)$ occurs naturally, and is not measured or computed but is a result of the interaction between the system and vibrated component. Obviously, an oscillating fuel injection rate is not going to affect the jet engine in the same fashion as an oscillating throttle. Consequently, each actuation will be described by a different function $g(x, w, a)$. Since $g(x, w, a)$ depends on properties of the system (which are fixed) and the vibrated component, we can only control the choice of the component to oscillate and the frequency and amplitude of the vibration. This choice determines the form of $g(x, w, a)$, and since in certain cases there exist no $g(x, w, a)$ that will allow vibrational control, such control is not always feasible.

We now turn to the question of stability. Suppose the equilibrium point $x = 0$ of (1.10) is unstable, and that there exist one or more accessible system components or processes that can be vibrated, each associated with a function $g(x, w, a)$ that is known. The objective of the theory presented in this paper is to determine a stability criterion for (1.11). Consequently, if a certain $g(x, w, a)$ satisfies the derived stability criterion, then oscillation of the corresponding system component, with specific frequency w and amplitude a, will alter the stability of the system and result in vibrational control. Therefore, the developed criterion will determine if vibrational control is feasible for various accessible system components or processes in a given system.

Vibrational control has found various applications, including lasers [2] and particle beams [3]. Initial work on developing a general theory of vibrational control was carried out by Meerkov [4]. He discussed the effect of vibrational control upon stability, transient motion and response of the controlled system. In subsequent publications, several specific nonlinear problems were discussed [5], but no general vibrational control was proposed. Such a theory was outlined by Bellman, Bentsman and Meerkov [1], who presented criteria for the control of nonlinear systems by linear vibrational control. Further nonlinear results are discussed in [6], including conditions for and choice of stabilizing vibrations.

To discuss the results derived in [1], consider (1.11) and assume that the Jacobian matrix $\partial f(0)/\partial x = f'(0)$ of $f(x)$ in (1.11) has a positive trace. A classic theorem in linear algebra states that the trace of a matrix equals the sum of its eigenvalues (see for example [7, p.251]). Consequently, if the trace is positive, then at least one of the

eigenvalues must have a positive real part and the equilibrium point is unstable. This does not imply, however, that if the trace is negative the equilibrium point is stable. A negative trace is a necessary but not a sufficient condition for stability.

Bellman, Bentsman and Meerkov [1] only considered linear vibrational control, which limited the analysis to linear functions $g(x,a,w) = Mx$ in (1.11). They proved that if the Jacobian $f'(0)$ has a positive trace and $g(x,a,w)$ is linear, then vibrational control is not feasible, indicating that no matrix M can stabilize the system (1.11). In this paper we consider a more general case of vibrational control via a nonlinear, slowly varying $g(x,a,w)$. In other words, we consider functions whose rate of change with respect to x is bounded (i.e., $\|\partial g/\partial x\| \leq w\delta_1$). We show that in this case, vibrational control may be possible even if the trace of the Jacobian Matrix is positive. Specifically, it will be shown that there exist nonlinear functions $g(x,a,w)$ that stabilize the system (1.11) even if its Jacobian $f'(0)$ has a positive trace.

The main point of this paper is that nonlinearities in $g(x,a,w)$ may not be negligible, and can affect the stability of (1.11). This result is of practical importance for the following reason. In engineering, it is common practice to linearize a system before analyzing its stability. However, if a linear system is considered, then Bellman, Bentsman and Meerkov's result indicates that vibrational control is not feasible when the Jacobian has a positive trace (note that positive traces occur in a wide variety of engineering systems e.g., liquid rockets [8]). Most engineering systems are, however, nonlinear and it is possible that nonlinearities in $g(x,a,w)$ may stabilize the system even if its Jacobian trace is positive. This implies that one should not discount vibrational control for systems that exhibit a positive trace. Instead, one should investigate the nonlinear functions $g(x,a,w)$ associated with vibrational open loop control to determine if they satisfy the stability criteria derived in this paper. We also note that the theory presented in this paper agrees almost exactly with numerical solutions (see section. 3.1).

2 General Derivation

Consider once again the nonlinear system

$$\dot{x} = f(x) + h(wt)g(x,w,a), \tag{2.1}$$

where $h(wt) = \sin(wt)$, $x \in \mathbb{R}^n$ is the state space vector and $x = 0$ is an equilibrium point of (1.10), which is not necessarily an equilibrium point of the forced system (2.1). It is assumed that $f(x)$ is three times continuously differentiable and $g(x)$ is four times continuously differentiable.

We will show that the nonautonomous system (2.1) can be approximated by an autonomous system

$$\dot{y} = F(y). \tag{2.2}$$

This approximation means that there exists a function $u(t,y)$, which is small for all time, such that $x(t) = y(t)+u(t,y)$. Consequently, if $Y(t)$ is a solution of (2.2) and $X(t)$ is a solution of (2.1), then $X(t)-Y(t) = u(t,Y(t))$ is small for all time t. Approximately, $Y(t)$ corresponds to the time average of $X(t)$, and it describes the slow response of the system, while $u(t,Y(t))$ corresponds to the small amplitude high frequency system oscillations excited by the small amplitude, high frequency control input. In essence, there exist two time scales. A fast time scale corresponding to the high frequency control input and the resulting high frequency system response $u(t,Y(t))$, and the slow time scale describing the time averaged system response $Y(t)$. Since $Y(t)$ is a slow or averaged response, it is described by a time averaged equation. In the case of vibrational control, the control input coupled with the system response $u(t,Y(t))$ yields a non-zero average that can stabilize the system.

We will use the following notation. Since w and a are constant, we will express $g(x,w,a)$ as $g(x)$. Also, we define the Jacobian matrix $J = f'(0) = \partial f(0)/\partial x$ and let

$$p(x) = f(x) - Jx, \tag{2.3}$$

$$\phi(wt) = -\epsilon^2 Jg(0)\sin(wt) - \epsilon g(0)\cos(wt), \tag{2.4}$$

where $\epsilon = 1/w$, and $p(x)$ is the sum of all terms of second order and higher in the Taylor expansion of $f(x)$

around $x = 0$. Furthermore, we introduce the constant vector b

$$b = \left[\frac{1}{T}\int_0^T p(\phi(wt))dt - \frac{\epsilon^2 g'(0)Jg(0)}{2}\right], \tag{2.5}$$

where $T = 2\pi/w$ and $g'(0)$ is the Jacobian matrix of $g(x)$, and the constant matrix A,

$$A = \left[J - \frac{\epsilon^2}{2}\frac{\partial(g'(y)Jg(y))}{\partial y}(0)\right], \tag{2.6}$$

where $g'(y)$ is the derivative of $g(y)$ evaluated at y, and $\partial[g'(y)Jg(y)](0)/\partial y$ denotes the derivative of $g'(y)Jg(y)$ evaluated at zero. Finally, we let

$$\zeta = \delta^2 + \epsilon^2\delta_0\delta_1 + \delta\delta_1^2 + \delta_0\delta_1^3/\epsilon + \delta\delta_1^4/\epsilon + \delta_0^3 + \delta_0^2\delta_1 + \delta\delta_0^2 + \delta\delta_0\delta_1 + \epsilon^3\delta_0^2 \tag{2.7}$$

and denote a ball of radius δ centered at a as $B(a,\delta)$.

Theorem 2.1 *Consider the nonlinear system (2.1) and suppose that $f(0) = 0$, $\|g(0)\| \le w\delta_0$, and $\|g'(\xi)\| \le w\delta_1$ for all $\xi \in B(0,\delta)$. Then for sufficiently small δ, δ_0 and δ_1, and sufficiently large w, there exists a function $u(t,y)$ that satisfies the following properties: $\|u(t,y)\| < 2(\delta_0 + \delta\delta_1)$ for all t and for all $y \in B(0,\delta)$, it is $2\pi/w$ periodic in t, and for any y has zero mean value. Furthermore, for $x(t)$ governed by the differential equation (2.1), $y(t) = x(t) - u(t,y)$ is governed by*

$$\dot{y} = Ay + b + O(\zeta) \tag{2.8}$$

for all $y \in B(0,\delta)$ and b, A and ζ defined in (2.5), (2.6) and (2.7), respectively.

While a detailed proof of Theorem (2.1) is given in the Appendix, an outline of the proof is provided below. A transformation $u(s,y)$ is constructed that satisfies the properties of the theorem. We then substitute the equation $y(t) = x(t) - u(t,y)$ into (2.1) and bound various terms so that we can rewrite (2.1) as the approximate system $\dot{y} = F(t,y)$. Next, we apply the method of averaging to derive the averaged equation $\dot{y} = F_{av}(y)$. Linearization of $\dot{y} = F_{av}(y)$ at the origin yields the result of the theorem.

The analysis in this paper includes Taylor terms up to second order in δ_0 and δ_1. Consequently, the resulting error ζ is of third order. If higher accuracy is desired, then more Taylor terms can be included although more stringent smoothness constraints will be imposed because we will have to ensure that higher order derivatives exist for the functions $f(x)$ and $g(x)$. We note that for the examples considered, a second order analysis is sufficient and is in excellent agreement with numerical integration results (see example 3.1).

2.1 Example: The Inverted Pendulum

Consider the vertically vibrated pendulum described by (1.1) and (1.2). These equations are of the form of (2.1). Since $g(0) = 0$, (2.4) implies that $\phi(wt) = 0$ and (2.3) shows that $p(0) = f(0) - 0 = 0$. Consequently, the vector b defined in (2.5) equals zero. The matrix A is defined in (2.6) and can be expressed in the following form,

$$A = \left[J - \frac{\epsilon^2}{2}\frac{\partial(g'(y)Jg(y))}{\partial y}(0)\right] = J - \frac{\epsilon^2}{2}\frac{\partial}{\partial y}\left\{\begin{bmatrix} 0 & 0 \\ aw^2D\cos(y_1) & 0 \end{bmatrix}\begin{bmatrix} 0 & 1 \\ C & -B \end{bmatrix}\begin{bmatrix} 0 \\ aw^2D\sin(y_1) \end{bmatrix}\right\}$$

$$= \begin{bmatrix} 0 & 1 \\ C & -B \end{bmatrix} - \frac{\partial}{\partial y}\begin{bmatrix} 0 \\ a^2w^2D^2\cos(y_1)\sin(y_1)/2 \end{bmatrix} = \begin{bmatrix} 0 & 1 \\ C-(awD)^2/2 & -B \end{bmatrix}. \tag{2.9}$$

Consequently, Theorem (2.1) indicates that the averaged behaviour of the system is governed by

$$\begin{bmatrix} \dot{y}_1 \\ \dot{y}_2 \end{bmatrix} = \begin{bmatrix} 0 & 1 \\ C-(awD)^2/2 & -B \end{bmatrix}\begin{bmatrix} y_1 \\ y_2 \end{bmatrix} \tag{2.10}$$

which is in agreement with the result of [4]. Note that the term $C - (awD)^2/2$ is negative for sufficiently large a or w, indicating that the equilibrium point is asymptotically stable. We also note that even though the method in this paper is restricted to slowly varying $g(x)$, (i.e., $\|g'(x)\| \leq w\delta_1 < w$) the above result is also valid for $\|g'(x)\| \not< w$. We impose the slowly varying restriction to permit inverting the matrix $[I + u_y]$ in (5.21). In the case of the pendulum, we can show that the matrix $[I + u_y]$ has an inverse even if $\|g'(x)\| \not< w$, which eliminates the slowly varying restriction.

3 Discussion of Results

Theorem (2.1) implies that vibrational control can result in an equilibrium shift. For such a shift to occur, the vector b defined in (2.5) has to be nonzero. Equations (2.3),(2.4) and (2.5) imply that such an equilibrium shift can occur only if $g(0)$ is nonzero. In this case there are two possibilities. The first possibility is that the average of $p(\phi(wt))$ is nonzero. Since $p(x)$ is defined in (2.3) as the nonlinear terms of $f(x)$, this implies that nonlinearities in $f(x)$ can cause an equilibrium shift. Such an equilibrium shift would be of order $O(\|\phi\|^2) = O(\delta_0^2)$. The second possibility is that the term $g'(0)Jg(0)$ is nonzero, indicating that the naturally occurring feedback function $g(x)$ can also cause an equilibrium shift. In this case, the equilibrium shift would be of order $O(\epsilon^2\|g'(0)Jg(0)\|) = O(\delta_0\delta_1)$. In either case, if the equilibrium shift is larger than δ our analysis fails because we are forced outside the ball $B(0,\delta)$.

Theorem (2.1) also yields a useful linear result. Consider a linear system of the form

$$\dot{x} = [J + \sin(wt)B]x, \tag{3.1}$$

where $\|B\| < w\delta_1$. In this case, $g(x) = Bx$ and $g'(x) = B$. Therefore $g(0) = 0$ and we can set $\delta_0 = 0$ with no loss of generality. Application of Theorem (2.1) yields the averaged equation

$$\dot{y} = [J - \epsilon^2 BJB/2]y + O\left(\delta(\delta + \delta_1^2 + \delta_1^4/\epsilon)\right). \tag{3.2}$$

However, the most interesting implication of Theorem (2.1) is the following: the operator $g'(y)Jg(y)$ in (2.6) is a nonlinear operator in $g(y)$. Consequently, nonlinearities in $g(y)$ may result in linear terms in the averaged equation (2.8), and can influence local stability. This indicates that the local stability of the nonlinear system (1.11) is not the same as the stability of a corresponding linearized system. It is possible to show that the nonlinearities in $g(y)$ can alter the stability of a system with a positive Jacobian trace. Stabilization of a system with a positive trace is illustrated in the next example.

3.1 Example: A System with a Positive Jacobian Trace

In this example we consider a second-order system with a positive trace. Specifically, we consider the second-order system derived in [8] for the flow potential of a liquid rocket combustor,

$$\ddot{x} + A_1\dot{x} + A_0 x = 0, \tag{3.3}$$

where x is a nondimensional flow potential perturbation and t is a normalized time. In an unstable liquid rocket, unsteady combustion provides negative damping that drives the instability. Since the damping is determined by A_1, negative damping corresponds to a negative coefficient A_1. To illustrate the point, we let $A_1 = -0.2$ and $A_0 = 1$, and rewrite (3.3) as the following second order system

$$\begin{bmatrix} \dot{x}_1 \\ \dot{x}_2 \end{bmatrix} = \begin{bmatrix} 0 & 1 \\ -A_0 & -A_1 \end{bmatrix} \begin{bmatrix} x_1 \\ x_2 \end{bmatrix} = \begin{bmatrix} 0 & 1 \\ -1 & 0.2 \end{bmatrix} \begin{bmatrix} x_1 \\ x_2 \end{bmatrix}. \tag{3.4}$$

The Jacobian matrix of (3.4) has a positive trace, indicating that the equilibrium point $x = 0$ is unstable.

Bellman, Bentsman and Meerkov [1] prove that it is not possible to vibrationally control a system with a positive trace if the function $g(x)$ is linear. Consequently, postulate the existence of a nonlinear function $g(x)$

$$g(x) = \begin{bmatrix} 0 \\ \alpha + \beta x_1 x_2 \end{bmatrix} \tag{3.5}$$

that describes the effect produced by forcing a system component. We stress once again that such a $g(x)$ would have to occur naturally. We will now show that if such a nonlinear $g(x)$ exists, it will stabilize the system (we do not claim that such a $g(x)$ is possible in rocket motors). A discussion of the reasoning for choosing the specific nonlinear $g(x)$ given in (3.5) is provided in Section (5.3) in the Appendix.

Given the above choice of $g(x)$, we write the forced equation as

$$\begin{bmatrix} \dot{x}_1 \\ \dot{x}_2 \end{bmatrix} = \begin{bmatrix} 0 & 1 \\ -A_0 & -A_1 \end{bmatrix} \begin{bmatrix} x_1 \\ x_2 \end{bmatrix} + \begin{bmatrix} 0 \\ \alpha + \beta x_1 x_2 \end{bmatrix} \sin(wt). \tag{3.6}$$

Let $w = 70$, $\alpha = 15$ and $\beta = 200$. For these values, (3.6) becomes

$$\begin{bmatrix} \dot{x}_1 \\ \dot{x}_2 \end{bmatrix} = \begin{bmatrix} 0 & 1 \\ -1 & 0.2 \end{bmatrix} \begin{bmatrix} x_1 \\ x_2 \end{bmatrix} + \begin{bmatrix} 0 \\ 15 + 200 x_1 x_2 \end{bmatrix} \sin(wt). \tag{3.7}$$

It follows from (3.5) that $\|g(0)\| \leq \alpha \leq w\delta_0$ for $\delta_0 \approx 0.22$. Similarly $\|g'(x)\| \leq \beta(x_1 + x_2) < 2\beta\delta < w\delta_1$ for $\delta_1 \approx (5.72)\delta$. Consequently, both δ_0 and δ_1 are sufficiently small and we can apply Theorem (2.1).

We need to calculate the vector b and the matrix A defined in (2.5) and (2.6), respectively. Notice that $p(x)$, defined in (2.3), is zero because the system (3.4) is linear. Consequently, (2.5) yields

$$b = -\frac{\varepsilon^2 g'(0) J g(0)}{2}. \tag{3.8}$$

However,

$$g'(x) = \begin{bmatrix} 0 & 0 \\ \beta x_2 & \beta x_1 \end{bmatrix} \tag{3.9}$$

indicating that $g'(0) = 0$, which implies $b = 0$ and that there is no equilibrium shift.

Equation (2.6) yields the matrix A,

$$A = \left[J - \frac{\varepsilon^2}{2} \frac{\partial (g'(y) J g(y))}{\partial y}(0) \right] = J - \frac{\varepsilon^2}{2} \frac{\partial}{\partial y} \left\{ \begin{bmatrix} 0 & 0 \\ \beta y_2 & \beta y_1 \end{bmatrix} \begin{bmatrix} 0 & 1 \\ -A_0 & -A_1 \end{bmatrix} \begin{bmatrix} 0 \\ \alpha + \beta y_1 y_2 \end{bmatrix} \right\}$$

$$= J - \frac{\varepsilon^2}{2} \frac{\partial}{\partial y} \begin{bmatrix} 0 \\ \alpha\beta y_2 - A_1 \alpha\beta y_1 + \beta^2 y_1 y_2^2 - A_1 \beta^2 y_1^2 y_2 \end{bmatrix} = \begin{bmatrix} 0 & 1 \\ -A_0 + \varepsilon^2 A_1 \alpha\beta/2 & -A_1 - \varepsilon^2 \alpha\beta/2 \end{bmatrix}. \tag{3.10}$$

Consequently, Theorem (2.1) implies that the averaged motion of the system is governed by

$$\begin{bmatrix} \dot{y}_1 \\ \dot{y}_2 \end{bmatrix} = \begin{bmatrix} 0 & 1 \\ -A_0 + \varepsilon^2 A_1 \alpha\beta/2 & -A_1 - \varepsilon^2 \alpha\beta/2 \end{bmatrix} \begin{bmatrix} y_1 \\ y_2 \end{bmatrix}. \tag{3.11}$$

Substituting the numerical values for A_0, A_1, α, β and $\varepsilon = 1/w$ yields

$$\begin{bmatrix} \dot{y}_1 \\ \dot{y}_2 \end{bmatrix} = \begin{bmatrix} 0 & 1 \\ -1.061 & -0.106 \end{bmatrix} \begin{bmatrix} y_1 \\ y_2 \end{bmatrix} \tag{3.12}$$

which is asymptotically stable.

Since the solution $X(t)$ of (3.6) is given by $X(t) = Y(t) + u(t, Y(t))$, where $Y(t)$ is a solution of (3.12) and tends towards the origin as time tends to infinity, $X(t)$ must remain close to the origin for all time because $u(t, Y(t))$ is small for all time. The construction of $u(t, y)$, as defined in the Appendix (see (5.4),(5.8) and (5.9)), implies that if $g(0) \neq 0$ then $u(t, y) \not\to 0$ as $y \to 0$. In this case $g(0) \neq 0$, indicating that $u(t, Y(t))$ does not converge to zero as $Y(t)$ tends to zero. Consequently, $X(t)$ remains close to zero for all time but does not tend to zero as time goes to infinity. Strictly speaking, the equilibrium point $x = 0$ of (2.1) is not asymptotically stable; indeed $x = 0$ is not an equilibrium point but is the center of a small asymptotically stable limit cycle. This limit cycle is the asymptotically stable orbit $X(t) = u(t, 0) \neq 0$. We refer to $x = 0$ as a *slow equilibrium point* because $y = 0$ is an equilibrium point of the slow or time averaged system (2.8), and we say that $x = 0$ is

slowly asymptotically stable because the equilibrium point $y = 0$ of the slow system (2.8) is asymptotically stable. When we refer to *slow* equilibrium points or *slow* stability, we refer to the properties of the time averaged system (2.8). The true dynamics are small oscillations about the slow or averaged dynamics and hence display the same qualitative behaviour. From a practical point of view we have achieved our control objective to keep the system (2.1) in a small neighbourhood of the origin. Therefore, if there exists an accessible component in a liquid rocket motor that can produce a naturally occurring feedback function $g(x) = [0, \alpha + \beta x_1 x_2]^T$, then we can achieve vibrational control by vibrating this component.

It is interesting and instructive to compare results obtained by this analysis with a numerical simulation. We can analytically solve the time averaged equation (3.12) to derive the following analytic expression for $Y_1(t)$

$$Y_1(t) = e^{-0.053t}[Y_1(0)\cos(1.03t) + Y_2(0)\sin(1.03t)], \tag{3.13}$$

where $Y_1(0)$ is the initial displacement and $Y_2(0)$ is the initial velocity. Figure (1) compares $Y_1(t)$ of (3.13) with a $X_1(t)$ calculated by numerically solving (3.7). Since the initial conditions for the slow solution $Y(t)$ are not known, they are matched to the initial conditions shown by the numerical simulation. Figure (1) shows that the slow equilibrium point $x = 0$ of the forced system (3.6) is indeed slowly asymptotically stable (i.e., $X_1(t)$ approaches a small asymptotically stable limit cycle) but is not asymptotically stable ($X_1(t) \not\to 0$). Furthermore, Fig. (1) shows excellent agreement between the behaviour predicted by the developed theory and the numerical simulation.

4 Conclusion

In this paper we present a criterion for nonlinear vibrational open loop control. Previous work that was restricted to linear control is extended to include analysis of nonlinear, vibrational control. It has been previously shown that linear vibrational control is not feasible if the Jacobian matrix has a positive trace. This paper demonstrates that nonlinear vibrational control is possible even if the trace of the Jacobian is positive. This result is significant because a large number of nonlinear engineering systems exhibit a positive Jacobian trace and yet may be stabilized by nonlinear, open loop, vibrational control. Finally, it is shown that the theory developed in this paper is in excellent agreement with numerical results.

5 Appendix

In this section we prove Theorem (2.1) and discuss the corresponding change of variables $x(t) = y(t) + u(t, y)$. We begin by assuming that the investigated system is described by

$$\dot{x} = f(x) + h(wt)g(x, w, a), \tag{5.1}$$

where $x(t) \in \mathbb{R}^n$, $f \in C^3(\mathbb{R}^n, \mathbb{R}^n)$, $f(0) = 0$, $h(wt) = \sin(wt)$, $w \gg 1$, and $g \in C^4(\mathbb{R}^n \times \mathbb{R} \times \mathbb{R}, \mathbb{R}^n)$. We perform a local analysis that will be restricted to a ball of radius δ centered at the origin. In addition, since w and a are constant, we write $g(x, w, a)$ simply as $g(x)$ and impose the following smoothness constraints

$$\begin{array}{rcl} \|f'(0)\| & \leq & \sigma, \qquad 0 \leq \sigma, \\ \|g(0)\| & \leq & w\delta_0, \qquad 0 \leq \delta_0, \\ \|g'(\xi)\| & \leq & w\delta_1, \qquad 0 \leq \delta_1, \end{array} \tag{5.2}$$

where $f'(x)$ denotes the derivative of f evaluated at x and $\xi \in B(0, \delta)$. To simplify the algebra, we introduce a fast time variable $s = wt$, define $\epsilon = 1/w$, denote dx/ds as $\acute{x}$ and rewrite (5.1) in the fast time scale

$$\acute{x} = \epsilon f(x) + \epsilon h(s)g(x). \tag{5.3}$$

5.1 The Transformation

To prove Theorem (2.1) we introduce the change of variables $x(s) = y(s) + u(s, y)$. Next, we define the function $u(s, y)$ and determine some of its properties; that is,

$$u(s, y) = \alpha(y)\sin(s) + \beta(y)\cos(s), \tag{5.4}$$

where $\alpha(y), \beta(y) \in \mathbb{R}^n$. The functions $\alpha(y)$ and $\beta(y)$ are chosen so that $u(s, y)$ satisfies the partial differential equation

$$u_s(s, y) = \varepsilon J u(s, y) + \varepsilon h(s) g(y), \tag{5.5}$$

where $J = f'(0)$ is the Jacobian matrix and the subscript s denotes a partial derivative with respect to s. Note that for any fixed y the above equation is an ordinary differential equation in $u(\cdot, y)$. Substituting (5.4) into (5.5) and equating the coefficients of the sines and cosines yields

$$\begin{aligned} -\beta(y) - \varepsilon J\alpha(y) &= \varepsilon g(y), & (5.6)\\ \alpha(y) - \varepsilon J\beta(y) &= 0. & (5.7) \end{aligned}$$

Solving (5.6) and (5.7) for $\alpha(y)$ and $\beta(y)$ yields

$$\begin{aligned} \alpha(y) &= -\varepsilon^2[I + \varepsilon^2 J^2]^{-1} J g(y), & (5.8)\\ \beta(y) &= -\varepsilon J\alpha(y) - \varepsilon g(y), & (5.9) \end{aligned}$$

where the inverse matrix $[I+\varepsilon^2 J^2]^{-1}$ is well defined provided ε is small enough to satisfy the inequality $\|\varepsilon^2 J^2\| < 1$.

To derive approximate equations for $\alpha(y)$ and $\beta(y)$ we need the following bound on $g(y)$,

$$\|g(y)\| \le \|g(0) + g(y) - g(0)\| \le \|g(0)\| + \frac{\delta_1}{\varepsilon}\|y\| \le \frac{\delta_0 + \delta_1\delta}{\varepsilon}, \tag{5.10}$$

which holds for all $y \in B(0, \delta)$. Next, we represent the inverse matrix $[I + \varepsilon^2 J^2]^{-1}$ as the geometric series

$$[I + \varepsilon^2 J^2]^{-1} = I - \varepsilon^2 J^2 + \varepsilon^4 J^4 - \ldots = I + O(\varepsilon^2\sigma^2). \tag{5.11}$$

Using (5.8) through (5.11) yields the following approximate expressions

$$\begin{aligned} \alpha(y) &= -\varepsilon^2 J g(y) + O(\varepsilon^3\delta_0 + \varepsilon^3\delta\delta_1), & (5.12)\\ \beta(y) &= -\varepsilon g(y) + \varepsilon^3 J^2 g(y) + O(\varepsilon^4\delta_0 + \varepsilon^4\delta\delta_1). & (5.13) \end{aligned}$$

To complete the discussion of the properties of $u(s, y)$, we need bounds on $u(s, y)$ and the partial derivative $u_y(s, y)$. We begin by bounding the inverse matrix $[I + \varepsilon^2 J^2]^{-1}$. Equation (5.11) implies

$$\|[I + \varepsilon^2 J^2]^{-1}\| \le \|I\| + \varepsilon^2\|J^2\| + \ldots \le 1 + \varepsilon^2\sigma^2 + \ldots \le 1/(1 - \varepsilon^2\sigma^2). \tag{5.14}$$

It follows from (5.8), (5.9), (5.10) and (5.14) that

$$\begin{aligned} \|\alpha(y)\| &\le \frac{\varepsilon\sigma(\delta_0 + \delta\delta_1)}{1 - \varepsilon^2\sigma^2}, & (5.15)\\ \|\beta(y)\| &\le \frac{\delta_0 + \delta\delta_1}{1 - \varepsilon^2\sigma^2} & (5.16) \end{aligned}$$

for all $y \in B(0, \delta)$. To derive the desired bound on $u(s, y)$ we need only to note that (5.4) implies $\|u\| \le \|\alpha\| + \|\beta\|$, indicating that

$$\|u(s, y)\| \le \frac{(1 + \varepsilon\sigma)(\delta_0 + \delta\delta_1)}{1 - \varepsilon^2\sigma^2} < 2(\delta_0 + \delta\delta_1) = O(\delta_0 + \delta\delta_1), \tag{5.17}$$

which holds for all s and sufficiently small ϵ. The bound on $u_y(s,y) = \alpha'(y)\sin(s) + \beta'(y)\cos(s)$ is also straightforward. Since (5.8) and (5.9) imply

$$\alpha'(y) = -\epsilon^2[I + \epsilon^2 J^2]^{-1} J g'(y), \tag{5.18}$$

$$\beta'(y) = -\epsilon J \alpha'(y) - \epsilon g'(y), \tag{5.19}$$

then using, (5.10), (5.14), (5.18) and (5.19) one obtains

$$\|u_y(s,y)\| \leq \frac{(1+\epsilon\sigma)\delta_1}{1-\epsilon^2\sigma^2} = O(\delta_1), \tag{5.20}$$

which holds for all s.

5.2 Proof of Theorem 2.1.

We begin by noting that the transformation $u(s,y)$ constructed in the previous section satisfies the constraints outlined in the theorem. The transformation $x(s) = y(s) + u(s,y)$ implies $dx/ds = \dot{x} = \dot{y} + u_s + u_y\dot{y}$. Substituting this relationship into (5.3) yields

$$[I + u_y(s,y)]\dot{y} + u_s(s,y) = \epsilon f(y+u) + \epsilon h(s) g(y+u). \tag{5.21}$$

Equation (5.20) implies $\|u_y(s,y)\| < 1$ for sufficiently small δ_1, for all $y \in B(0,\delta)$ and for all s. Consequently, the inverse matrix $[I + u_y(s,y)]^{-1}$ is well defined and we can rewrite (5.21) as

$$\dot{y} = [I + u_y(s,y)]^{-1}[\epsilon f(y+u) + \epsilon h(s) g(y+u) - u_s(s,y)]. \tag{5.22}$$

The following relationships will be used to simplify (5.22),

$$p(x) = f(x) - Jx, \tag{5.23}$$

$$q(y,u) = g(y+u) - g(y) - g'(y)u. \tag{5.24}$$

where $p(x)$ is defined as before and $q(y,u)$ represents the sum of all terms of second order and higher in the Taylor expansion of $g(y+u)$ around $u = 0$. It follows that

$$p(0) = 0, \quad p'(0) = 0, \quad p(x) = O(\|x\|^2), \tag{5.25}$$

$$q(y,0) = 0, \quad q_u(y,0) = 0, \quad q(y,u) = O(\|u\|^2). \tag{5.26}$$

Using (5.23) and (5.24) we can rewrite (5.22) as

$$\dot{y} = [I + u_y(s,y)]^{-1}[\epsilon J y + \epsilon J u(s,y) + \epsilon p(y+u) + \epsilon h(s) g(y) + \epsilon h(s) g'(y) u(s,y) + \epsilon h(s) q(y,u) - u_s(s,y)]. \tag{5.27}$$

Substituting (5.5) into (5.27) yields

$$\dot{y} = [I + u_y(s,y)]^{-1}[\epsilon J y + \epsilon p(y+u) + \epsilon h(s) g'(y) u(s,y) + \epsilon h(s) q(y,u)]. \tag{5.28}$$

Approximating the inverse matrix $[I + u_y(s,y)]^{-1}$ as a two term series with a second order error,

$$[I + u_y(s,y)]^{-1} = I - u_y(s,y) + O(\|u_y\|^2) = I - u_y(s,y) + O(\delta_1^2), \tag{5.29}$$

and substituting (5.29) into (5.28) yields

$$\dot{y} = \epsilon[I - u_y(s,y) + O(\delta_1^2)][Jy + h(s) g'(y) u(s,y) + p(y + u(s,y)) + h(s) q(y, u(s,y))] = \epsilon F(s,y). \tag{5.30}$$

We are now in a position to apply the method of averaging. Since $F(s,y)$ is periodic in s with a period 2π, we can approximate the non-autonomous system $\dot{y} = \epsilon F(s,y)$ as the autonomous averaged system $\dot{y} = \epsilon F_{av}(y)$ where

$$F_{av}(y) = \frac{1}{2\pi}\int_0^{2\pi} F(\tau, y) d\tau, \tag{5.31}$$

(see [9, p.412] for a discussion of averaging). Consequently, the averaged equation is given by

$$\dot{y} = \frac{\epsilon}{2\pi}\int_0^{2\pi}[I - u_y(\tau,y) + O(\delta_1^2)][Jy + h(\tau)g'(y)u(\tau,y) + p(y+u(\tau,y)) + h(\tau)q(y,u(\tau,y))]d\tau. \tag{5.32}$$

Expanding (5.32) yields

$$\begin{aligned}\dot{y} \;= \tfrac{\epsilon}{2\pi}\textstyle\int_0^{2\pi}[\;& Jy + h(\tau)g'(y)u(\tau,y) + p(y+u(\tau,y)) + h(\tau)q(y,u(\tau,y)) - u_y(\tau,y)Jy \\ & - u_y(\tau,y)h(\tau)g'(y)u(\tau,y) - u_y(\tau,y)p(y+u(\tau,y)) - u_y(\tau,y)h(\tau)q(y,u(\tau,y)) \\ & + O(\delta\delta_1^2 + \delta_0\delta_1^3/\epsilon + \delta\delta_1^4/\epsilon + \delta_0^2\delta_1^2)\;]d\tau.\end{aligned} \tag{5.33}$$

The terms $u_y(\tau,y)Jy$ and $u_y(\tau,y)h(\tau)g'(y)u(\tau,y)$ consist of an odd number of sinusoidal functions and thus average to zero. The term Jy is constant with respect to τ and can be taken outside the integral. Finally, since $h(s) = \sin(s)$ and $u(s,y) = \alpha(y)\sin(s) + \beta(y)\cos(s)$, then averaging the term $h(\tau)g'(y)u(\tau,y)$ yields

$$\frac{1}{2\pi}\int_0^{2\pi} h(\tau)g'(y)u(\tau,y)d\tau = \frac{1}{2\pi}\int_0^{2\pi}\sin^2(\tau)g'(y)\alpha(y) + \sin(\tau)\cos(\tau)g'(y)\beta(y)d\tau = g'(y)\alpha(y)/2. \tag{5.34}$$

Using the approximate expression (5.12) for $\alpha(y)$ in (5.34) lets us rewrite (5.33) as

$$\dot{y} = \epsilon Jy - \frac{\epsilon^3}{2}g'(y)Jg(y) + \frac{\epsilon}{2\pi}\int_0^{2\pi}[p(y+u(\tau,y)) + h(\tau)q(y,u(\tau,y)) - u_y(\tau,y)p(y+u(\tau,y)) - u_y(\tau,y)h(\tau)q(y,u(\tau,y))]d\tau$$

$$+\epsilon O(\epsilon^2\delta_0\delta_1 + \delta\delta_1^2 + \delta_0\delta_1^3/\epsilon + \delta\delta_1^4/\epsilon + \delta_0^2\delta_1^2). \tag{5.35}$$

To complete the proof we have to bound the integral in the (5.35). The bounds on $u_y(\tau,y)p(y+u(\tau,y))$ and $u_y(\tau,y)h(\tau)q(y,u(\tau,y))$ follow from (5.17), (5.20), (5.25) and (5.26); that is,

$$u_y(\tau,y)p(y+u(\tau,y)) \;= O(\|u_y\|\|y+u\|^2) \;= O(\delta^2\delta_1 + \delta\delta_0\delta_1 + \delta_0^2\delta_1), \tag{5.36}$$

$$u_y(\tau,y)h(\tau)q(y,u(\tau,y)) \;= O(\|u_y\|\|u\|^2) \;= O(\delta_0^2\delta_1 + \delta\delta_0\delta_1 + \delta^2\delta_1^3). \tag{5.37}$$

In order to get bounds on the remaining terms, $p(y+u(\tau,y))$ and $h(\tau)q(y,u(\tau,y))$, we will require the following notation. Denote the second order Taylor expansion of $g(y+u)$ at $u=0$ as

$$g(y+u) = g(y) + g'(y)u + \frac{1}{2}g''(y)\langle u,u\rangle + O(\|u\|^3), \tag{5.38}$$

where $\langle u,u\rangle$ denotes a tensor and $g''(y)$ is the corresponding three dimensional array of coefficients evaluated at y. It follows that $q(y,u) = g''(y)\langle u,u\rangle/2 + O(\|u\|^3)$. Consequently, the average of $h(\tau)q(y,u(\tau,y))$ is written as

$$\frac{1}{2\pi}\int_0^{2\pi}h(\tau)q(y,u(\tau,y))d\tau = \frac{1}{4\pi}\int_0^{2\pi}h(\tau)g''(y)\langle u(\tau,y),u(\tau,y)\rangle d\tau + O(\|u\|^3). \tag{5.39}$$

Since each term of $h(\tau)\langle u(\tau,y),u(\tau,y)\rangle$ consists of an odd number of sinusoidal functions, the resulting average is zero. Hence, (5.39) is reduced to

$$\frac{1}{2\pi}\int_0^{2\pi}h(\tau)q(y,u(\tau,y))d\tau = O(\delta_0^3 + \delta\delta_0^2\delta_1 + \delta^2\delta_0\delta_1^2 + \delta^3\delta_1^3). \tag{5.40}$$

With the aid of the bounds (5.36), (5.37) and (5.40) we can rewrite (5.35) as

$$\dot{y} = \epsilon Jy - \frac{\epsilon^3}{2}g'(y)Jg(y) + \frac{\epsilon}{2\pi}\int_0^{2\pi}p(y+u(\tau,y))d\tau + \epsilon O(\epsilon^2\delta_0\delta_1 + \delta\delta_1^2 + \delta_0\delta_1^3/\epsilon + \delta\delta_1^4/\epsilon + \delta_0^3 + \delta\delta_0\delta_1 + \delta_0^2\delta_1). \tag{5.41}$$

Equation (5.41) is of the form $\dot{y} = F(y) + \varepsilon O(\ldots)$ where

$$F(y) = \varepsilon Jy - \frac{\varepsilon^3}{2} g'(y) J g(y) + \frac{\varepsilon}{2\pi} \int_0^{2\pi} p(y + u(\tau, y)) d\tau. \tag{5.42}$$

Since we are concerned with local behaviour at the origin, we linearize (5.41) about $y = 0$, to get

$$\dot{y} = F(0) + \left[\frac{\partial F}{\partial y}(0)\right] y + \varepsilon O(\delta^2 + \ldots). \tag{5.43}$$

Expanding the above yields

$$\dot{y} = \left[\frac{\varepsilon}{2\pi} \int_0^{2\pi} p(u(\tau, 0)) d\tau - \frac{\varepsilon^3 g'(0) J g(0)}{2}\right] + \varepsilon Jy - \frac{\varepsilon^3}{2} \left[\frac{\partial (g'(y) J g(y))}{\partial y}(0)\right] y + \left[\frac{\partial \left(\frac{\varepsilon}{2\pi} \int_0^{2\pi} p(y + u(\tau, y)) d\tau\right)}{\partial y}(0)\right] y$$

$$+ \varepsilon O(\delta^2 + \varepsilon^2 \delta_0 \delta_1 + \delta \delta_1^2 + \delta_0 \delta_1^3/\varepsilon + \delta \delta_1^4/\varepsilon + \delta_0^3 + \delta \delta_0 \delta_1 + \delta_0^2 \delta_1). \tag{5.44}$$

We now complete the proof by bounding the last term in (5.44). Since the derivative of $p(x)$ exists and is continuous by assumption, we can move the partial derivative $\partial/\partial y$ inside the integral to get

$$\left[\frac{\partial \left(\frac{\varepsilon}{2\pi} \int_0^{2\pi} p(y + u(\tau, y)) d\tau\right)}{\partial y}(0)\right] = \frac{\varepsilon}{2\pi} \int_0^{2\pi} \left\{\frac{\partial [p(y + u(\tau, y))]}{\partial y}(0)\right\} d\tau \tag{5.45}$$

where

$$\frac{\partial [p(y + u(\tau, y))]}{\partial y}(0) = p'(u(\tau, 0)) + p'(u(\tau, 0)) u_y(\tau, 0). \tag{5.46}$$

Since $p(x) \in \mathbb{R}^n$, then $p'(a) \in \mathbb{R}^{n \times n}$ is a matrix valued function. Letting $[M]_{ij}$ denote the ij'th element of the matrix M and $\ell_{ij}(a) = [p'(a)]_{ij} \in \mathbb{R}$, then using (5.46) lets us write the ij'th term of (5.45) as

$$\left[\frac{\partial \left(\frac{\varepsilon}{2\pi} \int_0^{2\pi} p(y + u(\tau, y)) d\tau\right)}{\partial y}(0)\right]_{ij} = \frac{\varepsilon}{2\pi} \int_0^{2\pi} \ell_{ij}(u(\tau, 0)) + \langle \ell_{ik}(u(\tau, 0)) [u_y(\tau, 0)]_{kj} \rangle d\tau, \tag{5.47}$$

where the tensor notation $\langle\ \rangle$ implies a summation over the index k. Expanding ℓ_{ij} and ℓ_{ik} as first and zero order Taylor series about the origin yields

$$\left[\frac{\partial \left(\frac{\varepsilon}{2\pi} \int_0^{2\pi} p(y + u(\tau, y)) d\tau\right)}{\partial y}(0)\right]_{ij} = \frac{\varepsilon}{2\pi} \int_0^{2\pi} \left\{\ell_{ij}(0) + \ell'_{ij}(0) u(\tau, 0) + \langle \ell_{ik}(0) [u_y(\tau, 0)]_{kj} \rangle\right\} d\tau + \varepsilon O(\|u\|^2 + \|u\| \|u_y\|). \tag{5.48}$$

Equation (5.25) implies $\ell_{ij}(0) = 0$ and the averages of $\ell'_{ij}(0) u(\tau, 0)$ and $\ell_{ik}(0) [u_y(\tau, 0)]_{kj}$ are zero. Consequently,

$$\left[\frac{\partial \left(\frac{\varepsilon}{2\pi} \int_0^{2\pi} p(y + u(\tau, y)) d\tau\right)}{\partial y}(0)\right] y = \varepsilon O(\|y\| \|u\|^2 + \|y\| \|u\| \|u_y\|) = O(\delta \delta_0^2 + \delta \delta_0 \delta_1 + \delta^2 \delta_1^2). \tag{5.49}$$

The bound (5.49) allows us to rewrite (5.44) as

$$\dot{y} = \left[\frac{\varepsilon}{2\pi} \int_0^{2\pi} p(u(\tau, 0)) d\tau - \frac{\varepsilon^3 g'(0) J g(0)}{2}\right] + \varepsilon Jy - \frac{\varepsilon^3}{2} \left[\frac{\partial (g'(y) J g(y))}{\partial y}(0)\right] y +$$

$$\varepsilon O(\delta^2 + \varepsilon^2 \delta_0 \delta_1 + \delta \delta_1^2 + \delta_0 \delta_1^3/\varepsilon + \delta \delta_1^4/\varepsilon + \delta_0^3 + \delta_0^2 \delta_1 + \delta \delta_0^2 + \delta \delta_0 \delta_1). \tag{5.50}$$

According to the definition (2.4)

$$\phi(\tau) = -\epsilon^2 Jg(0)\sin(\tau) - \epsilon g(0)\cos(\tau), \tag{5.51}$$

then (5.12) and (5.13) imply

$$\phi(\tau) = u(\tau, 0) + O(\epsilon^3\delta_0 + \epsilon^3\delta\delta_1). \tag{5.52}$$

Using (5.52) in (5.50) yields

$$\dot{y} = \left[\frac{\epsilon}{2\pi}\int_0^{2\pi} p(\phi(\tau))d\tau - \frac{\epsilon^3 g'(0)Jg(0)}{2}\right] + \epsilon Jy - \frac{\epsilon^3}{2}\left[\frac{\partial(g'(y)Jg(y))}{\partial y}(0)\right] y +$$

$$\epsilon O(\delta^2 + \epsilon^2\delta_0\delta_1 + \delta\delta_1^2 + \delta_0\delta_1^3/\epsilon + \delta\delta_1^4/\epsilon + \delta_0^3 + \delta_0^2\delta_1 + \delta\delta_0^2 + \delta\delta_0\delta_1 + \epsilon^3\delta_0^2). \tag{5.53}$$

Rewriting (5.53) in the original time scale t yields

$$\dot{y} = Ay + b + O(\zeta). \tag{5.54}$$

where A, b and ζ are as defined in the theorem. □

5.3 Choice of $g(x)$ in Positive Trace Example

In equation (3.5) we let $g(x) = [0, \alpha + \beta x_1 x_2]^T$. This hypothetical choice of $g(x)$ is not arbitrary. We know that the sign of A_1 creates an instability. Consequently we wish to change the sign of this coefficient by applying vibrational control. Consider the averaged equation (2.8). If we denote the vector $g'(x)Jg(x)$ as $[G_1(x), G_2(x)]^T$ then the matrix A defined in (2.6) can be written as

$$A = J - k\frac{\partial[G_1(x), G_2(x)]^T}{\partial x}(0) = J - k\begin{bmatrix} \partial G_1(0)/\partial x_1 & \partial G_1(0)/\partial x_2 \\ \partial G_2(0)/\partial x_1 & \partial G_2(0)/\partial x_2 \end{bmatrix} \tag{5.55}$$

where k is a positive constant. For A to have a negative trace either $\partial G_1(0)/\partial x_1$ or $\partial G_2(0)/\partial x_2$ must be positive, or both. Consequently, letting $\partial G_2(0)/\partial x_2 = c$ be a positive quantity implies $G_2(x) = cx_2$. It follows that

$$G_2(x) = g_2(x)\frac{\partial g_2}{\partial x_1} - g_1(x)\frac{\partial g_2}{\partial x_2} + 0.2g_2(x)\frac{\partial g_2}{\partial x_2} = cx_2. \tag{5.56}$$

If we consider the first term only, we can set

$$g_2(x)\frac{\partial g_2}{\partial x_1} = cx_2. \tag{5.57}$$

Equation (5.57) is a partial differential equation in $g_2(x)$, which can be solved by separation of variables. Unfortunately, the solution to (5.57) is $g_2(x) = \pm c_1\sqrt{|x_1 x_2|}$ which is singular at the origin and violates the assumption that $g(x)$ is continuously differentiable. Consequently, we let $g_2(x) = \alpha + \beta x_1 x_2$, approximating the square root dependance of $g_2(x)$ near the origin. If we now set $g_1(x) = 0$, then $g(x) = [0, \alpha + \beta x_1 x_2]^T$. It is noteworthy that the last term in (5.56) suggests that $g_2(x) = Kx_2$ might also be a viable feedback function. Such a choice requires, however, that $K > w$, which violates the assumption that $\|g'(x)\| \leq w\delta_1 < w$.

References

[1] R.E. Bellman, J. Bentsman, and S.M Meerkov. "Vibrational control of nonlinear systems: vibrational stabilizability". *IEEE Transactions on Automatic Control*, vol.AC-31:pp.710–724, Aug 1986.

[2] S.M. Meerkov and G.I. Shapiro. "Method of vibrational control in the problem of stabilization of ionization-thermal instability of a powerful continuous CO_2 laser". *Automatic Remote Control*, vol.37:pp.821–830, 1976.

[3] C. McGreavy and J.M. Thornton. "Stability studies of single catalyst particles". *Chemical Engineering*, vol.1:pp.296–301, 1970.

[4] S.M. Meerkov. "Principle of vibrational control: theory and applications". *IEEE Transactions on Automatic Control*, vol.AC-25:pp.755–762, Aug 1980.

[5] J. Guckenheimer and P. Holmes. *Nonlinear oscillations, dynamical systems, and bifurcations of vector fields.* New York: Springer Verlag, 1983.

[6] J. Bentsman. "Vibrational control of a class of nonlinear systems by nonlinear multiplicative vibrations". *IEEE Transactions on Automatic Control*, vol.AC-32:pp.711–716, Aug 1987.

[7] G. Strang. *Linear Algebra and its Applications.* New York: Harcourt Brace Jovanovich, Inc., 1988.

[8] E. Powell. *Nonlinear combustion instability in liquid propellant rocket engines.* PhD thesis, Georgia Institute of Technology, 1970.

[9] H.K. Khalil. *Nonlinear Systems.* New York: Macmillan Publishing Company, 1992.

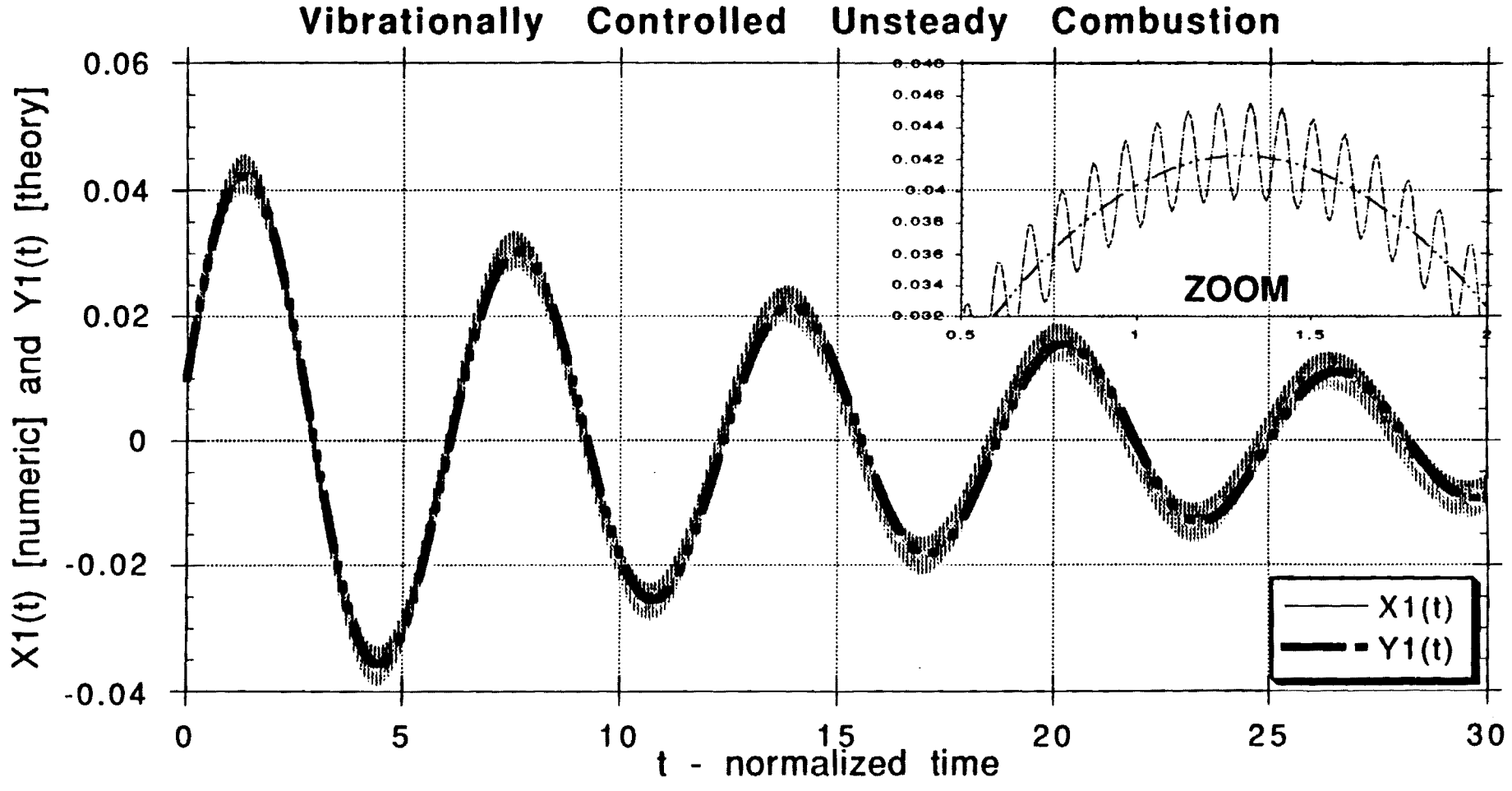

Figure 1: Damping of a liquid rocket instability by high frequency vibrational control